Joint PhD degree in Environmental Technology

Docteur de l'Université Paris-Est
Spécialité : Science et Technique de l'Environnement

Dottore di Ricerca in Tecnologie Ambientali

Degree of Doctor in Environmental Technology

Thesis for the degree of Doctor of Philosophy in Environmental Technology

Tesi di Dottorato – Thèse – PhD thesis – Väitöskirja

Ramita Khanongnuch

Hydrogen sulfide removal from synthetic biogas using anoxic biofilm reactors

21/05/2019, Tampere

In front of the PhD evaluation committee

Prof. David Gabriel	Reviewer and chair
Prof. Pavel Jeníček	Reviewer
Assoc. Prof. Marta Izquierdo Sanchis	Reviewer
Prof. Piet N.L. Lens	Promotor
Prof. Giovanni Esposito	Co-Promotor
Prof. Eric D. van Hullebusch	Co-Promotor
Asst. Prof. Aino-Maija Lakaniemi	Co-Promotor

Marie Skłodowska-Curie European Joint Doctorate Advanced Biological Waste-to-Energy Technologies

Evaluation committee

Reviewers/Examiners

Prof. David Gabriel
Department of Chemical, Biological and Environmental Engineering
Universitat Autònoma de Barcelona
Spain

Prof. Pavel Jeníček
Department of Water Technology and Environmental Engineering
University of Chemistry and Technology
Czech Republic

Assoc. Prof. Marta Izquierdo Sanchis
Chemical Engineering Department
University of Valencia
Spain

Thesis Promotor

Prof. Piet N. L. Lens
Department of Environmental Engineering and Water Technology
IHE Delft
The Netherlands

Thesis Co-Promotors

Prof. Giovanni Esposito
Department of Civil and Mechanical Engineering
University of Cassino and Southern Lazio
Italy

Prof. Hab. Eric D. van Hullebusch
University of Paris-Est Marne-la-Vallée
France

Asst. Prof. Aino-Maija Lakaniemi
Faculty of Engineering and Natural Sciences
Tampere University
Finland

Supervisory team

Thesis Supervisor

Prof. Piet N. L. Lens
Department of Environmental Engineering and Water Technology
IHE Delft
The Netherlands

Thesis Co-Supervisors

Asst. Prof. Aino-Maija Lakaniemi
Faculty of Engineering and Natural Sciences
Tampere University
Finland

Dr. Eldon R. Rene
Department of Environmental Engineering and Water Technology
IHE Delft
The Netherlands

Thesis Instructor

Dr. Francesco Di Capua
Department of Civil, Architectural and Environmental Engineering
University of Naples Federico II
Italy

This research was conducted in the framework of the Marie Skłodowska-Curie European Joint Doctorate (EJD) in Advanced Biological Waste-to-Energy Technologies (ABWET) and supported by the Horizon 2020 under grant agreement number 643071.

Abstract

The aim of this work was to develop and study anoxic bioreactors for the removal of reduced inorganic sulfur compounds from liquid and gaseous waste streams. In addition, the aim was to enable process integration for the simultaneous treatment of H_2S contaminated gas streams and NO_3^--containing wastewater.

The experiments related to sulfide oxidation in the liquid phase were conducted in two different attached growth bioreactors, i.e. a fluidized-bed reactor (FBR) and a moving bed biofilm reactor (MBBR), inoculated with the same mixed culture of sulfur-oxidizing nitrate-reducing (SO-NR) bacteria. The bioreactors were operated under different nitrogen-to-sulfur (N/S) molar ratios using $S_2O_3^{2-}$ and NO_3^- as an energy source and electron acceptor, respectively. Results revealed that both the FBR and MBBR achieved $S_2O_3^{2-}$ removal efficiencies (RE) >98% and completely removed NO_3^- at an N/S ratio of 0.5. Under severe nitrate limitation (N/S ratio of 0.1), the $S_2O_3^{2-}$ RE in the MBBR (37.8%) was higher than that observed in the FBR (26.1%). In addition, the MBBR showed better resilience to nitrate limitation than the FBR as the $S_2O_3^{2-}$ RE was recovered to 94% within 1 day after restoring the feed N/S ratio to 0.5, while it took 3 days to obtain 80% $S_2O_3^{2-}$ RE in the FBR. Artificial neural network models were successfully used to predict the FBR and MBBR performance, i.e. $S_2O_3^{2-}$ and NO_3^- RE as well as sulfate production.

The SO-NR biomass from the MBBR was used to inoculate an anoxic biotrickling filter (BTF), which was studied for simultaneous treatment of H_2S and NO_3^- containing waste streams. In the anoxic BTF, a maximum H_2S elimination capacity (EC) of 19.2 g S m^{-3} h^{-1} (99% RE) was obtained at an inlet H_2S load of 20.0 g S m^{-3} h^{-1} (~500 ppm_v) and an N/S ratio of ~1.7. As some NO_3^--containing wastewaters can also contain organic compounds, the anoxic BTF inoculated with *Paracoccus versutus* strain MAL 1HM19 was studied for the simultaneous treatment of H_2S, NO_3^- and organic carbon containing waste streams. With this BTF, NO_3^- and acetate removal rates of 16.7 g NO_3^--N m^{-3} h^{-1} and 42.0 g acetate m^{-3} h^{-1}, respectively, were achieved, which was higher than the values observed in the BTF inoculated with the mixed culture of autotrophic SO-NR bacteria (11.1 g NO_3^--N m^{-3} h^{-1} and 10.2 g acetate m^{-3} h^{-1}). Anoxic BTFs were operated under several transient conditions (i.e. varied gas and trickling liquid flow rates, intermittent NO_3^- supply and H_2S shock loads) to evaluate the impacts of sudden changes that usually occur in practical applications. The different transient conditions significantly affected the H_2S EC of the anoxic BTF. After applying H_2S shock loads, the H_2S RE fully recovered to >99% within 1.7 days after resuming normal operation.

In summary, the MBBR was more effective for the removal of $S_2O_3^{2-}$ than the FBR, especially under nitrate limited conditions. Based on the short recovery times after exposure to transient-state conditions, the anoxic MBBR and BTF were found to be resilient and robust systems for removal of reduced sulfur compounds under autotrophic and mixotrophic conditions.

Tiivistelmä

Tämän tutkimuksen tarkoituksena oli kehittää bioreaktoreita sulfidin poistamiseen nestemäisistä jätevirroista anoksisissa olosuhteissa. Lisäksi tavoitteena oli mahdollistaa rikkivetyä sisältävien kaasumaisten ja nitraattia sisältävien nestemäisten jätevirtojen yhtaikainen käsittely.

Ensiksi tutkittiin liukoisten epäorgaanisten rikkiyhdisteiden hapetusta rikkiä hapettavia ja nitraattia pelkistäviä (SO-NR) bakteereita sisältävällä mikrobiviljelmällä kahdessa erilaisessa bioreaktorissa, leijupetireaktorissa (FBR) ja kantajakappalereaktorissa (MBBR). Bioreaktoreiden toimintaa syötteen eri typen ja rikin moolisuhteilla vertailtiin käyttäen tiosulfaattia elektronidonorina ja nitraattia elektroniakseptorina. Molemmissa reaktoreissa saavutettiin yli 98 %:n tiosulfaatin poistotehokkuus ja nitraatti saatiin poistettua kokonaan N/S-suhteen ollessa 0,5. Erittäin typpirajoitteisissa olosuhteissa (NS suhde 0,1), MBBR:llä saavutettu tiosulfaatin poistotehokkuus (37,8 %) oli korkeampi kuin FBR:llä saavutettu tiosulfaatin poistotehokkuus (26,1 %). Kun syötteen N/S suhde palautettiin arvoon 0,5, MBBR:llä tiosulfaatin poistotehokkuus palautui yhden päivän aikana arvoon 94 %, kun taas FBR:llä kesti kolme päivää, että tiosulfaatin poistotehokkuus nousi arvoon 80 %. Kummallekin reaktorille kehitettiin oman neuroverkko-pohjainen malli, joka ennusti luotettavasti tiosulfaatin ja nitraatin poistotehokkuuksia eri olosuhteissa.

MBBR:ään rikastunutta SO-NR-viljelmää hyödynnettiin valutusbiosuodattimessa (BTF) rikkivetyä ja nitraattia sisältävien synteettisten jätevirtojen samanaikaiseen käsittelyyn. Anoksisella BTF:llä suurin saavutettu rikkivedyn poistokapasiteetti oli 19,2 g S m^{-3} h^{-1} (99 % poistotehokkuus) rikkivetykuorman ollessa 20,0 g S m^{-3} h^{-1} (~500 ppmv) ja N/S suhteen noin 1,7. Koska nitraattia sisältävät jätevedet voivat sisältää myös orgaanisia yhdisteitä toisessa BTF:ssä tutkittiin *Paracoccus versutus* MAL 1HM19 kannan kykyä poistaa samanaikaisesti rikkivetyä, nitraattia ja orgaanisia yhdisteitä. Tällä BTF:llä saavutettiin nitraatin poistonopeus 16,7 g NO_3^--N m^{-3} h^{-1} ja asetaatin poistonopeus 42,0 g-asetaattia m^{-3} h^{-1}. Saavutetut poistonopeudet olivat korkeampia kuin autotrofisia SO-NR bakteereja hyödyntävällä BTF:llä saavutetut arvot, jotka olivat 11,1 g NO_3^--N m^{-3} h^{-1} ja 10,2 g-asetaattia m^{-3} h^{-1}. SO-NR bakteerien hallitseman anoksisen BTF:n toimintaa tutkittiin vaihtuvissa olosuhteissa kuten muuttuva kaasun ja valutusnesteen virtausnopeus, katkonainen nitraatin syöttö ja rikkivedyn shokkikuormitus, sillä tällaiset häiriöt ovat mahdollisia käytännön sovelluksissa. Olosuhteiden ohimenevät muutokset vaikuttivat merkittävästi rikkivedyn poistokapasiteettiin. Esimerkiksi rikkivedyn shokkikuormituksen jälkeen kesti 1,7 päivää ennen kuin rikkivedyn poistotehokkuus palasi yli 99 %:n tasolle.

Yhteenvetona voidaan todeta, että MBBR mahdollisti tehokkaamman tiosulfaatin poiston kuin FBR erityisesti typpirajoitteisissa olosuhteissa. MBBR:n ja BTF:n osoitettiin palautuvan nopeasti ohimenevistä kuormitustilanteista ja mahdollistavan siis vakaan epäorgaanisten rikkiyhteisen poiston synteettisistä jätevirroista.

Sommario

Lo scopo di questo lavoro è stato quello di sviluppare e studiare bioreattori anossici per la rimozione di solfuro dai flussi di rifiuti liquidi e valutare l'integrazione di processi per il trattamento simultaneo di flussi di gas contaminati da H_2S e acque reflue contenenti NO_3^-.

Gli esperimenti relativi all'ossidazione del solfuro in fase liquida sono stati valutati in due diversi bioreattori di crescita collegati, ovvero un reattore a letto fluido (FBR) e un reattore a biomassa adesa a letto mobile (MBBR), inoculati con batteri riducenti il nitrato di zolfo (SO-NR). I bioreattori sono stati esaminati nell'ambito di diverse proporzioni molari di nitrato e zolfo (N/S) utilizzando rispettivamente $S_2O_3^{2-}$ e NO_3^- come fonte di energia e accettore di elettroni. I risultati hanno rivelato che sia l'FBR che l'MBBR hanno raggiunto tassi di rimozione (RE) di $S_2O_3^{2-}$ superiori al 98% e la rimozione completa di NO_3^- con un rapporto N/S di 0,5. In condizioni di forti limitazioni di nitrato (rapporto N/S di 0,1), il tasso di rimozione di $S_2O_3^{2-}$ nel MBBR (37.8%) era superiore a quello osservato nel FBR (26.1%). Di conseguenza, l'MBBR ha mostrato una migliore resilienza alla limitazione di nitrato rispetto al FBR, poiché il tasso di rimozione di $S_2O_3^{2-}$ è stato ripristinato al 94% entro 1 giorno dopo avere riportato il tasso N/S a 0,5, mentre l'FBR ha impiegato 3 giorni per ottenere l'80% di tasso di rimozione di $S_2O_3^{2-}$. Modelli di rete neurale artificiale sono stati utilizzati con successo per anticipare le prestazioni di FBR e MBBR, ad es. il tasso di rimozione di $S_2O_3^{2-}$ e NO_3^- e la produzione di solfato.

La biomassa SO-NR sviluppata nel MBBR è stata impiegata simultaneamente per trattare H_2S e NO_3^- contenenti flussi di rifiuti in un filtro anossico biotrickling (BTF). Il BTF anossico ha riportato una capacità di eliminazione (EC) di H_2S massima di 19,2 g S m^{-3} h^{-1} (99% RE) rispettivamente a un carico di H_2S in entrata di 20,0 g S m^{-3} h^{-1} (~500 ppm_v) e un rapporto N/S di ~1,7. Poiché alcune acque reflue contenenti NO_3^- possono contenere sostanze organiche, il BTF anossico inoculato con il ceppo *Paracoccus versutus* MAL 1HM19 è stato sviluppato per la rimozione simultanea di flussi di rifiuti contenenti H_2S, NO_3^- e carbonio organico. Dai risultati si è riscontrato che ha ottenuto tassi di rimozione di NO_3^- e acetato di 16,7 g NO_3^--N m^{-3} h^{-1} r 42,0 g di acetato m^{-3} h^{-1} rispettivamente, superiore ai valori osservati nel BTF inoculato con autotrofi (11,1 g NO_3^--N m^{-3} h^{-1} e 10,2 g di acetato m^{-3} h^{-1}). Il BTF anossico è stato fatto agire in diverse condizioni transitorie (es. tassi di portata di vari gas e di gocciolamento, fornitura intermittente di NO_3^- e forti cariche di H_2S) per valutare l'impatto delle variazioni sulle variabili di processo che di solito si verificano nelle applicazioni pratiche. Le diverse condizioni transitorie hanno influenzato significativamente la capacità di eliminazione di H_2S del BTF anossico. Con l'applicazione di forti cariche di H_2S, il tasso di eliminazione di H_2S si è completamente ristabilito quasi del 100% entro 40 h dalla ripresa del normale funzionamento.

In sintesi, l'MBBR si è rivelato più efficace per la rimozione di $S_2O_3^{2-}$ rispetto all'FBR. In base a un tempo di recupero istantaneo dopo aver tollerato le condizioni transitorie, l'MBBR anossico e il BTF anossico si presentano come sistemi di biofilm resilienti e robusti per il trattamento di composti di zolfo ridotti in condizioni autotrofe e mixotrofiche.

Résumé

L'objectif de cette étude a été de développer et étudier des bioréacteurs anoxiques pour l'élimination du soufre des flux de déchets liquides, et d'évaluer l'intégration du processus pour le traitement simultané des flux gazeux contaminés au H_2S et des eaux usées contenant du NO_3^-.

Les expériences relatives à l'oxydation du soufre dans la phase liquide ont été évaluées dans deux bioréacteurs à croissance fixe différents, à savoir un réacteur à lit fluidisé (RLF) et un réacteur filtrant sur lit mobile (RFLM), inoculés par une bactérie ayant la capacité de réduire les nitrates et d'oxyder le soufre (SO-NR). Les bioréacteurs ont été évalués sous différent ratios molaires azote/soufre (N/S) en utilisant le $S_2O_3^{2-}$ et le NO_3^- comme source d'énergie et accepteur d'électrons, respectivement. Les résultats ont révélé que le RLF et le RFLM sont parvenus à des capacités d'extraction (CE) du $S_2O_3^{2-}$ supérieures à 98 %, et à extraire complètement le NO_3^- au ratio N/S de 0,5. En conditions de forte limitation en nitrate (ratio N/S de 0,1), la CEx du $S_2O_3^{2-}$ dans le RFLM (37,8 %) était supérieure à celle observée dans le RLF (26,1 %). En conséquence, le RFLM a montré une meilleure résilience à la limitation en nitrate que le RLF puisque la CEx du $S_2O_3^{2-}$ a été ramenée à 94 % en une journée après restauration du ratio N/S à 0,5, alors que le RLF a pris 3 jours pour obtenir une CEx de 80 % pour le $S_2O_3^{2-}$. Les modèles de réseau neuronal artificiel ont pu être utilisés pour prédire les performances du RLF et du RFLM, à savoir la CE du $S_2O_3^{2-}$ et du NO_3^-ainsi que la production de sulfate.

La biomasse SO-NR développée dans le RFLM a été utilisée pour traiter simultanément les flux de déchets contenant du H_2S et du NO_3^- dans un biofiltre (BF) anoxique. Le BF anoxique a obtenu une capacité d'élimination (CEl) maximale du H_2S de 19,2 g de S m-3 h-1 (CEx) pour un apport de 20,0 g S m^{-3} h^{-1} (~500 ppm_v) en H_2S et un ratio N/S d'environ 1,7, respectivement. Comme certaines eaux usées contenant du NO_3^-peuvent contenir des produits organiques, le RLF anoxique inoculé avec du *Paracoccus versatus* souche MAL 1HM19 a été développé pour l'extraction simultanée du H_2S, du NO_3^- et du carbone organique contenus dans les flux de déchets. Les résultats ont montré des taux d'extraction respectifs de 16,7 g NO_3^--N m^{-3} h^{-1} et 42,0 g d'acétate m^{-3} h^{-1}, ce qui est supérieur aux valeurs observées dans le BF inoculé avec des autotrophes (11,1 g NO_3^--N m^{-3} h^{-1} et 10,2 g d'acétate m^{-3} h^{-1}). Le BF anoxique a été opéré sous différentes conditions transitoires (i.e. gaz divers et plusieurs vitesses de flux de ruissellement liquides, un apport intermittent en NO_3^- et apports élevés en H_2S) afin d'évaluer l'impact des modifications sur les variables du processus qui se produisent généralement dans les applications pratiques. Les différentes conditions transitoires ont significativement affecté la CEl du H_2S dans le BF anoxique. En appliquant des apports élevés en H_2S, la CEx du H_2S a été presque totalement rétabli à 100 % dans les 40 heures suivant la reprise de l'opération normale.

En résumé, le RFLM s'est montré plus efficace que le RLF pour l'extraction du $S_2O_3^2$. D'après un moment de récupération instantanée après tolérance des conditions transitoires, le RFLM anoxique et le RLF anoxique s'avèrent être de résilients et robustes systèmes de biofilms pour le traitement des composés soufrés réduits en conditions autotrophes et mixotrophes.

Samenvatting

Het doel van dit werk was om anoxische bioreactoren te ontwikkelen en bestuderen voor het verwijderen van sulfide uit vloeibare afvalstromen en het evalueren van procesintegratie voor de gelijktijdige behandeling van gasstromen vervuild met H_2S en afvalwater met NO_3^-.

De experimenten gerelateerd aan sulfide-oxidatie in de vloeibare fase werden geëvalueerd in twee verschillende bioreactoren, d.w.z. een wervelbedreactor (FBR) en een bewegend bed biofilmreactor (MBBR), geïnoculeerd met bacteriën die zwavel oxideren en nitraat reduceren (SO-NR). De bioreactoren werden geëvalueerd onder verschillende stikstof-tot-zwavel (N/S) molaire verhoudingen waarbij $S_2O_3^{2-}$ en NO_3^-, respectievelijk, als een energiebron en elektronenacceptor werden gebruikt. De resultaten toonden aan dat zowel de FBR als de MMBR een verwijderingsrendement (RE, 'Removal efficiency') van meer dan 98% behaalden voor $S_2O_3^{2-}$ en NO_3^- helemaal verwijderden bij een N/S-verhouding van 0,5. Bij een zware nitraatbeperking (N/S-verhouding van 0,1), was de $S_2O_3^{2-}$ RE in de MBBR (37,8%) hoger dan dat van de FBR (26,1%). Het gevolg was dat de MBBR een betere weerstand had tegen de nitraatlimitatie dan de FBR aangezien de $S_2O_3^{2-}$ RE binnen 1 dag tot 94% werd hersteld na het herstellen van de N/S-verhouding tot 0,5 terwijl de FBR 3 dagen nodig had om tot 80% van de $S_2O_3^{2-}$ RE te komen. Kunstmatige neurale netwerkmodellen werden met succes gebruikt om de prestaties van de FBR en MBBR te voorspellen, d.w.z. de $S_2O_3^{2-}$ en NO_{3-} RE en de productie van sulfaat.

De SO-NR biomassa die in de MBBR ontwikkelde, werd gebruikt om tegelijkertijd afvalstromen waarin H_2S en NO_3^- zat te behandelen in een anoxische biowasfilter (BTF, 'Biotrickling Filter'). De anoxische BTF behaalde een maximum H_2S eliminatiecapaciteit (EC) van 19,2 g S m^{-3} h^{-1} (99% RE) bij, respectievelijk, een inlaat H_2S belasting van 20,0 g S m^{-3} h^{-1} (~500 ppm_v) en een N/S-verhouding van ~1,7. Aangezien afvalwater met NO_3^- ook organische stoffen kan bevatten, werd de anoxische BTF geïnoculeerd met *Paracoccus versutus* stam MAL 1HM19 voor het tegelijkertijd verwijderen van H_2S, NO_3^- uit afvalstromen met organische koolstof. De resultaten toonden aan dat de afnamesnelheden van 16, 7 g NO_3^--N m^{-3} h^{-1} en 42,0 g acetaat m^{-3} h^{-1} werden bereikt, iets dat hoger was dan de waarden waargenomen in de BTF geïnoculeerd met autotrofe bacteriën (respectievelijk 11,1 g NO_3^--N m^{-3} h^{-1} en 10.2 g acetaat m^{-3} h^{-1}). De anoxische BTF blootgesteld enkele kortstondige condities (d.w.z. gevarieerde gas en recirculatie vloeistofstroomsnelheden, periodieke NO_3^- aanvoer en H_2S schokbelastingen) om de impact van veranderingen op de procesvariabelen te meten die gewoonlijk plaatsvinden bij praktische toepassingen. De verschillende kortstondige condities hadden een significante invloed op de H_2S EC van de anoxische BTF. Na de H_2S-schokladingen herstelde de H_2S RE bijna helemaal tot 100% binnen 40 uren na het begin van terug normaal functioneren.

Samenvattend, toonde deze studie aan dat de MBBR effectiever was bij het verwijderen van $S_2O_3^{2-}$ dan de FBR. De anoxische MBBR en de anoxische BTF zijn robuuste biofilmsystemen voor het behandelen van afvalstromen met een hoog zwavelgehalte onder autotrofe en mixotrofe condities.

Preface

This thesis is based on the experimental work performed at Tampere University of Technology (TUT), Finland and during the research at IHE Delft, The Netherlands. This research was supported by the Marie Skłodowska-Curie European Joint Doctorate (EJD) Advanced Biological Waste-To-Energy Technologies (ABWET) funded by the European Union's Horizon 2020 research and innovation programme grant agreement no. 643071.

I would like to thank my supervisor, Prof. Piet Lens, for his guidance during my research journey and for the valuable comments on my manuscripts. I am profoundly grateful to thank my instructors, Asst. Prof. Aino-Maija Lakaniemi, Dr. Eldon Rene and Dr. Francesco Di Capua who encouraged me and gave critical comments and suggestions on my research works.

I sincerely thank the lab staff and technicians for kindly providing facilities in laboratory, particularly Antti Nuottajärvi and Tarja Ylijoki- Kaiste from TUT and lab staffs from IHE Delft, The Netherlands. I am grateful to thank all my colleagues from ABWET, TUT, ETe-CoS^3, and staff in TUT for creating very nice working environment, the grateful support and discussion during work and free time. I would like to give special thanks to my families and all my friends who always cheer me up and be good listeners about my research during the entire PhD journey.

Tampere, 2019

Ramita Khanongnuch

Contents

Abbreviations

ANN	Artificial neural networks
BTF	Biotrickling filter
COD	Chemical oxygen demand
CSTR	Continuous stirred tank reactor
DGGE	Denaturing gradient gel electrophoresis
EBRT	Empty bed residence time
EC	Elimination capacity
FBR	Fluidized bed reactor
HRT	Hydraulic retention time
MBBR	Moving bed biofilm reactor
PCR	Polymerase chain reaction
RE	Removal efficiency
RTD	Residence time distribution
SS	Suspended solid
SO-NR	Sulfur-oxidizing nitrate-reducing
VSS	Volatile suspended solid

List of Publications

I. Khanongnuch, R., Di Capua, F., Lakaniemi, A.-M., Rene, E.R., Lens, P.N.L. 2018. Effect of N/S ratio on anoxic thiosulfate oxidation in a fluidized bed reactor: experimental and artificial neural network model analysis, *Process Biochem*., 68, 171–181.

II. Khanongnuch, R., Di Capua, F., Lakaniemi, A.-M., Rene, E.R., Lens, P.N.L. 2019. Long-term performance evaluation of an anoxic sulfur oxidizing moving bed biofilm reactor under nitrate limited conditions, *Environ. Sci.: Water Res. Technol.*, In Press.

III. Khanongnuch, R., Di Capua, F., Lakaniemi, A.-M., Rene, E.R., Lens, P.N.L. 2019. H_2S removal and microbial community composition in an anoxic biotrickling filter under autotrophic and mixotrophic conditions, *J. Hazard. Mater.*, 367, 397-406.

IV. Khanongnuch, R., Di Capua, F., Lakaniemi, A.-M., Rene, E.R., Lens, P.N.L. 2019. Transient-state operation of an anoxic biotrickling filter for H_2S removal. *J. Hazard. Mater.*, In Press.

V. Watsuntorn, W., Khanongnuch, R., Chulalaksananukul, W., Rene, E.R., Lens, P.N.L. 2019. Anoxic biotrickling filter inoculated with pure culture of *Paracoccus* strain MAL 1HM19. *Submitted for publication*.

Author's Contribution

Papers I-IV: Ramita Khanongnuch performed the experiments and all the related analysis, wrote the manuscript and is the corresponding author. Francesco Di Capua, Aino-Maija Lakaniemi, Eldon Rene and Piet Lens participated in planning the experiments, helped in data interpretation and thoroughly revised the manuscript.

Paper V: Wannapawn Watsuntorn performed the experiments and the related analysis, wrote the manuscript. Ramita Khanongnuch helped in data interpretation, performed the microbial community analysis and developed the neural network-based model. Warawut Chulalaksananukul, Eldon Rene and Piet Lens participated in planning the experiments, helped in data interpretation and thoroughly revised the manuscript.

Chapter 1 Introduction

1.1 Background

Sulfur compounds utilized and released during anthropogenic processes cause an imbalance to the sulfur cycle in nature and lead to environmental problems, such as acid rain, odor problems, corrosion and sulfide toxicity (Pokorna and Zabranska, 2015). The sulfur pollutants released from anthropogenic sources include hydrogen sulfide (H_2S), thiosulfate ($S_2O_3^{2-}$), sulfite (SO_3^{2-}) and sulfate (SO_4^{2-}). Reduced sulfur compounds, H_2S and its ionic forms (HS^- and S^{2-}), are commonly found in both liquid and gaseous streams generated in the petrochemical industry and anaerobic digesters (Mattiusi et al., 2015; Pokorna and Zabranska, 2015). In addition, some industrial wastewaters, e.g. from tannery effluents as well as pulp and paper production wastewaters, generally contain elevated concentrations of sulfur in the form of $S_2O_3^{2-}$, $S_nO_6^{2-}$, SO_3^{2-} and SO_4^{2-} which are inevitably reduced to H_2S under anaerobic conditions (Pokorna and Zabranska, 2015).

H_2S causes odor nuisance at concentrations as low as 0.025 ppm_v and represents an immediate hazard to human health at concentrations exceeding 600 ppm_v (Yalamanchili and Smith, 2008). H_2S levels in contaminated gas streams, i.e. flue gas and biogas, must be significantly reduced to prevent damage to equipment and gas distribution systems. For instance, the H_2S concentrations in biogas must be less than 1000 ppm_v for direct combustion of biogas, whereas for the application as a fuel in internal combustion engines or compressed natural gas production (CNG), the H_2S concentration must be less than 100 ppm_v and 16 ppm_v, respectively (Khanal and Li, 2017). Additionally, the presence of dissolved sulfide in the liquid phase can result in the corrosion of water transport systems and accumulation of metal precipitates in the sludge (Krayzelova et al., 2015).

1.2 Problem statement

The removal of sulfides from both liquid and gaseous streams can be accomplished using various physico-chemical methods, including scrubbing, adsorption, absorption and chemical precipitation (Muñoz et al., 2015; Nielsen et al., 2005). However, these technologies have high operating costs as well as negative environmental impacts due to the generation of chemical wastes (Abatzoglou and Boivin, 2009; Muñoz et al., 2015). Biological processes for sulfide removal are considered to be cleaner and less expensive alternatives compared to conventional technologies using chemicals (Cano et al., 2018). Aerobic and anoxic bioreactors have been operated for sulfide removal from both liquid and gas streams (Almenglo et al., 2016b; Bayrakdar et al., 2016; Can-Dogan et al., 2010; Mahmood et al., 2007). Anoxic bioreactors are more practically applicable than the aerobic ones in terms of ease of use and operational costs (Cano et al., 2018; Fernández et al., 2014), because use of oxygen as an electron acceptor can cause formation of polysulfides and mass transfer limitations of oxygen to the microorganisms due to low water solubility of oxygen (Krishnakumar et al., 2005). In aerobic biotrickling filters (BTF) treating H_2S-contaminated gas streams, insufficient oxygen supply can result in S^0 precipitation and bioreactor clogging, subsequently leading to reduced mass transfer and decreased bioreactor performance (Khoshnevisan et al., 2017; Rodriguez et al., 2014). In aerobic bioreactors for biogas cleaning, it is also necessary to carefully control the oxygen to methane ratio in order to avoid explosive mixtures of methane and oxygen (Fernández et al., 2013).

Some wastewaters, such as petroleum refinery wastewaters and tannery industry effluents, contain both nitrogen and reduced sulfur compounds. These kind of nitrate (NO_3^-) containing wastewaters and/or nitrified wastewaters can be treated via denitrification coupled to sulfur oxidation (Lofrano et al., 2013; Reyes-Avila et al., 2004). NO_3^- can be introduced externally when the concentrations of NO_3^- and nitrite (NO_2^-) in the influent wastewater are insufficient to sustain oxidation of all reduced sulfur compounds present in the waste stream (Yang et al., 2005). Hence, a continuous system for treating simultaneously a nitrified/NO_3^--contaminated wastewater and sulfide-contaminated wastewater/waste gas could be a sustainable technology, if both types of waste streams are available in sufficient amount at the same location (Cano et al., 2018).

The nitrogen to sulfur (N/S) ratio is one of the key operational factors for anoxic sulfide-oxidizing bioreactors, since it affects the metabolism of the sulfur-oxidizing bacteria and the ratio of the end-products (S^0 and SO_4^{2-}) formed during sulfide oxidation (Bayrakdar et al., 2016; Dolejs et al., 2015; Moraes et al., 2012). However, previous studies have not focused on the long-term performance and microbial community evolution under different N/S ratios. Some nitrified/NO_3^- contaminated wastewaters such as municipal wastewater, and effluents from systems treating swine wastewaters (Hunt et al., 2009)

or effluents from faecal sludge treatment (Forbis-Stokes et al., 2018) can also contain organic carbon. Therefore, the effect of organic carbon on the performance of an autotrophic bioreactor and activity of autotrophic microorganisms needs also to be investigated.

Among the different bioreactor configurations, biofilm systems are an attractive option, because of their ability to retain high biomass levels in the system. This results in less problems related to biomass wash-out and enables higher solid retention times (SRT) compared to reactor types relying solely on the activity of suspended microorganisms such as continuous stirred-tank reactors (CSTR) (Di Capua et al., 2015; Papirio et al., 2013). Hence, the development of appropriate biofilm systems containing sulfur-oxidizing nitrate-reducing (SO-NR) bacteria are promising approaches for the removal of reduced sulfur compounds (RSCs) from both liquid and gas streams under anoxic conditions.

During practical bioreactor applications, unexpected or transient conditions such as variable pollutant concentrations, transient emission patterns, and intermittent inlet gas flow rates are regularly encountered and can affect microbial activity and bioreactor stability (Rodriguez et al., 2014; San-Valero et al., 2017). Recent studies have investigated the impact of transient conditions, i.e. pollutant shock loads and starvation periods, on the performance of aerobic BTFs removing H_2S and other gaseous pollutants (López et al., 2017; Mohammad et al., 2017; Rene et al., 2010). In addition to the steady-state operation of anoxic bioreactors, the response and resilience of SO-NR bacteria in the anoxic bioreactors to transient conditions require further investigations such as the bioreactor operation under NO_3^- limiting conditions, H_2S shock loads as well as intermittent gas and liquid waste flow rates. Furthermore, collecting data of bioreactor performance under transient-state operation is useful for preparing operational strategy for further operations.

Modelling of the performance of biological systems can enhance process control to optimize operational conditions. Several mathematical models developed for wastewater and waste-gas treatment system required large data on sensitive parameters, e.g. microbial growth rate, target compound consumption rate, mass transfer and diffusion coefficients (Spigno and De Faveri, 2005). Recently, no model is available for predicting the dynamic performance of the biological treatment systems due to the process complexity and microbial activity (Rene et al., 2011). A neural network-based model is one of the most efficient black-box modelling tools for predicting and describing the non-linear performance of biological processes. Furthermore, this model has been successfully implemented for forecasting effluent quality and reducing energy consumption in full-scale wastewater treatment plants (Han et al., 2018; Lee et al., 2011).

1.3 Research objectives

The main objective of this thesis was to develop anoxic bioreactor configurations for treating inorganic sulfur-containing waste streams using NO_3^- as an electron acceptor. The specific objectives were the following:

1) To evaluate the performance of different bioreactor configurations for $S_2O_3^{2-}$ removal from the liquid waste streams using NO_3^- as an electron acceptor:
   a) by comparing the removal performance of a fluidized bed reactor (FBR) and a moving bed biofilm reactor (MBBR) operated under different N/S molar ratios
   b) by developing a neural network-based model for prediction and optimization of the bioreactor performance considering sulfur (i.e. $S_2O_3^{2-}$) and NO_3^- removal efficiencies and SO_4^{2-} production
2) To optimize the performance of an anoxic biotrickling filter (BTF) for H_2S removal from gas streams:
   a) by evaluating the removal performance of the BTF under autotrophic and mixotrophic conditions
   b) by developing the anoxic BTF for the simultaneous removal of H_2S-contaminated gas streams and wastewater containing NO_3^- and carbon pollutants using the inoculation of specific bacteria
   c) by evaluating the response of the BTF to transient-state conditions and suggesting an appropriate process control strategy

1.4 Structure of the thesis

This thesis comprises of eight chapters. The outline of the contents of the individual chapters (Figure 1.1) is described below:

Chapter 1 gives a general overview of this thesis including the background, problem statement, research objectives and thesis structure. **Chapter 2** reviews the existing knowledge on physical and chemical and biological technologies for biogas cleaning and upgrading. The chapter provides basic information on the techniques commercially used and/or studied for the removal of different contaminants present in biogas, particularly H_2S and CO_2. As technologies for biological removal of H_2S have been widely used in full-scale applications, the feasibility of simultaneous removal of H_2S and other contaminants are also highlighted.

Chapters 3 and 4 report the performance of two different bioreactors for $S_2O_3^{2-}$ removal from liquid streams including the evaluation of their biofilm activity, microbial community

composition and neural network-based models to predict and optimize the reactor performance with the focus on removal efficiencies of $S_2O_3^{2-}$ and NO_3^-. **Chapter 3** focuses on the SO-NR process in an anoxic FBR under different N/S ratios using $S_2O_3^{2-}$ and NO_3^- as a sulfur source and electron acceptor, respectively. Kinetic parameters of the FBR biomass are also evaluated based on batch activity tests. **Chapter 4** focuses on an anoxic MBBR operated under low N/S ratios (nitrate-limiting conditions) using $S_2O_3^{2-}$ as a sulfur source. This chapter also evaluates the specific $S_2O_3^{2-}$ and NO_3^- removal rates of biomass obtained from different experimental phases from the MBBR in batch tests.

Chapters 5, 6 and 7 focus on the performance of an anoxic BTF packed with polyurethane foam (PUF) cubes for H_2S removal from gas phase using NO_3^- as electron acceptor. In **Chapter 5,** the performance of the laboratory-scale anoxic BTF for H_2S removal was investigated using the biomass obtained from the anoxic MBBR used in **Chapter 4**. This chapter establishes the H_2S removal efficiency and microbial community composition under both autotrophic and heterotrophic conditions. In **Chapter 6,** a laboratory-scale anoxic BTF was inoculated with a pure culture of mixotrophic *Paracoccus* strain MAL 1HM19 for H_2S removal via mixotrophic denitrification. This chapter reveals the feasibility of the simultaneous removal of H_2S-contaminated gas stream, NO_3^- and organic carbon containing wastewater. **Chapter 7** focuses on the response of the anoxic BTF to short-term transient-state conditions, including intermittent influent H_2S and NO_3^- flow rates, H_2S shock loads, the wet-dry bed operations as well as the bioaugmentation of the existing anoxic BTF used in **Chapters 5 and 7** with *Paracoccus* strain MAL 1HM19.

Chapter 8 summarizes the knowledge gained from this dissertation and discusses the practical implications of this work. The recommendations and future perspectives are also provided in this chapter.

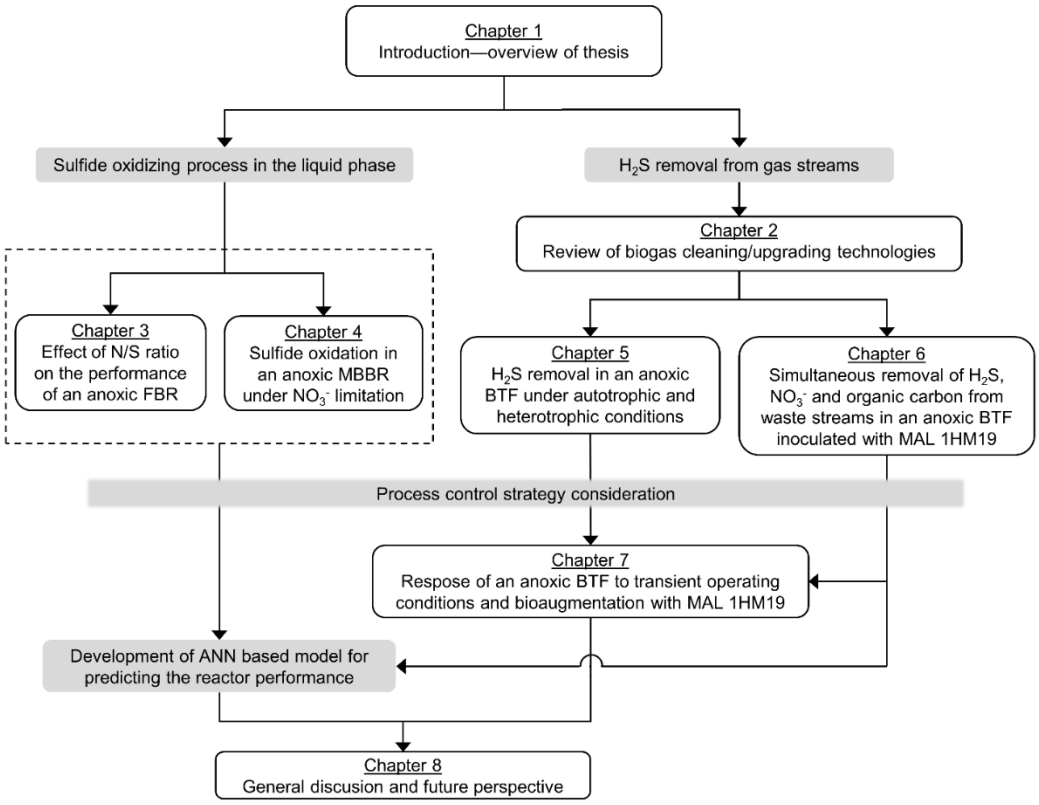

Figure 1.1. Overview of this PhD thesis.

1.5 References

Abatzoglou, N., Boivin, S., 2009. A review of biogas purification processes. Biofuels, Bioprod. Biorefining 3, 42–71.

Almenglo, F., Ramírez, M., Gómez, J.M., Cantero, D., 2016. Operational conditions for start-up and nitrate-feeding in an anoxic biotrickling filtration process at pilot scale. Chem. Eng. J. 285, 83–91.

Bayrakdar, A., Tilahun, E., Calli, B., 2016. Biogas desulfurization using autotrophic denitrification process. Appl. Microbiol. Biotechnol. 100, 939–948.

Can-Dogan, E., Turker, M., Dagasan, L., Arslan, A., 2010. Sulfide removal from industrial wastewaters by lithotrophic denitrification using nitrate as an electron acceptor. Water Sci. Technol. 62, 2286–2293.

Cano, P.I., Colón, J., Ramírez, M., Lafuente, J., Gabriel, D., Cantero, D., 2018. Life cycle assessment of different physical-chemical and biological technologies for biogas desulfurization in sewage treatment plants. J. Clean. Prod. 181, 663–674.

Di Capua, F., Papirio, S., Lens, P.N.L., Esposito, G., 2015. Chemolithotrophic denitrification in biofilm reactors. Chem. Eng. J. 280, 643–657.

Dolejs, P., Paclík, L., Maca, J., Pokorna, D., Zabranska, J., Bartacek, J., 2015. Effect of

S/N ratio on sulfide removal by autotrophic denitrification. Appl. Microbiol. Biotechnol. 99, 2383–2392.

Fernández, M., Ramírez, M., Gómez, J.M., Cantero, D., 2014. Biogas biodesulfurization in an anoxic biotrickling filter packed with open-pore polyurethane foam. J. Hazard. Mater. 264, 529–535.

Fernández, M., Ramírez, M., Pérez, R.M., Gómez, J.M., Cantero, D., 2013. Hydrogen sulphide removal from biogas by an anoxic biotrickling filter packed with Pall rings. Chem. Eng. J. 225, 456–463.

Forbis-Stokes, A.A., Rocha-Melogno, L., Deshusses, M.A., 2018. Nitrifying trickling filters and denitrifying bioreactors for nitrogen management of high-strength anaerobic digestion effluent. Chemosphere 204, 119–129.

Han, H.G., Zhang, L., Liu, H.X., Qiao, J.F., 2018. Multiobjective design of fuzzy neural network controller for wastewater treatment process. Appl. Soft Comput. J. 67, 467–478.

Hunt, P.G., Stone, K.C., Matheny, T.A., Poach, M.E., Vanotti, M.B., Ducey, T.F., 2009. Denitrification of nitrified and non-nitrified swine lagoon wastewater in the suspended sludge layer of treatment wetlands. Ecol. Eng. 35, 1514–1522.

Khanal, S.K., Li, Y., 2017. Biogas Production and Applications, in: Li, Y., Khanal, S.K. (Eds.), Bioenergy: Principles and Applications. John Wiley & Sons, Inc., New York. pp. 338–360.

Khoshnevisan, B., Tsapekos, P., Alfaro, N., Díaz, I., Fdz-Polanco, M., Rafiee, S., Angelidaki, I., 2017. A review on prospects and challenges of biological H_2S removal from biogas with focus on biotrickling filtration and microaerobic desulfurization. Biofuel Res. J. 4, 741–750.

Krayzelova, L., Bartacek, J., Díaz, I., Jeison, D., Volcke, E.I.P., Jenicek, P., 2015. Microaeration for hydrogen sulfide removal during anaerobic treatment: a review. Rev. Environ. Sci. Biotechnol. 14, 703–735.

Krishnakumar, B., Majumdar, S., Manilal, V.B., Haridas, A., 2005. Treatment of sulphide containing wastewater with sulphur recovery in a novel reverse fluidized loop reactor (RFLR). Water Res. 39, 639–647.

Lofrano, G., Meriç, S., Zengin, G.E., Orhon, D., 2013. Chemical and biological treatment technologies for leather tannery chemicals and wastewaters: A review. Sci. Total Environ. 461–462, 265–281.

López, M.E., Rene, E.R., Boger, Z., Veiga, M.C., Kennes, C., 2017. Modelling the removal of volatile pollutants under transient conditions in a two-stage bioreactor using artificial neural networks. J. Hazard. Mater. 324, 100–109.

Mahmood, Q., Zheng, P., Cai, J., Wu, D., Hu, B., Li, J., 2007. Anoxic sulfide biooxidation using nitrite as electron acceptor. J. Hazard. Mater. 147, 249–256.

Mattiusi, E.M., Kaminari, N.M.S., Ponte, M.J.J.S., Ponte, H.A., 2015. Behavior analysis of a porous bed electrochemical reactor the treatment of petrochemical industry wastewater contaminated by hydrogen sulfide (H_2S). Chem. Eng. J. 275, 305–314.

Mohammad, B.T., Rene, E.R., Veiga, M.C., Kennes, C., 2017. Performance of a thermophilic gas-phase biofilter treating high BTEX loads under steady- and transient-state operation. Int. Biodeterior. Biodegrad. 119, 289–298.

Moraes, B.S., Souza, T.S.O., Foresti, E., 2012. Effect of sulfide concentration on autotrophic denitrification from nitrate and nitrite in vertical fixed-bed reactors. Process Biochem. 47, 1395–1401.

Muñoz, R., Meier, L., Diaz, I., Jeison, D., 2015. A review on the state-of-the-art of physical/chemical and biological technologies for biogas upgrading. Rev. Environ. Sci. Biotechnol. 14, 727–759.

Nielsen, A.H., Lens, P., Vollertsen, J., Hvitved-Jacobsen, T., 2005. Sulfide-iron interactions in domestic wastewater from a gravity sewer. Water Res. 39, 2747–2755.

Papirio, S., Villa-Gomez, D.K., Esposito, G., Pirozzi, F., Lens, P.N.L., 2013. Acid mine drainage treatment in fluidized-bed bioreactors by sulfate-reducing bacteria: a critical review. Crit. Rev. Environ. Sci. Technol. 43, 2545–2580.

Pokorna, D., Zabranska, J., 2015. Sulfur-oxidizing bacteria in environmental technology. Biotechnol. Adv. 33, 1246–1259.

Lee, J.-W., Suh, C., Hong, Y.-S.T., Shin, H.-S., 2011. Sequential modelling of a full-scale wastewater treatment plant using an artificial neural network. Bioprocess Biosyst. Eng. 34, 963–973.

Rene, E.R., López, M.E., Veiga, M.C., Kennes, C., 2011. Neural network models for biological waste-gas treatment systems. N. Biotechnol. 29, 56–73.

Rene, E.R., López, M.E., Veiga, M.C., Kennes, C., 2010. Steady- and transient-state operation of a two-stage bioreactor for the treatment of a gaseous mixture of hydrogen sulphide, methanol and α-pinene. J. Chem. Technol. Biotechnol. 85, 336–348.

Reyes-Avila, J., Razo-Flores, E., Gomez, J., 2004. Simultaneous biological removal of nitrogen, carbon and sulfur by denitrification. Water Res. 38, 3313–3321.

Rodriguez, G., Dorado, A.D., Fortuny, M., Gabriel, D., Gamisans, X., 2014. Biotrickling filters for biogas sweetening: oxygen transfer improvement for a reliable operation. Process Saf. Environ. Prot. 92, 261–268.

San-Valero, P., Gabaldón, C., Penya-roja, J.M., Quijano, G., 2017. Enhanced styrene removal in a two-phase partitioning bioreactor operated as a biotrickling filter: towards full-scale applications. Chem. Eng. J. 309, 588–595.

Spigno, G., De Faveri, D.M., 2005. Modeling of a vapor-phase fungi bioreactor for the abatement of hexane: Fluid dynamics and kinetic aspects. Biotechnol. Bioeng. 89, 319–328.

Yalamanchili, C., Smith, M.D., 2008. Acute hydrogen sulfide toxicity due to sewer gas exposure. Am. J. Emerg. Med. 26, 7–9.

Yang, W., Vollertsen, J., Hvitved-Jacobsen, T., 2005. Anoxic sulfide oxidation in wastewater of sewer networks. Water Sci. Technol. 52, 191–199.

Chapter 2 Biogas cleaning and upgrading technologies

2.1 Introduction

The increased consumption of fossil fuels results in emission of greenhouse gases (GHGs), such as carbon dioxide (CO_2). It has been estimated that about 90% of the CO_2 emissions is generated from fossil fuel combustion (IEA, 2015). Furthermore, the reliability of the energy supply is a challenge due to limitations of natural resources, e.g. fossil fuels, which can cause energy source deficiency in the future. In this context, alternative energy production from bioresources has gained interest and it is widely applied at industrial scales to achieve sustainable and more environmentally friendly energy sources.

Bioenergy, particularly biogas produced from anaerobic digestion of organic wastes, is a promising alternative energy source (Guo et al., 2015; Yentekakis and Goula, 2017). Anaerobic digestion is a waste stabilizing process that transforms organic matter to a gaseous fraction, i.e. biogas, and a solid residue, i.e. an anaerobic digestate. The latter contains nutrients which are easily available to plants and can therefore be used as a fertilizer (Daniel-Gromke et al., 2018; Surendra et al., 2015). Biogas mainly consists of methane (CH_4) and CO_2, but also other gases such as hydrogen sulfide (H_2S), ammonia (NH_3), water vapor, siloxanes and halogenated hydrocarbons (Angelidaki et al., 2018; Barbusinski et al., 2017). The composition of biogas varies due to differences in biodegradable compounds and their quantities present in organic wastes, such as agricultural waste, sewage sludge, landfill and industrial wastes/wastewaters. The biogas contaminants can cause corrosion and failure of the process equipment and pipeline systems and have negative impacts to public health and environment (Sun et al., 2015). In addition, the presence of such impurities can reduce the final CH_4 content in biogas, which in turn reduces its calorific value during combustion. Thus, biogas is required to be cleaned up or even upgraded for economic considerations and from an environmental

perspective. After biogas upgrading, high quality biomethane (CH_4-rich biogas) can be obtained and used as a substitute for natural gas (Guo et al., 2015).

Biogas cleaning technologies refer to the removal of biogas contaminants, e.g. H_2S, NH_3, water vapor and siloxanes, to achieve the criteria for syngas production, direct combustion or combined heat and power (CHP) generation. Besides, the use of biogas for natural gas grid injection or production of added-value products requires technologies for biogas upgrading, particularly the removal of CO_2, to obtain a purified biogas with high quality as a natural gas (Figure 2.1).

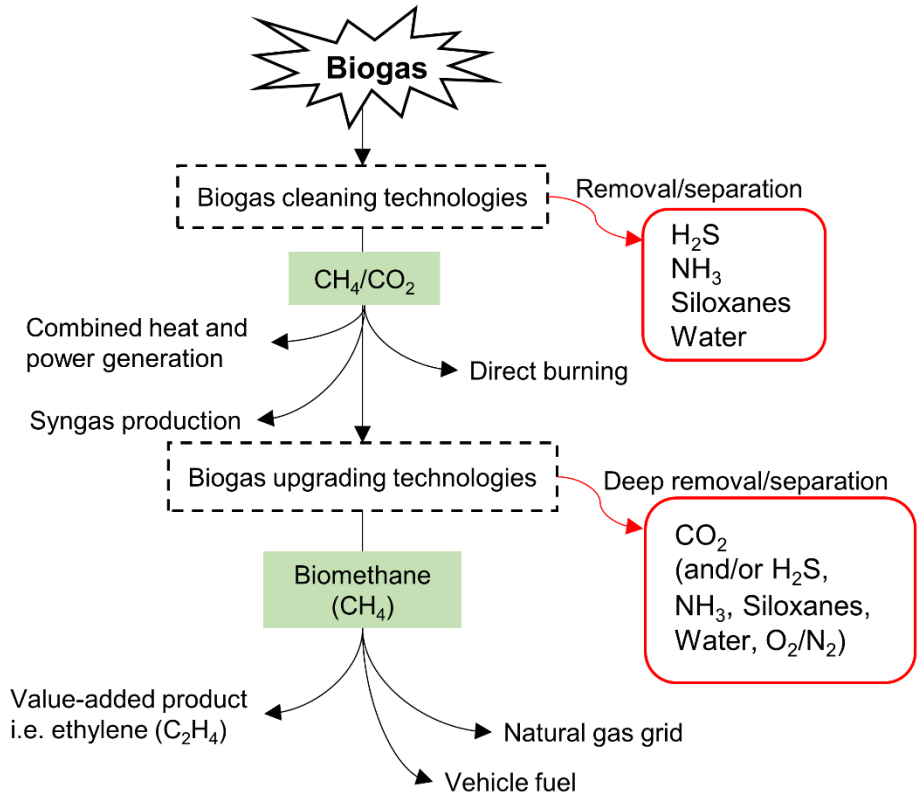

Figure 2.1. Possible pathways of various biogas applications as well as options for removal of contaminants from biogas.

2.2 Biogas production and utilization

Biogas is produced via anaerobic digestion of organic matter, such as that present in municipal wastes, agricultural waste as well as from landfills. Biogas technology has been successfully implemented in large-scale applications, e.g. agricultural or food processing industries (Prasertsan and Sajjakulnukit, 2006) as well at a small scale used in livestock farms or households (Lijó et al. 2017; Rajendran et al., 2012). Biogas technol-

ogy is, thus, a potential technology for waste management which also allows the production of renewable energy and value-added chemicals, e.g. methanol and ethylene (Yentekakis and Goula, 2017). In Europe, the number of biogas plants has increased during 2010-2014 (Achinas et al., 2017). Several countries have applied biomethane as a fuel source for vehicles, particularly in European countries like Germany and Sweden (IEA, 2017; Sorda et al., 2013). The potential use of biogas for renewable transport fuels in Sweden has been estimated to meet the vehicle gas demand in Stockholm County by 2020 and it is expected to increase by 2030 (Lönnqvist et al., 2015).

Biogas produced from anaerobic digestion contains approximately 50-75% CH_4, 25-50% CO_2 and <5% other compounds including H_2S, NH_3, siloxanes, oxygen (O_2), nitrogen (N_2) and halogenated hydrocarbons (Surendra et al., 2014). However, the content of CH_4 in biogas varies depending on the organic substrate used (Table 2.1). CH_4 is a valuable renewable energy source which has a lower calorific value (LCV) of 36 MJ m^{-3} at standard temperature and pressure (STP), while the LCV of raw biogas is approximately 20 MJ m^{-3} (Angelidaki et al., 2018). Hence, biogas should contain as high amounts of CH_4 as possible to obtain the high quality of biomethane to substitute natural gas. Other compounds present in biogas are considered as pollutants and need to be removed from the biogas stream, because they reduce the calorific value and limit the flammability of biogas as well as cause corrosion problems (Table 2.1).

2.3 Biogas upgrading technologies (CO_2 removal)

Different techniques for biogas cleaning and upgrading are available and the application of each technique is based on the purpose of the use of biogas. The use of biogas for electricity or heat generation requires the removal of corrosive contaminants, e.g. H_2S, NH_3 and moisture, while the transformation of biogas to biomethane requires the removal of CO_2 and a purity of CH_4 greater than 95%. The techniques for CO_2 removal available at the commercial scale are mostly physical/chemical technologies which have been conventionally used for several decades due to their high reliability and commercial availability (Table 2.2). Some amounts of other contaminants (e.g. H_2S and N_2/O_2) can be simultaneously removed with CO_2. According to IEA (2017), the technologies used in the market include water scrubbers (30%), membranes (25%), chemical scrubbers (18%), pressure swing adsorption (PSA) (14%), organic physical scrubbers (4%), cryogenic separation (2%) and other techniques (7%). Biological technologies for CO_2 removal are still limited at the commercial scale, but are widely investigated at laboratory and pilot scales, i.e. photobioreactors and biogas upgrading processes based on hydrogenotrophic methanogens (Angelidaki et al., 2018).

Table 2.1. Composition of natural gas and biogas produced from different sources (Rasi, 2007; Sun et al., 2015; Yentekakis et al. 2017).

Compounds	Natural gas	Biogas source			Negative effect of biogas contaminants
		Landfill gas	Anaerobic digestion at WWTP	Agricultural wastes	
CH_4 (%)	85-92	35-65	60-70	55-75	-
CO_2 (%)	0.2-1.5	25-40	30-40	35-40	• Decrease in heating value
H_2S (ppm_v)	1-6	20-500	0-34000	30-7200	• Odor • Corrosion in equipment and gas transportation systems • Immediate hazard to human health at concentrations >100 ppm_v • SO_x emission during combustion
NH_3 (ppm_v)	-	<5	<100	70-150	• NO_x emission during combustion
N_2 and O_2 (%)	<0.5	15	0-8	1-2	• Decrease in heating value
Siloxanes (mg m^{-3})	-	7-24	n.a.	n.a.	• Corrosion of equipment and gas transportation systems

Note: WWTP = Wastewater treatment plant; n.a. = data not available

Table 2.2. Physico-chemical technologies available at the industrial scale for biogas upgrading (Bauer et al., 2013; Hoyer et al., 2016; Muñoz et al., 2015; Wilken et al., 2017).

	Pressure swing adsorption	Water scrubbing	Organic solvent scrubbing	Chemical Scrubbing	Membrane separation	Cryogenic technique
Main pollutants removed	CO_2	CO_2 or H_2S	CO_2	CO_2 or H_2S	CO_2	CO_2
Co-contaminants removed	N_2/O_2, halogenates, siloxane	H_2S	H_2S, NH_3	H_2S <300 ppm_v	H_2S, N_2/O_2	H_2S, N_2/O_2
Mechanism	Physical adsorption	Physical absorption	Physical absorption	Chemical absorption	Physical separation/liquid absorption	Physical separation
Chemical/Material required for the reaction	Activated carbon, zeolites	Water	Glycol	Amines	Hollow fiber,	Not required
Operation pressure (bar)	3-10	4-10	4-8	Atmospheric		80
Required temperature (°C)	ambient	ambient	40-80	100-180	ambient	low to -150
Cost (€ Nm^{-3} h^{-1})	1000-3000	n.a.	n.a.	1500-3500	1500- 6000	n.a.
Power consumption (KWh Nm^{-3})	0.20-0.30	0.25-0.30	0.20-0.30	0.06-0.17	n.a	n.a.
CH_4 losses (%)	1.5-2.5	0.5-2	1-4	<0.5	0.5	1.8
Waste product of the process	CO_2	Polluted water	Solvent	Solvent	CO_2	CO_2
Example of well-known commercial scale	CarboTech	Malmberg	Genosob®, Seloxol®	DGE GmbH	DMT carborex	Cryo Pur

Note: n.a. = data not available

2.3.1 Absorption

Absorption is one of the most widely used technologies for biogas upgrading to remove gaseous contaminants that have higher solubility in water than CH_4. In order to increase solubility of gaseous compounds, biogas is compressed before feeding to the bottom of an absorption column in counter-current mode with a scrubbing liquid (Figures 2.2a and b). The absorption is carried out in a scrubber column packed with a carrier material to enhance the contact between the biogas and liquid. The absorbent can be water, organic solvent or an amine solvent (Yentekakis et al. 2017).

Water scrubbers (Figure 2.2a) enable a high CO_2 separation efficiency and can achieve a CH_4 content greater than 97% after a drying step (Sun et al., 2015). Most water scrubbers are operated at a pressure range of 6-10 bar and the inlet biogas temperature should not exceed 60 °C due to safety reasons (Rotunno et al., 2017). Prior to CO_2 removal in a water scrubber, H_2S should be removed to concentrations <300 ppm_v to avoid fouling (Allegue and Hinge, 2014). The disadvantage of this technique is a high power consumption, particularly the use of electricity for biogas compression, cooling and pumping (Ryckebosch et al., 2011). As water scrubbers require a large amount of water, most applications of water scrubbers are preferred to reuse scrubbing water from a desorption unit, referred to as regenerative absorption, which is more economical and eco-friendly than a single pass scrubbing process (Sun et al., 2015).

Organic solvents can be used in scrubbing to enable higher solubility of CO_2, lower water requirement, smaller unit volume and lower operation pressure (typically 4-8 bar) compared to water scrubbers (Wilken et al., 2017). However, solvent regeneration processes require high temperatures up to 80 °C (Wilken et al., 2017). The most common organic solvent used for CO_2 scrubbing is polyethylene glycol, used in well-known commercial Selexol® and Genosorb® processes (Miltner et al., 2017). In physical scrubbers utilizing organic solvents, other contaminants (e.g. H_2S, N_2/O_2 and water vapor) can be simultaneously removed with CO_2 and the CH_4 content of the upgraded biogas can be above 97%. However, the use of scrubbers results in the production of two waste streams, i.e. gas stream contaminated with CO_2 and liquid stream containing chemicals (Petersson and Welinger, 2009).

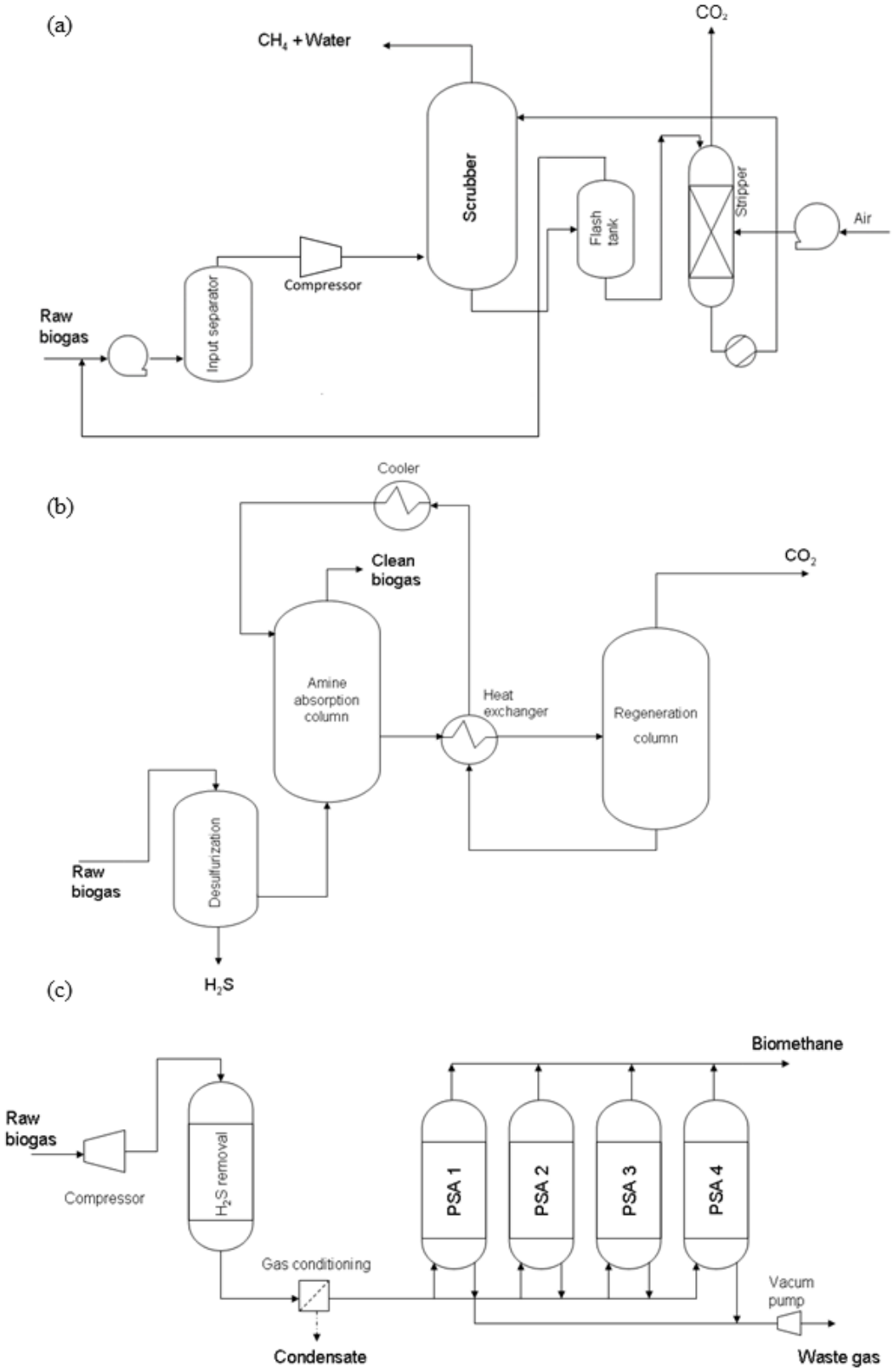

Figure 2.2. Typical configurations of (a) a water scrubber with a water regeneration unit, (b) a chemical scrubber with an absorbent regeneration unit and (c) a 4-stage pressure swing adsorption (PSA) for CO_2 removal and biomethane upgrading (adapted from de Hullu et al., 2008).

Chemical scrubbing is also widely used in commercial scale for CO_2 removal due to its lower power requirement than other physical/chemical techniques (Hoyer et al., 2016). The absorbents used in this technique are alkanol amine solutions, i.e. mono ethanol amine (MEA), di-methyl ethanol amine (DMEA) or tertiary amines. The chemical scrubbing can also be done by using amine-based nanofluids and nanoparticles (Al_3O and SiO_2) in wetted conditions for the simultaneous removal of CO_2 and H_2S (Taheri et al., 2016). The chemical scrubbing unit consists of two main parts, i.e. an absorption column and a regeneration column (Figure 2.2b). CO_2 reacts with the chemical solution in an absorption column packed with chemically inert material to increase mass transfer and provide a large wetted surface area between the gas and the scrubbing liquid (Ryckebosch et al., 2011). The treated biogas stream is released at the top of the absorption column, while the solution containing CO_2 is passed through the bottom of the column to the regeneration column which regenerates the absorbent and releases CO_2 to the atmosphere. The reaction of CO_2 in the absorption column and regeneration unit to desorb CO_2 from the absorbent are shown in the following equations:

Absorption: $2RNH_2 + CO_2 \rightarrow RNHCOO^- + RNH_3^+$ (2.1)

Desorption: $RNHCOO^- + RNH_3^+ \rightarrow 2RNH_2 + CO_2$ (2.2)

2.3.2 Pressure swing adsorption

Pressure swing adsorption (PSA) is one of the most common techniques used at the industrial scale (Hoyer et al., 2016). The upgraded biogas from the PSA process can achieve a CH_4 content >99% and the process does not require the use of solvents and heat for liquid regeneration. PSA is a dry method for the separation of CO_2 from the biogas stream by adsorption onto the surface of specific adsorbents, i.e. activated carbon, zeolites and carbon molecular sieve (Augelletti et al., 2017; Canevesi et al., 2018). The system consists of several process units (Figure 2.2c) working in parallel with an alternative cycle of adsorption, regeneration and pressure build-up. Initially, compressed biogas (4-10 bars) is injected to an adsorption column containing the adsorbing material that separates CH_4 and CO_2. Then, the CH_4-rich stream on the top of the column is evacuated to atmospheric pressure (1 atm). When the adsorbing material in the column becomes saturated, the biogas is sent to another column in which the adsorbing material has already been regenerated.

Regarding the regeneration of the adsorbent, the pressure is reduced to almost atmospheric pressure to evacuate the CO_2-rich gas stream which is subsequently released into the atmosphere or sent to further treatment. Practically, H_2S and the water content are removed from raw biogas before feeding it through the PSA to avoid corrosion problems, while N_2 and O_2 are simultaneously removed with CO_2. Wu et al. (2015) suggested that

the use of a metal-organic framework as an adsorbent could reduce the energy consumption in the PSA process compared to using zeolites. It was due to PSA using the metal-organic framework adsorbent having a linear CO_2 isotherm that induced easier desorption of CO_2. However, PSA has also some disadvantages including that the separated CO_2-rich gas stream requires additional treatment before being released to the atmosphere, i.e. a lean gas burner.

2.3.3 Novel CO_2 removal technologies

2.3.3.1 Membrane separation

In recent decades, separation techniques, i.e. membrane and cryogenic separation, for CO_2 removal from biogas have been gradually developed. With the membrane techniques, biogas contaminants, e.g. CO_2, H_2S and NH_3, are separated from the biogas stream based on selective permeability properties of the membranes. Membranes are made of materials that are permeable to CO_2, water and NH_3. Two membrane techniques commonly used for biogas upgrading include: a high-pressure gas separation with gas-phases on both sides of the membrane (Figure 2.3a), and a low-pressure gas-liquid separation where a liquid absorbs the molecules diffusing through the membrane (Figure 2.3b) (Deng and Hägg, 2010; Petersson and Wellinger, 2009). In case of the gas-liquid membranes, H_2S, NH_3 and siloxanes should be removed from the gas streams prior to feeding into the membrane unit to avoid the reduction of membrane performance. Membrane separation techniques have 60% lower operational costs than PSA or chemical scrubbing (Žák et al., 2018). The membranes can also operate at high pressure in the presence of water vapor.

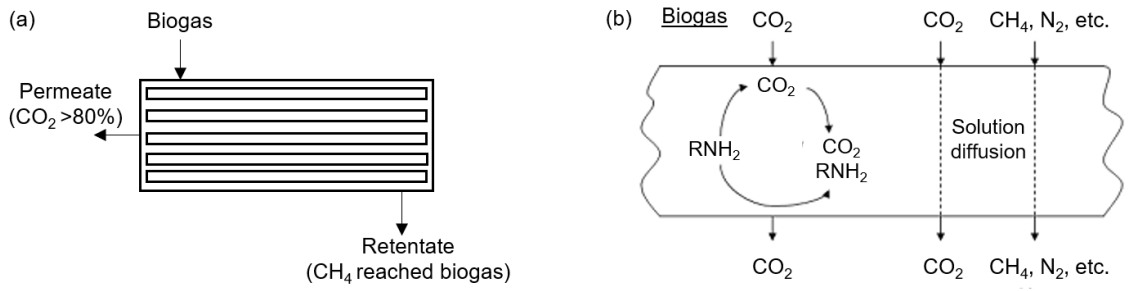

Figure 2.3. Principle of CO_2 removal from biogas using membrane techniques: (a) high-pressure gas separation and (b) low-pressure gas-liquid separation (adapted from Deng and Hägg, 2010).

2.3.3.2 Cryogenic separation

The cryogenic separation process is based on the difference of boiling and sublimation points between CH_4 and the impurities. Theoretically, CH_4 has a boiling point of -160°C at atmospheric pressure, whereas CO_2 has a boiling point of -78°C (Persson et al., 2006). This means that CO_2 condensates at higher temperatures than CH_4. This implies that

CO_2 can be separated from the biogas as a liquid by cooling the gas mixture at elevated pressure (Pellegrini et al., 2018). Additionally, water and siloxanes are also removed during the biogas cooling.

Cooling usually takes place in several steps in order to remove the different pollutants present in the biogas individually and to optimize the energy recovery (Allegue and Hinge, 2012). After CO_2 is removed as a liquid, the biogas stream can be cooled further to condensate the CH_4. The separated CO_2 in the liquid phase is clean and can be further used elsewhere or sold as chemical. To avoid freezing and other problems during the cryogenic compression-expansion process, water and H_2S need to be removed from the raw biogas. As biomethane obtained from the process has a very low temperature, this technique is more effective and profitable for biogas upgrading to liquefied biomethane (LBM) than obtaining gaseous biomethane (Pellegrini et al., 2018). However, cryogenic technology still has several disadvantages including its very high energy requirement for cooling and heating processes and the equipment clogged by frozen CO_2 (Wilken et al., 2017).

2.4 Technologies for biogas desulfurization

The H_2S present in biogas is a result of metabolic activity of sulfate reducing microorganisms during anaerobic degradation of waste streams with high protein content and/or high sulfate concentration (Pokorna and Zabranska, 2015). H_2S, which is a colorless and inflammable gas, is harmful to human health at 100 ppm_v (OSHA, 2005) and causes corrosion to facilities and equipment, e.g. pipelines, cogeneration engines and biogas distribution units (Soreanu et al., 2008a). The combustion of H_2S also produces SO_x emissions which are known as an acid rain precursor and air pollutants. Thus, H_2S needs to be removed from biogas to achieve the requirements for the different biogas application (Table 2.3).

Table 2.3. H_2S concentration requirements for various biogas applications (Allegue and Hinge, 2012).

Biogas utilization	H_2S (ppm_v)
Natural gas	<4
Kitchen stoves	<10
Internal combustion engines	<50
Stirling and boiler engines	<1,000
Turbines	<10,000
Micro-turbines	<70,000

The removal of H_2S from biogas can be achieved by conventional physico-chemical methods including scrubbing, adsorption, absorption and chemical precipitation (Muñoz et al., 2015). However, these technologies have limitations in terms of operating cost and generating chemical wastes as a side product of the process which can cause a negative

environmental impact (Abatzoglou and Boivin, 2009; Muñoz at al., 2015). For example, chemical absorption using alkaline solution requires large volumes of liquid solvents, which can lead the negative environmental impact (Tippayawong and Thanompongchart, 2010). The biological processes for H_2S removal are considered as an alternative to the conventional technologies due to their low operational costs and the benefit of the recovery of end-products (Cano et al., 2018). However, bioreactor technologies are high sensitive to changing operational conditions and require high attention in maintenance and operation due to e.g. excess biomass growth as well as the long-term start-up period of bioreactors compared to the physico-chemical techniques (Miltner et al., 2012).

2.4.1 Physical/chemical processes

2.4.1.1 Absorption

Chemical absorption is a conventional technique for H_2S removal from biogas streams. Typically, the absorption has been done by using alkaline solutions, e.g. sodium hydroxide (NaOH) which react with H_2S to form sodium sulfide (Na_2S) and/or sodium hydrogen sulfide (NaHS). In this process, the demands of water and electricity for pumping are reduced (Miltner et al., 2012) because the use of chemicals as scrubbing water, e.g. NaOH, enhances the water absorption capacity. However, the major drawback of chemical scrubbing is the production of large amounts of aqueous liquid contaminated with Na_2S. Chemical scrubbing is a potential choice for biogas streams containing high H_2S concentrations and the purpose of elemental sulfur (S^0) recovery (Petersson and Wellinger, 2009).

Other chemical solutions, e.g. iron (II) chloride ($FeCl_2$) and iron (III) hydroxide ($Fe(OH)_3$), can be used as absorption liquids; however, they cause the formation of insoluble compounds, such as FeS or Fe_2S_3 which cannot be regenerated (Ryckebosch et a., 2011). Additionally, the chemical absorption can be done by iron-chelated (Fe-EDTA) solutions to oxidize H_2S into S^0 which is easily recovered from the process. With this technique, H_2S removal efficiencies of 99.99% can be achieved. However, the system commonly faces some clogging and foaming problems (Allegue et al., 2014). The system generally includes two stages (Figure 2.4): (i) H_2S is dissolved to the liquid phase and oxidized to S^0 by the Fe-EDTA solution (Eq. 2.3) and (ii) ferric solution is regenerated by oxygenation (Eq. 2.4) according to the following reactions (de Hullu et al., 2018):

$$S^{2-} + Fe^{3+} \leftrightarrow S^0 + Fe^{2+} \quad (2.3)$$

$$Fe^{2+} + O_2\,(aq) \leftrightarrow Fe^{3+} + H_2O \quad (2.4)$$

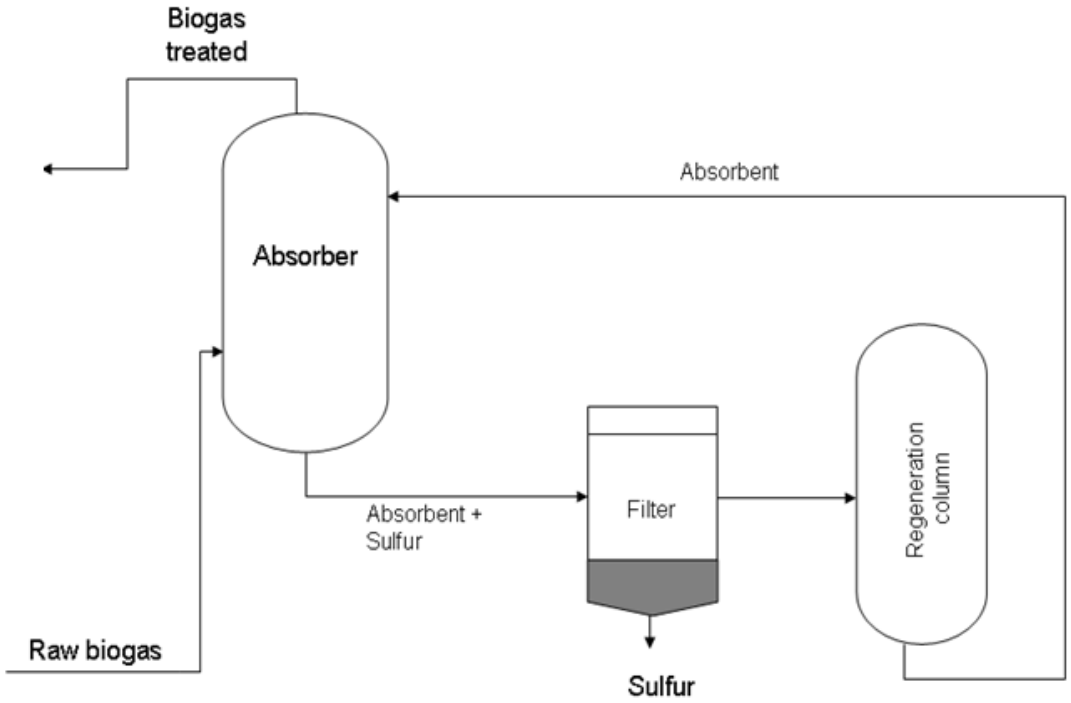

Figure 2.4. Schematic of a chemical absorption column for H_2S removal from biogas (adapted from de Hullu et al., 2008). The process consists of an absorption column for H_2S followed by units for S^0 recovery and regeneration of the absorbent.

2.4.1.2 Adsorption

Adsorption by impregnated activated carbon is a practically applied process for H_2S removal. The impregnated activated carbon is usually used for the removal of H_2S at the inlet concentration <3000 ppm_v due to the prolonged regeneration period (Allegue and Hinge, 2014). The adsorbents used for H_2S removal include zeolites for H_2S removal (Ozekmekci et al., 2015), nanoparticles of Cu-Zn-Ni loaded activated carbons and Ni-Co nanoparticles loaded alumina (γ-Al_2O_3) (Daneshyar et al., 2017). In the adsorption column, H_2S is chemically oxidized by O_2 into S^0 and water under the operational conditions of temperatures at 50-70°C and pressure at 7-8 bars (Allegue and Hinge, 2014). The produced S^0 is adsorbed by the activated carbon which is easily removed from the system. When the activated carbon bed is saturated, it can be replaced by a fresh one, or regenerated by washing with water. During biogas upgrading, the adsorption by the impregnated activated carbon for H_2S removal is commonly integrated with other techniques, e.g. a chemical scrubber or a pressure swing adsorption for CO_2 removal (Figure 2.2).

2.4.2 Biological technologies for H_2S removal

2.4.2.1 Biocatalysts

Biological H_2S removal can be achieved by numerous microorganisms under aerobic, anoxic and anaerobic conditions (Table 2.4). The potential source depends on the type of microorganisms, e.g. hot springs and sediments (Behera et al., 2014; Watsuntorn et al., 2017), or biological treatment processes, e.g. biomass or effluent from wastewater treatment systems and compost units (Chaiprapat et al., 2015; Fernández et al., 2014; Montebello et al., 2013; Ryu et al., 2009). In bioprocesses, sulfur oxidizing bacteria oxidizes H_2S to S^0, SO_4^{2-} or H_2SO_4 as the end-products depending on the operational parameters, i.e. pH, electron acceptor types and the ratio between H_2S and the electron acceptor (i.e., H_2S/O_2 and H_2S/NO_3^-). Aerobic oxidation of H_2S occurs according to the following equations:

$$H_2S + 0.5O_2 \rightarrow S^0 + H_2O \quad (2.5)$$

$$H_2S + 2O_2 \rightarrow SO_4^{2-} + H_2O \quad (2.6)$$

Degradation of H_2S under anoxic conditions is based on the denitrification process in which chemolithotrophic bacteria play a main role in the sulfide oxidizing process using NO_3^- and/or NO_2^- as electron acceptor in the absence of oxygen. The important stoichiometric reactions involved in the process are shown by the following equations (Pokorna and Zabranska, 2015):

$$5HS^- + 8NO_3^- + 3H^+ \rightarrow 5SO_4^{2-} + 4N_2 + 4H_2O \qquad \Delta G^0 = -3848 \text{ kJ/mol} \quad (2.7)$$

$$5HS^- + 2NO_3^- + 7H^+ \rightarrow 5S^0 + N_2 + 6H_2O \qquad \Delta G^0 = -1264 \text{ kJ/mol} \quad (2.8)$$

$$S^{2-} + 0.67NO_2^- + 2.67H^+ \rightarrow S^0 + 0.33N_2 + 1.33H_2O \qquad \Delta G^0 = -240.3\text{kJ/reaction} \quad (2.9)$$

The major type of microorganisms is the phototrophic bacteria, such as green sulfur-oxidizing bacteria (GSB) and purple sulfur-oxidizing bacteria (PSB). Sulfide is oxidized using CO_2 as the terminal electron acceptor and light to oxidize sulfide to elemental sulfur or sulfate and carbohydrate, as shown in the following equations:

$$2H_2S + CO_2 + \text{Light} \rightarrow 2S^0 + CH_2O + H_2O \quad (2.10)$$

$$H_2S + 2CO_2 + 2H_2O + \text{Light} \rightarrow H_2SO_4 + 2CH_2O \quad (2.11)$$

Table 2.4. Microorganisms capable of H_2S removal obtained from various inoculum sources.

Microorganisms	Electron acceptor (s)	Products	Specific operational conditions in bioreactor	Original inoculum source	Reference
Acidithiobacillus ferrooxidans	O_2	Fe^{3+}, SO_4^{2-}	• using Fe^{2+} as another electron donor • acidic pH (0.5-2.5)	Acid mine drainage	Lin et al. (2013)
Acidithiobacillus thiooxidans	O_2	H_2SO_4	• acidic pH (2.0) • gas stream at 10°C	Domestic wastewater sludge plant	Namgung and Song (2015)
Bacillus thermoleovorans	O_2	SO_4^{2-}	• 60°C	High-temperature compost	Ryu et al. (2009)
Thiobacillus thioparus	O_2	S^0, SO_4^{2-}	• neural	Mesophilic anaerobic stabilization tank[a]	Pokorna-Krayzelova et al. (2018)
Thiobacillus denitrificans	O_2, NO_3^-, NO_2^-	S^0, SO_4^{2-}, N_2	• neural	Soil containing sulfur	Ma et al. (2006)
Paracoccus 1HM19	O_2, NO_3^-, NO_2^-	S^0, SO_4^{2-}, N_2	• saline conditions (7% NaCl)	Hot spring	Watsuntorn et al. (2017)
Chlorobium sp. and *Chloronema giganteum*	CO_2	S^0, SO_4^{2-}	• phototrophic conditions (requirement of light)	Effluent from UASB[b] reactor treating domestic sewage	Garcia et al. (2015)

Note: [a]from a municipal wastewater treatment plant (WWTP)
[b]UASB = Upflow anaerobic sludge blanket

2.4.2.2 Microaeration

Microaeration is the simplest biological technique for biogas desulfurization which can be performed directly in anaerobic digesters. In principle, the small amount of air or O_2 is directly into headspace to oxidize H_2S to elemental sulfur (Eq. 2.5). The air or O_2 dosage is required around 1-1.8% of O_2 concentration in biogas to avoid the biogas dilution and the explosive limit from the mixture of CH_4 and O_2 (Muñoz et al., 2015). This technique has been applied in full-scale anaerobic digestion of sewage sludge from wastewater treatment plant (WWTP) since last decade (Jenicek et al., 2010, 2008; Jeníček et al., 2017). The removal efficiency of H_2S from biogas could reach 99% at an initial H_2S concentration of ~5000 ppm_v (Jeníček et al., 2017). During the process, the authors also observed the decrease of COD in the sludge liquor. Recently, the microaeration has been used for H_2S removal in anaerobic digestors (e.g. UASB and FBR) treating industrial wastewaters that the H_2S concentration 20000-67000 (Krayzelova et al., 2015). In this context, the H_2S removal efficiency was 70-80% under microaerobic conditions. The important operational parameters include air dosage, dosing point, biogas residence time in the reactor headspace and temperature (Khoshnevisan et al., 2017).

Microaeration provides low cost operation for 4-6 times compared to aerobic/anoxic biotrickling filter (Khoshnevisan et al., 2017). However, the limitation of this technique is that the application is available for specific reactor headspaces which were suitable for this purpose. One of the major challenges is that S^0 accumulation on the wall of headspace top of anaerobic digestors.

2.4.2.3 Aerobic biofilter/biotrickling filter

Biofilters (BF) and biotrickling filters (BTF) have been used for removal of gaseous H_2S which is fed through a packed bed (Figures 2.5b and c). The contaminants in the gas streams are transferred to the liquid phase and adsorbed/absorbed to the biofilm growing on the packed bed. The biodegradation of pollutants is carried out by the microorganisms attached on the filter media (Figure 2.5a). These bioreactor configurations contain packing materials such as organic materials (compost, soil or peat) or synthetic plastic packing. Compared to the BF, the BTF continuously provides trickling liquid to the packed bed (Kennes et al., 2009a). Biotrickling filters are more complex than biofilters, yet they have been used in field situations to remove H_2S from biogas. Fortuny et al. (2008) reported that the BTF was able to recover quickly from accidental shutdowns and after applying shock loads.

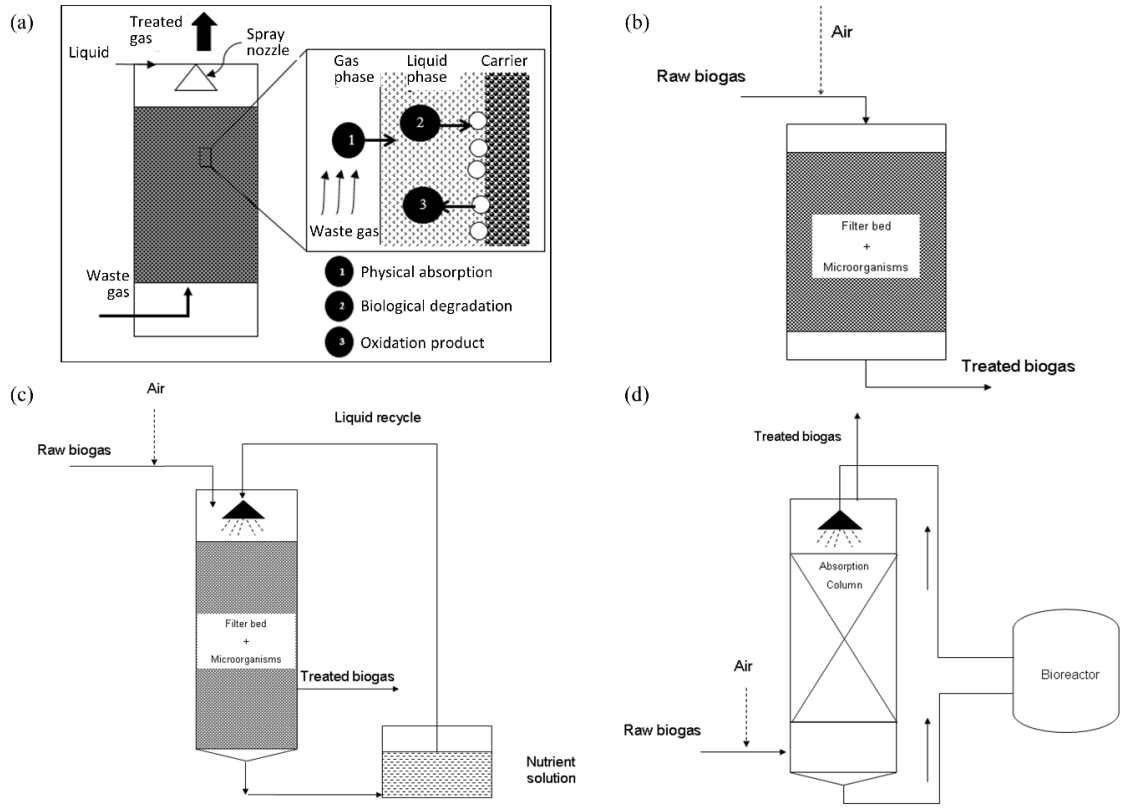

Figure 2.5. Biofiltration systems used for H_2S removal (a) the removal mechanism in the packing material, (b) biofilter, (c) biotrickling filter (BTF) and (d) bioscrubber (adapted from de Hullu et al., 2008).

Aerobic BF and BTF have been commercialized under various trademarks, e.g. BioSulfurex®, Biopuric®, BiogasCleaner®. Profactor Produktionsforschungs GmbH® (Allegue and Hinge, 2014) designed a BTF inoculated with aerobic sulfur-oxidizing bacteria for H_2S removal from biogas. In the system, the O_2 is provided by directly suppling air into the bioreactor, ~4-10% of the inlet gas stream. The Biopuric® process is used for removing H_2S concentrations of 1000-15000 ppm_v under acidic conditions (pH of 1-3), and the process converts H_2S into H_2SO_4 and S^0 with a H_2S removal efficiency of 90-99% (Allegue and Hinge, 2014).

López et al. (2016) tested an aerobic BTF for treating synthetic biogas containing H_2S of 2000-10000 ppm_v and suggested that BTF operation required the regulation of the trickling liquid velocity and flow pattern to improve the gas-liquid O_2 mass transfer in the BTF. The aerobic BTF has been recognized as one of the most effective and attractive techniques for biogas desulfurization due to its lower operational costs and environmental impact than other physical/chemical technologies (Cano et al., 2018).

2.4.2.4 Bioscrubber

The bioscrubber is a two-stage process including physical or chemical absorption of gaseous H_2S into sulfide ions (i.e. HS^- and S^{2-}) in an absorption column, followed by biological oxidation of the liquid streams containing sulfide ions in a bioreactor unit (Figure 2.5d). The THIOPAQ^{TM} process, which is a well-known bioscrubber and currently applied in full scale applications, is operated under alkaline (pH of 8.2-9.0) and aerobic conditions, wherein biodegradation is carried out by sulfur-oxidizing bacteria, particularly *Thiobacillus spp.* (Allegue and Hinge, 2014). This process can achieve H_2S removal efficiencies >99% and recovers elemental sulfur for further utilization. However, the use of conventional bioscrubbers requires large amounts of chemicals, e.g. NaOH, thus the economic aspects and environmental impact should be considered.

Recently, Tilahun et al. (2018) developed a hybrid membrane bioscrubber consisting of a polydimethylsiloxane membrane immerged into an absorption liquid for the treatment of a synthetic biogas (CH_4:CO_2:H_2S = 60:39: 1% *v/v*) which was directly bubbled into the bioreactor. The process was operated at inlet H_2S concentration of 148 g H_2S m^{-3}, dissolved oxygen (DO) concentrations <1 mg L^{-1}, pH of 7.0, temperature of 30°C and resulted in a H_2S removal efficiency of 97% and >74% S^0 recovery. The authors reported that the system also achieved a CO_2 removal efficiency of 50% and no fouling, wetting or dilution problems were observed during 180 operational days.

2.4.2.5 Fluidized bed biofilm reactor (FBR)

This bioreactor configuration generally contains carriers with small particle size, such as sand, activated carbon, glass and clay. To obtain a good performance, the carriers inside the bioreactor are required to maintain a proper fluidization rate which is an important parameter affecting biofilm formation on the carrier. The sulfur-oxidizing bacteria are present in the FBR as suspended and attached growth forms. The reactor is fluidized by high recirculation rates and can be operated in both up- and down-flow mode. Annachhatre and Suktrakoolvait (2001), who initiated the sulfide removal in a fluidized bed biofilm (FBR), found that a FBR operated at upflow velocities of 16-26 m h^{-1} could achieve a sulfide removal efficiency of >90% at sulfide loading rates of 0.13-1.6 kg S m^{-3} d^{-1}. When a FBR was operated at a DO less than 0.1 mg L^{-1}, the S^0 production was 65-75% of the removed sulfide.

Krishnakumar et al. (2005) studied the performance of a reverse fluidized loop reactor (RFLP) for oxidizing sulfide in the liquid phase and recovering sulfur from the process. This reactor was operated under alkaline pH (pH of 8.0) and it was able to achieve 90% sulfide oxidation at the maximum sulfide loading rate at 30 kg S m^{-3} d^{-1}, and 65% of sulfur was recovered. Moreover, this bioreactor type can be combined with other reactors for H_2S removal.

2.4.2.6 Photobioreactors

In photobioreactors for H_2S removal, sulfide is oxidized using CO_2 as a terminal electron acceptor and light to oxidize sulfide to elemental sulfur or sulfate and carbohydrates (Eqs. 2.10 and 2.11). Phototrophic H_2S removal coupled with S^0 recovery has been studied in phototube bioreactors, which allowed the bacteria to grow on the inner wall of the tubes, inoculated by pure cultures of green sulfur bacterium *Chlorobium limicola* (Henshaw et al., 1999; Henshaw and Zhu, 2001; Syed and Henshaw, 2005). As the phototube bioreactors required energy consumption and increased sulfide loading rates, Syed and Henshaw (2005) applied a light-emitting diode (LED) light source instead of an infrared light bulb. Phototrophic H_2S removal under anaerobic conditions has limitations during practical applications due to the problems related to slow growth rate and light source when operating at large scale.

Garcia et al. (2016, 2015) investigated the treatment of sulfide containing anaerobic effluents (1-6 mg S^{2-} L^{-1}) in phototrophic bioreactors exposed to sunlight located in a wastewater treatment plant (Brazil) and reported the microbial community composition using pyrosequencing. The system achieved sulfide removal efficiencies of 65% and >90% at a HRT of 24 and 12 h, respectively. The authors observed green-colored biomass developed in the systems, high amounts of S^0 (20 mg S^0 g^{-1} VTS at HRT of 12 h) and green and purple sulfur-oxidizing bacteria, e.g. *Chlorobium* sp., *Chloronema giganteum*, and *Chromatiaceae*, were detected in the system. These studies suggest the potential application of photobioreactors for the simultaneous removal of sulfide, organic matter and methane from anaerobic effluents. However, the use of natural light still requires further investigation, e.g. the effect of light intensity used in the system and the light duration applied to the microorganisms.

2.5 Technologies integrating biological biogas desulfurization with the removal of other contaminants

2.5.1 Hybrid of bubble column and high rate algal ponds

In recent years, the transformation of biogas to biomethane has been studied using photosynthetic systems which are the integration of a bubble column and a high rate algal pond (HRAP) for CO_2 and H_2S removal from biogas (Bahr et al., 2014; Meier et al., 2018; Posadas et al., 2015; Serejo et al., 2015; Toledo-Cervantes et al., 2018, 2016; Zhao et al., 2015). The mechanism behind this technique is that O_2 produced during CO_2 fixation of microalgae in the HRAP is provided as an electron acceptor for sulfide-oxidizing bacteria to oxidize H_2S in the subsequent bubble column. The upgraded biogas from this technique reaches the quality requirements for electricity production (Toledo-Cervantes

et al., 2018). Bahr et al. (2014) reported that the combined adsorption column-HRAP system treating a synthetic biogas containing 30% of CO_2 and 5000 ppm_v of H_2S enabled H_2S and CO_2 removal efficiencies of 100% and 90%, respectively. Furthermore, the microalgal biomass grown in the HRAP during CO_2 capture could be harvested and used for further biogas production with a CH_4 yield of 0.21-0.27 L g^{-1} of volatile suspended solids. In the phototrophic system, the presence of H_2S in biogas (up to 5000 ppm_v) did not affect the CO_2 removal (Bahr et al., 2014; Meier et al., 2018).

2.5.2 Simultaneous removal of H_2S and NH_3

In biogas contaminated with low NH_3 concentrations, NH_3 can be simultaneously removed using physico-chemical techniques for biogas upgrading, e.g. drying or adsorption processes. In some cases, NH_3 concentrations can be up to 2000 ppm_v in biogas produced from animal manure (Guo et al., 2009), and hence a separate unit for NH_3 removal is required. The simultaneous removal of NH_3 and H_2S can be carried out in a biofilter inoculated with *T. thioparus* and a mixed nitrifying culture or a biotrickling filter inoculated with *Pseudomonas putida* and *Arthrobacter oxydans* (Chung et al., 2005; Kim et al., 2002). Jiang et al. (2009) developed a horizontal biotrickling filter packed with exhausted activated carbon for the simultaneous removal of NH_3 and H_2S at inlet concentrations of 20-400 ppm_v for both pollutants. The biotrickling filter, inoculated with sulfide-oxidizing and nitrifying bacteria enriched from activated sludge, enabled H_2S and NH_3 removal efficiencies >98% (44 g NH_3 m^{-3} h^{-1}) and 95% (36 g H_2S m^{-3} h^{-1}), respectively. At high concentrations of H_2S (400 ppm_v), the authors observed inhibition of NH_3 degradation due to the accumulation of elemental sulfur and ammonium sulfate in the system.

Rabbani et al. (2016) studied the simultaneous removal of H_2S and NH_3 in a pilot-scale biofilter and observed that H_2S was removed by sulfur-oxidizing bacteria, while NH_3 was chemically oxidized with SO_4^{2-} to form $(NH_4)_2SO_4$ in acidic conditions (pH of 1.51-3.67). However, the recovery of a solid form of $(NH_4)_2SO_4$ from the biofilter should be further studied.

2.5.3 Simultaneous H_2S removal and treatment of NO_3^--contaminated wastewater

The anoxic BTF for H_2S removal from biogas entails the use of a soluble electron acceptor (NO_3^- or NO_2^-) and elimination of gas-liquid-biofilm mass transfer limitations of O_2 experienced in aerobic systems (Soreanu et al., 2009, 2008b, 2008a; Krishnakumar et al., 2005). The final product of H_2S oxidation in anoxic systems depends on the nitrogen-to-sulfur (N/S) ratio: mainly SO_4^{2-} is produced at N/S ratio >1.6, while S^0 production (in the range of 50-70%) is typically observed at N/S ratios <0.7 (Eqs. 2.7 and 2.8).

Biogas desulfurization has been studied in anoxic BTFs which performed efficiently: a high H_2S elimination capacity of 127-171 g S m^{-3} h^{-1} (at inlet H_2S 1400-14600 ppm_v) was obtained using NO_3^- solution (e.g. KNO_3 and $Ca(NO_3)_2$) as a trickling liquid (Almenglo et al., 2016b; Fernández et al., 2013, 2014; Montebello et al., 2012). Open-pore polyurethane foam and Pall rings are the packing materials commonly used in the anoxic BTFs. Jaber et al. (2017) studied the use of expended Schist and cellular concrete waste as a packing material in an anoxic BTF and reported that the H_2S elimination capacity was 10.5 g m^{-3} h^{-1} and H_2S removal efficiency of 100% at inlet H_2S concentrations of 133 ppm_v and EBRT of 63 s. The authors reported that the anoxic BTF packed with concrete wastes showed lower pressure drops (3-16 Pa m^{-1}) than other synthetic packing materials.

Anoxic H_2S removal from biogas has also been conducted in a two-stage reactor comprised of a scrubber (physico-chemical method) and an anoxic upflow fixed bed inoculated with sludge taken from the denitrification tank of a local WWTP (Bayrakdar et al., 2016). The bioreactor was operated at a HRT of 4 h, S/N ratio of 2.5 and sulfide loading rate of 451 mg S L^{-1} d^{-1}. The authors reported removal of 98% and 97% for H_2S and NO_3^-, respectively, and the operational problem with S^0 clogging was also reported by the authors.

Baspinar et al. (2011) studied the simultaneous removal of H_2S from biogas produced from anaerobic digester (13000-37000 ppm_v) and nitrogen (NO_3^- and NO_2^-) from the effluent of an activated sludge treatment plant without external carbon source addition. The study was conducted using a pilot scale hybrid system comprising of a bubble column and bioscrubber (2.4 m^3) using the NO_3^--containing wastewater as a scrubbing liquid. An H_2S elimination capacity in the range of 83-167 g S^{2-} m^{-3} h^{-1}, with outlet H_2S concentrations <1000 ppm_v was achieved.

2.6 Conclusions

The use of biogas for syngas production, direct combustion and electricity generation requires the removal of corrosive contaminants, e.g. H_2S and NH_3. In this context, biological technologies are attractive, cost effective, environmentally friendly and offer the possibility to recover value-added products. Compared to physico-chemical technologies, bioreactors have shown great potential, particularly for H_2S removal, as they can be operated under various operational conditions and were shown to be robust under transient conditions. However, bioreactor technologies require periodic maintenance to remove excess biomass that frequently causes clogging and/or channeling problems. The start-up period of bioreactors also takes long time, from several days up to a few months. For full-scale operation, physical/chemical technologies are preferable for biogas upgrading.

The selection of biogas cleaning and upgrading technologies can be considered from various aspects, e.g. limited installation area, technical optimization as well as operational and maintenance costs. However, the environmental impact and high energy consumption are still their major drawbacks. Biological technologies for removing CO_2 and H_2S, e.g. via the integration of a bubble column and a high rate algal pond, have gained attention as the biomass produced during CO_2 capture can also be harvested for further applications.

2.7 References

Achinas, S., Achinas, V., Euverink, G.J.W., 2017. A technological overview of biogas production from biowaste. Engineering 3, 299–307.

Allegue, L.B., Hinge, J., 2014. Biogas upgrading: Evaluation of methods for H_2S removal. Danish Technological Institue, Denmark.

Allegue, L.B., Hinge, J., 2012. Biogas and bio-syngas upgrading. Danish Technological Institue, Denmark.

Almenglo, F., Ramírez, M., Gómez, J.M., Cantero, D., 2016. Operational conditions for start-up and nitrate-feeding in an anoxic biotrickling filtration process at pilot scale. Chem. Eng. J. 285, 83–91.

Angelidaki, I., Treu, L., Tsapekos, P., Luo, G., Campanaro, S., Wenzel, H., Kougias, P.G., 2018. Biogas upgrading and utilization: Current status and perspectives. Biotechnol. Adv. 36, 452–466.

Annachhatre, A.P., Suktrakoolvait, S., 2001. Biological sulfide oxidation in a fluidized bed reactor. Environ. Technol. 22, 661–672.

Augelletti, R., Conti, M., Annesini, M.C., 2017. Pressure swing adsorption for biogas upgrading. A new process configuration for the separation of biomethane and carbon dioxide. J. Clean. Prod. 140, 1390–1398.

Bahr, M., Díaz, I., Dominguez, A., González-Sánchez, A., Muñoz, R., 2014. Microalgal-biotechnology as a platform for an integral biogas upgrading and nutrient removal from anaerobic effluents. Environ. Sci. Technol. 48, 573–581.

Barbusinski, K., Kalemba, K., Kasperczyk, D., Urbaniec, K., Kozik, V., 2017. Biological methods for odor treatment – A review. J. Clean. Prod. 152, 223–241.

Baspinar, A.B., Turker, M., Hocalar, A., Ozturk, I., 2011. Biogas desulphurization at technical scale by lithotrophic denitrification: Integration of sulphide and nitrogen removal. Process Biochem. 46, 916–922.

Bauer, F., Hulteberg, C., Persson, T., Tamm, D., 2013. Biogas upgrading – Review of commercial technologies, Swedish Gas Technology Centre (SGC), Malmö.

Bayrakdar, A., Tilahun, E., Calli, B., 2016. Biogas desulfurization using autotrophic denitrification process. Appl. Microbiol. Biotechnol. 100, 939–948.

Behera, B.C., Mishra, R.R., Dutta, S.K., Thatoi, H.N., 2014. Sulphur oxidising bacteria in mangrove ecosystem: A review. African J. Biotechnol. 13, 2897–2907.

Canevesi, R.L.S., Andreassen, K.A., da Silva, E.A., Borba, C.E., Grande, C.A., 2018. Pressure swing adsorption for biogas upgrading with carbon molecular sieve. Ind. Eng. Chem. Res. 57, 8057–8067.

Cano, P.I., Colón, J., Ramírez, M., Lafuente, J., Gabriel, D., Cantero, D., 2018. Life cycle assessment of different physical-chemical and biological technologies for biogas desulfurization in sewage treatment plants. J. Clean. Prod. 181, 663–674.

Chaiprapat, S., Charnnok, B., Kantachote, D., Sung, S., 2015. Bio-desulfurization of biogas using acidic biotrickling filter with dissolved oxygen in step feed recirculation. Bioresour. Technol. 179, 429–435.

Chung, Y.C., Lin, Y.Y., Tseng, C.P., 2005. Removal of high concentration of NH_3 and coexistent H_2S by biological activated carbon (BAC) biotrickling filter. Bioresour. Technol. 96, 1812–1820.

Converti, A., Oliveira, R.P.S., Torres, B.R., Lodi, A., Zilli, M., 2009. Biogas production and valorization by means of a two-step biological process. Bioresour. Technol. 100, 5771–5776.

Daneshyar, A., Ghaedi, M., Sabzehmeidani, M.M., Daneshyar, A., 2017. H_2S adsorption onto Cu-Zn–Ni nanoparticles loaded activated carbon and Ni-Co nanoparticles loaded γ-Al_2O_3: Optimization and adsorption isotherms. J. Colloid Interface Sci. 490, 553–561.

Daniel-Gromke, J., Rensberg, N., Denysenko, V., Stinner, W., Schmalfuß, T., Scheftelowitz, M., Nelles, M., Liebetrau, J., 2018. Current developments in production and utilization of biogas and biomethane in Germany. Chemie Ing. Tech. 90, 17–35.

de Hullu, J., Maassen, J., van Meel, P., Shazad, S., Vaessen, J., Bini, L., Reijenga, J., 2008. Comparing different biogas upgrading techniques. Dirkse Milieutechniek BV, Eindhoven.

Deng, L., Hägg, M.B., 2010. Techno-economic evaluation of biogas upgrading process using CO_2 facilitated transport membrane. Int. J. Greenh. Gas Control 4, 638–646.

Fernández, M., Ramírez, M., Gómez, J.M., Cantero, D., 2014. Biogas biodesulfurization in an anoxic biotrickling filter packed with open-pore polyurethane foam. J. Hazard. Mater. 264, 529–535.

Fernández, M., Ramírez, M., Pérez, R.M., Gómez, J.M., Cantero, D., 2013. Hydrogen sulphide removal from biogas by an anoxic biotrickling filter packed with Pall rings. Chem. Eng. J. 225, 456–463.

Fortuny, M., Baeza, J.A., Gamisans, X., Casas, C., Lafuente, J., Deshusses, M.A., Gabriel, D., 2008. Biological sweetening of energy gases mimics in biotrickling filters. Chemosphere 71, 10–17.

Garcia, G.P.P., Diniz, R.C.O., Bicalho, S.K., Franco, V., Pereira, A.D., Brandt, E.F., Etchebehere, C., Chernicharo, C.A.L., Araujo, J.C., 2016. Microbial community and sulphur behaviour in phototrophic reactors treating UASB effluent under different operational conditions. Int. Biodeterior. Biodegradation 119, 486–498

Garcia, G.P.P., Diniz, R.C.O., Bicalho, S.K., Franco, V.A.S., Gontijo, E.M.O., Toscano, R.A., Canhestro, K.O., Santos, M.R., Carmo, A.L.R.D., Lobato, L.C.S., Brandt, E.M.F., Chernicharo, C.A.L., Araujo, J.C, 2015. Biological sulphide removal from anaerobically treated domestic sewage: reactor performance and microbial community dynamics. Environ. Technol. 36, 2177–2189.

Guo, M., Song, W., Buhain, J., 2015. Bioenergy and biofuels: History, status, and perspective. Renew. Sustain. Energy Rev. 42, 712–725.

Guo, X., Tak, J.K., Johnson, R.L., 2009. Ammonia removal from air stream and biogas by a H_2SO_4 impregnated adsorbent originating from waste wood-shavings and biosolids. J. Hazard. Mater. 166, 372–376.

Henshaw, P., Medlar, D., McEwen, J., 1999. Selection of a support medium for a fixed-film green sulphur bacteria reactor. Water Res. 33, 3107–3110.

Henshaw, P.F., Zhu, W., 2001. Biological conversion of hydrogen sulphide to elemental sulphur in a fixed-film continuous flow photo-reactor. Water Res. 35, 3605–3610.

Hoyer, K., Hulteberg, C., Svensson, M., Jenberg, J., Nørregård, Ø., 2016. Biogas upgrading: Technical review. Energiforsk, Sweden.

IEA, 2017. IEA Bioenergy Task 37: Country report summaries 2017. IEA Energy.

IEA (International Energy Agency), 2015. World Energy Outlook Special Report “Energy and Climate Change”. OECD/IEA. https://doi.org/10.1038/479267b, Assessed date: 8 October 2018.

Jaber, M.B., Couvert, A., Amrane, A., Le Cloirec, P., Dumont, E., 2017. Hydrogen sulfide removal from a biogas mimic by biofiltration under anoxic conditions. J. Environ. Chem. Eng. 5, 5617–5623.

Jiang, X., Yan, R., Tay, J.H., 2009. Simultaneous autotrophic biodegradation of H_2S and NH_3 in a biotrickling filter. Chemosphere 75, 1350–1355.

Jeníček, P., Horejš, J., Pokorná-Krayzelová, L., Bindzar, J., Bartáček, J., 2017. Simple biogas desulfurization by microaeration – Full scale experience. Anaerobe 46, 41–45.

Jenicek, P., Keclik, F., Maca, J., Bindzar, J., 2008. Use of microaerobic conditions for the improvement of anaerobic digestion of solid wastes. Water Sci. Technol. 58, 1491–1496.

Jenicek, P., Koubova, J., Bindzar, J., Zabranska, J., 2010. Advantages of anaerobic digestion of sludge in microaerobic conditions. Water Sci. Technol. 62, 427–434.

Kennes, C., Montes, M., López, M.E., Veiga, M.C., 2009. Waste gas treatment in bioreactors: Environmental engineering aspects. Can. J. Civ. Eng. 36, 1887–1894.

Kennes, C., Thalasso, F., 1998. Review waste gas biotreatment technology. J. Chem. Technol. Biotechnol. 72, 303–319.

Khoshnevisan, B., Tsapekos, P., Alfaro, N., Díaz, I., Fdz-Polanco, M., Rafiee, S., Angelidaki, I., 2017. A review on prospects and challenges of biological H2S removal from biogas with focus on biotrickling filtration and microaerobic desulfurization. Biofuel Res. J. 4, 741–750. https://doi.org/10.18331/BRJ2017.4.4.6

Kim, H., Kim, Y.J., Chung, J.S., Xie, Q., 2002. Long-term operation of a biofilter for simultaneous removal of H_2S and NH_3. J. Air Waste Manag. Assoc. 52, 1389–1398.

Krayzelova, L., Bartacek, J., Díaz, I., Jeison, D., Volcke, E.I.P., Jenicek, P., 2015. Microaeration for hydrogen sulfide removal during anaerobic treatment: a review. Rev. Environ. Sci. Biotechnol. 14, 703–735.

Krishnakumar, B., Majumdar, S., Manilal, V.B., Haridas, A., 2005. Treatment of sulphide containing wastewater with sulphur recovery in a novel reverse fluidized loop reactor (RFLR). Water Res. 39, 639–647.

Lin, W.C., Chen, Y.P., Tseng, C.P., 2013. Pilot-scale chemical-biological system for efficient H_2S removal from biogas. Bioresour. Technol. 135, 283–291.

Lijó, L., Lorenzo-Toja, Y., González-García, S., Bacenetti, J., Negri, M., Moreira, M.T., 2017. Eco-efficiency assessment of farm-scaled biogas plants. Bioresour. Technol. 237, 146–155.

Lönnqvist, T., Sanches-Pereira, A., Sandberg, T., 2015. Biogas potential for sustainable transport e a Swedish regional case. J. Clean. Prod. 108, 1105–1114.

López, L.R., Bezerra, T., Mora, M., Lafuente, J., Gabriel, D., 2016. Influence of trickling liquid velocity and flow pattern in the improvement of oxygen transport in aerobic biotrickling filters for biogas desulfurization. J. Chem. Technol. Biotechnol. 91, 1031–1039.

Ma, Y.L., Yang, B.L., Zhao, J.L., 2006. Removal of H_2S by *Thiobacillus denitrificans* immobilized on different matrices. Bioresour. Technol. 97, 2041–2046.

Meier, L., Stará, D., Bartacek, J., Jeison, D., 2018. Removal of H_2S by a continuous microalgae-based photosynthetic biogas upgrading process. Process Saf. Environ. Prot. 119, 65–68.

Miltner, M., Makaruk, A., Krischan, J., Harasek, M., 2012. Chemical-oxidative scrubbing for the removal of hydrogen sulphide from raw biogas: Potentials and economics. Water Sci. Technol. 66, 1354–1360.

Montebello, A.M., Bezerra, T., Rovira, R., Rago, L., Lafuente, J., Gamisans, X., Campoy, S., Baeza, M., Gabriel, D., 2013. Operational aspects, pH transition and microbial shifts of a H_2S desulfurizing biotrickling filter with random packing material. Chemosphere 93, 2675–2682.

Montebello, A.M., Fernández, M., Almenglo, F., Ramírez, M., Cantero, D., Baeza, M., Gabriel, D., 2012. Simultaneous methylmercaptan and hydrogen sulfide removal in the desulfurization of biogas in aerobic and anoxic biotrickling filters. Chem. Eng. J. 200–202, 237–246.

Muñoz, R., Meier, L., Diaz, I., Jeison, D., 2015. A review on the state-of-the-art of physical/chemical and biological technologies for biogas upgrading. Rev. Environ. Sci. Biotechnol. 14, 727–759.

Namgung, H.K., Song, J.H., 2015. The effect of oxygen supply on the dual growth kinetics of *Acidithiobacillus thiooxidans* under acidic conditions for biogas desulfurization. Int. J. Environ. Res. Public Health 12, 1368–1386.

OSHA (U.S. Occupational, Safety and Health Administration), 2005. Fact sheet: Hydrogen sulfide. https://www.osha.gov/OshDoc/data_Hurricane_Facts/hydrogen_sulfide_fact.html, Accessed date: 21 September 2017.

Ozekmekci, M., Salkic, G., Fellah, M.F., 2015. Use of zeolites for the removal of H_2S: A mini-review. Fuel Process. Technol. 139. 49–60.

Pellegrini, L.A., De Guido, G., Langé, S., 2018. Biogas to liquefied biomethane via cryogenic upgrading technologies. Renew. Energy 124, 75–83.

Persson, M., Jönsson, O., Wellinger, A., 2006. Biogas upgrading to vehicle fuel standards and grid injection, in: Task 37 - Energy from biogas and landfill gas. IEA Bioenergy, pp. 1–34.

Petersson, A., Wellinger, A., 2009. Biogas upgrading technologies–developments and innovations. IEA Bioenergy Task 37. http://www.iea-biogas.net/files/daten-redaktion/download/publi-task37/upgrading_rz_low_final.pdf, Accessed date: 9 February 2016.

Pokorna-Krayzelova, L., Bartacek, J., Theuri, S.N., Segura Gonzalez, C.A., Prochazka, J., Volcke, E.I.P., Jenicek, P., 2018. Microaeration through a biomembrane for biogas desulfurization: lab-scale and pilot-scale experiences. Environ. Sci. Water Res. Technol. 4, 1190–1200.

Pokorna, D., Zabranska, J., 2015. Sulfur-oxidizing bacteria in environmental technology. Biotechnol. Adv. 33, 1246–1259.

Posadas, E., Serejo, M.L., Blanco, S., Pérez, R., García-Encina, P.A., Muñoz, R., 2015. Minimization of biomethane oxygen concentration during biogas upgrading in algal-bacterial photobioreactors. Algal Res.

Prasertsan, S., Sajjakulnukit, B., 2006. Biomass and biogas energy in Thailand: Potential, opportunity and barriers. Renew. Energy 31, 599–610.

Rabbani, K.A., Charles, W., Kayaalp, A., Cord-Ruwisch, R., Ho, G., 2016. Pilot-scale biofilter for the simultaneous removal of hydrogen sulphide and ammonia at a wastewater treatment plant. Biochem. Eng. J. 107, 1–10.

Rajendran, K., Aslanzadeh, S., Taherzadeh, M.J., 2012. Household biogas digesters-A review, Energies. 5, 2911–2942

Rasi, S., Veijanen, A., Rintala, J., 2007. Trace compounds of biogas from different biogas production plants. Energy 32, 1375–1380.

Rotunno, P., Lanzini, A., Leone, P., 2017. Energy and economic analysis of a water scrubbing based biogas upgrading process for biomethane injection into the gas

grid or use as transportation fuel. Renew. Energy 102, 417–432.

Ryckebosch, E., Drouillon, M., Vervaeren, H., 2011. Techniques for transformation of biogas to biomethane. Biomass and Bioenergy. 25, 1623–1645.

Ryu, H.W., Yoo, S.K., Choi, J.M., Cho, K.S., Cha, D.K., 2009. Thermophilic biofiltration of H_2S and isolation of a thermophilic and heterotrophic H_2S-degrading bacterium, *Bacillus* sp. TSO3. J. Hazard. Mater. 168, 501–506.

Serejo, M.L., Posadas, E., Boncz, M.A., Blanco, S., García-Encina, P., Muñoz, R., 2015. Influence of biogas flow rate on biomass composition during the optimization of biogas upgrading in microalgal-bacterial processes. Environ. Sci. Technol. 49, 3228–3236.

Sorda, G., Sunak, Y., Madlener, R., 2013. An agent-based spatial simulation to evaluate the promotion of electricity from agricultural biogas plants in Germany. Ecol. Econ. 89, 43–60.

Soreanu, G., Béland, M., Falletta, P., Edmonson, K., Seto, P., 2008a. Laboratory pilot scale study for H_2S removal from biogas in an anoxic biotrickling filter. Water Sci. Technol. 57, 201–207.

Soreanu, G., Béland, M., Falletta, P., Ventresca, B., Seto, P., 2009. Evaluation of different packing media for anoxic H_2S control in biogas. Environ. Technol. 30, 1249–1259.

Soreanu, G., Falletta, P., Béland, M., Seto, P., 2008b. Study on the performance of an anoxic biotrickling filter for the removal of hydrogen sulphide from biogas. Water Qual. Res. J. Canada 43, 211–218.

Sun, Q., Li, H., Yan, J., Liu, L., Yu, Z., Yu, X., 2015. Selection of appropriate biogas upgrading technology-a review of biogas cleaning, upgrading and utilisation. Renew. Sustain. Energy Rev. 51, 521–532.

Surendra, K.C., Sawatdeenarunat, C., Shrestha, S., Sung, S., Khanal, S.K., 2015. Anaerobic digestion-based biorefinery for bioenergy and biobased products. Ind. Biotechnol. 11, 103–112.

Surendra, K.C., Takara, D., Hashimoto, A.G., Khanal, S.K., 2014. Biogas as a sustainable energy source for developing countries: Opportunities and challenges. Renew. Sustain. Energy Rev. 31, 846–859.

Syed, M.A., Henshaw, P.F., 2005. Light emitting diodes and an infrared bulb as light sources of a fixed-film tubular photobioreactor for conversion of hydrogen sulfide to elemental sulfur. J. Chem. Technol. Biotechnol. 80, 119–123.

Taheri, M., Mohebbi, A., Hashemipour, H., Rashidi, A.M., 2016. Simultaneous absorption of carbon dioxide (CO_2) and hydrogen sulfide (H_2S) from CO_2-H_2S-CH_4 gas mixture using amine-based nanofluids in a wetted wall column. J. Nat. Gas Sci. Eng. 28, 410–417.

Tilahun, E., Sahinkaya, E., Çalli, B., 2018. A hybrid membrane gas absorption and bio-oxidation process for the removal of hydrogen sulfide from biogas. Int. Biodeterior. Biodegrad. 127, 69–76.

Toledo-Cervantes, A., Morales, T., González, Á., Lebrero, R., 2018. Long-term photosynthetic CO_2 removal from biogas and flue-gas: Exploring the potential of closed photobioreactors for high-value biomass production. Sci. Total Environ. 640–641, 1272–1278.

Toledo-Cervantes, A., Serejo, M.L., Blanco, S., Pérez, R., Lebrero, R., Muñoz, R., 2016. Photosynthetic biogas upgrading to bio-methane: Boosting nutrient recovery via biomass productivity control. Algal Res. 17, 46–52.

Watsuntorn, W., Ruangchainikom, C., Rene, E.R., Lens, P.N.L., Chulalaksananukul, W., 2017. Hydrogen sulfide oxidation under anoxic conditions by a nitrate-reducing, sulfide-oxidizing bacterium isolated from the Mae Um Long Luang hot spring, Thailand. Int. Biodeterior. Biodegradation 124, 196–205.

Wilken, D., Strippel, F., Hofmann, F., Maciejczyk, M., Klinkmüller, L., Wagner, L., Bontempo, G., Münch, J., Scheidl, S., Conton, M., Deremince, B., Walter, R., Zetsche, N., Findeisen, C., 2017. Biogas to Biomethane. Fachverband Biogas e. V., Freising.

Wu, B., Zhang, X., Xu, Y., Bao, D., Zhang, S., 2015. Assessment of the energy consumption of the biogas upgrading process with pressure swing adsorption using novel adsorbents. J. Clean. Prod. 101, 251–261.

Yentekakis, I. V., Goula, G., 2017. Biogas Management: Advanced utilization for production of renewable energy and added-value chemicals. Front. Environ. Sci. 5, 7.

Žák, M., Bendová, H., Friess, K., Bara, J.E., Izák, P., 2018. Single-step purification of raw biogas to biomethane quality by hollow fiber membranes without any pretreatment – An innovation in biogas upgrading. Sep. Purif. Technol. 203, 36–40.

Zhao, Y., Sun, S., Hu, C., Zhang, H., Xu, J., Ping, L., 2015. Performance of three microalgal strains in biogas slurry purification and biogas upgrade in response to various mixed light-emitting diode light wavelengths. Bioresour. Technol. 187, 338–345.

Chapter 3 Anoxic sulfide oxidation in fluidized bed reactor (FBR): experimental and artificial neural network (ANN) model analysis

This chapter has been published in modified form:

Khanongnuch, R., Di Capua, F., Lakaniemi, A.-M., Rene, E.R., Lens, P.N.L. 2018. Effect of N/S ratio on anoxic thiosulfate oxidation in a fluidized bed reactor: experimental and artificial neural network model analysis, *Process Biochem*. 68, 171–181.

Anoxic thiosulfate ($S_2O_3^{2-}$) oxidation using autotrophic denitrification by a mixed culture of sulfur-oxidizing nitrate-reducing (SO-NR) bacteria was studied in a fluidized bed reactor (FBR). The long-term performance of the FBR was evaluated for 306 days at three nitrogen-to-sulfur (N/S) molar ratios (0.5, 0.3 and 0.1) and a hydraulic retention time (HRT) of 5 h. $S_2O_3^{2-}$ removal efficiencies >99% were obtained at a N/S ratio of 0.5 and a $S_2O_3^{2-}$ and nitrate (NO_3^-) loading rate of 820 (± 84) mg $S_2O_3^{2-}$-S L^{-1} d^{-1} and 173 (± 10) mg NO_3^--N L^{-1} d^{-1}, respectively. The $S_2O_3^{2-}$ removal efficiency decreased to 76% and 26% at N/S ratios of 0.3 and 0.1, respectively, and recovered to 80% within 3 days after increasing the N/S ratio from 0.1 back to 0.5. The highest observed half-saturation (K_s) and inhibition (K_I) constants of the biofilm-grown SO-NR bacteria obtained from batch cultivations were 172 and 800 mg $S_2O_3^{2-}$-S L^{-1}, respectively. *Thiobacilus denitrificans* was the dominant microorganism in the FBR. Artificial neural network modelling successfully predicted $S_2O_3^{2-}$ and NO_3^- removal efficiencies and SO_4^{2-} production in the FBR. Additionally, results from the sensitivity analysis showed that the effluent pH was the most influential parameter affecting the $S_2O_3^{2-}$ removal efficiency.

3.1 Introduction

Sulfide compounds (S^{2-}, HS^- and H_2S) present in wastewater and biogas streams, particularly in industrial discharges from fermentation of molasses, pulp and paper industry and latex production, can cause odor and corrosion problems (Guerrero et al., 2015; Rattanapan et al., 2009). The removal of sulfide from both liquid and gaseous phases has been implemented by various physico-chemical methods, including scrubbing, adsorption, absorption and chemical precipitation (Muñoz et al., 2015; Nielsen et al., 2005). However, these technologies have high operating costs as well as negative environmental impacts due to the generation of chemical wastes (Abatzoglou and Boivin, 2009; Muñoz et al., 2015).

Biological processes for sulfide removal are considered as cleaner and less expensive alternatives compared to conventional technologies using chemicals. Aerobic and anoxic bioreactors have been operated for sulfide removal from both liquid and gas streams (Almenglo et al., 2016b; Bayrakdar et al., 2016; Can-Dogan et al., 2010; Mahmood et al., 2007). Anoxic bioreactors are more practically applicable than the aerobic ones in terms of ease of use and operational costs (Almenglo et al., 2016b; Fernández et al., 2014). Particularly, the use of aerobic bioreactors for biogas cleaning can cause various problems, including the dilution of biogas by oxygen. For safety reasons, it is also necessary to control the oxygen to methane ratio in order to avoid reaching explosive limits (Fernández et al., 2013).

Different bioreactor configurations have been operated under anoxic conditions for sulfide removal from liquid waste streams. Dolejs et al. (2015) studied sulfide removal using autotrophic denitrification in a continuous stirred tank reactor (CSTR) and reported that the sulfide removal efficiency decreased from 96% to 55% and the denitrification was completely inhibited when the CSTR was operated at a N/S ratio lower than 0.42. In another study using an activated sludge augmented with *T. denitrificans*, the $S_2O_3^{2-}$ removal efficiency became very unstable when the N/S ratio was decreased from 1.0 to 0.9 (Manconi et al., 2007). CSTRs are, however, susceptible to biomass wash-out and therefore require a high solid retention time (SRT) resulting in larger reactor volumes than biofilm systems, which can efficiently retain biomass (Di Capua et al., 2015; Papirio et al., 2013). Biofilm systems, e.g. fluidized bed reactors (FBR), have been widely used for sulfide removal under aerobic and micro-aerobic conditions (Annachhatre and Suktrakoolvait, 2001; Krayzelova et al., 2015; Krishnakumar et al., 2005; Midha et al., 2012). Using oxygen as an electron acceptor can cause the formation of polysulfides as well as mass transfer limitations of oxygen and sulfide to the immobilized biomass (Krishnakumar et al., 2005). Recently, FBRs have been extensively studied for NO_3^- removal using RSCs as electron donors at different temperatures and pH conditions (Di Capua et al., 2017c, 2017a; Zou et al., 2016).

Sulfide-oxidizing, nitrate-reducing (SO-NR) bacteria such as *Thiobacillus denitrificans* and *Sulfurimonas denitrificans* can oxidize sulfide and other RSCs such as elemental sulfur (S^0) and thiosulfate ($S_2O_3^{2-}$) by using NO_3^- as electron acceptor in the absence of oxygen (Di Capua et al., 2016a; Manconi et al., 2007). The stoichiometry of anoxic HS^- and $S_2O_3^{2-}$ oxidation by SO-NR bacteria is represented by the following reactions (Mora et al., 2014a, 2014c):

$$HS^- + 1.23NO_3^- + 0.573H^+ + 0.027CO_2 + 0.438HCO_3^- + 0.093NH_4^+ \rightarrow SO_4^{2-} + 0.614N_2 + 0.866H_2O + 0.093C_5H_7O_2N \quad (3.1)$$

$$S_2O_3^{2-} + 1.16NO_3^- + 0.124H_2O + 0.035CO_2 + 0.519HCO_3^- + 0.11NH_4^+ \rightarrow 2SO_4^{2-} + 0.578N_2 + 0.435H^+ + 0.110C_5H_7O_2N \quad (3.2)$$

The application of artificial neural networks (ANNs) for modeling non-linear bioprocesses is effective in evaluating the performance of biological waste gas treatment systems, particularly biofilters and biotrickling filters (Nair et al., 2016; Rene et al., 2011). Recently, ANNs have been used to predict FBR performance in various applications, i.e. treatment of sulfate-rich wastewaters and heap bioleaching solutions (Janyasuthiwong et al., 2016; Midha et al., 2013; Ozkaya et al., 2008; Reyes-Alvarado et al., 2017). The ANN model was for example successfully applied to predict the removal efficiencies of SO_4^{2-} and COD, and S^{2-} production in a biological SO_4^{2-} reduction process with a network topology

of 5-11-3 (Reyes-Alvarado et al., 2017). The authors also carried out a sensitivity analysis in order to ascertain the relationship between the input parameters and their effects on the outputs, which showed that the influent pH mainly affected the sulfidogenic process.

Previous studies have shown that the nitrogen to sulfur (N/S) ratio is one of the key operational factors for anoxic sulfide-oxidizing bioreactors, since it affects the metabolism of the sulfide-oxidizing bacteria and the ratio of the end-products formed during sulfide oxidation, i.e. S^0 and sulfate (SO_4^{2-}) (Bayrakdar et al., 2016; Dolejs et al., 2015; Moraes et al., 2012). These studies, however, did not test the long-term performance and microbial community evolution under different N/S ratios, neither used ANN modeling to evaluate the performance and relationship of the process variables of anoxic H_2S or $S_2O_3^{2-}$ oxidation. In this study, $S_2O_3^{2-}$ was used as the model sulfur compound for H_2S due to be the first intermediate formed by SO-NR bacteria during H_2S oxidation and its high solubility which is easier to handle in laboratory-scale experiments compared to H_2S (Luo et al., 2013).

The objective of this study was to evaluate the long-term performance of an FBR for $S_2O_3^{2-}$ oxidation using NO_3^- as the electron acceptor at different N/S ratios (0.5, 0.3 and 0.1) using the following tests: (1) the resilience of the FBR to long-term NO_3^- limiting conditions by operating at an extreme low N/S ratio (N/S ratio 0.1) for over 40 days; (2) batch activity tests to evaluate the kinetic parameters of the immobilized biomass under steady-state at each studied N/S ratio; (3) polymerase chain reaction-denaturing gradient gel electrophoresis (PCR-DGGE) to study the evolution of the microbial community in the FBR biofilms and (4) ANN modeling to predict the $S_2O_3^{2-}$ and NO_3^- removal efficiencies and SO_4^{2-} concentration in the FBR for $S_2O_3^{2-}$ oxidation, while the modelled data was subjected to a sensitivity analysis to determine the key parameters affecting the $S_2O_3^{2-}$ and NO_3^- removal efficiencies.

3.2 Materials and methods

3.2.1 Medium preparation

The mineral medium used in this study was composed of $Na_2S_2O_3$ (470 g L^{-1}), KNO_3, (72-280 g L^{-1}), $NaHCO_3$ (1 g L^{-1}), KH_2PO_4 (2 g L^{-1}), NH_4Cl (1 g L^{-1}), $MgSO_4 \cdot 7H_2O$ (0.8 g L^{-1}), $FeSO_4 \cdot 7H_2O$ (2 g L^{-1}) and 2 mL L^{-1} of a trace element solution as described by Zou et al. (2016). The influent pH was adjusted to 7.0 using 37% HCl. All chemicals used in this study were of laboratory grade.

3.2.2 Experimental set-up and operating conditions

The lab-scale FBR (Figure 3.1) had an empty bed volume of 0.58 L and a height of 40 cm, similar to the configuration described by Zou et al. (2016). The reactor was operated at a hydraulic retention time (HRT) of 5 h and at room temperature (20 ± 2 °C). Filtrasorb®200 granular activated carbon (GAC) (Calgon Carbon, USA) was used as the carrier material. The expansion of the reactor bed was maintained at 20-25% of the bed height. The FBR was previously operated for 705 days to study thiosulfate-driven denitrification at different nitrogen loading rates (NLR) (Zou et al., 2016), pH and temperature (Di Capua et al., 2017c, 2017a). The influent tank was connected to a Tedlar gasbag filled with N_2 to prevent oxygen diffusion into the tank and to maintain the dissolved oxygen (DO) concentration as low as possible.

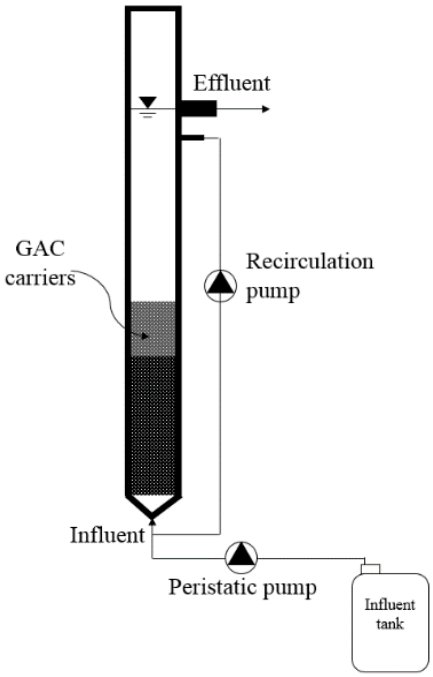

Figure 3.1. Schematic of a fluidized bed reactor used in this study.

In this study, $S_2O_3^{2-}$ and NO_3^- removal efficiencies were evaluated under three different N/S molar ratios (0.5, 0.3 and 0.1) for 306 days (Table 3.1). The FBR operation was divided into four experimental periods in which the influent $S_2O_3^{2-}$ concentration was maintained at 200 mg $S_2O_3^{2-}$-S L^{-1}, whereas the influent NO_3^- concentration was decreased stepwise from 40 mg NO_3^--N L^{-1} (N/S 0.5, period I) to 20 (N/S 0.3, period II) and 10 mg NO_3^--N L^{-1} (N/S 0.1, period III), respectively. During period IV, the N/S ratio was increased to 0.5 in order to evaluate the recovery of the $S_2O_3^{2-}$ oxidation efficiency after a 42-day starvation period at a N/S ratio of 0.1. Steady-state conditions in each period of FBR operation were assumed when the relative standard deviation (%RSD) of the

$S_2O_3^{2-}$ removal efficiency was <10%. The loading rate (LR), removal efficiency (RE) and volumetric removal rate (VRR) of $S_2O_3^{2-}$ and NO_3^- in the FBR were estimated using the following equations:

$$\text{LR (mg L}^{-1}\text{ d}^{-1}) = \frac{C_{in} \times Q}{V} \quad (3.3)$$

$$\text{RE (\%)} = \frac{C_{in} - C_{out}}{C_{out}} \times 100 \quad (3.4)$$

$$\text{VRR (g L}^{-1}\text{ d}^{-1}) = LR \times \frac{RE\ (\%)}{100} \quad (3.5)$$

where C_{in} and C_{out} are influent and effluent concentrations of NO_3^- (mg NO_3^--N L^{-1}) or $S_2O_3^{2-}$ (mg $S_2O_3^{2-}$-S L^{-1}), respectively.

Table 3.1. Operational conditions and performance of the FBR during the four operation periods

Parameters	Period I	Period II	Period III	Period IV
Steady-state duration (days)	101-115	188-207	235-249	292-306
Effluent pH	6.84 ± 0.16	7.11 ± 0.05	7.30 ± 0.05	7.18 ± 0.05
Influent NO_3^--N (mg L^{-1})	38.7 ± 10	27.9 ± 1.3	10.7 ± 0.4	39.8 ± 0.8
NO_3^--N loading (mg L^{-1} d^{-1})	173 ± 10	125 ± 6	48 ± 2	178 ± 7
NO_3^--N removal efficiency (%)	100	100	100	100
Influent $S_2O_3^{2-}$-S (mg L^{-1})	184 ± 19	188 ± 11	193 ± 7	183 ± 7
$S_2O_3^{2-}$-S loading (mg L^{-1} d^{-1})	822 ± 84	836 ± 54	862 ± 30	817 ± 29
$S_2O_3^{2-}$-S removal rate (mg L^{-1} d^{-1})	814 ± 80	642 ± 55	187 ± 94	660 ± 52
$S_2O_3^{2-}$-S removal efficiency (%)	99.1 ± 0.9	76.3 ± 2.7	26.0 ± 2.0	80.8 ± 4.1
SO_4^{2-}-S concentration in the effluent (mg L^{-1})	245 ± 19	192 ± 10	74 ± 22	225 ± 20
Influent N/S ratio	0.49 ± 0.03	0.34 ± 0.03	0.13 ± 0.00	0.50 ± 0.02
Consumed N/S ratio	0.49 ± 0.03	0.45 ± 0.05	0.49 ± 0.06	0.62 ± 0.06

3.2.3 Batch activity tests

Batch activity tests were performed in duplicate in order to measure the specific uptake rate of $S_2O_3^{2-}$ and to determine the affinity of the biomass to $S_2O_3^{2-}$. For each test, 10-mL of biofilm-coated GAC was collected from the FBR during steady-state conditions of experimental periods II, III and IV (on days 196, 244 and 305) and used in three separate batch activity tests (tests A, B and C). A sample of 400 (± 50) mg VSS L^{-1} biomass was added to 120 mL serum bottles with 40 mL headspace. The medium used in these batch assays was the same as in the FBR experiment. The batch bottles were placed on a HS 501 horizontal shaker (IKA, USA) with 220 rpm mixing and maintained at 20 (± 2) ˚C.

The initial concentrations of $S_2O_3^{2-}$ and NO_3^- used in the batch activity tests are reported in Table 3.2. $S_2O_3^{2-}$ oxidation coupled to NO_3^- reduction was described using the Haldane model (Eq. 3.6). Besides a Haldane term describing the potential substrate inhibition by $S_2O_3^{2-}$, a Michaelis-Menten term was also considered to take into account NO_3^- limitation (Eq. 3.6).

$$r_S = \frac{r_{max_S} \times S}{K_s + S + \frac{S^2}{K_I}} \times \frac{N}{K_n + N} \quad (3.6)$$

where S, K_s and K_I are the concentration, half-saturation constant and inhibition constant for $S_2O_3^{2-}$ (mg S L^{-1}), respectively, N and K_n are the concentration and half-saturation constant for NO_3^- (mg N L^{-1}), respectively, and r_{max_S} is the maximum specific uptake rate for $S_2O_3^{2-}$ (mg S g VSS^{-1} h^{-1}).

Table 3.2. Experimental conditions of batch activity tests and the obtained Haldane kinetic coefficients of the nitrate reducing, sulfide oxidizing bacteria taken from the FBR at different N/S ratios

		Initial concentrations		Kinetic coefficients			
Test	N/S ratio	$S_2O_3^{2-}$ (mg $S_2O_3^{2-}$-S L^{-1})	NO_3^- (mg NO_3^--N L^{-1})	r_{max} (mg $S_2O_3^{2-}$-S g^{-1} VSS h^{-1})	K_S (mg $S_2O_3^{2-}$-S L^{-1})	K_I (mg $S_2O_3^{2-}$-S L^{-1})	K_n (mg NO_3^--N L^{-1})
A	0.3	50, 90 180, 200, 300, 550	7, 14, 30, 45, 65	145.8	21.8	466.1	4.53
B	0.1	50, 90, 200, 300, 550	2, 4, 8, 12, 25	331.3	171.9	247.7	0.25
C	0.5	50, 90, 200, 300, 550	9, 20, 40, 70, 160	127.0	45.1	798.6	6.32

3.2.4 Residence time distribution (RTD) test

The RTD test was conducted at the end of the FBR experiments in order to determine the hydrodynamic behavior of the FBR. A tracer, 10-mL of a 1 M KCl solution, was pulse injected into the influent stream. During the test, the conductivity of the effluent was measured using a Multiparameter inoLab Multi Level 1 meter equipped with a KLE 325 probe (WTW, Germany). In order to validate the RTD test, two flow rates of 360 and 108 mL h^{-1} were applied. The hydrodynamic behavior of the FBR was determined using Eqs. 3.7-3.9. The Morrill Dispersion Index (MDI) (Eq. 3.10) was used to evaluate the flow characteristics in the FBR.

$$\text{RTD function } (E(t)) = \frac{C_i}{\sum C_i \Delta t_i} \quad (3.7)$$

Mean residence time $(t_m) = \frac{\sum t_i C_i \Delta t_i}{\sum C_i \Delta t_i}$ (3.8)

Experimental amount of outlet tracer $= \sum C_i \Delta t_i$ (3.9)

MDI $= \frac{t_{90}}{t_{10}}$ (3.10)

where C_i is KCl concentration in the effluent (mg L^{-1}), t_i is the measuring time (h), t_{90} and t_{10} are times when 90% and 10% of the tracer passes through the FBR, respectively.

3.2.5 Analytical techniques

The liquid samples collected from the FBR and batch bottles were filtered through 0.45 µm Chromafil Xtra PET-202125 membrane syringe filters (Mechery-Nagel, Germany) prior to the measurement of nitrite (NO_2^-), NO_3^-, $S_2O_3^{2-}$ and SO_4^{2-} concentrations by ion chromatography (IC) as described by Di Capua et al. (2017c). The total dissolved sulfide in the FBR effluent was measured using the Cord-Ruwisch method (Cord-Ruwisch, 1985). The pH of the FBR influent and effluent was measured using a pH 3110 portable meter fitted with a SenTix 21 electrode (WTW, Germany). The DO concentration was measured directly in the FBR using a HQ40d portable multimeter equipped with an Intellical™ LDO101 probe (HACH, USA). Alkalinity and volatile suspended solid (VSS) concentrations of the FBR biofilm were measured according to the procedures described in Standard Methods (APHA/AWWA/WEF, 1999). To prepare the biomass for the VSS measurement, two samples of 1 mL GAC were mixed in a 15 mL Falcon tube with deionized (DI) water to detach the biofilm from GAC by manual shaking. Subsequently, the liquid portion containing the detached biomass was used to measure the VSS concentration. This procedure was repeated until all biofilm was detached from the GAC based on visual observation.

The concentration of S^0 in the biofilm-coated GAC was estimated by modified cyanolysis (Kelly and Wood, 2000). Deionized water containing the cells detached from 1 mL of GAC by manual shaking was mixed with 10 mL of acetone. 200 µL of the obtained solution was mixed with 100 µL of 100 mM KCN and incubated at room temperature (20 ± 2 °C) for 10 min. After incubation, 500 µL of PO_4^{3-} buffer solution (containing 50 ml of 0.2 M NaH_2PO_4 and 39 ml of 0.2 M NaOH) and 100 µL of 1.5 M $Fe(NO_3)_3$ in 4 M $HClO_4$ were added to the mixture. After centrifugation for 1 min at 14,000 rpm, the optical density (OD) of the supernatant was measured using a UV-1601 spectrophotometer (Shimadzu, Japan) at a wavelength of 460 nm.

3.2.6 Microbial community analysis

The microbial community of the FBR biofilm was analyzed by polymerase chain reaction denaturing gradient gel electrophoresis (PCR-DGGE) followed by sequencing. Two samples of 1 mL of biofilm-coated GAC were collected from the FBR during steady-state operations of each experimental period (days 114, 196, 242 and 306), and sonicated for 2 min in sterile de-ionized water to detach all the bacterial cells from the carrier material. The solution containing the microorganisms was filtered through a Cyclopore track etched 0.2 µm membrane (Whatman, USA), and the biomass samples collected on the filters were stored at -20 ºC for further analysis.

DNA was extracted from the defrosted filters using a PowerSoil® DNA isolation kit (MO BIO Laboratories, Inc., USA) according to the manufacturer's instructions. A primer pair Bac357F-GC and Un907R was used for amplifying the partial bacterial 16S rRNA genes by using a T3000 thermalcycler (Biometra, Germany) as described by Kolehmainen et al. (2007). DGGE was performed with a INGENY phorU2 × 2 - system (Ingeny International BV, GV Goes, The Netherlands) as reported by Kolehmainen et al. (2007). The amplified samples were sequenced by Macrogen (South Korea). The obtained sequences were analyzed using the Bioedit software (version 7.2.5, Ibis Biosciences, USA) and compared with the sequences available at the National Center for Biotechnology Information (NCBI) database (http://blast.ncbi.nlm.nih.gov).

3.2.7 ANN model development

The ANN modeling was performed using the Neural Net Fitting application in the Neural Network Toolbox 11.0 of MATLAB® R2017b (MathWorks Inc., USA). The multilayer perceptron described in Figure 3.2 was a feed-forward network in which the neurons in the input layer received the normalized input signals and passed those signals to the hidden layer after multiplying them with the respective connection weights. A tan-sigmoidal transfer function was used in the hidden layer, while a linear (PURELIN) transfer function was used in the output layer, respectively.

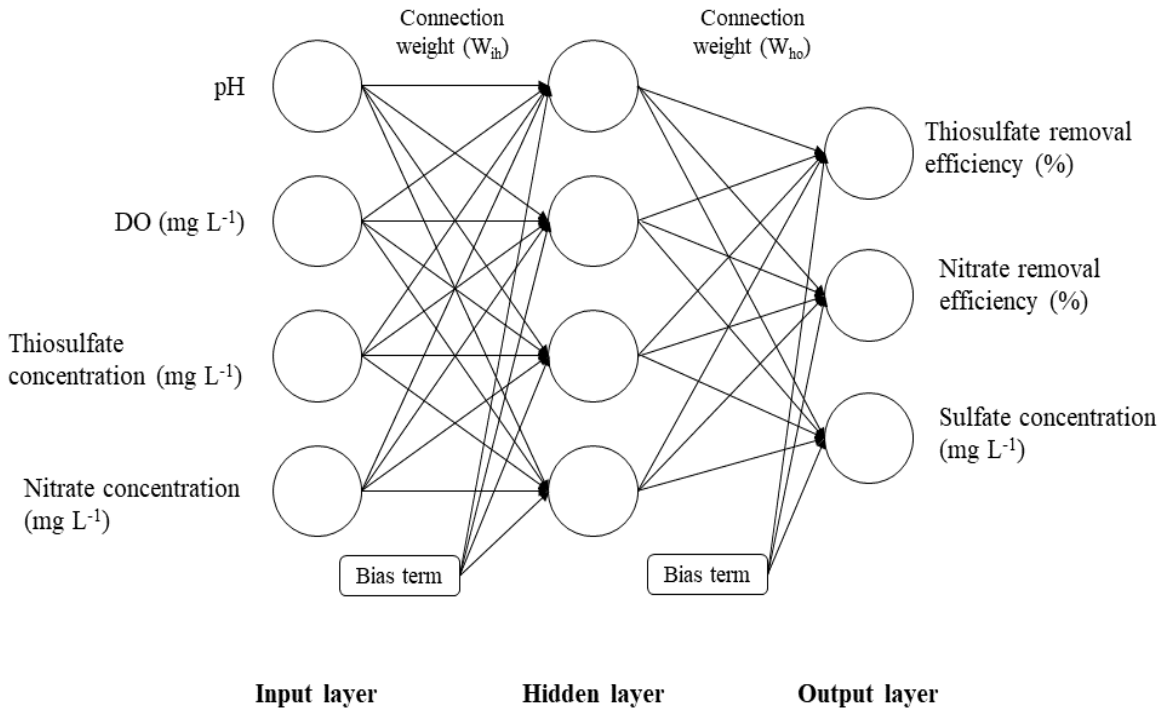

Figure 3.2. Architecture of a multilayer perceptron used for predicting the fluidized bed reactor performance by artificial neural network (input-hidden-output = 4-4-3)

The inputs to the ANN model consisted of pH, DO, influent concentrations of $S_2O_3^{2-}$ ($S_2O_3^{2-}{}_{in}$) and NO_3^- ($NO_3^-{}_{in}$), respectively, while the ANN outputs were $S_2O_3^{2-}$ ($S_2O_3^{2-}$-RE) and NO_3^- (NO_3^--RE) removal efficiencies and SO_4^{2-} production ($SO_4^{2-}{}_{ef}$), respectively. Table 3.3 shows the basic statistics of the training, validation and test data used to develop the ANN model. In order to suit the transfer function and avoid outliers, the raw input and output data were normalized to the range of 0-1, according to Eq. (3.11). The experimental data (days 45-306) was randomly divided into training (70%), validation (10%) and testing (20%) sample sets.

$$\hat{X} = \frac{X - X_{min}}{X_{max} - X_{min}} \tag{3.11}$$

where $\hat{X}$ is the normalized value, X_{min} and X_{max} are the minimum and maximum values of X, respectively.

Table 3.3. Basic statistics of the training, validation and test data used to develop the artificial neural network model

	Mean	Minimum	Maximum
Dissolved oxygen in the FBR	0.25	0.16	0.40
pH	7.13	6.60	7.57
Influent $S_2O_3^{2-}$ concentration, $S_2O_3^{2-}{}_{in}$ (mg L^{-1})	333.52	267.50	374.94
Influent NO_3^- concentration, $NO_3^-{}_{in}$ (mg L^{-1})	138.02	44.88	194.30
$S_2O_3^{2-}$ removal efficiency, $S_2O_3^{2-}$-RE (%)	77.35	22.25	100.00
NO_3^- removal efficiency, NO_3^--RE (%)	99.99	99.00	100.00
Effluent SO_4^{2-} concentration, $SO_4^{2-}{}_{ef}$ (mg L^{-1})	591.44	186.48	839.48

The ANN was trained using the Levenberg-Marquardt back-propagation algorithm (*trainlm* function), while the mean squared error (MSE) and regression analysis were used for estimating the error between the model fitted and the experimental data. The strength of the relationship between the output and input variables was evaluated by sensitivity analysis, which was performed using the shareware version of the multivariable statistical modelling software, NNMODEL (PA, USA).

3.2.8 Data analysis

The statistical analysis of the data was performed using the Minitab 16 software. The one-way analysis of variance (ANOVA) was conducted in order to compare the pH, DO, $S_2O_3^{2-}$ and NO_3^- concentrations and the respective removal efficiencies and SO_4^{2-} production at the steady-state of each operational period. The significant level was set at 95% ($P \leq 0.05$). To determine the kinetic parameters, the Haldane equation (Eq. 3.6) was applied using the non-linear programming solver (fminsearch) in MATLAB® R2017b (MathWorks Inc., USA) in order to optimize the experimental data using r_{max_S}, K_s, K_I and K_n as the optimization variables.

3.3 Results

3.3.1 FBR performance

Figure 3.3 shows the profiles of effluent pH, NO_3^-, NO_2^-, $S_2O_3^{2-}$, SO_4^{2-} and DO concentration during the 306 days of operation. The influent pH was maintained at 6.9 (± 0.1). The consumed N/S ratio slightly fluctuated but remained close to 0.5, while the alkalinity consumption varied in the range of 25 to 145 mg HCO_3^- L^{-1} during the entire FBR operation. NO_2^- was never detected in the effluent during the study. During the entire experiment, the VSS concentration of the FBR biofilm was relatively constant, being 21.7 (±

4.9) g VSS L^{-1} of GAC, based on measurements conducted on days 0, 60, 114, 196, 242 and 306. S^0 was visually observed on the GAC carrier as white particles and its concentration showed an increasing trend as the feed N/S ratios were deceased. The measured S^0 concentration of the biofilm-coated GAC was approximately 9, 13 and 26 mg L^{-1} on days 200, 240 and 300, respectively.

During period I (N/S ratio of 0.5), the loading rates of $S_2O_3^{2-}$ and NO_3^- were 820 (± 84) mg $S_2O_3^{2-}$-S L^{-1} d^{-1} and 173 (± 10) mg NO_3^--N L^{-1} d^{-1}, respectively. During the first 38 days of operation, the concentrations of $S_2O_3^{2-}$, SO_4^{2-} and DO in the FBR effluent were not stable (Figure 3.3). Therefore, the DO concentration in the reactor was decreased from 0.43 (± 0.07) (days 0-38) to 0.25 (± 0.05) (days 39-306) mg L^{-1} by connecting a N_2 gasbag to the influent tank. During steady-state operation of period I (days 101-115), $S_2O_3^{2-}$ and NO_3^- removal efficiencies were 99% and 100%, respectively, with SO_4^{2-} as the main end-product. The volumetric removal rate of $S_2O_3^{2-}$ was 810 (± 80) g $S_2O_3^{2-}$-S L^{-1} d^{-1} and the effluent SO_4^{2-} concentration was 740 (± 60) mg L^{-1}, 35% higher than the theoretical value in period I (550 mg L^{-1}) calculated according to Eq. (3.2). The effluent pH during period I was 6.8 (± 0.2).

During periods II (N/S ratio 0.3) and III (N/S ratio 0.1), the feed NO_3^- loading rate was decreased from 175 (period I) to 125 and 50 g NO_3^--N L^{-1} d^{-1}, respectively (Table 3.1). NO_3^- was completely consumed in both periods II and III, whereas the $S_2O_3^{2-}$ removal efficiency decreased to 76% in period II and further to 26% in period III (under steady-state operation), resulting in effluent SO_4^{2-} concentrations of 580 (± 30) and 200 (± 15) mg L^{-1}, respectively. The effluent pH gradually increased from 6.8 (± 0.2) (period I) to 7.1 (± 0.1) and 7.3 (± 0.1) in periods II and III, respectively. During period III (N/S ratio 0.1), biofilm detachment from the GAC was also visually observed.

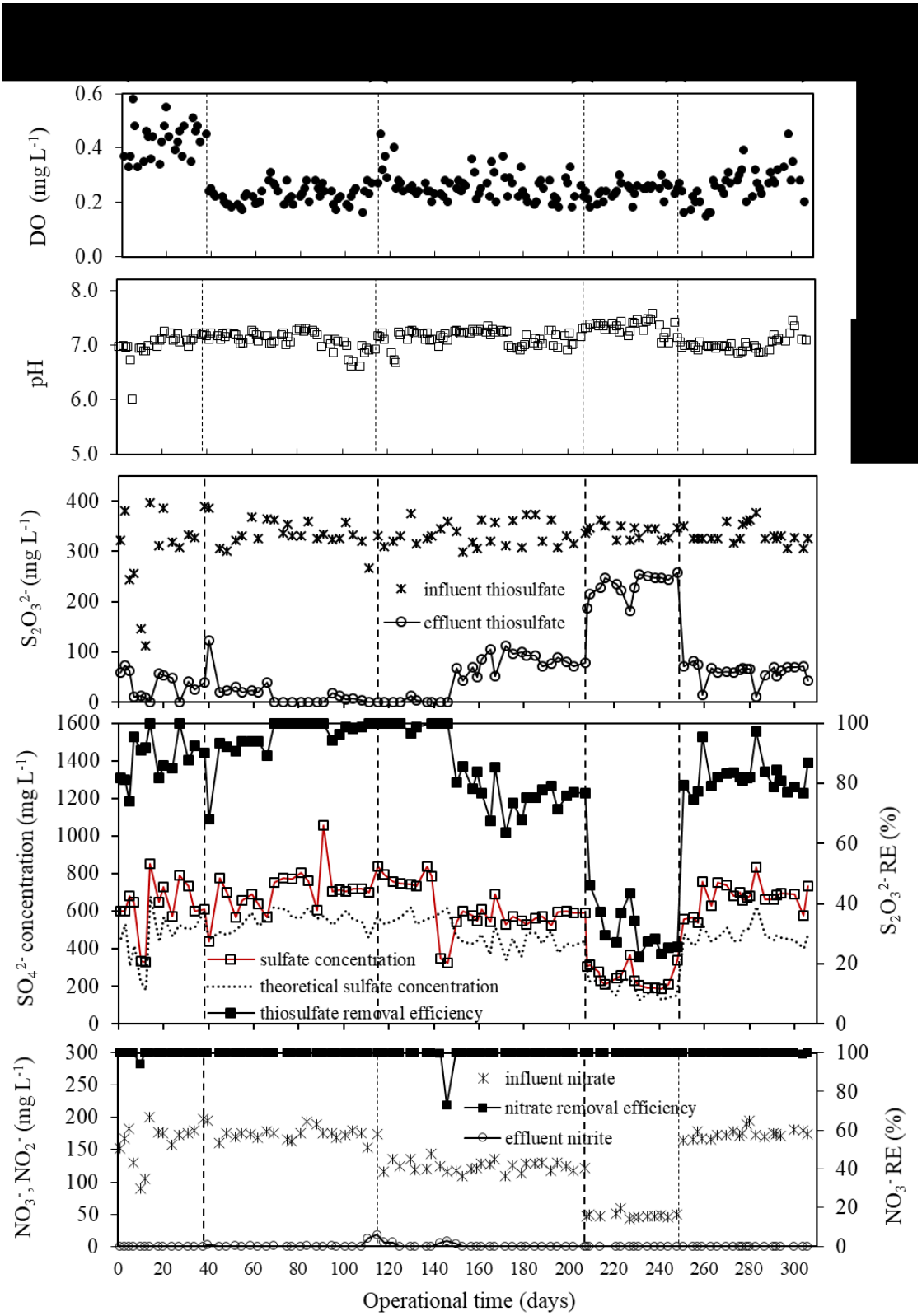

Figure 3.3. Time course profiles of dissolved oxygen, pH, $S_2O_3^{2-}$ removal efficiency (RE) in the fluidized bed reactor and influent and effluent concentrations of NO_3^-, NO_2^- and SO_4^{2-}.

During period IV, the N/S ratio was increased to 0.5 as in period I. As a result, the $S_2O_3^{2-}$ removal efficiency increased from 26% in period III to 80% in period IV in 3 days. Although the $S_2O_3^{2-}$ removal efficiency in period IV was 20% lower than in period I, the SO_4^{2-} concentration in the effluent (680 ± 60 mg L^{-1}) was only 8% lower than in period I. During period IV, the effluent pH was 7.2 (± 0.1), higher than the one measured at the same N/S ratio in period I.

3.3.2 Batch activity tests

Figure 3.4 shows the maximum specific uptake rate, half-saturation and inhibition constants for $S_2O_3^{2-}$ (r_{max}, K_s and K_I, respectively) estimated from the batch activity tests A, B and C (Table 3.2). The highest half-saturation constant, K_n, for NO_3^- reduction was 6.32 mg NO_3^--N L^{-1} and was obtained with the SO-NR bacteria cultivated during period IV (N/S ratio of 0.5). The biomass taken during period III (N/S ratio 0.1) showed the lowest K_I for $S_2O_3^{2-}$ oxidation, while it was the highest with the biomass taken at a N/S ratio of 0.5 (period IV). The $S_2O_3^{2-}$ removal efficiencies obtained in tests A, B and C were 84.5 (± 12.8)%, 26.3 (± 3.5)% and 91.6 (± 8.4)%, respectively (data not shown). NO_2^- was found as an intermediate of the process, but no NO_2^- was detected at the end of the batch activity tests (data not shown).

3.3.3 Hydrodynamic flow characteristics of the FBR

The RTD curves of the FBR at the flow rates of 360 and 108 mL h^{-1} are shown in Figure 3.5. The mass recovery of KCl used as a tracer was 90%. Most of the tracer was washed out within 1 and 2 h at flow rates of 360 and 108 mL h^{-1}, respectively, while the rest of the tracer was slowly removed (Figure 3.5). The results obtained from the RTD curves indicated that the effective mean residence time in the FBR at flow rates of 360 and 108 mL h^{-1} were 2.1 and 6.7 h, respectively. The computed MDI values (MDI = 9 and 11) for the two flow rates described the hydraulic regime in the FBR as semi-complete mixing. In the case of an effective plug flow, the MDI has a value of 2 or less, whereas the value for a completely mixed system is 22 (Metcalf & Eddy Inc. et al., 2014).

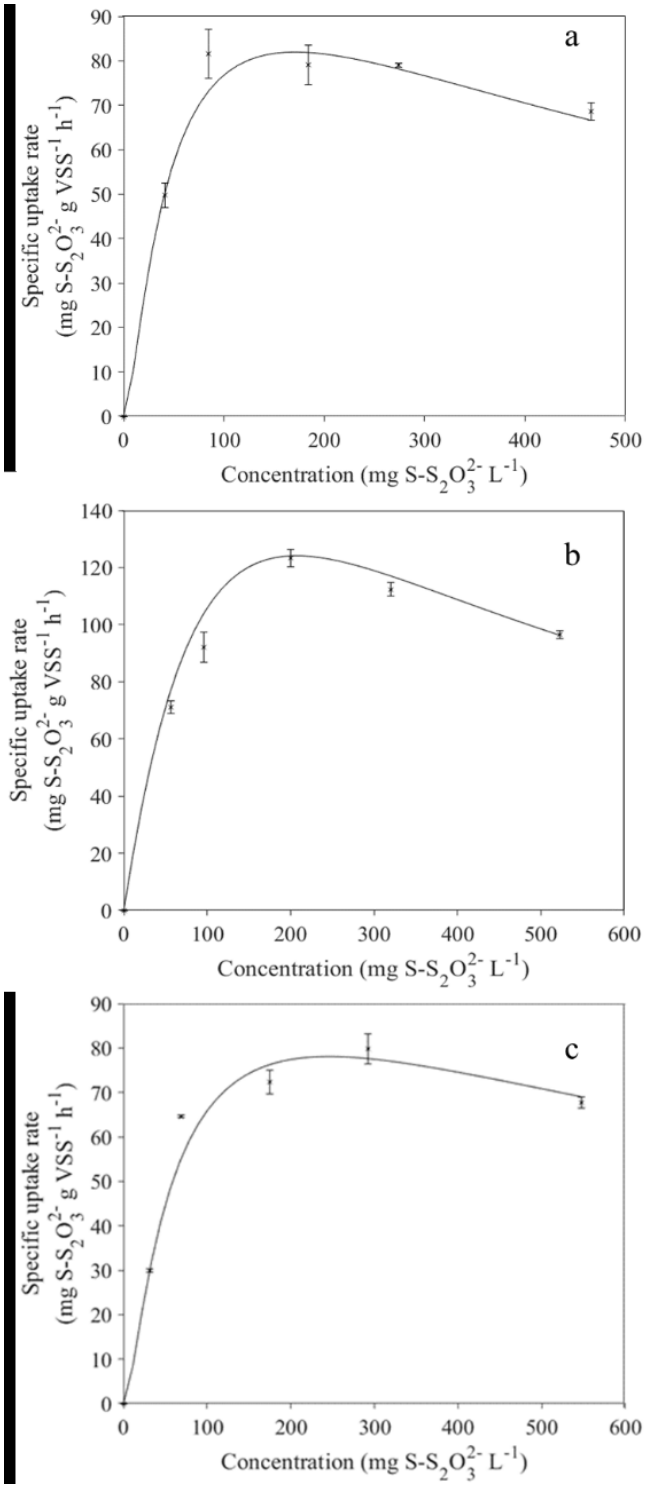

Figure 3.4. Haldane plots of thiosulfate uptake rate from batch activity tests at different N/S ratios: (a) 0.3, (b) 0.1 and (c) 0.5. Dots and lines represent experimental and model fitted data, respectively. The error bars indicated the standard error between the experimental and model fitted data.

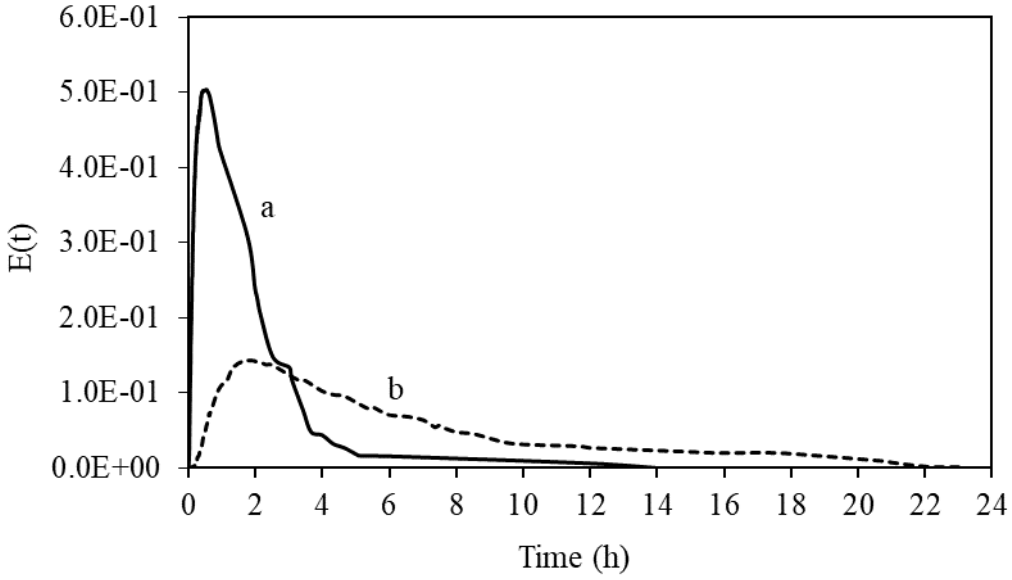

Figure 3.5. The residence time distribution (RTD) curves for the FBR at flow rates of (a) 360 and (b) 108 mL h^{-1}.

3.3.4 Microbial community profiling in the FBR

The microbial community profiles of the FBR biofilm during periods I, II, III and IV showed that operation at different N/S ratios resulted in changes in the microbial community composition (Figure 3.6). Based on the affiliations of the nucleotide sequences obtained from the BLAST analysis, 8 of the 15 sequenced bands were identified as known facultative autotrophic sulfide-oxidizing bacteria (Table 3.4, bands 1, 6-10, 12 and 13). The closest relatives of the known bacteria were *T. denitrificans* (band 8, 99% similarity) and *T. thioparus* (bands 6 and 7, 92-99.8% similarity). Bands 1 and 9 were also detected as a *Thiobacillus* genus; however, the sequence results were shown as uncultured representative of the genus with no species-level information. During period IV (N/S ratio 0.5), the band representing *T. denitrificans* (band 8) faded away and was replaced by bands identified as *T. thioparus* (bands 6 and 7). The band associated to *Thiomonas* sp. (band 13) and uncultured *Sulfuritalea* (band 12) showed a higher intensity at N/S ratios of 0.3 and 0.1 than at a N/S ratio of 0.5. The chemo-organotrophic *Flavobacteriaceae* (bands 2 and 3), *Chryseobacterium* sp. (band 4) and *Simplicispira* sp. (band 10) were detected at all N/S ratios tested. Additionally, *Desulfovibrio* sp. (band 14), a SO_4^{2-} reducing bacterium, was detected in the FBR biofilm throughout the entire experiment.

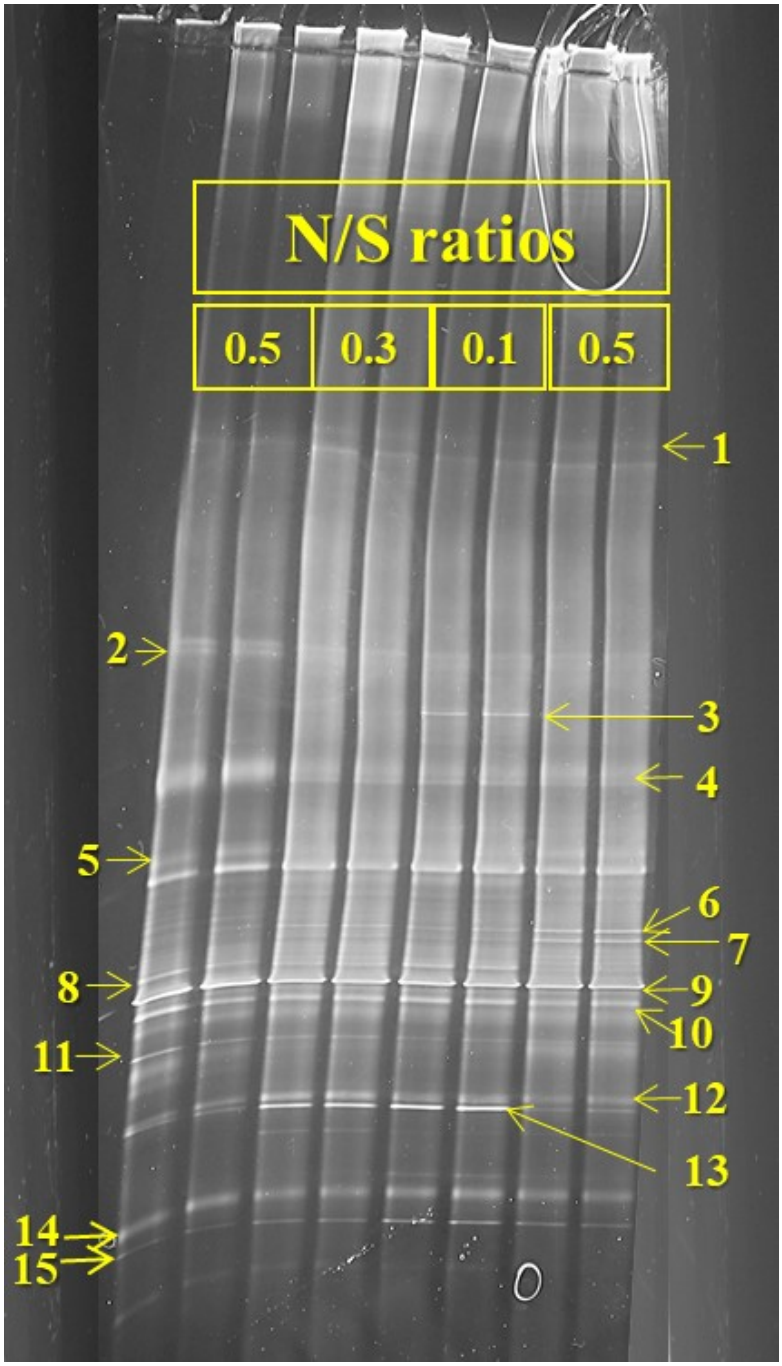

Figure 3.6. Microbial community profiling of the fluidized bed reactor biofilm at different N/S ratios. Two duplicate samples were analyzed from each operational period. The affiliations of the bands are given in Table 3.4.

Table 3.4. Identification of the microorganisms in the FBR biofilm based on the denaturing gradient gel electrophoresis band sequences (16S rDNA).

Band label	Affiliation (sequence ID)	Matching length	Similarity (%)	Bacterial class
1	Uncultured *Thiobacilus* sp. (FJ933304.1)	425	92.0	β-Proteobacteria
2, 3	Uncultured *Flavobacteriaceae* bacterium (EU642061.1)	433-434	91.3-99.3	Flavobacteriales
4	Uncultured *Chryseobacterium* sp. (JQ724349.1)	437	99.3	Flavobacteriales
5	Uncultured bacterium partial 16S rRNA gene, isolate EFW618 (LN889996.1)	463	96.1	
6, 7	*Thiobacillus thioparus* (HM535225.1)	456-474	99.4-99.8	β-Proteobacteria
8	*Thiobacillus denitrificans* (NR_025358.1)	431	99.1	β-Proteobacteria
9	Uncultured *Thiobacilus* sp. (KM200026.1)	451-453	99.1-99.8	β-Proteobacteria
10	*Simplicispira* sp. Iso11-01 gene (AB795522.1)	437	98.6	β-Proteobacteria
11	Denitrifying bacterium (Y09967.1)	407	93.9	β-Proteobacteria
12	Uncultured sulfuritalea (JX493272.1)	488	97.6	β-Proteobacteria
13	*Thiomonas* sp. (LN864654.1)	467	98.9	β-Proteobacteria
14	*Desulfovibrio* sp. (JX828422.1)	429	99.3	δ-Proteobacteria
15	Uncultured bacterium clone QKAB4ZG071 (KJ707249.1)	404	94.8	

3.3.5 ANN modeling

Figure 3.7 shows the experimentally verified and ANN predicted profiles of the $S_2O_3^{2-}$ and NO_3^- removal efficiencies and SO_4^{2-} concentration. The network topology was obtained at the following settings of the internal network parameters: learning rate (1.0) and epoch size (10). The performance of the Levenberg-Marquardt back-propagation algorithm was achieved with a MSE of 0.006523, while the determination coefficient (R^2) of the training, validation, test and overall predicted data were 0.90, 0.95, 0.88 and 0.90, respectively. At the best network topology for the FBR as 4-4-3, the connection weights and the bias terms were obtained for the interconnections between the neurons in different layers of the multilayer perceptron (Table 3.5).

The sensitivity analysis of the ANN model was represented in terms of the absolute average sensitivity (AAS) and the average sensitivity (AS), as shown in Table 3.6. Table 3.6 shows that the removal efficiency of $S_2O_3^{2-}$ was affected by the effluent pH and DO concentrations with AAS values of 0.53 and 0.24, respectively. The removal efficiency of NO_3^- was affected by the influent $S_2O_3^{2-}$ and NO_3^- concentrations with AAS values of 0.54

and 0.36, respectively. Besides, the SO_4^{2-} production depended on the $S_2O_3^{2-}$ and DO concentrations.

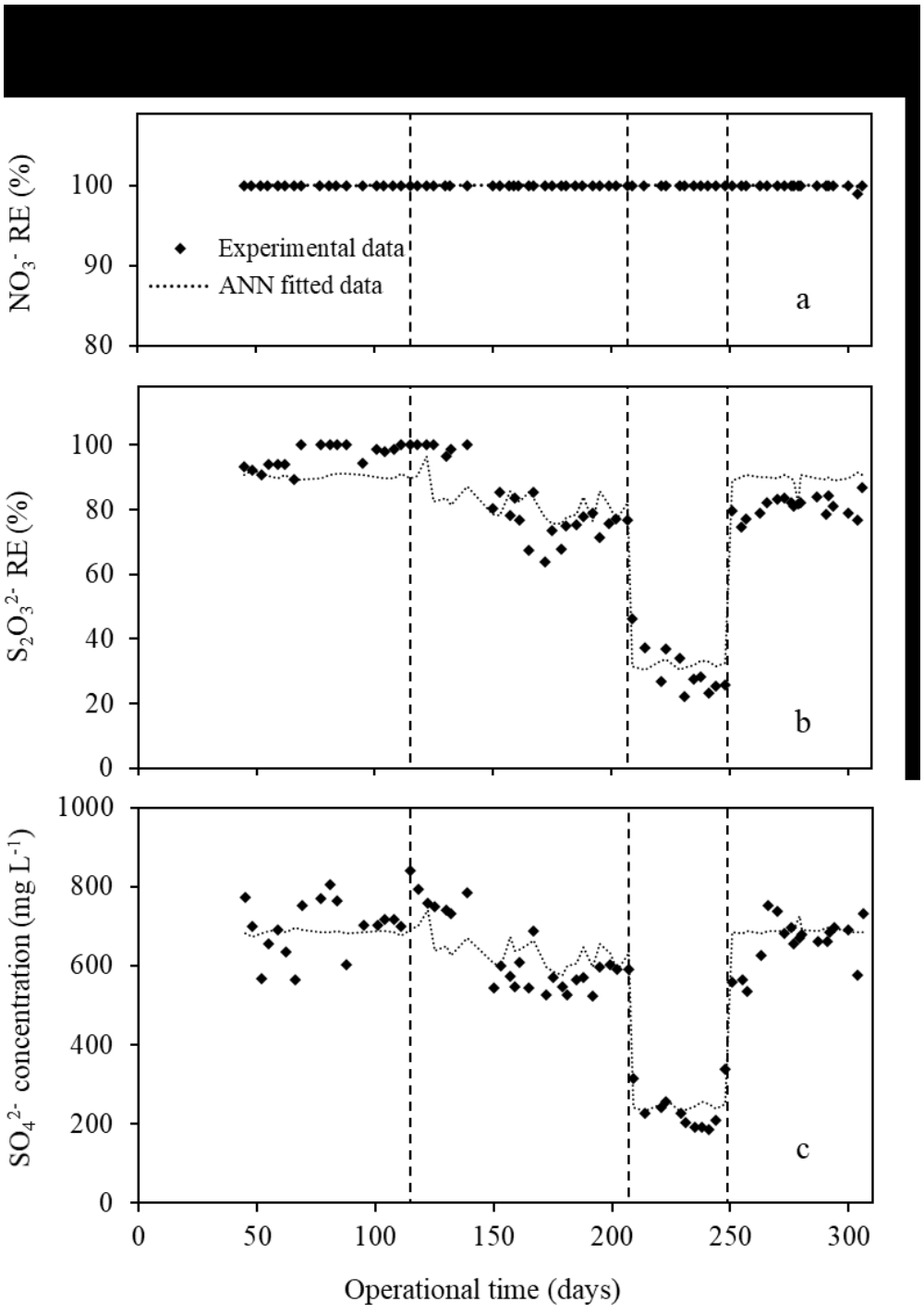

Figure 3.7. ANN model fitted data for (a) NO_3^- and (b) $S_2O_3^{2-}$ removal efficiency and (c) SO_4^{2-} concentration in the effluent. Dots and lines represent experimental and predicted model data, respectively.

Table 3.5. Connection weights between the input → hidden layers (W_{ih}), and the hidden → output layers (W_{ho}) of the artificial neural network model.

Model input	Input → hidden layers (W_{ih})				Hidden → output layers (W_{ho})			
	HID-1	HID-2	HID-3	HID-4		NO_3^--RE	$S_2O_3^{2-}$-RE	$SO_4^{2-}{}_{ef}$
DO	-1.3883	1.9379	-0.0189	-0.35864	HID-1	0.39572	0.42553	-0.12227
pH	-0.75667	-0.05606	0.48028	0.60495	HID-2	-0.34833	0.74721	0.52792
$S_2O_3^{2-}{}_{in}$	-0.31489	-1.2136	-0.24311	-0.79393	HID-3	0.00334	0.82527	0.76574
$NO_3^-{}_{in}$	-0.50078	-0.6068	2.2425	1.3638	HID-4	-0.63191	0.16955	-0.24917
Bias term	2.3203	-2.2994	0.69113	-2.5176	Bias term	-0.3693	0.4252	0.2072

Table 3.6. Sensitivity analysis of artificial neural network model inputs.

Model inputs	NO_3^--RE (%)		$S_2O_3^{2-}$-RE (%)		$SO_4^{2-}{}_{ef}$ (mg L^{-1})	
	AAS	AS	AAS	AS	AAS	AS
DO (mg L^{-1})	0.0758	+0.0758	0.2377	-0.2377	0.3606	-0.3606
pH	0.0290	+0.0290	0.5311	-0.5311	0.1167	+0.1167
$S_2O_3^{2-}{}_{in}$ (mg L^{-1})	0.5369	+0.5369	0.1456	-0.1456	0.359	+0.3590
$NO_3^-{}_{in}$ (mg L^{-1})	0.3583	-0.3583	0.0855	-0.0855	0.1637	-0.1637

Note: RE = removal efficiency; AAS and AS = absolute average sensitivity and average sensitivity, respectively

3.4 Discussion

3.4.1 Effect of NO_3^- limitation on FBR performance

This study showed that NO_3^- dosing can be used to remove sulfur compounds, i.e. $S_2O_3^{2-}$ as model for H_2S, from waste or scrubbing wasters. The SO-NR bacteria in the FBR showed high stability to $S_2O_3^{2-}$ oxidation at all N/S ratios tested, evidenced by the comparison between the fed and consumed N/S ratios during the entire experiment (Table 3.1). The consumed N/S ratio was close to 0.5 during periods I, II and III, while it slightly increased close to 0.6 during period IV (Table 3.1). During the latter period, the $S_2O_3^{2-}$ removal efficiency of the FBR decreased because NO_3^- was completely depleted over time (Figure 3.3).

The FBR showed high robustness and resiliency since the $S_2O_3^{2-}$ oxidation efficiency rapidly recovered after operating under extreme nitrate-limiting conditions (period III), i.e. N/S ratio 0.1 compared to the stoichiometric requirement of N/S ratio 0.6 as shown as Eq. (3.2) (Figure 3.3). Starvation periods have often been applied to test the robustness and resilience of bioreactors. Chen et al. (2016) applied a H_2S starvation period of 15 days in a two-layer biotrickling filter (BTF), observing an increase in H_2S removal efficiency from 65% to 99% during the 4 days starvation period. Recently, *Thiobacillus*-dominated FBR biofilms have shown extremely high sulfur oxidation and NO_3^- reduction rates even under extreme operational conditions, such as low temperature (<5°C) (Di Capua et al., 2017c), low pH of 5.0 (Di Capua et al., 2017a) and high heavy metal concentrations, i.e. 20-100 mg Ni L^{-1} (Di Capua et al., 2017b) or 86.6 mg Co L^{-1} (Zou et al., 2014). The high biomass concentrations of the FBR biofilm (Table 3.7) likely played an important role in providing resistance to substrate fluctuations during this study. However, the $S_2O_3^{2-}$ removal efficiency during period IV (N/S ratio 0.1) was about 20% lower than in period I at the same N/S ratio. The lower $S_2O_3^{2-}$ removal efficiencies observed during period IV could be attributed to the changes in the microbial community of the FBR biofilm, particularly *T. denitrificans* was absent (below detection limit of DGGE) in period IV (Figure 3.6, Table 3.4).

In this study, SO_4^{2-} was the main product of $S_2O_3^{2-}$ oxidation (Figure 3.3). The reduction of 1 g of NO_3^--N under $S_2O_3^{2-}$ oxidation produced 19.4 (± 1.8) g of SO_4^{2-} in the FBR effluent, which is 31% higher than the theoretical value of 11.8 g of SO_4^{2-} calculated according to Eq. (3.2). The excess of SO_4^{2-} in the FBR effluent could be attributed to two mechanisms. The facultative anaerobic sulfur oxidizing bacteria, i.e. *Thiobacillus* sp. and *Thiomonas* sp., populating the FBR biofilm can also use oxygen as electron acceptor to oxidize the S^0 accumulated in the bioreactor during previous operation (Di Capua et al., 2017a; Zou et al., 2016). Alternatively, the unexpectedly high SO_4^{2-} concentrations in the effluent could be due to sulfur disproportionation under anoxic conditions, which occurs as described by Eq. (3.12) (Finster et al., 1998):

$$4S^0 + 4H_2O \rightarrow 3H_2S + SO_4^{2-} + 2H^+ \quad (3.12)$$

During this study, S^0 was also measured and visually observed as white particles attached on the GAC carrier material of the FBR. Previous studies have reported the accumulation of S^0 during S^{2-} and $S_2O_3^{2-}$ oxidation both in bioreactors (Dolejs et al., 2015; Moraes et al., 2012) and batch bioassays (Beristain-Cardoso et al., 2006) as a result of electron donor overloading or NO_3^- starvation (Mora et al., 2014a). Besides, Sahinkaya et al. (2011) reported that low NO_3^- loading rates could promote biological sulfur disproportionation in anoxic reactor columns packed with S^0.

Table 3.7. Comparative analysis of various bioreactors performing sulfide or thiosulfate oxidation using autotrophic denitrification.

Type of reactor	Reactor volume, L	Microorganisms	Biomass concentration	Substrate	Feed S-compounds	S removal rate	N loading rate (mg NO_3^--N L^{-1} d^{-1})	Operational N/S ratios (mol mol^{-1})	HRT (h)	References
GSAD	30	Mixed culture of autotrophic & heterotrophic denitrifying bacteria	7 g VSS L^{-1}	Dissolved sulfide (TDS)	100-150 mg TDS L^{-1}	0.18 - 0.63 (g S L^{-1} d^{-1})	90-330	0.5-0.7	5-20	Yang et al. (2016)
CSTR	2	Mixed culture containing T. denitrificans	0.5-0.85 g VSS L^{-1}	$S_2O_3^{2-}$ & S^{2-}	150-570 mg $S_2O_3^{2-}$-S L^{-1} & 96-125 mg S^{2-} L^{-1}	N.A.	150-500	0.5-1.0	12-20	Manconi et al. (2007)
CSTR	4	Activated sludge from a municipal treatment plant	0.6 g VSS L^{-1}	S^{2-}	18-176 mg S^{2-} L^{-1}	N.A.	29 -63	0.2-2.4	40	Dolejs et al. (2015)
FBR	0.58	Mix culture of autotrophic denitrifying bacteria	20-28 g VSS L^{-1} of carrier	$S_2O_3^{2-}$	190 mg $S_2O_3^{2-}$-S L^{-1}	0.2 - 0.8 (g $S_2O_3^{2-}$-S L^{-1} d^{-1})	50-180	0.1-0.5	5	This study

Note: GSAD = granular sludge autotrophic denitrification; N.A. = data not available; CSTR = continuous stirred tank reactor; FBR = fluidized bed reactor; TDS = total dissolved sulfide; S = sulfur; N = nitrogen

The biofilm detachment from the GAC in the FBR observed from period III onwards likely occurred as a response to NO_3^- starvation. Under this condition, the deeper biofilm layer experiences a lack of substrate that can lead to biofilm detachment and after a more extended period to reactor failure (Papirio et al., 2013). However, wash-out of suspended cells was minimal as the VSS concentration was relatively stable (21.7 ± 4.9 g VSS L^{-1} of GAC) during the entire experiment.

3.4.2 Effect of NO_3^- starvation on the microbial community of the FBR biofilm

The microbial community composition of the FBR biofilm changed during FBR operation at different N/S ratios (Figure 3.6). Sulfur-oxidizing bacteria of the genus *Thiobacillus* were found as the dominant microorganisms in the FBR biofilm during the whole operation (Table 3.4) and were mainly responsible for NO_3^- consumption. In particular, *T. denitrificans* (band 8) has a good ability to be immobilized with other microorganisms promoting biofilm formation (Pokorna and Zabranska, 2015). *T. thioparus* (bands 6-7) can reduce NO_3^- using $S_2O_3^{2-}$ as electron donor and has been reported to be less sensitive to high $S_2O_3^{2-}$ concentrations than *T. denitrificans* (Di Capua et al., 2016a). DGGE profiling (Figure 3.6) showed that long-term NO_3^- starvation favored *T. thioparus* over *T. denitrificans*.

During period IV, *T. thioparus* (band 6 and 7) outgrew both *T. denitrificans* (band 8) and *Thiomonas* sp. (band 13). This may also explain the lower $S_2O_3^{2-}$ consumption in period IV compared to period I, since *T. thioparus* can use $S_2O_3^{2-}$ only to reduce NO_3^- to NO_2^- (Pokorna and Zabranska, 2015). NO_2^- was, nevertheless, never detected in the FBR effluent, and it was presumably consumed by other denitrifying bacteria (e.g. band 11) present in the FBR biofilm.

Despite the presence of *Desulfovobrio sp.* in the microbial community of the FBR biofilm, SO_4^{2-} reduction rates were almost negligible, probably due to the lack of external electron donors. This was also confirmed by the observed SO_4^{2-} concentration in the effluent which was higher than the theoretical value, confirming that SO_4^{2-} consumption did not occur in this study. It is also possible that some other denitrifying bacteria were playing a role in the nitrogen bioconversion in the FBR but were present in concentrations below the detection limit of the PCR-DGGE.

3.4.3 Effect of N/S ratio on the $S_2O_3^{2-}$ oxidation kinetics based on batch bioassays

The highest affinity constant, K_s value of 171.9 mg L^{-1} obtained at a N/S ratio of 0.1 (Table 3.2), indicates a low $S_2O_3^{2-}$ oxidation activity by the SO-NR bacteria populating the FBR

biofilm at extreme nitrate-limiting conditions. The K_s values estimated at N/S ratios of 0.3 and 0.5 (Table 3.2) were closer to the values reported by Mora et al. (2015) (16.1 mg $S_2O_3^{2-}$-S L^{-1}) for a suspended culture of thiosulfate-oxidizing denitrifiers at a N/S ratio of 1.3. Biofilm cultures of SO-NR bacteria have higher K_s values compared to suspended-growth cultures (Sahinkaya et al., 2011) as a result of diffusion limitations of the substrates within the biofilm (Sierra-Alvarez et al., 2007).

The lowest value of the inhibition constant K_I (247.7 mg $S_2O_3^{2-}$ L^{-1}) was obtained at a N/S ratio of 0.1, indicating that substrate inhibition by $S_2O_3^{2-}$ occurred at the highest $S_2O_3^{2-}$ concentration tested in the batch bioassays (Table 3.2, Figure 3.4). Substrate inhibition by $S_2O_3^{2-}$ was also observed in previous studies performing batch tests with both suspended (Campos et al., 2008) and biofilm (Di Capua et al., 2016a) cultures of SO-NR bacteria at concentrations exceeding 2.2 g $S_2O_3^{2-}$-S L^{-1}. However, the results of this study (Table 3.2) showed that $S_2O_3^{2-}$ can also inhibit SO-NR bacteria activity at lower concentrations, i.e. 800 mg $S_2O_3^{2-}$-S L^{-1}.

3.4.4 ANN modeling and sensitivity analysis

The AAS and AS values could be used to identify the most influential input parameters (pH, DO, $NO_{3\text{-}in}^{-}$ and $S_2O_{3\text{-}in}^{2-}$) affecting the FBR performance (Rene et al., 2009), i.e. $S_2O_3^{2-}$ and NO_3^- removal efficiency as well as SO_4^{2-} production. According to the removal of sulfur compounds in anoxic FBRs, the change in input parameters could have significant impact on the overall bioreactor performance (Annachhatre and Suktrakoolvait, 2001; Di Capua et al., 2017c; Zou et al., 2016). The ANN model was able to provide adequate information in the form of a contour plot to reveal the effects of different operational conditions on the FBR performance (Figure 3.8). Accordingly, the influent NO_3^- concentration should be >100 mg NO_3^- L^{-1} in order to achieve $S_2O_3^{2-}$ removal efficiencies >80%, and the effluent pH should be maintained at values >4.0. This observation is strongly supported by the experimental results of this study in which the effluent pH during the entire experiment was higher than 7.0 (Figure 3.3). Besides, a previously operated FBR wherein the thiosulfate-driven NO_3^- removal was achieved at a pH of 4.8 to 6.9, resulting in an increase in the removal efficiency at higher pH values (Di Capua et al., 2017a). The sensitivity analysis results also revealed that the DO concentrations strongly affected both the $S_2O_3^{2-}$ removal efficiency (AS = -0.24) and effluent SO_4^{2-} concentrations (AS = -0.36). These results from the sensitivity analysis were in good agreement with the experimental result obtained during days 0-38, which showed that a high DO concentration led to fluctuations in $S_2O_3^{2-}$ removal efficiency (Figure 3.3).

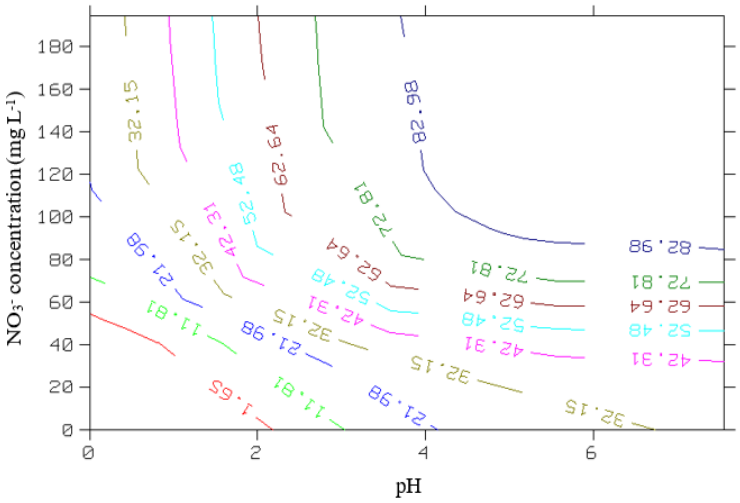

Figure 3.8. Contour plot showing the effect of effluent pH and influent NO_3^- concentration on the artificial neural network model predicted $S_2O_3^{2-}$ removal efficiency.

3.4.5 Practical implications: use of NO_3^- dosing for sulfide removal

For full scale operation, the FBR can be considered as a reliable technology to scale-up for the removal of $S_2O_3^{2-}$ and other sulfur compounds (e.g. HS^- and S^{2-}) under anaerobic conditions, e.g. using NO_3^- as the electron acceptor. Long-term reactor operation can lead to unexpected events, such as substrate starvation, which can dramatically reduce the bioreactor performance. The FBR used in this study demonstrated good robustness and resilience, particularly, the FBR was able to recover 80% of the initial $S_2O_3^{2-}$ removal efficiency within 3 days following starvation (period III, N/S ratio 0.1). However, changes in the microbial community of the FBR biofilm during the starvation period may affect the sulfide oxidation rates and must thus be avoided in practice.

In full-scale, wastewater and waste gas treatment systems are usually controlled with online monitoring equipment, such as programmable sensors which can be integrated with the ANN model in order to control and predict the reactor performance (Rene et al., 2011). The results from the ANN modeling associated with the sensitivity analysis obtained from this study (Figure 3.7) suggest that ANN can be used offline for monitoring and assessing the performance of full-scale FBR using autotrophic denitrification treating wastewater containing both $S_2O_3^{2-}$ and NO_3^-, e.g. mining or $H_2S/S_2O_3^{2-}$ containing scrubbing liquors used for treating H_2S contaminated gases.

3.5 Conclusions

High (99%) $S_2O_3^{2-}$ removal efficiencies were obtained in a FBR using NO_3^- as electron acceptor using the following parameters: N/S ratio of 0.5, 20 ºC, HRT of 5 h and influent pH of 6.9 (± 0.1). Batch activity tests indicated that decreasing the N/S ratio resulted in increasing the biomass affinity constant, K_s, and decreasing the inhibition constant, K_I, of the SO-NR bacteria immobilized in the FBR. The $S_2O_3^{2-}$ oxidation efficiency in the FBR recovered to 80% within 3 days following an increase in N/S ratio to 0.5 after a 42-day starvation period (N/S of 0.1). *Thiobacillus* sp. was the dominant microorganism in the FBR biofilm and primarily responsible for $S_2O_3^{2-}$ oxidation using NO_3^- as electron acceptor. The ANN model successfully predicted the performance parameters of the FBR, i.e. $S_2O_3^{2-}$ and NO_3^- removal efficiency and effluent SO_4^{2-} concentration. The sensitivity analysis results showed that effluent pH was the most influential parameter affecting the $S_2O_3^{2-}$ removal efficiency. Besides, the influent $S_2O_3^{2-}$ concentration affected the NO_3^- removal efficiency and the effluent SO_4^{2-} concentration.

3.6 References

Abatzoglou, N., Boivin, S., 2009. A review of biogas purification processes. Biofuels, Bioprod. Biorefin. 3, 42–71.

Almenglo, F., Ramírez, M., Gómez, J.M., Cantero, D., 2016. Operational conditions for start-up and nitrate-feeding in an anoxic biotrickling filtration process at pilot scale. Chem. Eng. J. 285, 83–91.

Annachhatre, A.P., Suktrakoolvait, S., 2001. Biological sulfide oxidation in a fluidized bed reactor. Environ. Technol. 22, 661–672.

APHA/AWWA/WEF, 1999. Standard methods for the examination of water and wastewater, 20th ed. American Public Health Association/American Water Works Association/Water Environment Federation, Washington D.C.

Bayrakdar, A., Tilahun, E., Calli, B., 2016. Biogas desulfurization using autotrophic denitrification process. Appl. Microbiol. Biotechnol. 100, 939–948.

Beristain-Cardoso, R., Sierra-Alvarez, R., Rowlette, P., Flores, E.R., Gómez, J., Field, J.A., 2006. Sulfide oxidation under chemolithoautotrophic denitrifying conditions. Biotechnol. Bioeng. 95, 1148–1157.

Campos, J.L., Carvalho, S., Portela, R., Mosquera-Corral, A., Méndez, R., 2008. Kinetics of denitrification using sulphur compounds: Effects of S/N ratio, endogenous and exogenous compounds. Bioresour. Technol. 99, 1293–1299.

Can-Dogan, E., Turker, M., Dagasan, L., Arslan, A., 2010. Sulfide removal from industrial wastewaters by lithotrophic denitrification using nitrate as an electron acceptor. Water Sci. Technol. 62, 2286–2293.

Chen, Y., Wang, X., He, S., Zhu, S., Shen, S., 2016. The performance of a two-layer biotrickling filter filled with new mixed packing materials for the removal of H_2S from air. J. Environ. Manage. 165, 11–16.

Cord-Ruwisch, R., 1985. A quick method for the determination of dissolved and precipitated sulfides in cultures of sulphate-reducing bacteria. J. Microbiol. Methods 4, 33–36.

Di Capua, F., Ahoranta, S.H., Papirio, S., Lens, P.N.L., Esposito, G., 2016. Impacts of sulfur source and temperature on sulfur-driven denitrification by pure and mixed cultures of *Thiobacillus*. Process Biochem.

Di Capua, F., Lakaniemi, A.-M., Puhakka, J.A., Lens, P.N.L., Esposito, G., 2017a. High-rate thiosulfate-driven denitrification at pH lower than 5 in fluidized-bed reactor. Chem. Eng. J. 310, 282–291.

Di Capua, F., Milone, I., Lakaniemi, A.-M., Hullebusch, E.D., Lens, P.N.L., Esposito, G., 2017b. Effects of different nickel species on autotrophic denitrification driven by thiosulfate in batch tests and a fluidized-bed reactor. Bioresour. Technol. 238, 534–541.

Di Capua, F., Milone, I., Lakaniemi, A.-M., Lens, P.N.L., Esposito, G., 2017c. High-rate autotrophic denitrification in a fluidized-bed reactor at psychrophilic temperatures. Chem. Eng. J. 313, 591–598.

Di Capua, F., Papirio, S., Lens, P.N.L., Esposito, G., 2015. Chemolithotrophic denitrification in biofilm reactors. Chem. Eng. J. 280, 643–657.

Dolejs, P., Paclík, L., Maca, J., Pokorna, D., Zabranska, J., Bartacek, J., 2015. Effect of S/N ratio on sulfide removal by autotrophic denitrification. Appl. Microbiol. Biotechnol. 99, 2383–2392.

Fernández, M., Ramírez, M., Gómez, J.M., Cantero, D., 2014. Biogas biodesulfurization in an anoxic biotrickling filter packed with open-pore polyurethane foam. J. Hazard. Mater. 264, 529–535.

Fernández, M., Ramírez, M., Pérez, R.M., Gómez, J.M., Cantero, D., 2013. Hydrogen sulphide removal from biogas by an anoxic biotrickling filter packed with Pall rings. Chem. Eng. J. 225, 456–463.

Finster, K., Liesack, W., Thamdrup, B., 1998. Elemental sulfur and thiosulfate disproportionation by *Desulfocapsa sulfoexigens* sp. nov., a new anaerobic bacterium isolated from marine surface sediment. Appl. Environ. Microbiol. 64, 119–125.

Guerrero, L., Montalvo, S., Huiliñir, C., Campos, J.L., Barahona, A., Borja, R., 2015. Advances in the biological removal of sulphides from aqueous phase in anaerobic processes: A review. Environ. Rev. 24, 84–100.

Janyasuthiwong, S., Rene, E.R., Esposito, G., Lens, P.N.L., 2016. Effect of pH on the performance of sulfate and thiosulfate-fed sulfate reducing inverse fluidized bed reactors. J. Environ. Eng. 142, 1–11.

Kelly, D.P., Wood, A.P., 2000. Reclassification of some species of *Thiobacillus* to the newly designated genera *Acidithiobacillus* gen. nov., *Halothiobacillus* gen. nov. and *Thermithiobacillus* gen. nov. Int. J. Syst. Evol. Microbiol. 50, 511–516.

Kolehmainen, R.E., Langwaldt, J.H., Puhakka, J.A., 2007. Natural organic matter (NOM) removal and structural changes in the bacterial community during artificial groundwater recharge with humic lake water. Water Res. 41, 2715–2725.

Krayzelova, L., Bartacek, J., Díaz, I., Jeison, D., Volcke, E.I.P., Jenicek, P., 2015. Microaeration for hydrogen sulfide removal during anaerobic treatment: a review. Rev. Environ. Sci. Biotechnol. 14, 703–735.

Krishnakumar, B., Majumdar, S., Manilal, V.B., Haridas, A., 2005. Treatment of sulphide containing wastewater with sulphur recovery in a novel reverse fluidized loop reactor (RFLR). Water Res. 39, 639–647.

Luo, J., Tian, G., Lin, W., 2013. Enrichment, isolation and identification of sulfur-oxidizing bacteria from sulfide removing bioreactor. J. Environ. Sci. 25, 1393–1399.

Mahmood, Q., Zheng, P., Cai, J., Wu, D., Hu, B., Li, J., 2007. Anoxic sulfide biooxidation using nitrite as electron acceptor. J. Hazard. Mater. 147, 249–256.

Manconi, I., Carucci, A., Lens, P., 2007. Combined removal of sulfur compounds and nitrate by autotrophic denitrification in bioaugmented activated sludge system. Biotechnol. Bioeng. 98, 551–560.

Metcalf & Eddy Inc., Tchobanoglous, G., Stensel, H.D., Tsuchihashi, R., Burton, F.L., 2014. Wastewater Engineering: Treatment and Resource Recovery, 5th ed. McGraw-Hill Education, New York.

Midha, V., Jha, M.K., Dey, A., 2013. Neural network prediction of fluidized bed bioreactor performance for sulfide oxidation. Korean J. Chem. Eng. 30, 385–391.

Midha, V., Jha, M.K., Dey, A., 2012. Sulfide oxidation in fluidized bed bioreactor using nylon support material. J. Environ. Sci. 24, 512–519.

Mora, M., Dorado, A.D., Gamisans, X., Gabriel, D., 2015. Investigating the kinetics of autotrophic denitrification with thiosulfate: Modeling the denitritation mechanisms and the effect of the acclimation of SO-NR cultures to nitrite. Chem. Eng. J. 262, 235–241.

Mora, M., Fernández, M., Gómez, J.M., Cantero, D., Lafuente, J., Gamisans, X., Gabriel, D., 2014a. Kinetic and stoichiometric characterization of anoxic sulfide oxidation by SO-NR mixed cultures from anoxic biotrickling filters. Appl. Microbiol. Biotechnol. 99, 77–87.

Mora, M., López, L.R., Gamisans, X., Gabriel, D., 2014b. Coupling respirometry and titrimetry for the characterization of the biological activity of a SO-NR consortium.

Chem. Eng. J. 251, 111–115.

Moraes, B.S., Souza, T.S.O., Foresti, E., 2012. Effect of sulfide concentration on autotrophic denitrification from nitrate and nitrite in vertical fixed-bed reactors. Process Biochem. 47, 1395–1401.

Muñoz, R., Meier, L., Diaz, I., Jeison, D., 2015. A review on the state-of-the-art of physical/chemical and biological technologies for biogas upgrading. Rev. Environ. Sci. Biotechnol. 14, 727–759.

Nair, V. V., Dhar, H., Kumar, S., Thalla, A.K., Mukherjee, S., Wong, J.W.C., 2016. Artificial neural network based modeling to evaluate methane yield from biogas in a laboratory-scale anaerobic bioreactor. Bioresour. Technol. 217, 90–99.

Nielsen, A.H., Lens, P., Vollertsen, J., Hvitved-Jacobsen, T., 2005. Sulfide-iron interactions in domestic wastewater from a gravity sewer. Water Res. 39, 2747–2755.

Ozkaya, B., Sahinkaya, E., Nurmi, P., Kaksonen, A.H., Puhakka, J.A., 2008. Biologically Fe^{2+} oxidizing fluidized bed reactor performance and controlling of Fe^{3+} recycle during heap bioleaching: An artificial neural network-based model. Bioprocess Biosyst. Eng. 31, 111–117.

Papirio, S., Villa-Gomez, D.K., Esposito, G., Pirozzi, F., Lens, P.N.L., 2013. Acid mine drainage treatment in fluidized-bed bioreactors by sulfate-reducing bacteria: A critical review. Crit. Rev. Environ. Sci. Technol. 43, 2545–2580.

Pokorna, D., Zabranska, J., 2015. Sulfur-oxidizing bacteria in environmental technology. Biotechnol. Adv. 33, 1246–1259.

Rattanapan, C., Boonsawang, P., Kantachote, D., 2009. Removal of H_2S in down-flow GAC biofiltration using sulfide oxidizing bacteria from concentrated latex wastewater. Bioresour. Technol. 100, 125–130.

Rene, E.R., López, M.E., Veiga, M.C., Kennes, C., 2011. Neural network models for biological waste-gas treatment systems. New Biotechnol. 29, 56–73.

Rene, E.R., Veiga, M.C., Kennes, C., 2009. Experimental and neural model analysis of styrene removal from polluted air in a biofilter. J. Chem. Technol. Biotechnol. 84, 941–948.

Reyes-Alvarado, L.C., Okpalanze, N.N., Kankanala, D., Rene, E.R., Esposito, G., Lens, P.N.L., 2017. Forecasting the effect of feast and famine conditions on biological sulphate reduction in an anaerobic inverse fluidized bed reactor using artificial neural networks. Process Biochem. 55, 146–161.

Sahinkaya, E., Dursun, N., Kilic, A., Demirel, S., Uyanik, S., Cinar, O., 2011. Simultaneous heterotrophic and sulfur-oxidizing autotrophic denitrification process for drinking water treatment: Control of sulfate production. Water Res. 45, 6661–6667.

Sierra-Alvarez, R., Beristain-Cardoso, R., Salazar, M., Gómez, J., Razo-Flores, E., Field, J.A., 2007. Chemolithotrophic denitrification with elemental sulfur for groundwater treatment. Water Res. 41, 1253–1262.

Yang, W., Lu, H., Khanal, S.K., Zhao, Q., Meng, L., Chen, G.H., 2016. Granulation of sulfur-oxidizing bacteria for autotrophic denitrification. Water Res. 104, 507–519.

Zou, G., Papirio, S., Lakaniemi, A.-M., Ahoranta, S.H., Puhakka, J.A., 2016. High rate autotrophic denitrification in fluidized-bed biofilm reactors. Chem. Eng. J. 284, 1287–1294.

Zou, G., Papirio, S., Ylinen, A., Di Capua, F., Lakaniemi, A.-M., Puhakka, J.A., 2014. Fluidized-bed denitrification for mine waters. Part II: Effects of Ni and Co. Biodegradation 25, 417–423.

Chapter 4 Anoxic sulfide oxidation in moving bed biofilm reactor (MBBR): experimental and artificial neural network (ANN) model analysis

This chapter has been submitted in modified form:

Khanongnuch, R., Di Capua, F., Lakaniemi, A.-M., Rene, E.R., Lens, P.N.L. 2019. Long-term performance evaluation of an anoxic sulfur oxidizing moving bed biofilm reactor under nitrate limited conditions, *Environ. Sci.: Water Res. Technol*., In Press.

An anoxic sulfur-oxidizing moving bed biofilm reactor (MBBR) treating sulfur and nitrate-contaminated synthetic wastewater was monitored for 306 days under feed nitrogen-to-sulfur (N/S) molar ratios of 0.5, 0.3 and 0.1. Thiosulfate ($S_2O_3^{2-}$) removal efficiencies (REs) exceeding 98% were observed at a N/S ratio of 0.5 and a $S_2O_3^{2-}$ loading rate of 0.9 g $S_2O_3^{2-}$-S L^{-1} d^{-1}, whereas REs of 82.3 (± 2.6)% and 37.7 (± 3.4)% were observed at N/S ratios of 0.3 and 0.1, respectively. Complete nitrate (NO_3^-) removal was obtained at all tested N/S ratios. A comparison between the kinetic parameters of the MBBR biomass under the same after stoichiometric conditions (N/S ratio of 0.5) revealed a 1.3-fold increase of the maximum specific rate of $S_2O_3^{2-}$ oxidation (r_{max}) and a 30-fold increase of the affinity constant for $S_2O_3^{2-}$ (K_s) compared to those observed after long-term NO_3^- limitation (N/S ratio of 0.1). The MBBR showed optimal resilience to NO_3^- limitation as the $S_2O_3^{2-}$ RE recovered from 37.3% to 94.1% within two days after increasing the N/S ratio from 0.1 to 0.5. Based on PCR-DGGE analysis, sulfur-oxidizing, nitrate-reducing bacteria, i.e. *Thiobacillus* sp. and *Sulfuritalea* sp., dominated in the MBBR biofilm during the entire study. An artificial neural network (ANN) model with a topology of 4-4-3 was successfully developed to predict the $S_2O_3^{2-}$ and NO_3^- RE and sulfate concentration during MBBR operation.

4.1 Introduction

Wastewaters such as pig manure, tannery effluents and pulp and paper processing effluents generally contain elevated concentrations of sulfur in the form of thiosulfate ($S_2O_3^{2-}$), polythionate ($S_nO_6^{2-}$), elemental sulfur (S^0), sulfite (SO_3^{2-}) and sulfate (SO_4^{2-}), which are reduced to hydrogen sulfide (H_2S) during anaerobic digestion (Pokorna and Zabranska, 2015). The presence of sulfide species (H_2S, HS^- and S^{2-}) in gaseous and wastewater streams is highly detrimental due to their ability to cause corrosion and harm the environment (Krayzelova et al., 2015).

The removal of sulfur contaminants such as H_2S and $S_2O_3^{2-}$ using nitrate (NO_3^-) as the electron acceptor has gained increasing interest since reduced sulfur compounds and NO_3^- can be simultaneously removed from waste streams by a single anaerobic process (Di Capua et al., 2016b, 2019; Fernández et al., 2014; Khanongnuch et al., 2018; Zou et al., 2016). The operation of anoxic sulfur-oxidizing bioreactors entails the use of a highly soluble electron acceptor (i.e. NO_3^-) and eliminates oxygen gas-liquid-biofilm mass transfer limitations commonly experienced in aerobic systems (Krishnakumar et al., 2005). Moreover, the operation of anoxic bioreactors has low environmental impacts and operational costs if nitrified wastewater or NO_3^--containing wastewater is provided as a source of NO_3^- (Cano et al., 2018; Di Capua et al., 2015). The reaction involved in the anoxic

oxidation of $S_2O_3^{2-}$ and sulfide in the presence of NO_3^- is described by Eqs. (4.1) and (4.2), respectively (Mora et al., 2014b):

$$S_2O_3^{2-} + 1.16NO_3^- + 0.124H_2O + 0.035CO_2 + 0.519HCO_3^- + 0.11NH_4^+ \rightarrow 2SO_4^{2-} + 0.578N_2 + 0.110C_5H_7O_2N + 0.435H^+ \quad (4.1)$$

$$HS^- + 1.23NO_3^- + 0.573H^+ + 0.438HCO_3^- + 0.027CO_2 + 0.093NH_4^+ \rightarrow SO_4^{2-} + 0.614N_2 + 0.866H_2O + 0.093C_5H_7O_2N \quad (4.2)$$

Moving bed biofilm reactors (MBBR) have been widely used for the treatment of domestic and industrial wastewaters due to their effective biomass retention (Chai et al., 2014; Hatika Abu Bakar et al., 2017; Yuan et al., 2015). However, studies focusing on the operation of anoxic MBBRs for treating sulfur contaminated wastewaters is still limited. Full-scale sulfur-oxidizing bioreactors may experience fluctuations in the influent NO_3^- concentration as well as an unexpected increase or decrease of sulfur loading, which can lead to severe NO_3^- limitation in the system. Furthermore, when the concentrations of NO_3^- and nitrite (NO_2^-) in the influent wastewater are insufficient to sustain the process, NO_3^- source (e.g., $NaNO_3$, KNO_3, $Ca(NO_3)_2$) can be supplied externally to maintain the process efficiency (Yang et al., 2005). Dosing must be strictly controlled to minimize the addition of chemicals and the operational costs. As a result, it is important to evaluate the performance of an anoxic MBBR under NO_3^- limitation as well as the response and resilience of the sulfur-oxidizing nitrate-reducing (SO-NR) MBBR biofilm to long-term NO_3^- limited conditions. Process control evaluation and microbial community analysis are important to better understand the operational and biological variables determining the performance of the system.

Modelling of the process is one way to enable enhanced process control and artificial neural network (ANN) is one of the most efficient black-box modelling tools for predicting and describing the performance of biological processes, in which the process variables are non-linear in nature. ANNs have been successfully applied to optimize the operational conditions for enhancing the process control, monitoring the effluent quality, reducing energy consumption and dynamic forecasting in full-scale wastewater treatment plants (Han et al., 2018; Lee et al., 2011) and industrial biohydrogen production plants (Han et al., 2018; Lee et al., 2011; Zamaniyan et al., 2013).

In this study, the performance and microbial community evolution of an anoxic sulfur-oxidizing MBBR were monitored under different N/S ratios (0.5 and 0.3 and 0.1) for 306 days. An ANN model coupled with a sensitivity analysis was implemented to predict the $S_2O_3^{2-}$ and NO_3^- removal efficiencies (RE) and SO_4^{2-} production based on the collected data during long-term operation.

4.2 Materials and methods

4.2.1 Inoculum source and influent solution composition

The MBBR was inoculated with biofilm-coated granular activated carbon (GAC) collected from a laboratory-scale fluidized-bed reactor (FBR) previously operated to study the effects of temperature, hydraulic retention time (HRT) and pH on thiosulfate-driven denitrification (Di Capua et al., 2017a, 2017c). The microbial community of the biofilm-coated GAC was dominated by sulfur-oxidizing bacteria, i.e. *Thiobacillus denitrificans* and *Thiobacillus thioparus*. The GAC-attached biomass had total solid (TS) and volatile solid (VS) concentrations of 23.0 (± 1.5) and 17.3 (± 1.3) g L^{-1} of GAC, respectively. The VS/TS ratio was approximately 0.75-0.76.

The influent solution used in this study contained 200 mg $S_2O_3^{2-}$-S L^{-1} (added as $Na_2S_2O_3 \cdot 5H_2O$), 10-45 mg NO_3^--N L^{-1} (added as KNO_3), 1 g L^{-1} of $NaHCO_3$, nutrients (mg L^{-1}) as follows: KH_2PO_4 (200), NH_4Cl (100), $MgSO_4 \cdot 7H_2O$ (80), $FeSO_4 \cdot 7H_2O$ (2) and 0.2 mL L^{-1} of a trace element solution as described by Zou et al. (2016). The pH of the influent solution was adjusted to 7.0 using 37% HCl. $S_2O_3^{2-}$ was used as the representative reduced sulfur compound due to its ease of handling and stability at circumneutral pH (Luo et al., 2013; Mora et al., 2014b).

4.2.2 Experimental set-up and operation

The MBBR used in this study was made of glass and had a working volume of 0.825 L (Figure 4.1). The MBBR was filled with 350 (± 5) pieces of Kaldnes-K1 carriers [specific surface area: 500 m^2 m^{-3}, effective area: 410 mm^2 $piece^{-1}$, density: 0.95 g cm^{-3}, diameter × height: 9 × 7 mm], corresponding to a 40% filling ratio. The influent was fed to the MBBR at a flow rate of 4.0 L d^{-1} (Masterflex® Easy Load II L/S driven by Masterflex® L/S, Cole-Parmer, USA), corresponding to a theoretical hydraulic retention time (HRT) of 5 h. Mixing was provided with a Heidolph RZR 2052 mechanical stirrer (Heidolph Instrument GmbH & Co. KG, Germany) operated at a speed of 65 rpm. The MBBR was operated at room temperature (20 ± 2) °C.

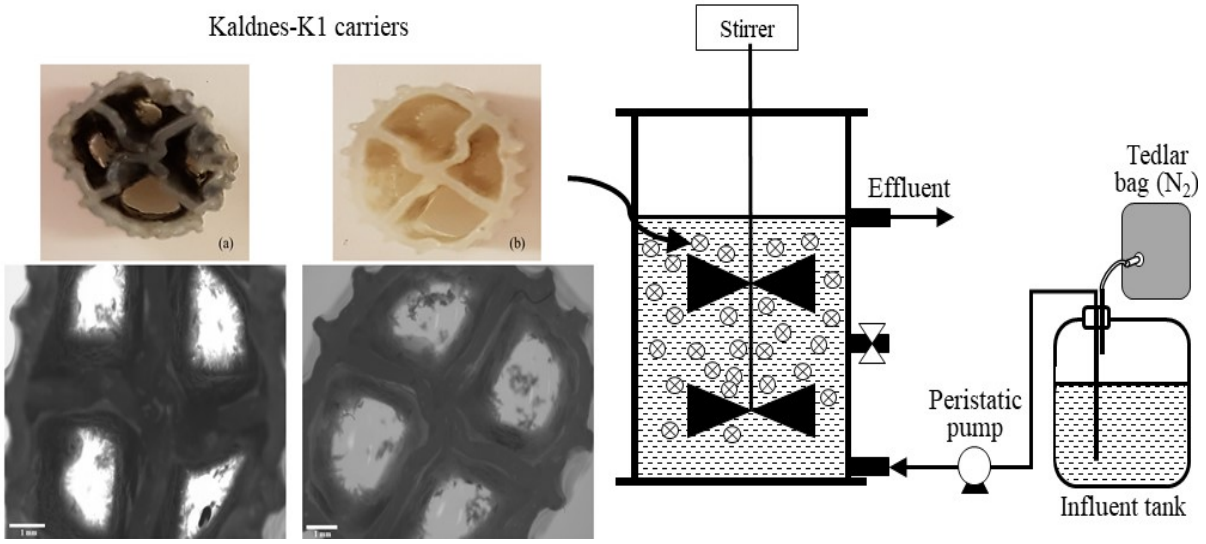

Figure 4.1. Schematic representation the MBBR used in this study, including a photograph of the two different biofilm types attached to the Kaldnes-K1 carriers: (a) thick-dark brown biofilm, and (b) thin-light brown biofilm.

Initially, the MBBR was filled with 180 pieces of K1 carriers (51% of total carriers) was initially filled with the influent solution up to 800 mL and 10 mL of biofilm-coated GAC as inoculum. The MBBR was purged with N_2 for 15-20 minutes to ensure the anoxic conditions and operated in batch mode for 14 days. Batch operation was stopped when the $S_2O_3^{2-}$ and NO_3^- RE exceeded 90% and biofilm formation was visually observed on the K1 carriers. Afterwards, the GAC was completely removed and 170 pieces of K1 carriers added to the MBBR prior to starting continuous operation.

Continuous MBBR operation (306 days) was divided into five experimental periods (Table 4.1). During the entire experiment, the influent $S_2O_3^{2-}$ concentration was kept constant at ~200 mg $S_2O_3^{2-}$-S L^{-1}, corresponding to an inlet $S_2O_3^{2-}$ loading rate of 0.91 (± 0.05) kg $S_2O_3^{2-}$-S m^{-3} d^{-1}, while the influent NO_3^- concentration was varied between 10.6 and 40.5 mg NO_3^--N L^{-1} in order to adjust the N/S ratio (Table 4.1). During period I (days 0-45), the microbial community in the MBBR was acclimated to continuous operation at a stoichiometric N/S ratio of 0.5 (Table 4.1) to ensure that the biofilm formed on the K1 carriers could sustain the simultaneous removal of $S_2O_3^{2-}$ and NO_3^-. The dissolved oxygen (DO) concentration in the MBBR was 0.87 (± 0.31) mg L^{-1}. In period II (days 46-115), the operational conditions were similar to period I but the DO concentration was reduced to 0.45 (± 0.08) mg L^{-1} (Figure 4.2a) as a N_2-filled Tedlar bag was connected to the top of the influent tank in order to reduce oxygen intrusion and maintain the anoxic conditions.

Table 4.1. Conditions of the anoxic MBBR during the different operational periods.

Period	Time (days)	DO concentration (mg L^{-1})	Feed N/S ratio (mol mol^{-1})	Influent $S_2O_3^{2-}$ (mg $S_2O_3^{2-}$-S L^{-1})	Influent NO_3^- (mg NO_3^--N L^{-1})	Effluent pH
I	0-45	0.87 (± 0.31)	0.5	199.0 (± 26.1)	40.5 (± 3.4)	7.11 (± 0.25)
II	46-115	0.45 (± 0.08)	0.5	185.7 (± 4.7)	39.4 (± 1.5)	6.82 (± 0.13)
III	116-207	0.53 (± 0.09)	0.3	194.1 (± 12.4)	28.7 (± 1.7)	7.12 (± 0.12)
IV	208-249	0.52 (± 0.9)	0.1	197.2 (± 7.5)	10.6 (± 0.6)	7.28 (± 0.12)
V	250-306	0.54 (± 0.8)	0.5	186.8 (± 3.2)	39.6 (± 1.4)	6.93 (± 0.09)

During period III (days 116-207), the MBBR was operated at a N/S ratio of 0.3, corresponding to an influent NO_3^- concentration of 28.7 (± 1.7) mg NO_3^--N $L^{-1}$and an inlet NO_3^- loading rate of 0.14 kg NO_3^--N m^{-3} d^{-1}. In period IV (days 208-249), the influent NO_3^- concentration was decreased to 10.6 (± 0.6) mg NO_3^--N L^{-1}, corresponding to inlet NO_3^- loading rate of 0.05 kg NO_3^--N m^{-3} d^{-1}, and the MBBR operated at a N/S ratio of 0.1. During period V (days 250-306), an influent NO_3^- concentration of 39.4 (± 1.5) mg NO_3^--N L^{-1} (N/S ratio of 0.5) was used in order to investigate the MBBR potential to recover the $S_2O_3^{2-}$ RE after a 42-day operation under NO_3^- limited conditions (period IV).

The performance of the MBBR in each experimental period was evaluated during steady-state conditions. The steady-state condition was assumed when the relative standard deviation (%RSD) of the $S_2O_3^{2-}$ RE was ≤ 10%.

4.2.3 Batch kinetics bioassays

Batch bioassays were performed to determine the kinetic constants, i.e. the maximum specific rate of $S_2O_3^{2-}$ oxidation (r_{max}) and the affinities of the biofilm microorganisms to $S_2O_3^{2-}$ (K_s) and NO_3^- (K_n). Bioassays were performed in duplicate in 120 mL serum bottles with 60 mL headspace, and the medium solution (pH 7.0 ± 0.2) had the same composition as the influent solution used for the continuous MBBR operation. Biofilm-attached K1 carriers (9 pieces/bottle) were taken from the MBBR during steady-state conditions of operational periods II-V (days 117, 196, 244 and 305, respectively) and used as inoculum. The initial $S_2O_3^{2-}$ and NO_3^- concentrations used in these bioassays were as shown in Table 4.2. The bottles were purged with N_2 for 10 min and sealed with rubber septa and aluminum crimps to ensure anoxic conditions. Subsequently, the bottles were placed on a HS 501 horizontal shaker (IKA, USA) operated at 220 rpm and 20 (± 2) °C. In this study, the simultaneous $S_2O_3^{2-}$-oxidizing NO_3^--reducing process was described using a Monod model (Eq. 4.3):

$$r_S = \frac{r_{max_S} \times S}{K_s + S} \times \frac{N}{K_n + N} \qquad (4.3)$$

Table 4.2. Kinetic coefficients (Monod) of the attached biofilm collected from the MBBR during different operational periods.

Period	N/S ratio (mol mol^{-1}	Biomass concentration (mg VS L^{-1})	Initial concentrations		Kinetic coefficients		
			$S_2O_3^{2-}$ (mg $S_2O_3^{2-}$-S L^{-1})	NO_3^- (mg NO_3^--N L^{-1})	r_{max} (mg $S_2O_3^{2-}$-S g^{-1} VS h^{-1})	K_s (mg $S_2O_3^{2-}$-S L^{-1})	K_n (mg NO_3^--N L^{-1})
II	0.5	495 (± 105)	0, 6, 85, 160, 180, 300	0, 1, 15, 26, 36, 62	109.4	1.7	6.3
III	0.3	465 (± 230)	0, 40, 80, 160, 270, 380	0, 6, 12, 24, 30,50	113.1	67.0	-
IV	0.1	320 (± 30)	0, 70, 130, 360, 480	0, 3, 6, 14, 20	69.2	109.3	-
V	0.5	490 (± 200)	0, 35, 70, 200, 300, 420	0, 7, 15, 45, 62, 85	143.9	50.6	8.9

However, the simplified Monod model (Eq. 4.4) was used when the affinity for NO_3^- (K_n) was much smaller than the affinity for $S_2O_3^{2-}$ (K_s) (Kopec et al., 2018). This was the case for microbial biofilm samples taken from the MBBR during low N/S ratio conditions (N/S ratios of 0.3 and 0.1).

$$r_S = \frac{r_{max_S} \times S}{K_s + S} \quad (4.4)$$

where S and K_s are the concentration and affinity constant for $S_2O_3^{2-}$ (mg $S_2O_3^{2-}$-S L^{-1}), respectively; N and K_n are the concentration and affinity constant for NO_3^- (mg NO_3^--N L^{-1}), respectively; and r_{max_S} is the maximum specific rate of $S_2O_3^{2-}$ oxidation (mg $S_2O_3^{2-}$-S g VS^{-1} h^{-1}).

4.2.4 Batch activity tests

The batch tests were performed in duplicate to study the SO-NR activity of the MBBR biomass by measuring the specific uptake rates of $S_2O_3^{2-}$ (STUR) and NO_3^- (SNUR) (Table 4.3). On days 117 (period II), the tests were performed to evaluate the metabolic activity of the two different types of biofilm formed on the K1 carriers, i.e. thick-dark biofilm and thin-light biofilm. At the end of the experiment (day 306, period IV), the fed-batch tests were performed to evaluate the response of carrier-attached and suspended biomass to sequential feeding that $S_2O_3^{2-}$ and NO_3^- were sequentially added before they were almost completely consumed.

Table 4.3. Experimental conditions of the batch activity tests performed with the MBBR biomass collected at different operational days.

Day	Experiment	Volume (mL)	No. of carriers used (pieces)	Initial concentrations		N/S ratio (mol/mol)	VSS concentration (mg L^{-1})	Removed $S_2O_3^{2-}$-S (mg L^{-1})	Produced SO_4^{2-}-S (mg L^{-1})	Specific uptake rate[a]	
				$S_2O_3^{2-}$-S (mg L^{-1})	NO_3^--N (mg L^{-1})					STUR (g $S_2O_3^{2-}$-S g VSS d^{-1})	SNUR (g NO_3^--N g VSS d^{-1})
107	Effect of different biofilm characteristics	40	5	200	100	0.45					
	- thick-dark brown biofilm						265 (± 20)	190 (± 4)	259 (± 10)	1.91 (± 0.04)	0.89 (± 0.02)
	- thin-light brown biofilm						175 (± 20)	189 (± 1)	271 (± 16)	1.69 (± 0.22)	0.88 (± 0.21)
306	Effect of sequential feeding on the biomass[b]	40		200	100	0.45					
	- carrier-attached biomass		5				260 (± 20)	125 (± 14) to 290 (±73)	178 (± 16) to 352 (± 85)	4.08 (± 0.19), 5.80 (± 1.40) and 4.09 (± 0.72)	0.84 (± 0.05), 1.81 (± 0.68) and 0.84 (± 0.13)
	- suspended biomass		32 mL				160 (± 60)	168 (± 9) to 268 (± 11)	173 (± 77) to 398 (± 38)	1.13 (± 0.07), 2.59 (± 0.21) and 4.91 (± 0.86)	0.28 (± 0.04), 0.69 (± 0.05) and 1.10 (± 0.08)

Note: [a]STUR = specific thiosulfate uptake rate; SNUR = specific nitrate uptake rate
[b]The three values reported for the removed $S_2O_3^{2-}$-S, produced SO_4^{2-}-S, STUR and SNUR were calculated before the first feeding, after the first feeding and after the second feeding, respectively

The nutrient solution was as described for the kinetic bioassays. K1 carriers (5 pieces/bottle) were taken from the MBBR and directly added as inoculum to 60-mL serum bottles with 20 mL headspace. The nutrient solution was as described for the kinetic bioassays.

4.2.5 Residence time distribution (RTD) test

The RTD test for the MBBR, at an theoretical HRT of 5 h, was performed on day 307 to determine the hydrodynamic behavior of the MBBR using the pulse input method as described by Khanongnuch et al. (2018) The procedure used to perform the RTD test and data analysis are described in Fogler (2016). The results obtained from the RTD test were used to determine Peclet number (Pe_r) that describes the mixing characteristics of the MBBR as shown in Eq. (4.5).

$$\frac{\sigma^2}{t_m^2} = \frac{2}{Pe_r} - \frac{2}{Pe_r^2}(1-e^{-Pe_r}) \quad (4.5)$$

where σ^2 and t_m are the variance and mean residence time of the RTD, respectively.

4.2.6 Microbial community analysis

Two pieces of K1 carrier were taken during the steady-state operation of the MBBR in periods II (day 115), III (day 196), IV (day 242) and V (day 306). To obtain the bacterial cells from the carrier material, a biofilm-attached K1 carrier was immersed in 10 mL of sterile milli-Q water and sonicated for 2 min. The obtained solution was filtered through a Cyclopore track etched 0.2 µm membrane (Whatman, USA). Subsequently, the membranes with the retained biomass were stored at -20 ºC for microbial community analysis by polymerase chain reaction denaturing gradient gel electrophoresis (PCR-DGGE). The DNA extraction was performed using a PowerSoil® DNA isolation kit (MO BIO Laboratories, Inc., USA) according to the manufacturer's instructions. PCR-DGGE analysis was performed according to the protocol described by Ahoranta et al. (2016). The amplified DNA samples were sequenced by Macrogen Inc. (The Netherlands). The sequence data was edited using the Bioedit software (version 7.2.5, Ibis Biosciences, USA) and compared with the sequences available in the National Center for Biotechnology Information (NCBI) database.

4.2.7 Analytical techniques

The concentrations of $S_2O_3^{2-}$, SO_4^{2-}, NO_3^- and NO_2^- in the MBBR influent and effluent were measured by ion chromatography (IC) as described by Di Capua et al. (2017c). Liquid samples were filtered through 0.45 µm Chromafil Xtra PET-202125 membrane

syringe filters (Mechery-Nagel, Germany) and stored at -20 °C prior to analysis. The DO concentration in the MBBR was measured with a HQ40d portable multimeter equipped with an Intellical™ LDO101 probe (HACH, USA). The influent and effluent pH of the MBBR were measured using a pH 3110 portable meter fitted with a SenTix 21 electrode (WTW, Germany). The pH of the liquid samples obtained from batch tests was measured using a pH 330i meter (WTW, Germany) fitted with a SlimTrode lab pH electrode (Hamilton, USA). Alkalinity was measured according to the procedure described in Standard Methods (APHA/AWWA/WEF, 1999).

During MBBR operation (days 44, 60, 90, 114, 196, 242 and 306), two pieces of K1 carrier were collected to measure the total solids (TS) and volatile solids (VS) of the K1 carrier-attached biomass. Each piece of K1 carrier was added into a 15 mL Falcon tube containing 10 mL of deionized water and the biofilm was detached by manual shaking. The procedure was repeated until all the biomass was detached from the carrier. The solution containing detached biomass was used for the determination of TS and VS of a carriers according to the same procedure of volatile suspended solids (VSS) concentration in liquid samples given in Standard Methods (APHA/AWWA/WEF, 1999). Elemental sulfur (S^0) was measured from K1 carriers collected on days 193, 240 and 300 using the modified cyanolysis method (Khanongnuch et al., 2018).

4.2.8 ANN model development

An ANN model was developed using MBBR experimental data from days 45 to 306 (78 data points). The ANN input parameters consisted of the influent concentrations of $S_2O_3^{2-}$ ($S_2O_3^{2-}{}_{in}$) and NO_3^- ($NO_3^-{}_{in}$), the effluent pH and the DO concentration. The output parameters of the ANN model were the $S_2O_3^{2-}$ and NO_3^- RE and the produced SO_4^{2-} concentration ($SO_4^{2-}{}_{out}$). The basic statistics of the training, validation and test data sets used to develop the ANN model are shown in Table 4.4. The experimental data were normalized in the range of 0-1 before being used in the Neural Network Toolbox 11.0 of MATLAB® R2018b (MathWorks Inc., USA), as described by Khanongnuch et al. (2018). The network topology selected for the ANN model to predict the $S_2O_3^{2-}$ and NO_3^- RE and the SO_4^{2-} concentration was a three-layered feed-forward back propagation neural network (Figure 4.3). The feed-forward network, where signals flow from the input layer to the hidden layer and then to the output layer in the forward direction (Figure 4.3), used in this study is the most commonly employed network architecture to model and predict the performance of bioreactors used in the field of environmental engineering (Nair et al., 2016; Rene et al., 2011; Sahinkaya, 2009). A three-layered feed-forward network also yields lower mean squared error (*MSE*) and higher coefficient of determination (R^2) values compared to an ANN coupled with hybrid methods (Fan et al., 2018). The network architecture consisted of four neurons in the input layer connected to four neurons in the

hidden layer, and three neurons in the output layer. To obtain the best network topology, the number of neurons in the hidden layer, the number of data points of training, validation and testing were selected using a trial and error approach based on the R^2 and *MSE* values that showed modelled output values closely fitting the experimental measurements (Table 4.5).

Table 4.4. Basic statistics of the training, validation and test data sets used to develop the artificial neural network (ANN) model.

	N	Mean	Minimum	Maximum
Dissolved oxygen in the MBBR	78	0.50	0.27	0.71
pH	78	7.13	6.63	7.67
$S_2O_3^{2-}{}_{in}$ (mg $S_2O_3^{2-}$-S L^{-1})	78	193	163	216
$NO_3^-{}_{in}$ (mg NO_3^--N L^{-1})	78	30.9	9.86	47.7
$S_2O_3^{2-}$-RE (%)	78	80.3	33.2	100
NO_3^--RE (%)	78	98.5	82.0	100
$SO_4^{2-}{}_{out}$ (mg L^{-1})	78	213	93.2	304

Note: N = number of experimental data points was used for training, validating and testing the ANN model

Table 4.5. Best values of the network parameters used to develop the ANN model for the moving bed biofilm reactor (MBBR).

Training parameters	Range of value tested	Best value
Number of training data set	43-54	50 (65%)
Number of validation data set	12-19	16 (20%)
Number of test data set	8-12	12 (15%)
Number of neurons in input layer (N_I)	4	4
Number of neurons in hidden layer (N_H)	4-8	4
Number of neurons in output layer (N_O)	3	3
Epoch size	21	15
Momentum term (μ)	0-1	0.000001

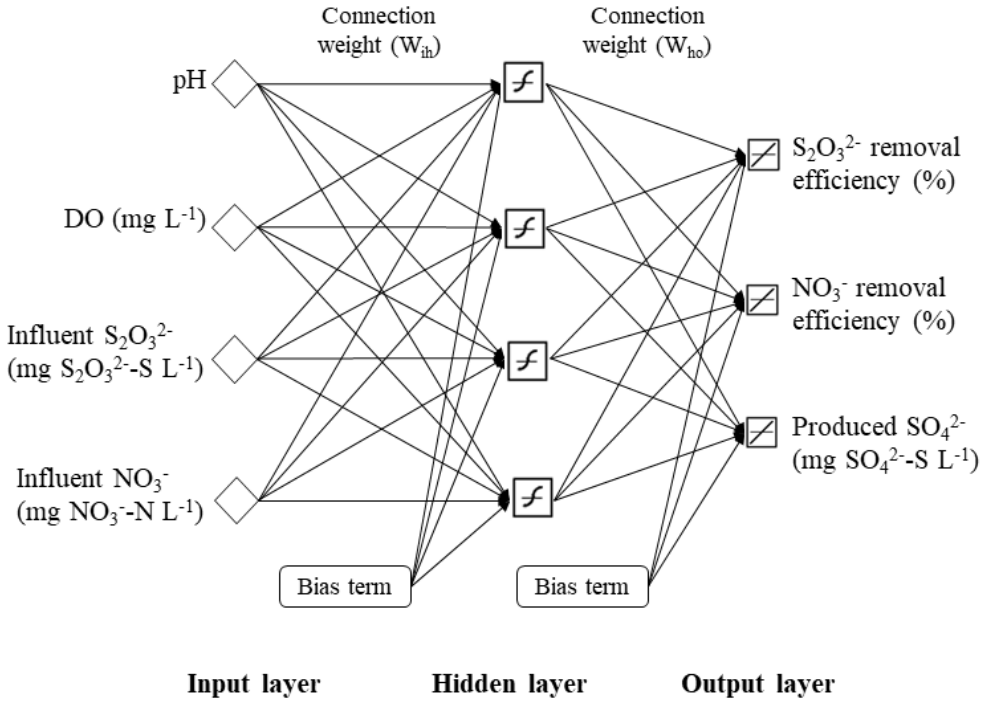

Figure 4.3. Artificial neural network topology developed for the prediction of $S_2O_3^{2-}$ and NO_3^- removal efficiencies and produced SO_4^{2-} concentration of the anoxic MBBR. ⊿ and ⊿ represent, respectively, the tan-sigmoid and linear (PURELIN) transfer function.

The ANN model was trained using the Levenberg-Marquardt back-propagation algorithm (*trainlm* function in the Neural Network Toolbox 11.0). This training algorithm is generally used for prediction and forecasting purposes because it is well suited for accurate training and has a fast convergence speed (Yetilmezsoy and Sapci-Zengin, 2009). In this algorithm, the input layer transfers the signal multiplied by the connection weights (W_{ih}) to the hidden layer. Subsequently, the hidden layer transfers the signal to the output layer, multiplied by the respective connection weights (W_{ho}). A tan-sigmoid transfer function was used in the hidden layer, while a linear (PURELIN) transfer function was used in the output layer.

4.2.9 Statistical analysis

A one-way analysis of variance (ANOVA) with Tukey's multiple comparison test was performed for data analysis using the Minitab 16 software (Minitab Inc., USA) to determine the statistical differences in each parameter during the steady-state operation of the MBBR. The significant difference was considered at 95% ($P \leq 0.05$). The kinetic constants of Monod (Eqs. 2 and 3) were determined using the non-linear programming solver (fminsearch) in MATLAB® R2018b (MathWorks Inc., USA).

The sensitivity analysis for the ANN model was performed using the multivariable statistical modelling software NNMODEL (PA, USA) to determine the absolute average sensitivity (AAS) and the average sensitivity (AS) values. The AAS value is the average of the absolute values of the change in the output. To normalize the data, the change in the output is divided by the change in the input. The calculation of AS is similar to the determination of AAS, except no consideration of absolute values. If the change in the output variable is in the same direction, both AAS and AS values would be similar. The absolute value AS matrix ($S_{ki,abs}$) is calculated as shown in Eq. (4.6):

$$S_{ki,\,abs} = \frac{\sum_{P=1}^{P} \left| S_{ki}^{(P)} \right|}{P} \tag{4.6}$$

Where, P is the number of training patterns of the network.

4.3 Results

4.3.1 MBBR performance at different N/S ratios

Figure 4.2 shows the MBBR performance at different N/S ratio operations. During period I (days 0-44), the $S_2O_3^{2-}$ RE was 95.2 (± 1.4)%, while the NO_3^- RE fluctuated between 48.7 and 100%, respectively. The effluent pH varied in the range of 6.86-7.36. During period II (N/S ratio of 0.5), the $S_2O_3^{2-}$ RE was 98.5 ± 0.7%. The effluent pH and alkalinity were 6.82 (± 0.13) and 342 (± 14) mg HCO_3^- L^{-1}, respectively. A NO_3^- RE higher than 99% was observed from day 60 onwards (Figure 4.2d). A similar $S_2O_3^{2-}$ removal rate of 0.85 (± 0.04) kg S m^{-3} d^{-1} was observed during periods I and II.

MBBR operation at N/S ratios below 0.5 resulted in lower $S_2O_3^{2-}$ removal rates and efficiencies than those observed in the first two operational periods. The $S_2O_3^{2-}$ RE was 82.3 (± 2.6)% at a N/S ratio of 0.3 (period III) and 37.7 (± 3.4)% at a N/S ratio of 0.1 (period IV), corresponding to $S_2O_3^{2-}$ removal rates of 0.62 (± 0.04) and 0.38 (± 0.01) kg S m^{-3} d^{-1}, respectively. The effluent pH and alkalinity were 7.12 (± 0.17) and 393 (± 15) mg HCO_3^- L^{-1} in period III and increased to 7.28 (± 0.12) and 440 (± 10) mg HCO_3^- L^{-1}, respectively, when the MBBR was operated at a N/S ratio of 0.1 (period IV) (Figure 4.2a). The $S_2O_3^{2-}$ RE increased from 37.3% (day 249) to 94.1% (day 251) in two days after increasing the N/S ratio from 0.1 to 0.5 (period V). The $S_2O_3^{2-}$ RE further increased slightly during period V and reached 99.5 (± 0.7)% at the end of the experiment (days 292-306), corresponding to a $S_2O_3^{2-}$ removal rate of 0.87 (± 0.02) g S m^{-3} d^{-1}.

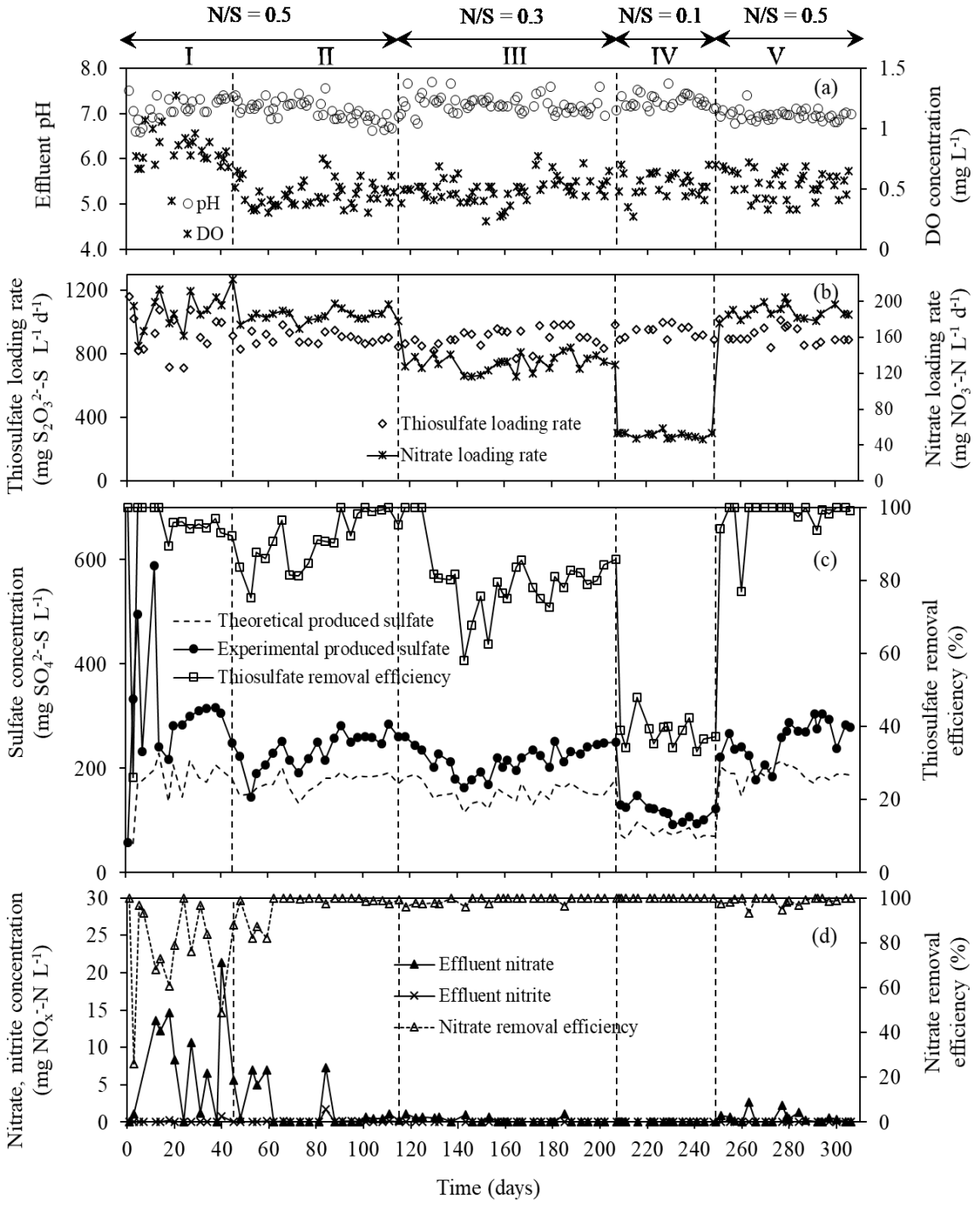

Figure 4.2. Time course profiles of (a) effluent DO and pH, (b) $S_2O_3^{2-}$ and NO_3^- loading rate, (c) removal efficiency of $S_2O_3^{2-}$ and effluent SO_4^{2-} concentration, (d) effluent NO_3^- and NO_2^- and removal efficiency of NO_3^- during the MBBR operation. The dashed line in (c) indicates the theoretical SO_4^{2-} production based on Eq. (4.1).

Figure 4.2c shows the effluent SO_4^{2-} concentration profile in the MBBR at different N/S ratios tested. The highest effluent SO_4^{2-} concentration (302 ± 14 mg SO_4^{2-}-S L^{-1}) was observed during the acclimation phase (period I, N/S ratio of 0.5), while the lowest (105 ± 11 mg SO_4^{2-}-S L^{-1}) was observed during period IV (N/S ratio of 0.1). In periods II and V (N/S ratio of 0.5), similar effluent SO_4^{2-} concentrations were observed, being 263 (± 14) and 279 (± 22) mg SO_4^{2-}-S L^{-1}, respectively. During period III (N/S ratio of 0.3), the effluent SO_4^{2-} concentration was 241 (± 9) mg SO_4^{2-}-S L^{-1}.

4.3.2 Residence time distribution

The mean residence time (t_m) in the MBBR obtained from the RTD analysis was 4.43 h, while the theoretical HRT of 5 h calculated based on the influent flow rate. Regarding the dimensionless RTD function ($E(\Theta)$) (Figure 4.4), the normalized time (Θ) was defined as the RTD profile time (t) divided by t_m. Thus, at Θ = 1 (the value of perfect completely mixed reactor) ($t = t_m$ = 4.43 h), 64% of the tracer had left the reactor, corresponding to an accumulative profile ($F(\Theta)$) of 0.64 (Figure 4.4). The tracer completely left the MBBR within 22 h after the pulse injection. According to the mixing characteristics, the Peclet number, Pe_r, of 0 represents an ideal completely mixed reactor, whereas the value of an ideal plug flow is infinity (∞). In the present study, the hydrodynamic behavior of the MBBR (Pe_r =1.31) was very close to that of an ideal completely mixed reactor, resulting in a uniform distribution of $S_2O_3^{2-}$ and NO_3^- in the reactor volume during the study.

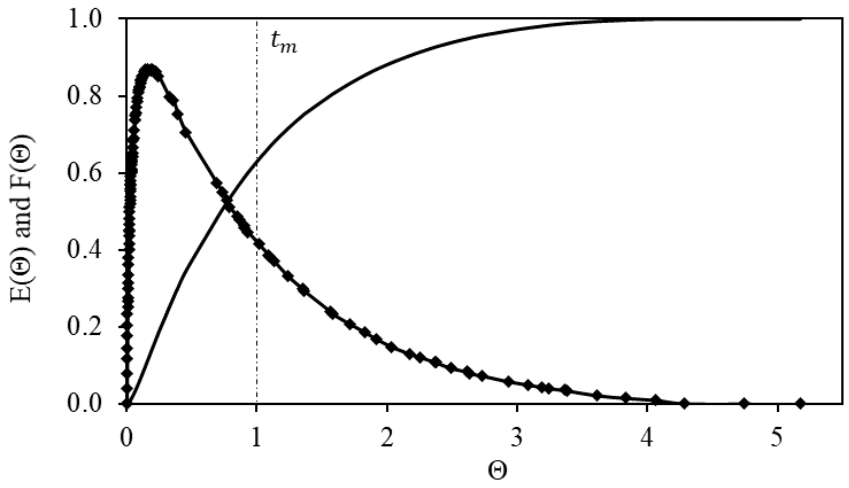

Figure 4.4. Residence time distribution (RTD) curve of the MBBR at a HRT of 5 h performed on day 307.

4.3.3 Biofilm quantity, characteristic and viability during MBBR operation

The weight of the carrier-attached and suspended biomass in the MBBR during continuous operation was as shown in Figure 4.5. The biofilm formed on K1 carriers added prior to starting the 14-day batch mode operation was thick-dark brown (Figure 4.1a), while the biofilm developed on the carriers added at the end of the batch mode operation was light brown and thinner (Figure 4.1b). The thick-dark brown was observed as a fine activated carbon particle attached to the surface K1 carriers. The weight of the carrier-attached biomass with thick-dark brown biofilm was 1.20 (± 0.14) mg VS carrier^{-1} on day 44 and gradually increased up to 2.17 (± 0.15) mg VS carrier^{-1} on day 90 (period II, N/S ratio of 0.5). Afterwards, the biomass quantity remained relatively stable until the end of the experiment (day 306). The quantity of the carrier-attached biomass on the carriers with thin-light brown biofilm was similar during this study (0.88 - 1.28 mg VS carrier^{-1}), except in period IV (day 242) when the weight was only 0.35 ± 0.14 mg VS carrier^{-1} (Figure 4.5). The similar metabolic activities (STUR and SNUR) were observed for the carrier-attached biomass with thick-dark brown and thin-light brown biofilm during period II (Table 4.3).

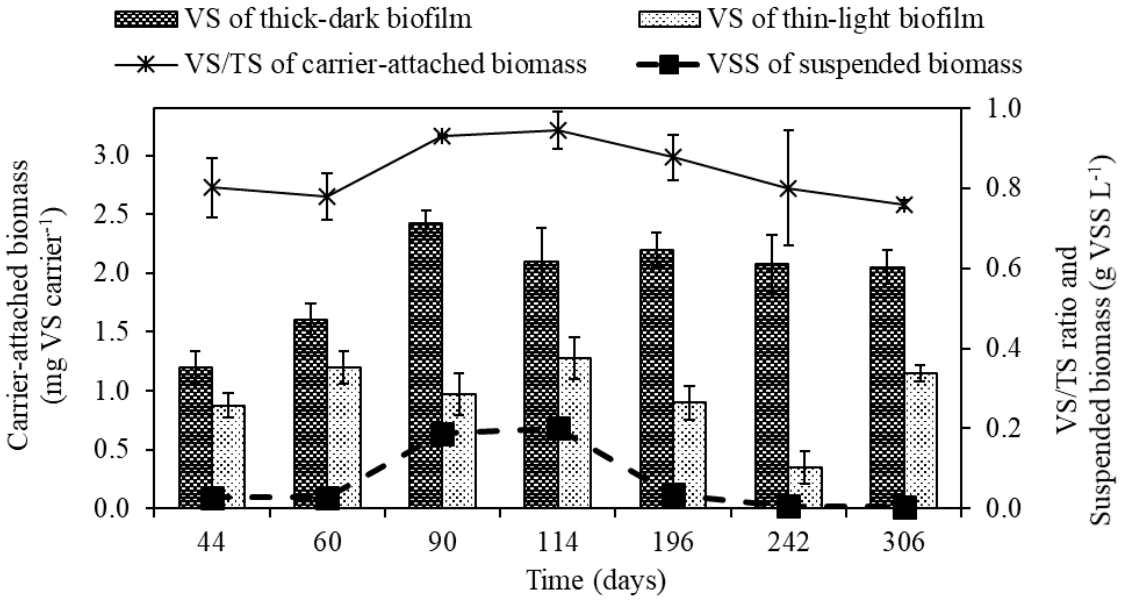

Figure 4.5. Biomass evolution in the MBBR during operational periods I (days 44, 60, 90 and 114), II (day 196), III (day 242) and IV (day 306).

Figure 4.6 shows the activity of carrier-attached and suspended biomass during the sequential feedings of $S_2O_3^{2-}$ and NO_3^- in batch activity tests. After the first, second and third sequential feeding, the carrier-attached biomass showed STUR and SNUR of 4.1-5.8 g $S_2O_3^{2-}$-S g VS d^{-1} and 0.84-1.81 g NO_3^--N g VS d^{-1}, respectively (Figure 4.6a, Table 4.3). STUR and SNUR of the suspended biomass increased from 1.13 (± 0.07) g $S_2O_3^{2-}$-S g VSS d^{-1} and 0.28 g NO_3^--N g VS d^{-1} after the first feeding to 4.91 (± 0.86) g $S_2O_3^{2-}$-

S g VSS d^{-1} and 1.10 (± 0.08) g NO_3^--N g VS d^{-1} after the third feeding, respectively (Figure 4.6b, Table 4.3).

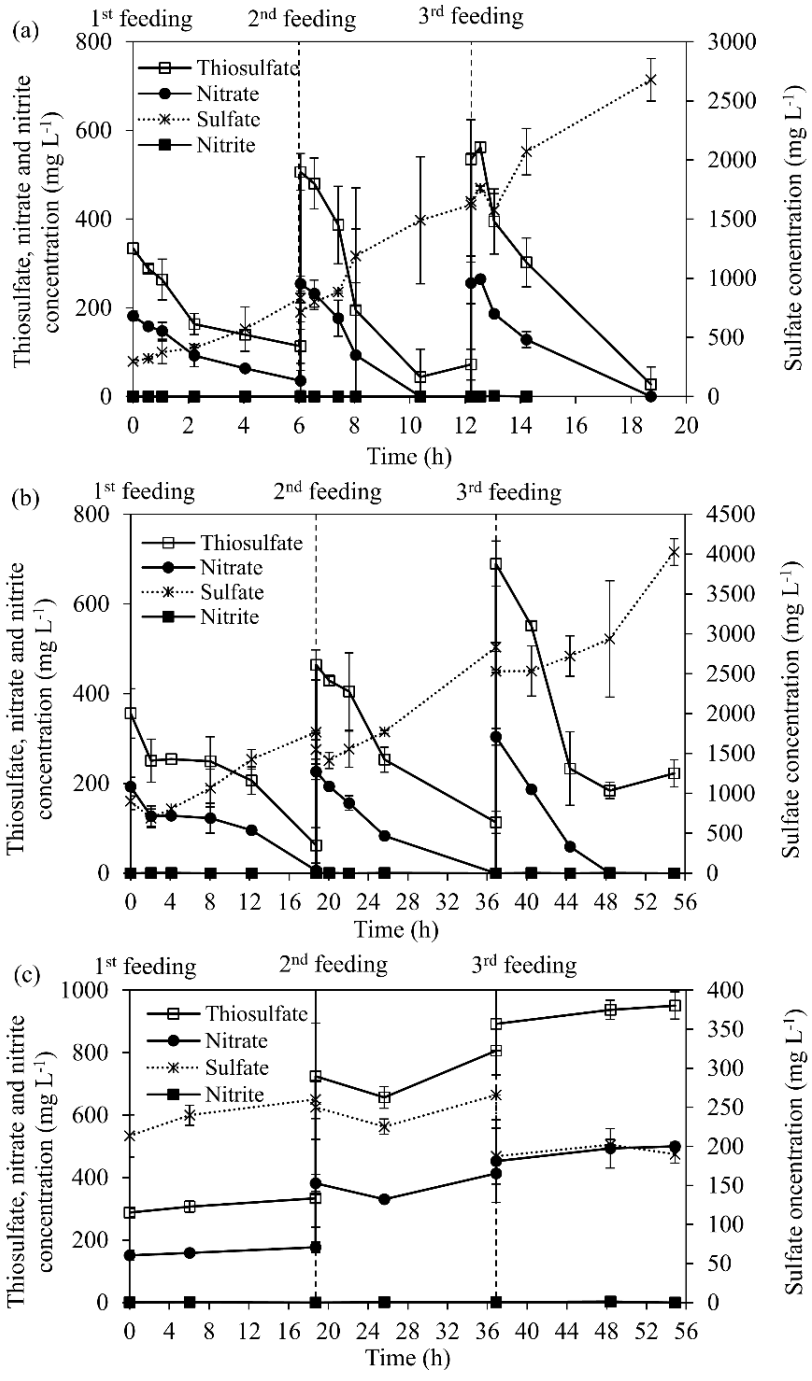

Figure 4.6. Thiosulfate, nitrate, nitrite and sulfate concentrations during sequential feeding in the batch bioassays performed with (a) carrier-attached biomass, (b) suspended biomass, and (c) without microorganisms (abiotic). Error bars represent the standard deviation.

A positive correlation between biomass weight on K1 carriers and the S^0 concentration in the MBBR was observed during this study (days 193, 240 and 300) (data not shown). The carriers with thick-dark biofilm (Figure 4.1a) contained a higher amount of S^0 (33.5-76.6 µg carrier^{-1}) than those with thin-light biofilm (Figure 4.1b) (8.2-14.6 µg carrier^{-1}).

4.3.4 Kinetic parameters of $S_2O_3^{2-}$ oxidation based on batch bioassays

The Monod model was successfully used to describe $S_2O_3^{2-}$ oxidation coupled to NO_3^- reduction at different N/S ratios during MBBR operation (Figure 4.7). The highest r_{max} (144.0 mg $S_2O_3^{2-}$-S g^{-1} VS h^{-1}) was obtained with the biomass taken in period V (N/S ratio of 0.5) after 42-day operation at severe NO_3^- limitation (N/S ratio 0.1, period IV), while similar r_{max} values (111.3 ± 1.8 mg $S_2O_3^{2-}$-S g^{-1} VS h^{-1}) were obtained in periods II (N/S ratio of 0.5) and III (N/S ratio of 0.3) (Table 4.2). The lowest biofilm affinity for $S_2O_3^{2-}$ (K_s = 1.70 mg $S_2O_3^{2-}$-S L^{-1}) was observed in bioassays performed during period II (N/S ratio of 0.5), while the highest K_s value (109.43 mg $S_2O_3^{2-}$-S L^{-1}) was observed during period IV (N/S ratio of 0.1).

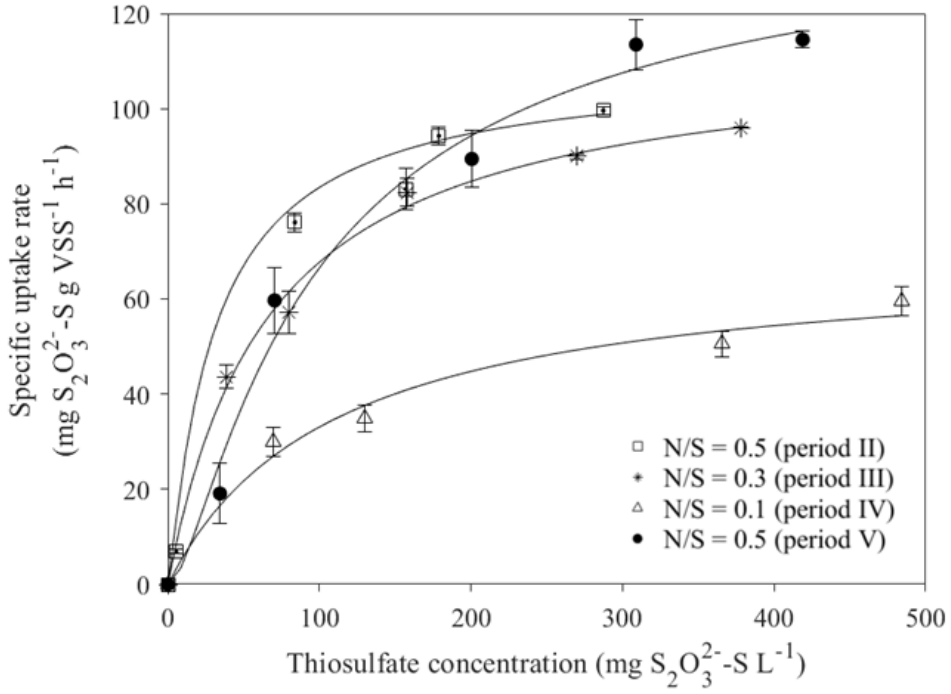

Figure 4.7. Monod model prediction for estimating the maximum rate of sulfur oxidation (r_{max}) as well as $S_2O_3^{2-}$ (K_s) and NO_3^- (K_n) affinity constants of MBBR biomass collected at different N/S ratios. Dots and lines represent experimental and model fitted data, respectively. The error bars indicate the standard errors between the experimental and model fitted data.

4.3.5 Microbial community profile

The results of the PCR-DGGE analysis showed that the microbial community structure of the carrier-attached biomass changed during long-term MBBR operation (Figure 4.8). The sequenced DGGE bands indicated that microorganisms having 97.6-99.6% similarity to *Thiobacillus* sp., *Chryseobacterium* sp., *Simplicispira* sp. and *Sulfuritalea* sp. were present in the MBBR biofilm during all the experimental periods. However, bands 9 and 11 related to a bacterium having 99.1-99.3% similarity to *T. denitrificans*, which were clearly visible in the DGGE profiles of periods I, III and IV, showed low intensity in period II. Bands 10 and 16, related to bacteria having 98.9 and 100% similarity to *Rhodocyclaceae* and *Thiomonas* sp., respectively, were detected in periods I, II and III but they faded away in period IV. Band 17, related to a bacterium with 99.3% similarity to *Desulfovibro* sp., was clearly detected in period III, whereas it had low intensity in periods I, II and IV. Bands 7 and 8 had no significant similarities to the bacteria in the database due to the poor quality of the sequenced DNA. The microbial community composition of the suspended biomass samples was very similar to the carrier-attached communities during each operational period (data not shown).

4.3.6 ANN modeling of MBBR performance

The best network topology of the ANN model developed for the MBBR had 4 neurons in the input layer, 4 neurons in the hidden layer and 3 neurons in the output layer (4-4-3). Altogether 50 data points were used for training, 16 for validation and 12 for testing, that corresponded to 65%, 20% and 15% of all data points, respectively (Table 4.5). The ANN model training was completed within 2 s and the best validation performance with a MSE of 0.013185 was achieved at an epoch size of 15. The values of coefficient of determination (R^2) of the training, validation and test data sets were 0.94, 0.92 and 0.95, respectively, which corresponded to an overall R^2 of 0.93 for the whole data set. The connection weights and the bias terms associated to the neurons in the three-layered ANN were as shown in Table 4.6. The $S_2O_3^{2-}$ RE and NO_3^- RE and the SO_4^{2-} production profiles predicted by the ANN model are shown in Figure 4.9.

.

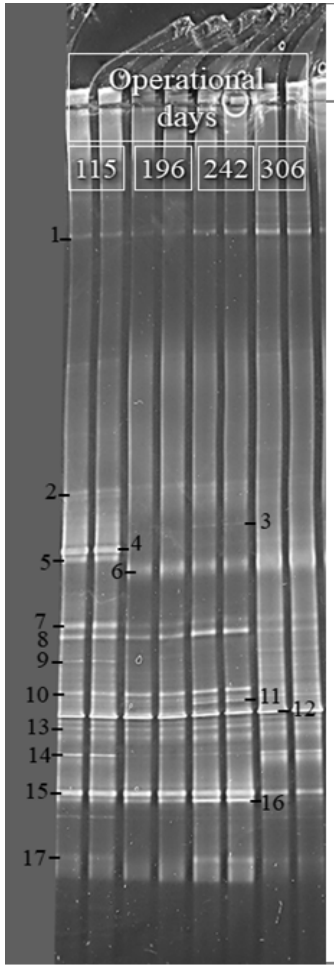

Band label	Affiliation	Class	Matching sequence length	Sequence ID	Similarity (%)
1	Uncultured bacterium clone LNH_9_9_11_Water.153675 16S ribosomal RNA gene		570	KM131698.1	100
2-3	*Flavobacteriaceae* bacterium	Flavobacteriales	410-434	EU642061.1	91.3-97.6
4-6	*Chryseobacterium* sp.	Flavobacteriales	451-526	EU706218.1	99.3-99.6
7	Uncultured bacterium partial 16S rRNA gene, isolate EFW618		463	LN889996.1	96.1
9, 11	*Thiobacillus denitrificans*	Betaproteobacteria	429-441	NR_025358.1	99.1-99.3
10	*Rhodocyclaceae* bacterium	Betaproteobacteria	434	FM207908.1	100
12	*Thiobacillus* sp.	Betaproteobacteria	458	KM595278.1	97.9
13	*Simplicispira* sp.	Betaproteobacteria	436	AB795522.1	98.6
14	Denitrifying bacterium	Betaproteobacteria	406	Y09967.1	93.9
15	*Sulfuritalea* sp.	Betaproteobacteria	488	JX493272.1	97.6
16	*Thiomonas* sp.	Betaproteobacteria	466	LN864654.1	98.9
17	*Desulfovibrio* sp.	Deltaproteobacteria	429	JX828422.1	99.3

Figure 4.8. PCR-DGGE profiling of the microbial community composition of the K1 carrier-attached biomass in the MBBR during experimental periods II (day 115), III (day 196), IV (day 242) and V (day 306). Each sample was run in duplicate.

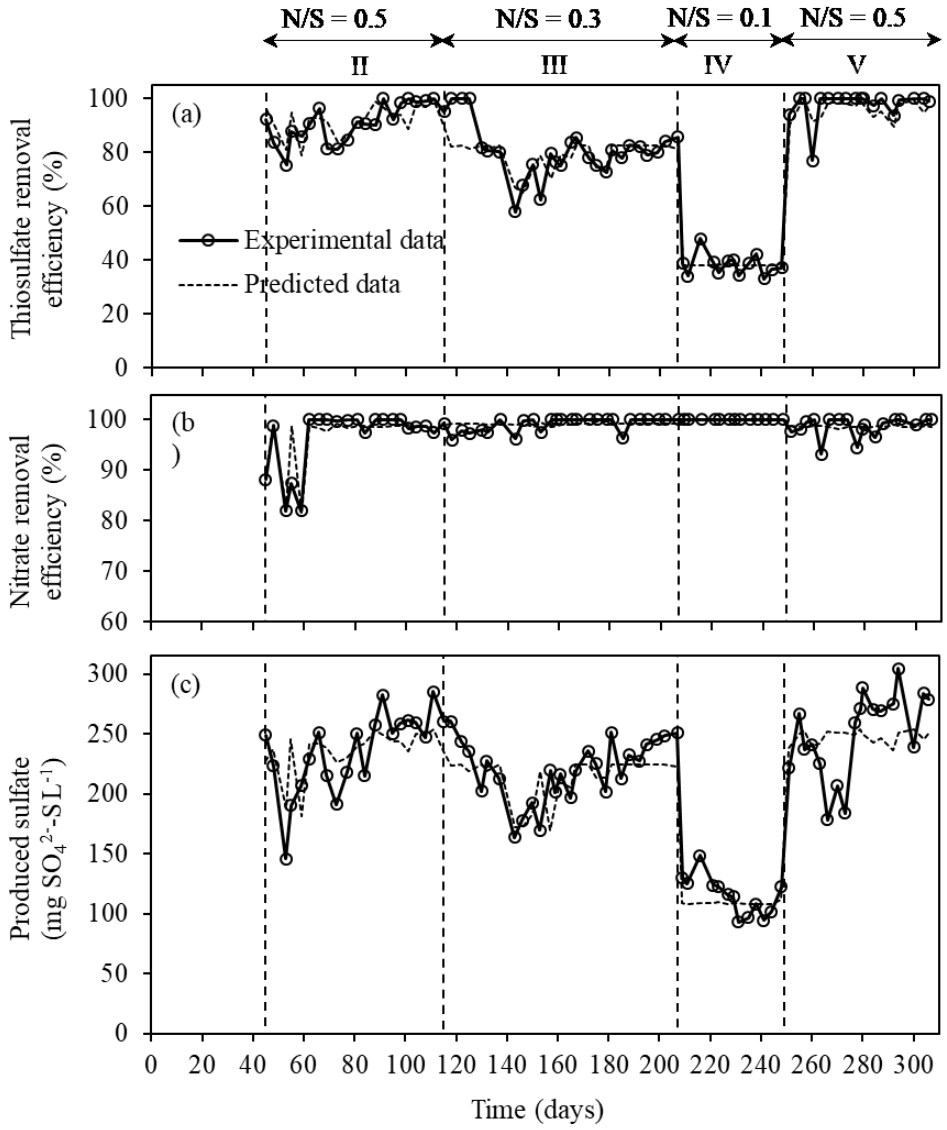

Figure 4.9. Artificial neural network model predicted and experimental data for (a) thiosulfate and (b) nitrate removal efficiency and (c) effluent sulfate during operational days 45 to 306.

Table 4.6. Connection weights between the input-hidden layer (W_{ih}) and hidden-output layer (W_{ho}) of the developed artificial neural network model (4-4-3).

Input	Input-hidden layer (W_{ih})				Hidden-output layer (W_{ho})		
	HID-1	HID-2	HID-3	HID-4	NO_3^- RE	$S_2O_3^{2-}$ RE	$SO_4^{2-}{}_{out}$
DO	-0.1629	-0.5262	14.8681	2.7219	-0.1003	0.4092	0.1756
pH	-2.7005	0.5462	-12.2174	0.3961	0.0386	-0.2569	-0.1379
$NO_3^-{}_{in}$	12.0382	-8.1713	-15.3434	7.1698	0.9873	0.1019	0.2297
$S_2O_3^{2-}{}_{in}$	-3.3725	0.2566	-0.0629	0.3265	0.0560	0.2580	0.3763
Bias term	4.4894	4.2162	19.1464	2.4816	-0.0707	-0.0312	-0.3966

Table 4.7 shows the absolute average sensitivity (AAS) and the average sensitivity (AS) values obtained from the sensitivity analysis of the developed ANN model. The AAS and AS values indicated that the influent NO_3^- and effluent pH were the most important factors affecting the $S_2O_3^{2-}$ RE (AAS = 0.4680 and 0.3528) and SO_4^{2-} production (AAS = 0.4357 and 0.3185). The NO_3^- RE was strongly influenced by the influent $S_2O_3^{2-}$ concentration (AAS = 0.3603) and the effluent pH (AAS = 0.3781).

Table 4.7. Sensitivity analysis of the artificial neural network model inputs.

Input variable	$S_2O_3^{2-}$ RE (%)		NO_3^- RE (%)		$SO_4^{2-}{}_{out}$ (mg L^{-1})	
	AAS	AS	AAS	AS	AAS	AS
$S_2O_3^{2-}{}_{in}$ (mg $S_2O_3^{2-}$-S L^{-1})	0.1513	-0.0656	0.3603	+0.1383	0.2180	-0.1258
$NO_3^-{}_{in}$ (mg NO_3^--N L^{-1})	0.3528	+0.3020	0.2180	-0.0094	0.3185	+0.3185
pH	0.4680	-0.4006	0.3781	-0.3781	0.4357	-0.3845
DO (mg L^{-1})	0.0279	+0.0145	0.0436	+0.0107	0.0278	+0.0278

Note: RE = removal efficiency; AAS and AS = absolute average sensitivity and average sensitivity, respectively

4.4 Discussion

4.4.1 Effect of NO_3^- limitation on MBBR performance

The $S_2O_3^{2-}$ RE in the MBBR was strictly correlated to NO_3^- loading rate (Figure 4.2). Decreasing the NO_3^- concentration in the feed reduced $S_2O_3^{2-}$ consumption and SO_4^{2-} production based on the stoichiometry described by Eq. (4.1). The $S_2O_3^{2-}$ REs (Figure 4.2c) during period V were higher than those observed in periods I and II, indicating that the sulfur-oxidizing capacity of the MBBR biofilm was enhanced after cultivation under severe NO_3^- limited conditions (N/S ratios of 0.3 and 0.1). In a previous work, the response of a sulfur-oxidizing FBR biofilm was investigated under the same NO_3^- limited conditions applied in this study (Khanongnuch et al., 2018). The $S_2O_3^{2-}$ RE of the FBR recovered to 80.8 (± 4.1)% 14 days after increasing the N/S ratio from 0.1 to 0.5. The MBBR operated in this study showed 8.2, 14.8 and 18.7% higher $S_2O_3^{2-}$ REs during operation at feed N/S ratios of 0.3, 0.1 and 0.5 (after severe NO_3^- limitation) and a much shorter recovery period (2 days) after restoring the N/S ratio to 0.5 (Khanongnuch et al., 2018). This was likely due to the different bioreactor configuration, microbial community structure as well as biomass and DO concentrations in the two reactors. The higher DO concentrations observed in the MBBR (0.45 mg L^{-1}) during the study compared to that maintained in the FBR (0.25 mg L^{-1}) likely stimulated bacteria capable sulfur oxidation using O_2 observed in the MBBR biofilm, i.e. *Thiomonas* sp. and *Thiobacillus* sp..

During this study, $S_2O_3^{2-}$ was oxidized to mainly SO_4^{2-} at all operational conditions. The effluent SO_4^{2-} concentrations exceeded the theoretical values (calculated based on Eq. 4.1) throughout the study (Figure 4.2c), being particularly high at the beginning of period I. The high SO_4^{2-} concentration observed in the MBBR effluent can be attributed to the oxidation of excess $S_2O_3^{2-}$ and other sulfur compounds formed in the system, i.e. H_2S and S^0. The biological disproportionation of excess $S_2O_3^{2-}$ into sulfide and SO_4^{2-} (according to Eq. 4.7) could have occurred in the MBBR:

$$S_2O_3^{2-} + H_2O \rightarrow SO_4^{2-} + 0.5H_2S + 0.5HS^- + 0.5H^+ \quad \Delta G^0 = -25 \text{ KJ mol}^{-1} \qquad (4.7)$$

Moreover, excess SO_4^{2-} production in the MBBR could be also produced by the complete oxidation of the biogenic S^0 accumulated intracellularly by the SO-NR bacteria during the previous long-term cultivation at extremely high $S_2O_3^{2-}$ concentrations and loading rates of the biomass used as inoculum (Di Capua et al., 2017c; Zou et al., 2016). NO_3^- limited conditions could promote partial $S_2O_3^{2-}$ oxidation to S^0 due to excess availability of electron donor compared to electron acceptor (Di Capua et al., 2017c). The S^0 disproportionation can be described by Eq. (4.8) (Finster et al., 1998):

$$4S^0 + 4H_2O \rightarrow 3H_2S + SO_4^{2-} + 2H^+ \qquad (4.8)$$

4.4.2 Effect of NO_3^- limited conditions on quantity and activity of the MBBR biomass

The MBBR showed good ability to develop a SO-NR biofilm, resulting in a VS/TS ratio up to 0.94 (Figure 4.5). The affinity constant of the SO-NR biomass for $S_2O_3^{2-}$ (K_s = 1.7 mg $S_2O_3^{2-}$ L, at N/S ratio of 0.5) observed in period II (N/S ratio of 0.5) was lower than values previously reported for sulfur-oxidizing biomass cultivated in other bioreactors, i.e. CSTR (16.1 mg $S_2O_3^{2-}$-S L^{-1}) and FBR (45.1 mg $S_2O_3^{2-}$-S L^{-1}) (Khanongnuch et al., 2018; Mora et al., 2015). The higher K_s observed at N/S ratios of 0.3 and 0.1 (Figure 4.7) were clearly due to the cultivation under NO_3^- limitation.

This study also revealed that the active SO-NR biomass decreased during cultivation at a N/S ratio of 0.1, resulting in the lowest r_{max}. The metabolic activity of the SO-NR bacteria populating the MBBR biofilm was enhanced after cultivation under severely NO_3^- limited conditions (N/S ratio of 0.1), as the highest r_{max} was observed during period V. The NO_3^- limited conditions probably also developed the density of active SO-NR biomass, as resulted higher of affinity constant but similar biomass concentration to periods II (N/S ratio of 0.5) (Table 4.2). Stress conditions such as nutrient limitation can induce a delay in biochemical conversions and enhance the EPS production, which serve as a supplementary substrate source and protect the bacterial cells from harmful toxic materials (Chénier et al., 2003). EPS overproduction can increase the adhesive properties of

the biofilm, enhancing its ability to withstand stress and harsh operating conditions (Garrett et al., 2008).

The results obtained from the sequential feeding experiment (Figure 4.6, Table 4.3) revealed that the suspended biomass in the MBBR could also remove $S_2O_3^{2-}$ and NO_3^- efficiently. As those sequential feedings resulted in an increase in the food to biomass ratio, i.e. high substrate availability, an increase in the STUR and SNUR was observed for the suspended biomass. This observation is in agreement with the results of Reboleiro-Rivas et al. (2013) who reported the utilization of high inlet organic loads with a lower biomass concentration in an aerobic moving bed membrane bioreactor treating municipal wastewater. In their study, the enzymatic activities, i.e. alkaline phosphatase, acid phosphatase and α-glucosidase activities, of the suspended biomass samples were higher than the activities observed in the attached biofilm samples due to better substrate diffusion. In biofilm reactors, fast-growing bacteria commonly grow in suspension, while the slow-growing bacteria aggregate to form a biofilm (Nogueira et al., 2002). However, NO_3^- limited conditions (N/S ratios of 0.3 and 0.1) strongly reduced the suspended biomass concentration, which decreased from 200 mg VSS L^{-1} (period I) to less than 5 mg VSS L^{-1} (period IV) (Figure 4.5). Conversely, the quantity of the attached growth biomass remained relatively constant after the acclimation period of the MBBR (day 90) (Figure 4.5), which confirms the good resilience of the SO-NR biofilm to withstand NO_3^- limited conditions.

During the MBBR operation, the observed fine activated carbon particles attached on the surface of the K1 carriers (thick-dark brown biofilm, Figure 4.1a) were able to maintain high and constant biomass quantity during the MBBR operation, particularly under severe NO_3^- limitation (Figure 4.5). Similarly, several studies reported that the activated carbon powder provided an efficient surface for the attached biomass and increase the resistant effect of fluctuating loading of substrate enhanced biofilm (Baêta et al., 2012; Skouteris et al., 2015; Woo et al., 2016).

4.4.3 Effect of NO_3^- limited conditions on microbial community composition

The MBBR enabled to effectively maintain and enrich autotrophic SO-NR bacteria such as *Thiobacillus* sp., *T. denitrificans* and *Sulfuritalea* sp., as they were detected at all tested N/S ratios (Figure 4.8). The growth of heterotrophic bacteria, such as *Thiomonas* sp., *Rhodocyclaceae* bacterium and *Chryseobacterium* sp., in the MBBR biofilm could be sustained by soluble microbial and cell lysis products (e.g. acetate, glucose and pyruvate) available under autotrophic conditions (Di Capua et al., 2017a; Khanongnuch et al., 2019; Wang et al., 2016). In particular, the reduction of biomass weight indicated that

biofilm degradation and detachment of the outer layer of the biofilm substantially occurred during period IV and were likely responsible for the enhanced growth of *Thiomonas*- and *Desulfovibrio*-like bacteria. *Desulfovibrio* are sulfate-reducing bacteria (SRB) commonly found in the inner parts of the biofilm and able of $S_2O_3^{2-}$ disproportionation to H_2S and SO_4^{2-} (Eqs. 4.7 and 4.8) (Di Capua et al., 2017b; Qian et al., 2015a).

4.4.4 ANN modeling and sensitivity analysis

Figure 4.9 shows that the experimental data was perfectly mapped by the ANN model with high R^2 values during training and testing (0.94 and 0.95, respectively). The R^2 of training (0.94) indicated that the model learned the relation between input output parameters (i.e. $S_2O_3^{2-}$ RE and NO_3^- RE and SO_4^{2-} production), while the R^2 of validation (0.92) demonstrated a good generalization capacity of the model (Antwi et al., 2017). The ANN developed in this study can be successfully used to predict the performance of full-scale MBBR operation in the future using influent pH, DO concentration and influent concentrations of $S_2O_3^{2-}$ or NO_3^- as input factors. Besides, other input parameters, such as the temperature or N_2 gas production could also be included as input factors to the model. In such cases, the number of neurons in the input and the hidden layers would change and the model should be trained offline to accommodate the new data set.

In practical situations, the ANN model can be trained using real-time data from the process and merged with previously recorded data in offline or online mode. In such cases, the software can be programmed to monitor the performance of the MBBR in real time and generate a set of signals that will raise an alarm to the plant operator about the faults that are occurring and enable suitable changes in the operational parameters to prevent failure of the MBBR using a set-point tracking control loop (M. E. López et al., 2017; Sadeghassadi et al., 2018).

4.5 Conclusions

Based on this study, the MBBR is a robust biofilm system able to sustain anoxic $S_2O_3^{2-}$ oxidation under severe NO_3^- limitation (feed N/S ratio 0.1). The SO-NR biofilm in the MBBR demonstrated high resiliency, being able to recover the $S_2O_3^{2-}$ RE from 37% to 94% within two days after increasing the feed N/S ratio from 0.1 to 0.5. The r_{max} and K_s of the NR-SO biofilm in the MBBR at a N/S ratio of 0.5 after severe NO_3^- limitation were 1.3-fold and 30-fold, respectively, higher than those at the same N/S ratio prior to cultivation at lower N/S ratios. Nevertheless, long-term operation at low N/S ratios reduced the amount of active SO-NR biomass in the system. Biomass sloughing due to long-term NO_3^- limitation sustained the growth of heterotrophic bacteria in the MBBR. An ANN

model coupled to a sensitivity analysis was able to predict and describe the effect of NO_3^- limited conditions on the MBBR performance.

4.6 References

Ahoranta, S.H., Kokko, M.E., Papirio, S., Özkaya, B., Puhakka, J.A., 2016. Arsenic removal from acidic solutions with biogenic ferric precipitates. J. Hazard. Mater. 306, 124–132.

Antwi, P., Li, J., Boadi, P.O., Meng, J., Shi, E., Deng, K., Bondinuba, F.K., 2017. Estimation of biogas and methane yields in an UASB treating potato starch processing wastewater with backpropagation artificial neural network. Bioresour. Technol. 228, 106–115.

APHA/AWWA/WEF, 1999. Standard methods for the examination of water and wastewater, 20th ed. American Public Health Association/American Water Works Association/Water Environment Federation, Washington D.C.

Baêta, B.E.L., Ramos, R.L., Lima, D.R.S., Aquino, S.F., 2012. Use of submerged anaerobic membrane bioreactor (SAMBR) containing powdered activated carbon (PAC) for the treatment of textile effluents. Water Sci. Technol. 65, 1540–1547.

Cano, P.I., Colón, J., Ramírez, M., Lafuente, J., Gabriel, D., Cantero, D., 2018. Life cycle assessment of different physical-chemical and biological technologies for biogas desulfurization in sewage treatment plants. J. Clean. Prod. 181, 663–674.

Chai, S., Guo, J., Chai, Y., Cai, J., Gao, L., 2014. Anaerobic treatment of winery wastewater in moving bed biofilm reactors. Desalin. Water Treat. 52, 1841–1849.

Chénier, M.R., Beaumier, D., Roy, R., Driscoll, B.T., Lawrence, J.R., Greer, C.W., 2003. Impact of seasonal variations and nutrient inputs on nitrogen cycling and degradation of hexadecane by replicated river biofilms. Appl. Environ. Microbiol.

Di Capua, F., Ahoranta, S.H., Papirio, S., Lens, P.N.L., Esposito, G., 2016. Impacts of sulfur source and temperature on sulfur-driven denitrification by pure and mixed cultures of *Thiobacillus*. Process Biochem. 51, 1576–1584.

Di Capua, F., Lakaniemi, A.-M., Puhakka, J.A., Lens, P.N.L., Esposito, G., 2017a. High-rate thiosulfate-driven denitrification at pH lower than 5 in fluidized-bed reactor. Chem. Eng. J. 310, 282–291.

Di Capua, F., Milone, I., Lakaniemi, A.-M., Hullebusch, E.D., Lens, P.N.L., Esposito, G., 2017b. Effects of different nickel species on autotrophic denitrification driven by thiosulfate in batch tests and a fluidized-bed reactor. Bioresour. Technol. 238, 534–541.

Di Capua, F., Milone, I., Lakaniemi, A.-M., Lens, P.N.L., Esposito, G., 2017c. High-rate autotrophic denitrification in a fluidized-bed reactor at psychrophilic temperatures. Chem. Eng. J. 313, 591–598.

Di Capua, F., Papirio, S., Lens, P.N.L., Esposito, G., 2015. Chemolithotrophic denitrification in biofilm reactors. Chem. Eng. J. 280, 643–657.

Di Capua, F., Pirozzi, F., Lens, P.N.L., Esposito, G., 2019. Electron donors for autotrophic denitrification. Chem. Eng. J. 362, 922–937.

Fan, M., Hu, J., Cao, R., Ruan, W., Wei, X., 2018. A review on experimental design for pollutants removal in water treatment with the aid of artificial intelligence. Chemosphere 200, 330–343.

Fernández, M., Ramírez, M., Gómez, J.M., Cantero, D., 2014. Biogas biodesulfurization in an anoxic biotrickling filter packed with open-pore polyurethane foam. J. Hazard. Mater. 264, 529–535.

Finster, K., Liesack, W., Thamdrup, B., 1998. Elemental sulfur and thiosulfate disproportionation by *Desulfocapsa sulfoexigens* sp. nov., a new anaerobic bacterium isolated from marine surface sediment. Appl. Environ. Microbiol. 64, 119–125.

Fogler, H.S., 2016. Elements of chemical reaction engineering, 5th ed. Prentice Hall, Indiana.

Garrett, T.R., Bhakoo, M., Zhang, Z., 2008. Bacterial adhesion and biofilms on surfaces. Prog. Nat. Sci. 18, 1049–1056.

Han, H.G., Zhang, L., Liu, H.X., Qiao, J.F., 2018. Multiobjective design of fuzzy neural network controller for wastewater treatment process. Appl. Soft Comput. J. 67, 467–478.

Abu Bakar, S.N.H., Abu Hasan, H., Mohammad, A.W., Abdullah, S.R.S., Haan, T.Y., Ngteni, R., Yusof, K.M.M., 2017. A review of moving-bed biofilm reactor technology for palm oil mill effluent treatment. J. Clean. Prod. 171, 1532–1545.

Khanongnuch, R., Di Capua, F., Lakaniemi, A.-M., Rene, E.R., Lens, P.N.L., 2019. H_2S

removal and microbial community composition in an anoxic biotrickling filter under autotrophic and mixotrophic conditions. J. Hazard. Mater. 367, 397–406.

Khanongnuch, R., Di Capua, F., Lakaniemi, A.-M., Rene, E.R., Lens, P.N.L., 2018. Effect of N/S ratio on anoxic thiosulfate oxidation in a fluidized bed reactor: experimental and artificial neural network model analysis. Process Biochem. 68, 171–181.

Kopec, L., Kopec, A., Drewnowski, J., 2018. The application of Monod equation to denitrification kinetics description in the moving bed biofilm reactor (MBBR). Int. J. Environ. Sci. Technol. 16, 1479–1486.

Krayzelova, L., Bartacek, J., Díaz, I., Jeison, D., Volcke, E.I.P., Jenicek, P., 2015. Microaeration for hydrogen sulfide removal during anaerobic treatment: a review. Rev. Environ. Sci. Biotechnol. 14, 703–735.

Krishnakumar, B., Majumdar, S., Manilal, V.B., Haridas, A., 2005. Treatment of sulphide containing wastewater with sulphur recovery in a novel reverse fluidized loop reactor (RFLR). Water Res. 39, 639–647.

Lee, J.-W., Suh, C., Hong, Y.-S.T., Shin, H.-S., 2011. Sequential modelling of a full-scale wastewater treatment plant using an artificial neural network. Bioprocess Biosyst. Eng. 34, 963–973.

López, M.E., Rene, E.R., Boger, Z., Veiga, M.C., Kennes, C., 2017. Modelling the removal of volatile pollutants under transient conditions in a two-stage bioreactor using artificial neural networks. J. Hazard. Mater. 324, 100–109.

Luo, J., Tian, G., Lin, W., 2013. Enrichment, isolation and identification of sulfur-oxidizing bacteria from sulfide removing bioreactor. J. Environ. Sci. 25, 1393–1399.

Mora, M., Dorado, A.D., Gamisans, X., Gabriel, D., 2015. Investigating the kinetics of autotrophic denitrification with thiosulfate: Modeling the denitritation mechanisms and the effect of the acclimation of SO-NR cultures to nitrite. Chem. Eng. J. 262, 235–241.

Mora, M., Guisasola, A., Gamisans, X., Gabriel, D., 2014. Examining thiosulfate-driven autotrophic denitrification through respirometry. Chemosphere 113, 1–8.

Nair, V. V., Dhar, H., Kumar, S., Thalla, A.K., Mukherjee, S., Wong, J.W.C., 2016. Artificial neural network based modeling to evaluate methane yield from biogas in a laboratory-scale anaerobic bioreactor. Bioresour. Technol. 217, 90–99.

Nogueira, R., Melo, L.F., Purkhold, U., Wuertz, S., Wagner, M., 2002. Nitrifying and heterotrophic population dynamics in biofilm reactors: effects of hydraulic retention time and the presence of organic carbon (vol 36, 469, 2002). Water Res. 36, 469–481.

Pokorna, D., Zabranska, J., 2015. Sulfur-oxidizing bacteria in environmental technology. Biotechnol. Adv. 33, 1246–1259.

Qian, J., Lu, H., Cui, Y., Wei, L., Liu, R., Chen, G.H., 2015. Investigation on thiosulfate-involved organics and nitrogen removal by a sulfur cycle-based biological wastewater treatment process. Water Res. 69, 295–306.

Reboleiro-Rivas, P., Martín-Pascual, J., Juárez-Jiménez, B., Poyatos, J.M., Hontoria, E., Rodelas, B., González-López, J., 2013. Enzymatic activities in a moving bed membrane bioreactor for real urban wastewater treatment: Effect of operational conditions. Ecol. Eng. 61, 23–33.

Rene, E.R., López, M.E., Veiga, M.C., Kennes, C., 2011. Neural network models for biological waste-gas treatment systems. N. Biotechnol. 29, 56–73.

Sadeghassadi, M., Macnab, C.J.B., Gopaluni, B., Westwick, D., 2018. Application of neural networks for optimal-setpoint design and MPC control in biological wastewater treatment. Comput. Chem. Eng.

Sahinkaya, E., 2009. Biotreatment of zinc-containing wastewater in a sulfidogenic CSTR: Performance and artificial neural network (ANN) modelling studies. J. Hazard. Mater. 164, 105–113.

Skouteris, G., Saroj, D., Melidis, P., Hai, F.I., Ouki, S., 2015. The effect of activated carbon addition on membrane bioreactor processes for wastewater treatment and reclamation - A critical review. Bioresour. Technol. 185, 399–410.

Wang, Y., Bott, C., Nerenberg, R., 2016. Sulfur-based denitrification: Effect of biofilm development on denitrification fluxes. Water Res. 100, 184–193.

Woo, Y.C., Lee, J.J., Shim, W.G., Shon, H.K., Tijing, L.D., Yao, M., Kim, H.S., 2016. Effect of powdered activated carbon on integrated submerged membrane bioreactor-nanofiltration process for wastewater reclamation. Bioresour. Technol. 210, 18–25.

Yang, W., Vollertsen, J., Hvitved-Jacobsen, T., 2005. Anoxic sulfide oxidation in wastewater of sewer networks. Water Sci. Technol. 52, 191–199.

Yetilmezsoy, K., Sapci-Zengin, Z., 2009. Stochastic modeling applications for the prediction of COD removal efficiency of UASB reactors treating diluted real cotton textile wastewater. Stoch. Environ. Res. Risk Assess. 23, 13–26.

Yuan, Q., Wang, H., Hang, Q., Deng, Y., Liu, K., Li, C., Zheng, S., 2015. Comparison of the MBBR denitrification carriers for advanced nitrogen removal of wastewater treatment plant effluent. Environ. Sci. Pollut. Res. 22, 13970–13979.

Zamaniyan, A., Joda, F., Behroozsarand, A., Ebrahimi, H., 2013. Application of artificial neural networks (ANN) for modeling of industrial hydrogen plant. Int. J. Hydrogen Energy 38, 6289–6297.

Zou, G., Papirio, S., Lakaniemi, A.-M., Ahoranta, S.H., Puhakka, J.A., 2016. High rate autotrophic denitrification in fluidized-bed biofilm reactors. Chem. Eng. J. 284, 1287–1294.

Chapter 5 H_2S removal and microbial community composition in an anoxic biotrickling filter (BTF) under autotrophic and mixotrophic conditions

This chapter has been submitted in modified form:

Khanongnuch, R., Di Capua, F., Lakaniemi, A.-M., Rene, E.R., Lens, P.N.L. 2019. H_2S removal and microbial community composition in an anoxic biotrickling filter under autotrophic and mixotrophic conditions, *J. Hazard. Mater.*, 367, 397-406.

Removal of H_2S from gas streams using NO_3^--containing synthetic wastewater was investigated in an anoxic biotrickling filter (BTF) at feed N/S ratios of 1.2-1.7 mol mol^{-1} with an initial nominal empty bed residence time of 3.5 min and a hydraulic retention time of 115 min. During 108 days of operation under autotrophic conditions, the BTF showed a maximum elimination capacity (EC) of 19.2 g S m^{-3} h^{-1} and H_2S removal efficiency (RE) above 99%. Excess biofilm growth reduced the HRT from 115 to 19 min and decreased the desulfurization efficiency of the BTF. When the BTF was operated under mixotrophic conditions by adding organic carbon (10.2 g acetate m^{-3} h^{-1}) to the synthetic wastewater, the H_2S EC decreased from 16.4 to 13.1 g S m^{-3} h^{-1}, while the NO_3^- EC increased from 9.9 to 11.1 g NO_3^--N m^{-3} h^{-1}, respectively. *Thiobacillus* sp. (98-100% similarity) was the only sulfur-oxidizing nitrate-reducing bacterium detected in the BTF biofilm, while the increased abundance of heterotrophic denitrifiers, i.e. *Brevundimonas* sp. and *Rhodocyclales*, increased the consumed N/S ratio during BTF operation. Residence time distribution tests showed that biomass accumulation during BTF operation reduced gas and liquid retention times by 17.1% and 83.5%, respectively.

5.1 Introduction

Hydrogen sulfide (H_2S) is generated by many industrial activities, livestock operations and anaerobic digestion of wastes (Kanjanarong et al., 2017; Pokorna and Zabranska, 2015). It is harmful to human health at 100 ppm_v (OSHA, 2005) and causes corrosion to equipment, e.g. pipelines, cogeneration engines and biogas distribution units (Soreanu et al., 2008). Particularly, H_2S needs to be removed from biogas to obtain a high quality, safe and convenient energy source from the anaerobic digestion of organic waste. The H_2S concentrations must be less than 1000 ppm_v for direct combustion of biogas, whereas for the application as a fuel in internal combustion engines or compressed natural gas production (CNG), the H_2S concentration must be less than 100 ppm_v and 16 ppm_v, respectively (Khanal and Li, 2017).

The use of anoxic biotrickling filters (BTF) for H_2S removal has received widespread industrial attention in the last few decades (Soreanu et al., 2009, 2008) as more environmentally friendly and cost-effective technologies than the conventional physico-chemical methods such as chemical precipitation and scrubbing (Almenglo et al., 2016b; Fernández et al., 2014). Anoxic H_2S oxidation via autotrophic denitrification proceeds according to Eqs. (5.1) and (5.2) by sulfur-oxidizing nitrate-reducing (SO-NR) bacteria (Mora et al., 2014):

$$HS^- + 1.23\ NO_3^- + 0.093\ NH_4^+ + 0.438\ HCO_3^- + 0.573\ H^+ + 0.027\ CO_2 \rightarrow 0.093\ C_5H_7O_2N + 0.614\ N_2 + SO_4^{2-} + 0.866\ H_2O \quad (5.1)$$

$$HS^- + 0.350\ NO_3^- + 0.013\ NH_4^+ + 0.059\ HCO_3^- + 1.4\ H^+ + 0.004\ CO_2 \rightarrow 0.013\ C_5H_7O_2N + 0.175\ N_2 + S^0 + 1.21\ H_2O \quad (5.2)$$

In recent years, H_2S removal in anoxic BTFs with recycling of the liquid medium has been studied at the laboratory-scale. In these studies, the authors have tested the performance of the BTF under the influence of different parameters and operational strategies such as the use of different packing materials, gas-liquid flow patterns, mode of reactor start-up and the effect of inlet H_2S concentrations (Table 5.1). When NO_3^- is supplied in batch feeding mode, the H_2S RE decreases once NO_3^- is completely consumed (Fernández et al., 2014; Soreanu et al., 2008). This leads to H_2S fluctuations during BTF operation which affects the stability of the BTF performance during long-term operation. Continuous NO_3^- supply can be applied to overcome the fluctuations typically observed in H_2S removal during BTF operation and reduce stress on microbial population due to NO_3^- starvation during discontinuous dosing (Almenglo et al., 2016c). López et al. (2018) showed that a feedforward control of NO_3^- dosing significantly reduces the impact of H_2S load fluctuation to the anoxic BTF performance, resulting in stable H_2S removal. In contrast, Li et al. (2016) observed no significant effects of the NO_3^- supplying strategy on H_2S removal at N/S ratios ranging from 0.25 to 1.0 and a constant H_2S concentration of ~1600 ppm_v. Additional research on the effects of H_2S concentration, N/S ratio and microbial community composition on anoxic desulfurization in BTF are still required.

Using chemical nitrate sources (e.g. $NaNO_3$ and KNO_3) increases the operating costs (Cano et al., 2018). Hence, a continuous system for H_2S removal from gas stream (e.g. biogas) using nitrified/NO_3^--containing wastewater would be a sustainable option, particularly if the H_2S treatment plant is located nearby a nitrification bioreactor (Cano et al., 2018). Since, some nitrified/NO_3^- contaminated wastewaters such as swine wastewaters, and effluents from nitrification units or fecal sludge treatment (Forbis-Stokes et al., 2018; Hunt et al., 2009; Jiang et al., 2013; Qian et al., 2015) can also contain residual organics, the effect of organic compound on the performance of a BTF relying on the activity of autotrophic microorganisms needs to be investigated. The main objective of this study was to evaluate the capability of an anoxic BTF for H_2S removal with continuous NO_3^- feeding under autotrophic and mixotrophic conditions at (i) different H_2S concentrations (from 100 to 500 ppm_v), (ii) different N/S ratios (1.2 and 1.7 mol mol^{-1}), and (iii) a feed acetate (CH_3COO^-) concentration of (51.4 ± 2.8 mg L^{-1}).

Table 5.1. H_2S removal selected anoxic biofilter/biotrickling filter studies conducted at different operational parameters.

Packing materials	Bed volume (L)	EBRT (min)	H_2S (ppm_v)	H_2S IL[b] (g S m^{-3} h^{-1})	The maximum EC[b] (g S m^{-3} h^{-1})	Gas flow rate (L h^{-1})	NO_3^- (mg L^{-1})	Trickling velocity (m h^{-1})	N/S ratio	pH of Liquid medium	Temperature (°C)	References
Plastic fiber	12.0	5-16	1000-4000	1-31	11.7	25-75	300-1800[c]	1.7	N.D. [d]	6.5	23 ± 2	Soreanu et al. (2008a)
Pall rings	2.40	2-17	1400-14600	9-201	170	8.4-60	50-600[c]	2.3-20.6	0.7-1.5	7.0	29 ± 1	Fernández et al. (2013)
OPUF[a]	2.40	2-6	850-8500	6-201	170	60	500-2400[c]	2.3-20.6	0.4-1.6	7.3-7.5	15-36	Fernández et al. (2014)
Concrete waste	7.85	1-5	25-1100	2-38	30.3	94-470	N.D.[d]	0.01[e]	0.4-1.6	7.0-9.0	N.D. [d]	Jaber et al. (2017)
PUF[a]	2.11	3	100-500	3-20	19.2	60	12-64	0.22	1.2-1.7	7.0 ± 2.0	24 ± 2	This study

Note: [a]OPUF and PUF = open-polyurethane foam and polyurethane foam, respectively
[b]IL and EC = inlet loading rate and elimination capacity, respectively
[c]Fresh NO_3^- was supplied once after NO_3^- in liquid medium was completely consumed
[d]N.D. = no data available[e] the liquid was trickled for 5 min each hour

5.2 Materials and methods

5.2.1 Synthetic nitrified wastewater

The synthetic nitrified wastewater used as the BTF medium had the following chemical composition (per liter): 0.07-0.46 g KNO_3, 1 g $NaHCO_3$, 0.2 g KH_2PO_4, 0.1 g NH_4Cl, 0.08 g $MgSO_4 \cdot 7H_2O$, 1 mL $FeSO_4 \cdot 7H_2O$ solution and 0.2 mL of trace element solution as described by Zou et al. (2016). Sodium acetate (230 g $CH_3COONa \cdot 3H_2O$ L^{-1}) was added as a model organic compound during the mixotrophic operation due to its ease of use and measurement. The pH of the synthetic wastewater was adjusted to ~7.0 with 37% HCl.

5.2.2 Source of inoculum and immobilization of biomass in the BTF

The inoculum was biofilm-attached K1 carriers (2.17 ± 0.15 VSS $carrier^{-1}$ and VSS/TSS ratio of 0.76) collected from a *Thiobacillus*-dominated lab-scale moving bed biofilm reactor (MBBR) previously operated for anoxic thiosulfate ($S_2O_3^{2-}$) oxidation (Khanongnuch et al., 2019). The inoculation was performed in a 5-L Schott-Duran bottle filled with 1.5 L of the polyurethane foam (PUF) cubes and 80 pieces of biofilm-attached K1 carriers. The bottle was filled with 3 L medium with 650 mg $S_2O_3^{2-}$-S L^{-1} and 140 mg NO_3^--N L^{-1}, respectively, and purged with N_2 gas for 10 min. After 14-day incubation at room temperature (22 ± 2 °C), the incubated PUF cubes were mixed with new PUF cubes and added to the BTF to obtain a bed height of 30 cm.

5.2.3 Bioreactor set-up and operation

The laboratory-scale BTF used in this study (Figure 5.1) was made of glass (Glass discovery, The Netherlands) and had an inner diameter and a bed height of 12 and 30 cm, respectively. The BTF packed-bed comprised of 264 pieces of PUF cubes (BVB Substrate, The Netherlands) with a cube size of 8 cm^3, a void ratio of 0.98 and a density of 28 kg m^{-3}, corresponding to total bed volume of 2.11 L occupied by PUF.

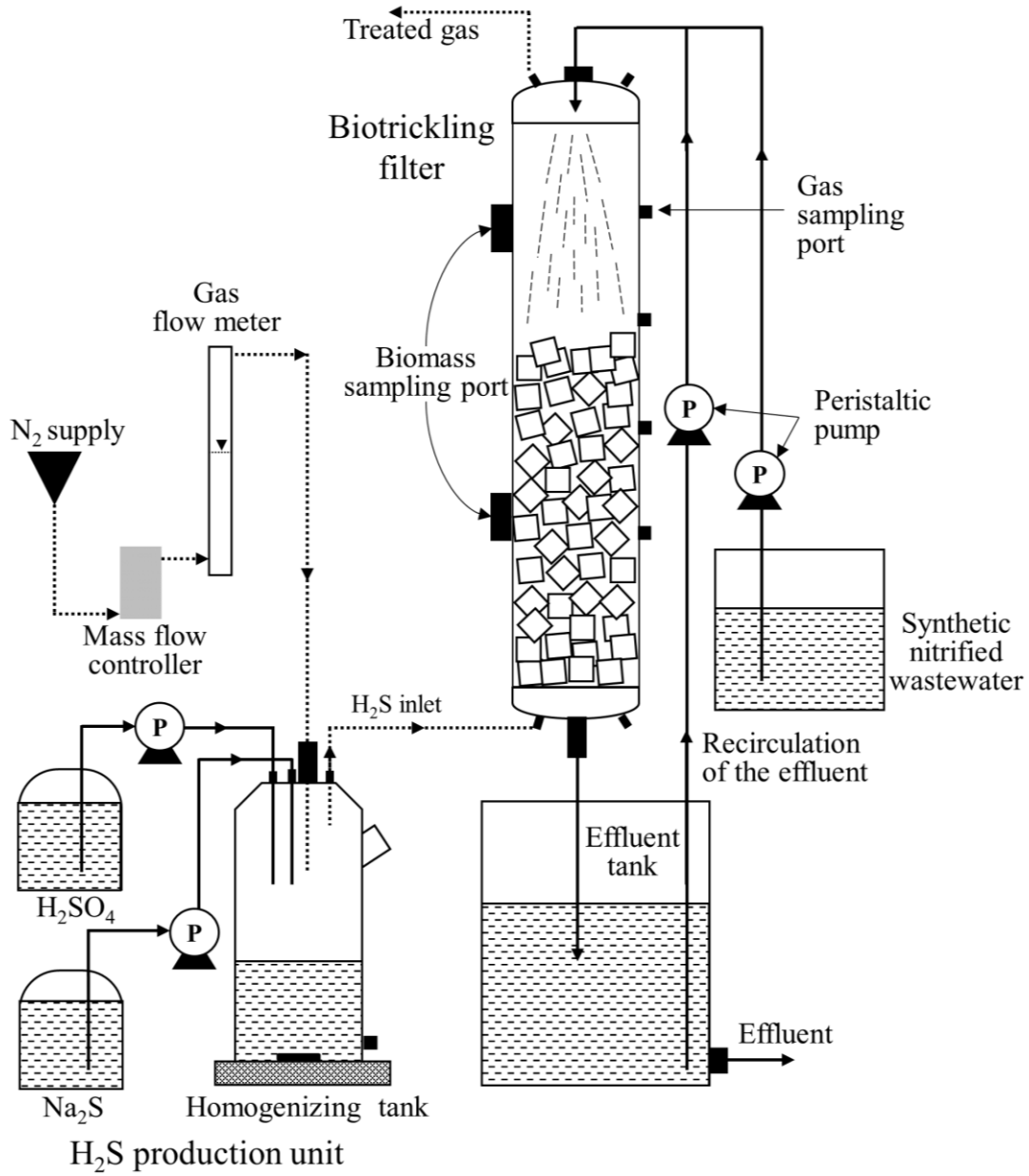

Figure 5.1. Schematic of the anoxic biotrickling filter for H_2S removal. Dotted and continuous lines represent the gas and liquid flows, respectively.

The gas stream fed to the BTF consisted of a mixture of N_2 gas and H_2S generated using solutions of Na_2S (0.1-0.3 N) and H_2SO_4 (1 N). The desired H_2S concentrations were obtained by controlling Na_2S concentrations and dripping rates using a peristaltic pump (Cole-Parmer, USA). The gas stream was fed to the BTF in counter-current mode, controlled by a Delta Smart II Mass Flow controller (Brooks instrument, USA) connected to a flow meter. The gas flow rate was maintained at 60 L h^{-1}, corresponding to a theoretical empty bed residence time (EBRT) of 3 min. The synthetic wastewater and recirculated

effluent were fed to the BTF from the top at a flow rate of 10 L d^{-1} and 50 L d^{-1} (Masterflex, Cole-Parmer, USA), respectively, to obtain a total trickling liquid flow rate of 60 L d^{-1}.

5.2.4 Residence time distribution (RTD) tests

The nominal EBRT and hydraulic residence time (HRT) of the BTF before and after the experiments (days -16 and 139, respectively) was estimated by residence time distribution (RTD) test and calculation described by Fogler (2016). The Bodenstein number (*Bo*) to characterize the axial dispersion in the BTF was determined based on the RTD test data. A potassium bromide solution (1 g KBr L^{-1}) was used as a tracer for determining the liquid residence time using the pulse input method as described by Fogler (2016). The KBr solution was injected through the influent and the KBr concentration in the effluent was monitored using a Cond3310 meter fitted with a TetraCon® 325 probe (WTW, Germany). To determine the gas residence time, CH_4 was used as a tracer and pulse injected to the influent gas stream. Effluent gas samples were collected once every 0.5 min to measure the CH_4 concentration using a SCION 456-GC gas chromatograph equipped with a PORABOND-Q capillary column (25 m × 0.53 mm × 10 mm) and a thermal conductivity detector (TCD) (SCION instrument, United Kingdom). The temperature of the oven and the detector were 25 and 140 °C, respectively. Helium was used as the carrier gas at a flow rate of 30 mL min^{-1}. The hydraulic retention time of NO_3^- in the BTF was determined using Eqs. (5.3)-(5.5).

$$\text{RTD function } (E(t)) = \frac{C_i}{\sum C_i \Delta t_i} \tag{5.3}$$

$$\text{Mean residence time } (t_m) = \frac{\sum t_i C_i \Delta t_i}{\sum C_i \Delta t_i} \tag{5.4}$$

$$\text{Experimental amount of outlet tracer} = \sum C_i \Delta t_i \tag{5.5}$$

where C_i is KCl concentration in the effluent (mg L^{-1}) and t_i is the measuring time (h).

The results obtained from the RTD tests were used to determine the Peclet number (Pe_r) is referred as Bodenstein number (*Bo*) (Fogler, 2016) that describes the mixing characteristics indicating the axial dispersion of the BTF as shown in Eq. (5.6), respectively.

$$\frac{\sigma^2}{t_m^2} = \frac{2}{Pe_r} - \frac{2}{Pe_r^2}\left(1-e^{-Pe_r}\right) \tag{5.6}$$

where σ^2 and t_m are the variance and mean residence time of the RTD, respectively.

The BTF was operated for 154 days in five different experimental phases (P1, P2, P3, P4 and P5) at a temperature of 24 (± 1) °C (Table 5.2). In phase P1, the BTF was filled

with 4 L of the synthetic wastewater containing initial concentrations of 67.4 (± 8.4) mg $S_2O_3^{2-}$-S L^{-1} and 15.5 (± 1.0) mg NO_3^--N L^{-1} and operated in batch mode for 11 days (days -15 to 0) to allow biofilm formation on the PUF cubes. From day 1 onwards (phase P2), the retaining synthetic wastewater was drained out from the BTF. The gas stream containing H_2S and the synthetic wastewater were continuously fed to the BTF. The inlet H_2S concentration in phase P2 was 111 (± 15) ppm_v and was increased to 434 (± 28) ppm_v from phase P3 onwards. NO_3^- concentrations were gradually increased from 12.2 (± 2.1) mg NO_3^--N L^{-1} in phase P2 to 62.1 (± 2.0) mg NO_3^--N L^{-1} in phase P5 (Table 5.2). In phase P5, acetate was added to the synthetic wastewater at a concentration of 51.4 (± 2.8) mg L^{-1}. Sulfur, nitrogen and carbon mass balances (Table 5.3) were performed based on the experimental data obtained during 3 days of steady-state observed in each experimental phase. Data from both gas and liquid phases were considered for sulfur and carbon mass balances, while nitrogen mass balance was based only on the liquid phase.

Table 5.2. Operational and influent characteristics during different phases of the biotrickling filter operation.

Phase	P1	P2	P3	P4	P5
Time (days)	-15-0	1-22	23-84	85-108	109-138
Feeding mode	Batch	Continuous	Continuous	Continuous	Continuous
H_2S (ppm_v)	-	111 (± 15)	434 (± 28)	433 (± 44)	428 (± 30)
IL[a] (g S m^{-3} h^{-1})	-	3.5-5.6	14.6-19.3	14.2-20.0	15.1-19.2
$S_2O_3^{2-}$-S (mg S L^{-1})	67.4 (± 8.4)	-	-	-	-
NO_3^--N (mg N L^{-1})	15.5 (± 1.0)	12.2 (± 2.1)	46.9 (± 2.6)	62.2 (± 1.8)	62.1 (± 2.0)
IL[a] (g N m^{-3} h^{-1})	-	1.8-2.9	8.3-10.2	11.8-12.9	11.4-15.0
CH_3COO^- (mg L^{-1})	-	-	-	-	51.4 (± 2.8)
Feed N/S ratio (mol mol^{-1})	0.53 (± 0.01)	1.18 (± 0.09)	1.21 (±0.05)	1.68 (± 0.18)	1.66 (± 0.12)

Note: [a] IL inlet loading rate

Table 5.3. Mass balances of sulfur, nitrogen and carbon in the anoxic biotrickling filter (BTF) during different experimental phases (P2-P5) of BTF operation.

EP[a]	Day	Sulfur (mg S d^{-1})								Nitrogen (mg N d^{-1})				Carbon (mg C d^{-1})					
		Influent			Effluent					Influent		Effluent		Influent			Effluent		
		H_2S	SO_4^{2-}	$S_2O_3^{2-}$	H_2S	SO_4^{2-}	$S_2O_3^{2-}$	S^{2-}	ΔS[b]	NO_3^-	NO_3^-	NO_2^-	ΔN[b]	HCO_3^-	CH_3COO^-	HCO_3^-	CH_3COO^-	CO_2	ΔC[b]
P2	20-22	226	256	3	0	477	30	0	-21	143	32	35	75	904	-	493	-	1	410
P3	48-50	867	217	3	55	909	22	20	82	474	50	2	422	979	-	502	-	13	442
P3	81-83	847	217	3	243	901	14	22	-112	484	27	2	455	914	-	524	-	36	354
P4	104-106	900	210	3	89	943	4	6	71	627	140	8	479	899	-	582	-	219	98
P5	135-137	844	224	3	265	728	3	12	63	640	18	5	617	920	227	748	2	1446	-1048

Note: [a]EP = experimental phase
[b]Δ = total influent load - total effluent load (ΔS and ΔC= estimated S^0 production and estimated carbon consumed, respectively, considering sulfur and carbon in both gas and liquid streams, while ΔN = estimated N_2 production estimated from nitrogen removed from liquid stream.)

5.2.5 Batch activity tests

Batch tests were performed at the end of each experimental phase to determine the SO-NR activity of the biomass attached on the PUF cubes. Tests I, II and III were conducted under autotrophic conditions with biomass collected during phases P3, P4 and P5 of BTF operation, respectively (Table 5.4). In addition, biomass collected during phase P5 was also tested with acetate in the medium (test IV). Three pieces of PUF cubes collected from the BTF were immediately cut into small pieces (2 × 0.67 × 0.67 cm^3) using a sterile surgical blade and divided into two 250-mL batch bottles (working volume of 200 mL), resulting in a total PUF volume of 12.1 (± 0.6) cm^3 per bottle. $Na_2S \cdot 9H_2O$ was added as the sulfide source to the synthetic nitrified wastewater. The bottles were purged with N_2 gas to ensure anoxic conditions and incubated at 22 (± 2) °C and 65 rpm mixing.

5.2.6 Microbial community analysis

Two pieces of PUF cubes were collected from the BTF at the end of each experimental phase (days 9, 25, 72, 112, and 138) for the microbial community analysis using polymerase chain reaction-denaturing gradient gel electrophoresis (PCR-DGGE). To detach the bacterial cells from the PUF, each PUF cube was immersed in 30 mL of sterile phosphate buffer solution (8.0 g L^{-1} NaCl, 0.20 g L^{-1} KCl, 0.97 g L^{-1} HPO_4^{2-} and 0.17 g L^{-1} H_2PO_4) and sonicated for 2 min. The solution was subsequently filtered through a Cyclopore track etched 0.2 µm membrane (Whatman, USA). The membranes containing the retained biomass were stored at -20 ºC for DNA extraction using the DNeasy® PowerSoil® Kit (QIAGEN, Germany). The procedure of polymerase chain reaction-denaturing gradient gel electrophoresis (PCR-DGGE) and reamplification of cut DGGE bands were performed according to Kolehmainen et al. (2007). DNA sequencing was performed by Marcrogen Europe Inc. (The Netherlands). The obtained sequencing data was analyzed using the BioEdit software (version 7.2.5) and compared with sequences in the National Center for Biotechnology Information (NCBI) database (https://blast.ncbi.nlm.nih.gov) using the Nucleotide BLAST (blastn) search tool.

5.2.7 Analytical methods

The liquid samples were filtered through 0.45 µm syringe filters (Sigma-Aldrich, USA) prior measurement of NO_3^-, $S_2O_3^{2-}$ and SO_4^{2-} concentrations using ion chromatography with a Dionex ICS-1000 (Thermo Fisher, USA) as described by Villa-Gomez et al. (2011). The pH of the solutions was measured using a Präzision-pH-Meter E510pH (Metrohm, Switzerland) equipped with a SenTix 21 pH electrode (WTW, Germany). The concentrations of total sulfide (S^{2-}), nitrite (NO_2^-) and COD were measured using colorimetric methods (APHA/AWWA/WEF, 1999) with a Lamda 365 UV/VIS spectrophotometer (Perkin-

Elmer, USA). Alkalinity was measured by potentiometric titration using a Titrino plus 848 titration meter equipped with a Metrohm 801 Stirrer (Metrohm AG, Switzerland). Acetate concentrations were measured using a Varian 430-GC gas chromatograph (Varian Inc., USA) as described by Eregowda et al. (2018). Gas composition (CH_4, CO_2 and N_2) was measured using a SCION 456-GC gas chromatograph as described in the Supplementary material. H_2S and O_2 concentrations in the gas phase were measured using a Dräger X-am® 7000 gas detector (Dräger, Germany).

Table 5.4. Specific sulfide and nitrate removal rate of biomass-attached polyurethane foam (PUF) cubes in the batch activity tests.

Day[a]	No.	Initial concentrations			Specific removal rates	
		S^{2-} (mg S L^{-1})	NO_3^--N (mg N L^{-1})	CH_3COO^- (mg L^{-1})	S^{2-} (g S m^{-3}_{PUF} h^{-1})	NO_3^- (g N m^{-3}_{PUF} h^{-1})
83	I	161 (± 16)	75.5 (± 1.1)	-	9.6 (± 1.2)	1.8 (± 0.4)
108	II	124 (± 8)	94.5 (± 2.1)	-	25.9 (± 4.0)	23.1 (± 3.2)
137	III	78.2 (± 1.7)	74.1 (± 5.0)	-	1131 (± 10)	359 (± 52)
137	IV	75.0 (± 0.2)	72.1 (± 4.4)	52.5 (± 3.5)	1061 (± 35)	1400 (± 57)

Note: [a] day of biomass harvesting

5.2.8 Data analysis

The statistical differences in the performance parameters during each phase of BTF operation, i.e. EC and RE, were determined using a one-way analysis of variance (ANOVA) in combination with Tukey's multiple comparison test (Minitab Inc., USA). The significant difference was considered at 95% ($P \leq 0.05$).

5.3 Results

5.3.1 H_2S and NO_3^- degradation behavior in the anoxic BTF

At the start of the experiments (day -16), based on the results of the RTD test the mean residence times of gas (EBRT) and liquid (HRT) in the BTF were 3.5 and 115 min, respectively (Figures 5.2 and 5.3). The initial Bodenstein number (*Bo*) in the BTF was 11.4, indicating a near typical plug-flow behavior ($Bo > 10$) (Kim and Deshusses, 2003). However, EBRT and HRT had decreased to 2.9 and 19 min, respectively, by the end of the experiment (Figures 5.2 and 5.3). As a result, *Bo* decreased to 9.4, which indicates that an axial dispersion of the gas phase, i.e. a nonuniform velocity profile, occurred in the BTF at the end of this study.

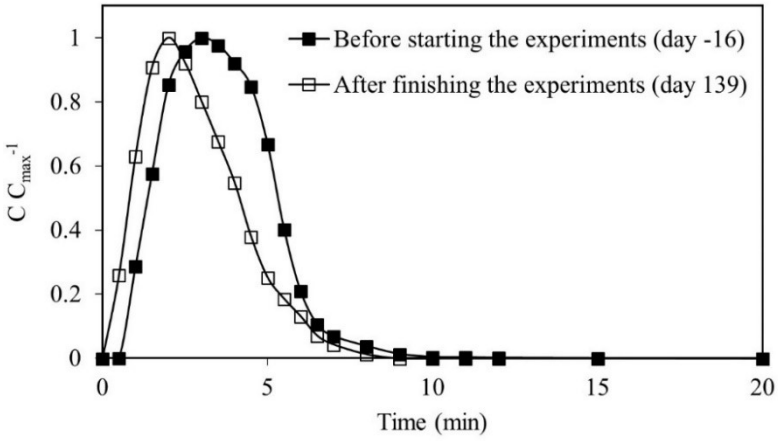

Figure 5.2. Residence time distribution (RTD) curves for the anoxic biotrickling filter obtained at a gas flow rate of 60 L h^{-1}.

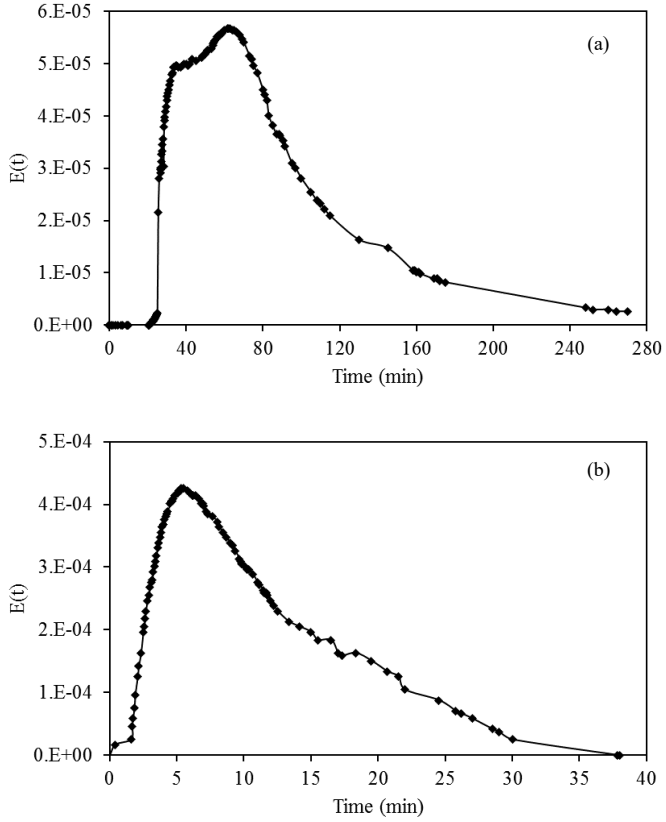

Figure 5.3. Residence time distribution (RTD) curves for the anoxic biotrickling filter (BTF) obtained with a liquid flow rate of 10 L d^{-1} (a) before starting the experiment (day -16) and (b) after finishing the experiment (day 139).

During phase P1 (days -15-0), the initial biofilm formation occurred and the obtained $S_2O_3^{2-}$ and NO_3^- RE were 65.2% and 94.2%, respectively (Figures 5.4c and e). The effluent pH increased from 7.2 to 7.8 between day -15 and day -13 and thereafter it gradually decreased to 7.0 (Figure 5.4a). In phase P2 (days 1-22), the H_2S feed was 111 (±

15) ppm_v, corresponding to an inlet loading rate (IL) of 3.5-5.6 g S m^{-3} h^{-1} and a N/S ratio of 1.18. The H_2S RE reached 100%, whereas the NO_3^- RE fluctuated between 26 and 82%. NO_2^- concentration, which was 22 mg NO_2^--N L^{-1} on day 0 and the concentration gradually decreased to 2.5 mg NO_2^--N L^{-1} by day 22. In phase P2, approximately 40% of the feed NO_3^- was converted to N_2 (Figure 5.5b). During phase P2, the effluent pH was 8.5 (± 0.3) and the effluent alkalinity concentration decreased from 555 mg HCO_3^- L^{-1} (day 1) to 188 mg HCO_3^- L^{-1} (day 22, Figure 5.4b).

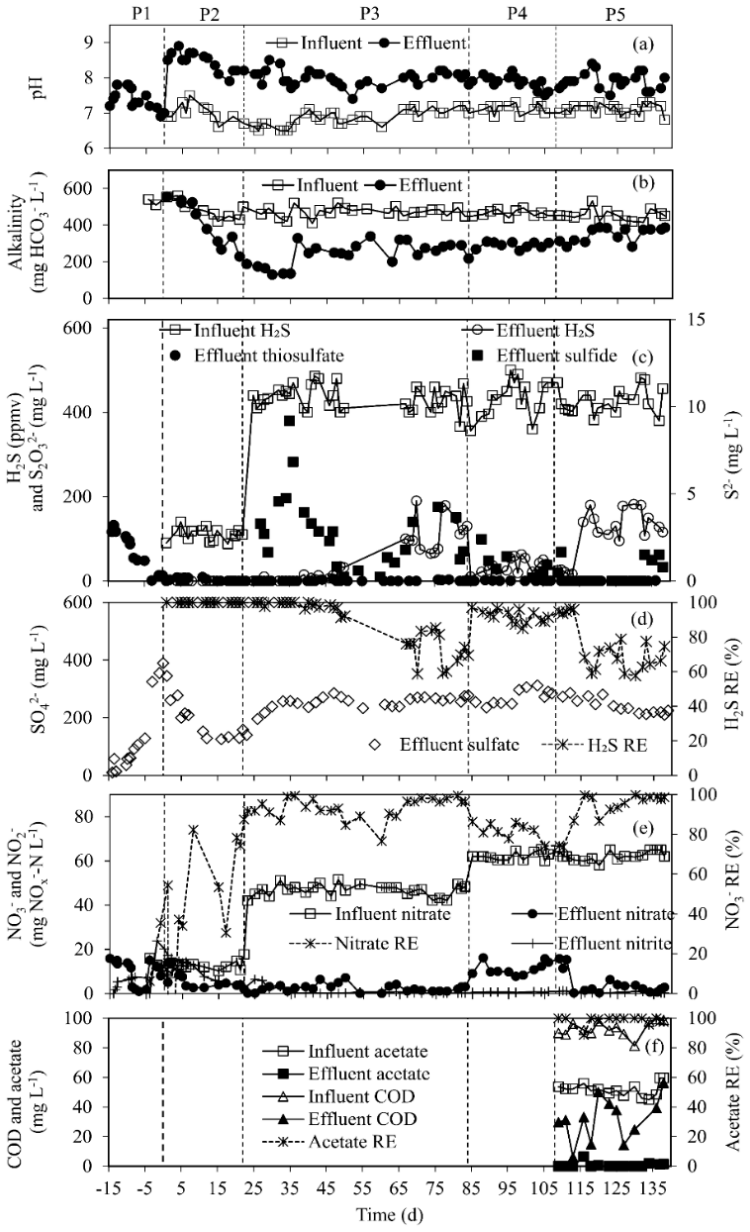

Figure 5.4. Time course profiles of influent and effluent pH, alkalinity, H_2S, S^{2-}, SO_4^{2-}, $S_2O_3^{2-}$, NO^{3-}, NO^{2-} and acetate concentrations and removal efficiency (RE) of H_2S and NO_3^- in the anoxic biotrickling filter.

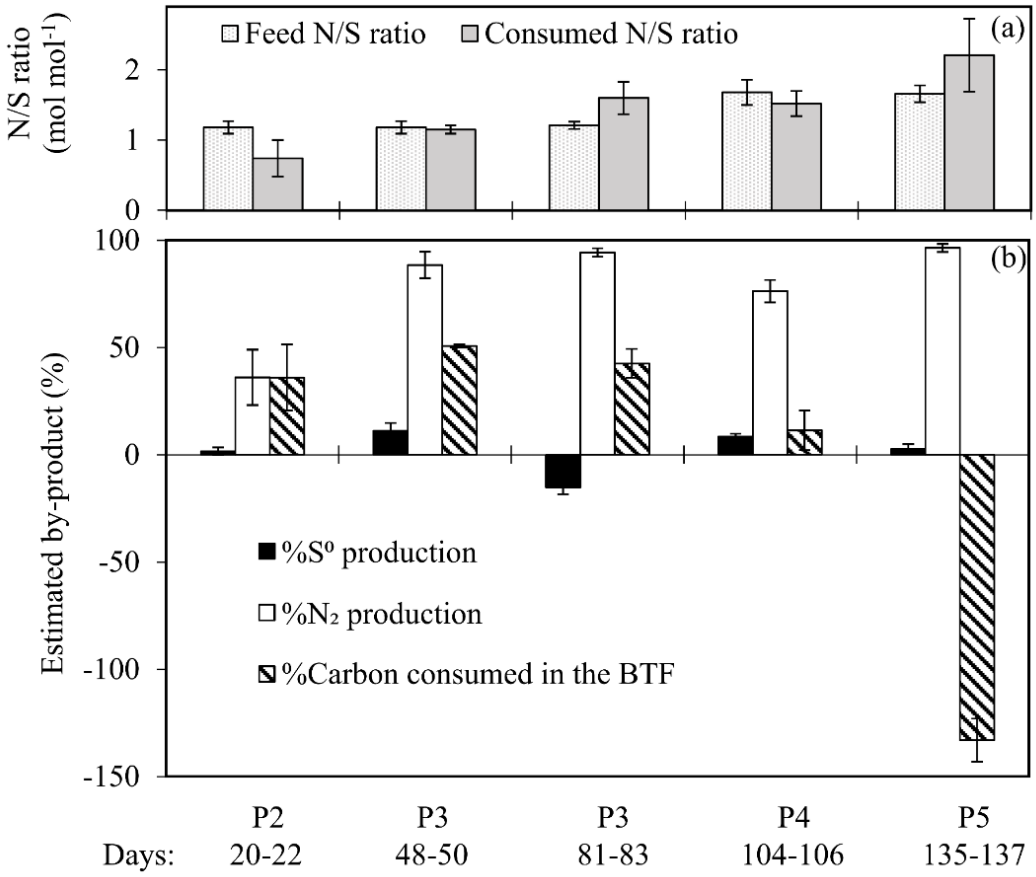

Figure 5.5. N/S ratios and the mass balances of sulfur, nitrogen and carbon during BTF operation. % S^0 production and % carbon consumed in the BTF was based on the influent and effluent concentrations of sulfur or carbon, while % N_2 production was estimated from NO_3^- and NO_2^- in the liquid phase.

In phase P3 (days 23-84), the inlet H_2S was increased to 434 (± 28) ppm_v (IL of 14.6-19.3 g S m^{-3} h^{-1}), while NO_3^- was kept constant (feed N/S ratio of 1.21). The effluent alkalinity was 269 (± 37) mg HCO_3^- L^{-1}, while pH remained stable at 7.9 (± 0.2) from phase P3 onwards (Figure 5.4a). During days 25-50, the H_2S RE was 98.2 (± 2.6)%, and a maximum elimination capacity (EC) of 19.2 g S m^{-3} h^{-1} was achieved on day 42. The consumed N/S ratio was 1.15 (± 0.06) and 11.2% of the fed H_2S was partially oxidized to S^0 (Figure 5.5). During days 51-66, the BTF was not monitored due to technical problems with the gas detector. Subsequently, the H_2S RE fluctuated in a range of 58-85% and the H_2S EC (12.4 ± 1.8 g S m^{-3} h^{-1}) was lower than that in phase P2 (Figure 5.6a), while the NO_3^- RE was >96% during days 67-83 (Figures 5.4c and e). The consumed N/S ratio (1.60 ± 0.23) was higher than the one observed during days 25-50 (Figure 5.5). NO_2^- was not detected in the effluent (<1 mg NO_2^--N L^{-1}) from phase P3 onwards (Figure 5.4e).

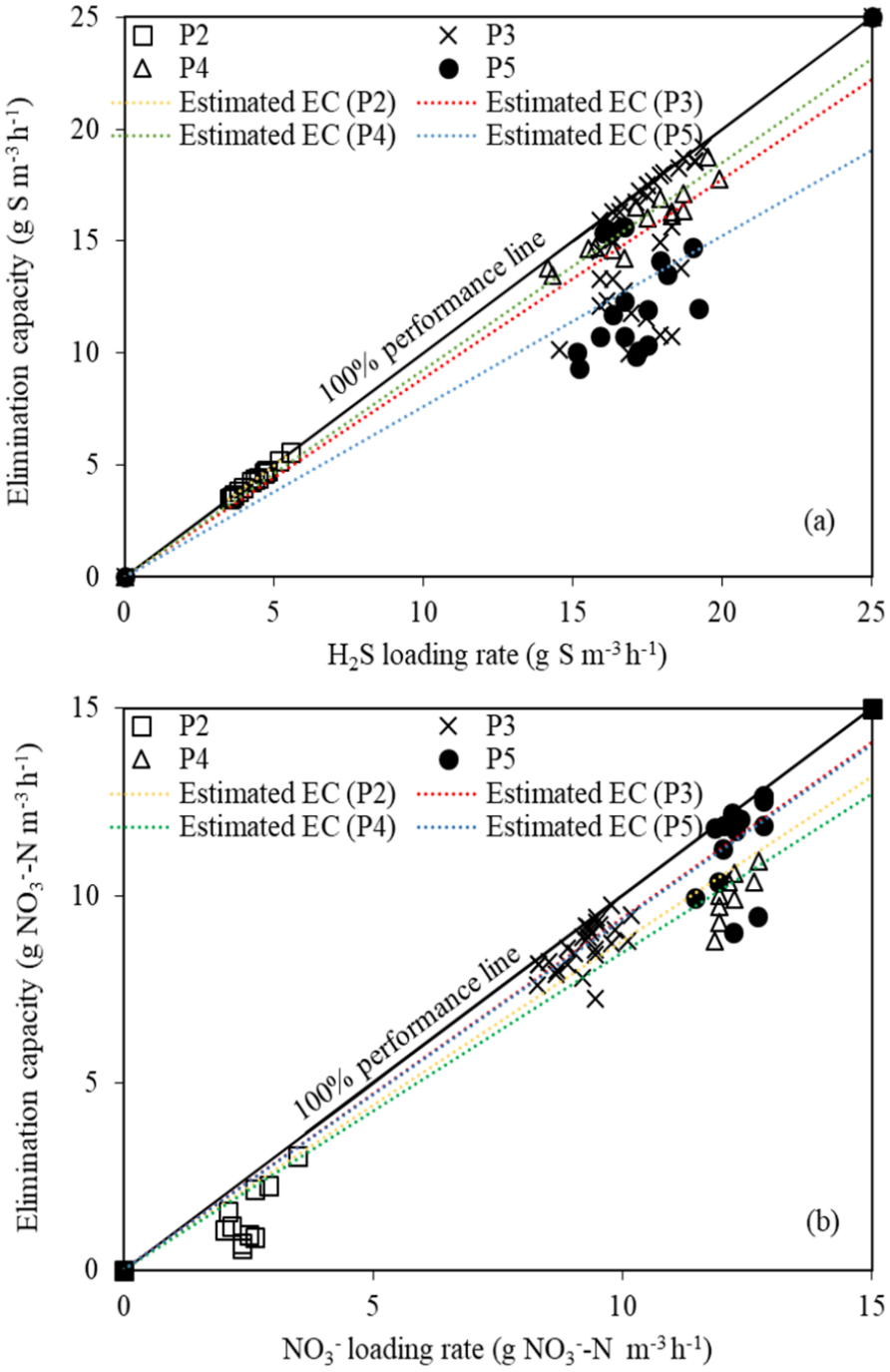

Figure 5.6. Elimination capacities (EC) of H_2S and NO_3^- during different experimental phases (P1-P5) of anoxic biotrickling filter operation.

To recover the H_2S RE that decreased during days 67-83 (phase P3), the influent NO_3^- IL was increased from 9.2 (± 0.55) (phase P3) to 12.3 (± 0.4) g N m^{-3} h^{-1} in phase P4 (Table 5.2). As a result, the average H_2S RE increased to 91.9 (± 3.7)% (EC of 16.4 ± 2.7 g S m^{-3} h^{-1}), while the NO_3^- RE slightly decreased to 82.1 ± 3.7% (days 85-108, Figure 5.4d). However, increasing NO_3^- IL increased the EC from 8.6 (± 0.6) in phase P3 to 10.0

(± 0.7) g N m^{-3} h^{-1} in phase P4. NO_3^- was partially reduced to NO_2^- (Table 5.3) and the estimated N_2 production (75%) was lower compared to phase P3 and P5 (Figure 5.5). Compared to the biomass taken from the BTF on day 83 (phase 3), the biomass collected on day 108 resulted in 2.7 and 12.8 times higher S^{2-} and NO_3^- removal rates, respectively (Table 5.4).

During phase P5, the feed acetate (10.2 g m^{-3} h^{-1}) was completely removed from the first day of the addition (Figure 5.4f). However, the H_2S RE decreased from 96.0% on day 113 to 67.3% on day 116. The NO_3^- RE and the maximum EC of the BTF in phase P5 were 96.5 (± 3.8)% and 11.1 (± 3.2) g NO_3^--N m^{-3} h^{-1} (day 134), respectively. The effluent alkalinity increased from 290 (± 18) mg HCO_3^- L^{-1} (phase P4) to 366 (± 33) mg HCO_3^- L^{-1} (phase P5) and the carbon production rate in the effluent of both gas and liquid phases increased to much higher values than those of the influent (Figure 5.5b). In batch tests conducted with biomass collected from phase P5 (day 137), the test without acetate addition (Table 5.4, test III) showed ~4 times lower specific NO_3^- removal rates compared to the test with acetate addition (Table 5.4, test IV). Besides, the specific S^{2-} removal rate in the test without acetate (1131 ± 10 g S m^{-3}_{PUF} h^{-1}) was slightly higher than the test with acetate (1061 ± 35 g S m^{-3}_{PUF} h^{-1}) (Table 5.4).

5.3.2 Microbial community in the BTF

The microbial community composition demonstrated by a DGGE profile showed an increase of in the number of DGGE bands during the BTF operation (Figure 5.7). Bacteria having 98-100% similarity to *Thiobacillus* sp. (bands 1, 9, 10, 12, 13, and 16) were dominant in the DGGE profiles of all experimental phases. The DGGE and sequencing results also indicated that *Stenotrophomonas* sp. (bands 3 and 14) and *Rhodobacter* sp. (bands 4, 15, and 17) were present in the culture during all the experimental phases of the BTF operation (Figure 5.7). Conversely, *Chryseobacterium* sp. (band 6) was observed only in the beginning (day 1). From day 84 onwards (the end of phase P3), the new DGGE bands were observed in the DGGE profile, i.e. *Brevundimonas* sp. (band 2), *Rhodocyclales* bacterium (band 11) and *Bacteroidetes* bacterium (bands 7 and 8).

.

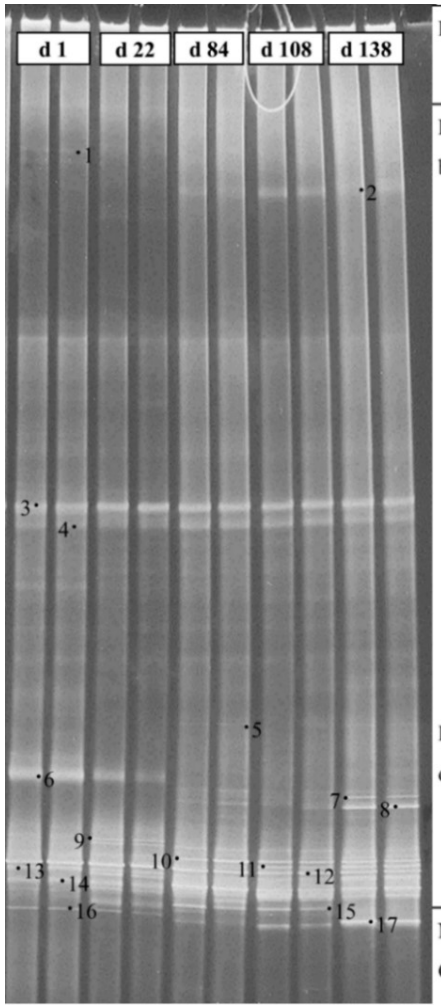

Phylum	Class/order/family	Affiliation[b]	Band(s)[a]	Accession number	Similarity (%)	Sequence length
Proteo-bacteria	*β*/Nitrosomonadales/ Thiobacillaceae	*Thiobacillus* sp.	1, 9, 10, 12, 13, 16	KM200026.1, JX530173.1, KM200014.1	98.0-100	433-508
	β/Rhodocyclales	*Rhodocyclales* bacterium	11	JQ723653.1	98.7	448
	β	Uncultured *β* proteobacterium	5	AY133108.1	92.6	448
	α/Caulobacterales/ Caulobacteraceae	*Brevundimonas* sp.	2	EF590244.1	100	425
	α/Rhodobacterales/ Rhodobacteraceae	*Rhodobacter* sp.	4, 15, 17	LN879886.1, JN648234.1	92.6-99.1	415-429
	γ/Xanthomonadales/ Xanthomonadaceae	*Stenotrophomonas* sp.	3, 14	KY490132.1, KM021209.1	91.8-94.5	456-510
Bacteroi detes	Flavobacteriia/Flavobacteriales/ Flavobacteriaceae	*Chryseobacterium* sp.	6	JQ724341.1	99.8	485
	-	*Bacteroidetes/Chlorobi* group bacterium	7, 8	KU685184.1, LN998004.1	96.2-96.3	416-418

Note: d= day, [a] Band label of DGGE-separated DNA fragments, and [b] Closet relative DGGE-separated DNA fragment in Genbank

Figure 5.7. Denaturing gradient gel electrophoresis (DGGE) profiles (left) and identification of the sequenced DGGE bands (right) of the biomass samples collected during the BTF operation.

5.4 Discussion

5.4.1 Effect of N/S ratio and organic carbon addition on H_2S removal in the anoxic BTF

The maximum H_2S EC of 19.2 g S m^{-3} h^{-1} (99% RE) obtained in this study was higher than the EC values reported in anoxic BTFs packed with lava rock (9.1 g S m^{-3} h^{-1}) (Soreanu et al., 2009) and plastic fibers (11.7 g S m^{-3} h^{-1}) (Soreanu et al., 2008), which were operated at ILs ranging from 2.0 to 23.5 g S m^{-3} h^{-1}. However, the H_2S EC in our study was lower than those observed in anoxic BTFs using open-pore PUF (Almenglo et al., 2016a; Fernández et al., 2014), pall ring (Fernández et al., 2013) and concrete waste (Jaber et al., 2017) (Table 5.1) as the packing material. In literature, BTFs in those studies were operated at very high H_2S IL (up to 200 g S m^{-3} h^{-1}) and a temperature of 30 °C, which is optimal for the activity of *Thiobacillus* sp. (Di Capua et al., 2016). As the EC trends during stable BTF operation (phase P1, P2 and P3) were very close to the 100% performance line (Figure 5.6a), probably higher ECs could still be attained if higher ILs were applied.

The complete H_2S oxidation to SO_4^{2-} in the presence of NO_3^- as the electron acceptor (Eq. 5.1) results in the production of 1.26 g SO_4^{2-}/g NO_3^- (stoichiometric N/S ratio of 1.2 mol mol^{-1}), whereas 1.47 g S^0/g NO_3^- (stoichiometric N/S ratio of 0.35) is produced during partial H_2S oxidation to elemental sulfur (Eq. 5.2). In this study, SO_4^{2-} was the main oxidation product during the entire BTF operation and its concentration in the effluent was close to the stoichiometric SO_4^{2-} production (Eq. 5.1). Jaber et al. (2017) studied anoxic biofilters packed with concrete waste at N/S ratios between 0.4 and 1.6 and observed that 55-57% of the inlet H_2S was oxidized to SO_4^{2-} at all tested N/S ratios. Other studies reported that systems operated at N/S ratios >1.6 mainly produce SO_4^{2-} (S^0 production <15%), while S^0 production in the range of 50-70% is typically observed at N/S ratios <0.7 (Fernández et al., 2014, 2013; Montebello et al., 2012).

The addition of organic carbon in the form of acetate (phase P5) led to mixotrophic conditions in the BTF which resulted in insufficient NO_3^- availability for H_2S removal by autotrophs. Conversely, acetate addition had a positive effect on NO_3^- removal, as the residual NO_3^- present in phase P4 was almost completely consumed via heterotrophic denitrification during phase P5 (Figures 5.4 and 5.5b). The batch activity tests also showed no substantial difference in the sulfide oxidation activity of the biomass cultivated in the BTF with and without acetate supplementation (Table 5.4 and Figure 5.8). This indicates that SO-NR bacteria were not inhibited by the growth of heterotrophic denitrifiers and

were abundantly present in the BTF biofilm during phase P5, as confirmed by the microbial community composition on day 138 (Figure 5.7). The consumption of residual NO_3^- at the beginning of phase P5 occurred simultaneously with a decrease in H_2S RE (day 116), indicating the fact that a shortage of NO_3^- decreased the desulfurization efficiency under mixotrophic conditions. Besides acting as an electron donor for denitrification, acetate addition also increases the alkalinity of the reactor (1.60 g HCO_3^-/g NO_3^-) according to the following equation (Bayrakdar et al., 2016):

$$NO_3^- + 0.63CH_3COO^- + 0.37CO_2 \rightarrow 0.5N_2 + 0.13H_2O + 1.63HCO_3^- \quad (5.7)$$

During phase P5, heterotrophic denitrification using acetate produced a large amount of alkalinity and CO_2 (Table 2), which act as a buffer and inorganic carbon source for the autotrophic microorganisms (Eq. 5.1).

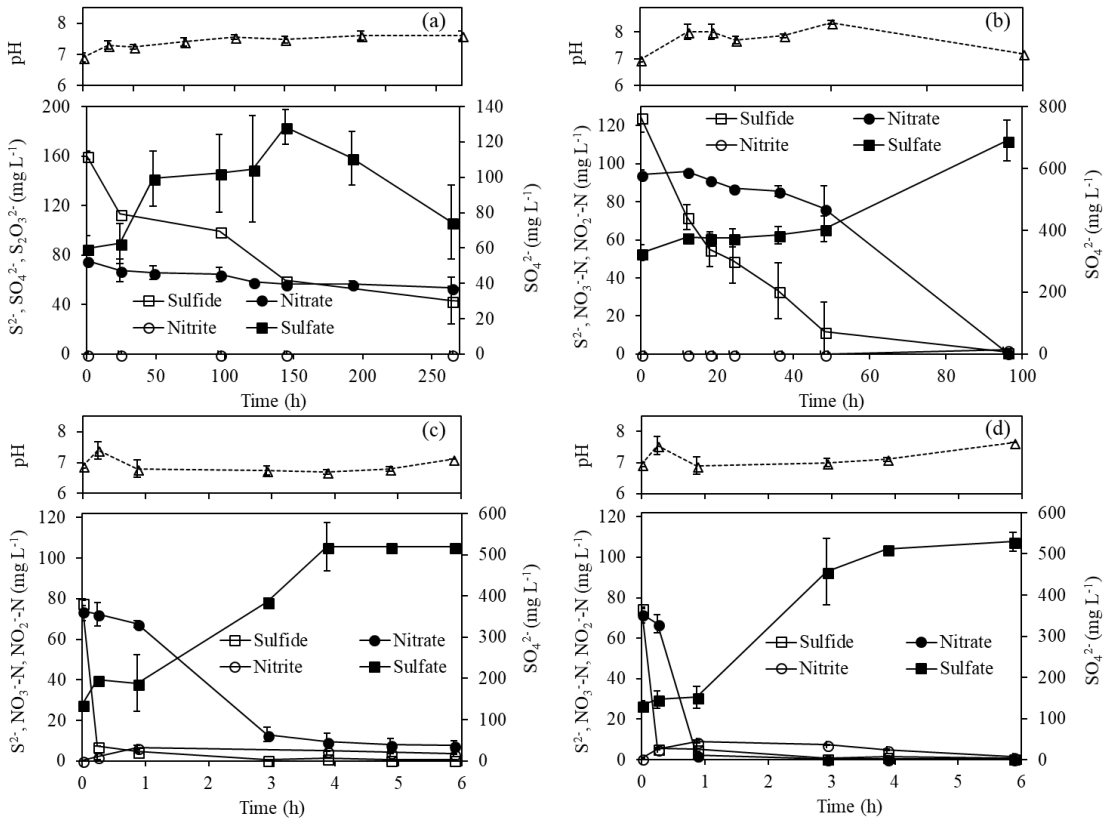

Figure 5.8. Profiles of sulfide (S^{2-}), nitrate (NO_3^-), nitrite (NO_2^-) and sulfate (SO_4^{2-}) concentrations in the batch activity tests with biofilm-attached PUF cubes collected from the BTF on days 83 (a), 108 (b) and 137 (c and d; with and without acetate addition, respectively).

5.4.2 Effect of substrate loads on microbial community profile in the anoxic BTF performance

Changes in microbial community profile were observed every time operational conditions were changed. Increase of both H_2S and NO_3^- ILs in phase P3 led to the appearance of new DGGE bands from day 84 onwards (Figure 5.7) representing *Brevundimonas* sp., *Rhodocyclales* bacterium and *Bacteroidetes* bacterium which are known heterotrophic denitrifiers (Tsubouchi et al., 2014). These microorganisms could compete for NO_3^- as electron acceptor with autotrophic denitrifiers in the anoxic BTF resulting in the decrease of H_2S RE in the end of phase P3 (Figure 5.4d). Huang et al. (2017, 2015) who studied the microbial community structure in five continuous stirred tank reactors (Huang et al., 2015) and three anaerobic sludge blanket reactors (Huang et al., 2017) for mixotrophic denitrifying sulfide removal also observed that microbial community was different at different NO_3^- and acetate ILs applied. Huang et al. (2017, 2015) reported that the optimized N/S molar ratio of 1.2 provided S^0 production of 75%, while the SO_4^{2-} was the main product of sulfide oxidation when the reactors were fed with higher or lower inlet NO_3^- and acetate loads (N/S ratio 0.4 and 1.8). Those studies (Huang et al., 2017, 2015) confirm our results: (i) the evolution of microbial community was due to the increase of H_2S and NO_3^- ILs from phase P2 to P3 (Table 5.2) and (ii) H_2S oxidation to S^0 or SO_4^{2-} was independent from N/S ratios, but related on NO_3^- and H_2S ILs, resulting in decreasing in $\%S^0$ production at the end of phase 3 which was likely caused by the insufficient NO_3^- IL (Figure 5.5).

Thiobacillus sp. was the only SO-NR bacterium observed in the BTF and therefore likely responsible for the simultaneous removal of H_2S and NO_3^- as described by Eq. (5.1) and (2). Based on those equations, *Thiobacillus* sp. also produced biomass by using bicarbonate as carbon source under autotrophic denitrification as evidenced by lower carbon in the effluents than in the influents during phases P2-P4 (Figure 5.5). *Stenotrophomonas* sp., a heterotrophic denitrifier detected since the first day of BTF operation, can survive by utilizing organic compounds excreted by autotrophs and microbial biomass ($C_5H_7O_2N$) produced during H_2S oxidation via autotrophic denitrification (Eq. 5.1) (Huber et al., 2016). Heterotrophic denitrifiers have also been detected from autotrophic systems, further verifying that their activity can be sustained by the organic material excreted by *Thiobacillus* sp. (Di Capua et al., 2017a, 2017b, 2017c). Figure 5.5 shows that carbon was bound to the biomass during the BTF operation under autotrophic conditions, and carbon was released during period P5, when acetate was added to the feed, indicating degradation of the previously formed biomass.

5.4.3 Effect of gas and liquid retention times on the BTF performance

During BTF operation, a trickling liquid velocity (TLV) of 0.22 m h^{-1} (flow rate of 2.5 L h^{-1}), H_2S RE >95% was observed without any operational problems such as clogging and bed drying. The TLV applied to the BTF in this study was much lower than those used in several previous studies, while gas flow rates were similar (Table 5.1). TLV typically has a low impact on the H_2S RE of anoxic BTFs as the electron acceptor (NO_3^-) is dissolved into the liquid phase (Brito et al., 2017; López et al., 2018), although high TLVs (>18.9 m h^{-1}) could severely impact the BTF performance by generating high pressure drops (Fernández et al., 2013) as well as biomass detachment (Fortuny et al., 2011). Biomass growth had a strong impact on the HRT of the BTF during the study. Based on the results of RTD tests, the HRT at the end of the study (day 139) was six times shorter than the initial HRT (day -16) (Figure 5.3), while the gas retention time was less affected (Figure 5.2). This suggests that the retention time of the liquid (synthetic nitrified wastewater) should be increased and optimized during BTF operation to maintain an optimal contact time between NO_3^- in the liquid phase and H_2S in the gas phase. The large decrease in the HRT during the study might explain the H_2S breakthrough observed at the end of phase P3 that required additional NO_3^- to maintain high desulfurization efficiency (Figures 5.4c and e). Conversely, the decrease of the EBRT from 3.5 to 2.9 min had less effect on the H_2S RE compared to that of the HRT reduction. The EBRTs tested in this study were in the range of commonly reported values for BTF operation under both anoxic (Table 5.1) and aerobic (Charnnok et al., 2013; Tomas et al., 2009) conditions. In a previous study involving mixtures of pollutants, Montebello et al. (2012) reported that a decrease of the EBRT in an anoxic BTF had much less effect on the H_2E RE than to the methylmercaptan (CH_3SH) RE due to the higher solubility of H_2S compared to that of CH_3SH.

5.4.4 Practical implications

The results from this study showed that H_2S removal could be achieved in an anoxic BTF using nitrified/NO_3^--contaminated wastewater as an electron acceptor. The anoxic BTF can be applied for biogas cleaning prior to CO_2 removal step or used in combined heat and power (CHP) unit without CH_4 dilution as N_2 and CO_2 production was not significant in the system. This study suggested that the BTF can be operated with wastewater containing organic carbon (C/N molar ratio of 0.2) as it is beneficial to increase the NO_3^- RE via mixotrophic denitrification and provides CO_2 as the endogenous carbon source instead of adding an external bicarbonate buffer (Bayrakdar et al., 2016). However, the NO_3^- IL should be optimized to serve sufficiently for both autotrophic and heterotrophic denitrifiers.

Acetate is a readily biodegradable organic carbon source that was chosen as a model organic compound in this study because it is easily available and measured. However, much more recalcitrant and slowly biodegradable organic matter would likely be available in the nitrified wastewater after aerobic oxidation. The presence of poorly soluble organic matter in the BTF may hamper gas/liquid mass transfer and the SO-NR activity, resulting in low H_2S and NO_3^- removal. Therefore, additional research on the effects of slowly biodegradable organic matter on BTF operation is therefore required.

5.5 Conclusions

The H_2S EC was achieved between 3.5 and 19.2 g S m^{-3} h^{-1} (>99% RE) using inlet NO_3^- loads of 2.9-12.9 NO_3^--N m^{-3} h^{-1} (N/S ratio=1.2-1.7) in the anoxic BTF. The addition of acetate reduced the H_2S RE from 92% to 67% and increased NO_3^- RE from 86% to 99%. *Thiobacillus* sp. was the sole SO-NR genus present in the biofilm of the BTF in all experimental phases, while populations of *Bacteroidetes* and *Rhodobacter* sp. were enhanced by acetate addition. Feed N/S ratios >1.7 are recommended for complete H_2S oxidation, although NO_3^- breakthrough in the effluent may occur at inlet loading rates 12.3 (± 0.4) g NO_3^--N m^{-3} h^{-1}. Low trickling liquid velocity (0.22 m h^{-1}) led to poor NO_3^- distribution and reduced the HRT during long-term anoxic BTF operation.

5.6 References

Almenglo, F., Bezerra, T., Lafuente, J., Gabriel, D., Ramírez, M., Cantero, D., 2016a. Effect of gas-liquid flow pattern and microbial diversity analysis of a pilot-scale biotrickling filter for anoxic biogas desulfurization. Chemosphere 157, 215–223.

Almenglo, F., Ramírez, M., Gómez, J.M., Cantero, D., 2016b. Operational conditions for start-up and nitrate-feeding in an anoxic biotrickling filtration process at pilot scale. Chem. Eng. J. 285, 83–91.

APHA/AWWA/WEF, 1999. Standard methods for the examination of water and wastewater, 20th ed. American Public Health Association/American Water Works Association/Water Environment Federation, Washington D.C.

Bayrakdar, A., Tilahun, E., Calli, B., 2016. Biogas desulfurization using autotrophic denitrification process. Appl. Microbiol. Biotechnol. 100, 939–948.

Jaber, M.B., Couvert, A., Amrane, A., Le Cloirec, P., Dumont, E., 2017. Hydrogen sulfide removal from a biogas mimic by biofiltration under anoxic conditions, J. Environ. Chem. Eng. 5, 5617–5623.

Cano, P.I., Colón, J., Ramírez, M., Lafuente, J., Gabriel, D., Cantero, D., 2018. Life cycle assessment of different physical-chemical and biological technologies for biogas desulfurization in sewage treatment plants. J. Clean. Prod. 181, 663–674.

Chaiprapat, S., Mardthing, R., Kantachote, D., Karnchanawong, S., 2011. Removal of hydrogen sulfide by complete aerobic oxidation in acidic biofiltration. Process Biochem. 46, 344–352.

Chen, C., Ren, N., Wang, A., Liu, L., Lee, D.J., 2010. Functional consortium for denitrifying sulfide removal process. Appl. Microbiol. Biotechnol. 86, 353–358.

Cheng, Z., Lu, L., Kennes, C., Yu, J., Chen, J., 2016. Treatment of gaseous toluene in three biofilters inoculated with fungi/bacteria: Microbial analysis, performance and starvation response. J. Hazard. Mater. 303, 83–93.

Di Capua, F., Ahoranta, S.H., Papirio, S., Lens, P.N.L., Esposito, G., 2016. Impacts of sulfur source and temperature on sulfur-driven denitrification by pure and mixed cultures of *Thiobacillus*. Process Biochem. 51, 1576–1584.

Di Capua, F., Lakaniemi, A.-M., Puhakka, J.A., Lens, P.N.L., Esposito, G., 2017. High-rate thiosulfate-driven denitrification at pH lower than 5 in fluidized-bed reactor. Chem. Eng. J. 310, 282-291.

Di Capua, F., Milone, I., Lakaniemi, A.-M., Hullebusch, E.D., Lens, P.N.L., Esposito, G., 2017a. Effects of different nickel species on autotrophic denitrification driven by thiosulfate in batch tests and a fluidized-bed reactor. Bioresour. Technol. 238, 534–541.

Di Capua, F., Milone, I., Lakaniemi, A.-M., Lens, P.N.L., Esposito, G., 2017b. High-rate autotrophic denitrification in a fluidized-bed reactor at psychrophilic temperatures. Chem. Eng. J. 313, 591–598.

Dumont, E., 2015. H_2S removal from biogas using bioreactors: a review. Int. J. Energy Environ. 6, 479–498.

Eregowda, T., Matanhike, L., Rene, E.R., Lens, P.N.L., 2018. Performance of a biotrickling filter for anaerobic utilization of gas-phase methanol coupled to thiosulphate reduction and resource recovery through volatile fatty acids production. Bioresour. Technol. 263, 591–600.

Feng, Q., Wang, Y., Wang, T., Zheng, H., Chu, L., Zhang, C., Chen, H., Kong, X., Xing, X.H., 2012. Effects of packing rates of cubic-shaped polyurethane foam carriers on the microbial community and the removal of organics and nitrogen in moving bed biofilm reactors. Bioresour. Technol. 117, 201–207.

Fernández, M., Ramírez, M., Gómez, J.M., Cantero, D., 2014. Biogas biodesulfurization in an anoxic biotrickling filter packed with open-pore polyurethane foam. J. Hazard. Mater. 264, 529–535.

Fernández, M., Ramírez, M., Pérez, R.M., Gómez, J.M., Cantero, D., 2013. Hydrogen sulphide removal from biogas by an anoxic biotrickling filter packed with Pall rings. Chem. Eng. J. 225, 456–463.

Ferrera, I., Massana, R., Casamayor, E.O., Balagué, V., Sánchez, O., Pedrós-Alió, C., Mas, J., 2004. High-diversity biofilm for the oxidation of sulfide-containing effluents. Appl. Microbiol. Biotechnol. 64, 726–734.

Fogler, H.S., 2016. Elements of chemical reaction engineering, 5th ed., Prentice Hall, Indiana.

Forbis-Stokes, A.A., Rocha-Melogno, L., Deshusses, M.A., 2018. Nitrifying trickling filters and denitrifying bioreactors for nitrogen management of high-strength anaerobic digestion effluent. Chemosphere 204, 119–129.

Hiraishi, A., Muramatsu, K., Urata, K., 1995. Characterization of new denitrifying *Rhodobacter* strains isolated from photosynthetic sludge for wastewater treatment. J. Ferment. Bioeng. 79, 39–44.

Huber, B., Herzog, B., Drewes, J.E., Koch, K., Müller, E., 2016. Characterization of sulfur oxidizing bacteria related to biogenic sulfuric acid corrosion in sludge digesters. BMC Microbiol. 16, 1–11.

Hunt, P.G., Stone, K.C., Matheny, T.A., Poach, M.E., Vanotti, M.B., Ducey, T.F., 2009. Denitrification of nitrified and non-nitrified swine lagoon wastewater in the suspended sludge layer of treatment wetlands. Ecol. Eng. 35, 1514–1522.

Jaber, M.B., Couvert, A., Amrane, A., Le Cloirec, P., Dumont, E., 2017. Hydrogen sulfide removal from a biogas mimic by biofiltration under anoxic conditions. J. Environ. Chem. Eng. 5, 5617–5623.

Kanjanarong, J., Giri, B.S., Jaisi, D.P., Oliveira, F.R., Boonsawang, P., Chaiprapat, S., Singh, R.S., Balakrishna, A., Khanal, S.K., 2017. Removal of hydrogen sulfide generated during anaerobic treatment of sulfate-laden wastewater using biochar: Evaluation of efficiency and mechanisms. Bioresour. Technol. 234, 115–121.

Khanal, S.K., Li, Y., 2017. Biogas Production and Applications, in: Li, Y., Khanal, S.K. (Eds.), Bioenergy: Principles and Applications. John Wiley & Sons Inc., New York, pp. 338–360.

Khanongnuch, R., Di Capua, F., Lakaniemi, A.-M., Rene, E.R., Lens, P.N.L., 2019. Long-term performance evaluation of an anoxic sulfur oxidizing moving bed biofilm reactor under nitrate limited conditions. Submitted for publication.

Kolehmainen, R.E., Langwaldt, J.H., Puhakka, J.A., 2007. Natural organic matter (NOM) removal and structural changes in the bacterial community during artificial groundwater recharge with humic lake water, Water Res. 41, 2715-2725.

Montebello, A.M., Mora, M., López, L.R., Bezerra, T., Gamisans, X., Lafuente, J., Baeza, M., Gabriel, D., 2014. Aerobic desulfurization of biogas by acidic biotrickling filtration in a randomly packed reactor. J. Hazard. Mater. 280, 200–208.

Mora, M., Fernández, M., Gómez, J.M., Cantero, D., Lafuente, J., Gamisans, X., Gabriel, D., 2014. Kinetic and stoichiometric characterization of anoxic sulfide oxidation by SO-NR mixed cultures from anoxic biotrickling filters. Appl. Microbiol. Biotechnol. 99, 77–87.

Morris, J.M., Jin, S., Crimi, B., Pruden, A., 2009. Microbial fuel cell in enhancing anaerobic biodegradation of diesel. Chem. Eng. J. 146, 161–167.

Pokorna, D., Zabranska, J., 2015. Sulfur-oxidizing bacteria in environmental technology. Biotechnol. Adv. 33, 1246–1259.

Rene, E.R., López, M.E., Veiga, M.C., Kennes, C., 2011. Neural network models for biological waste-gas treatment systems. New Biotechnol. 29, 56–73.

Reyes-Avila, J., Razo-Flores, E., Gomez, J., 2004. Simultaneous biological removal of nitrogen, carbon and sulfur by denitrification. Water Res. 38, 3313–3321.

Sahinkaya, E., Dursun, N., Kilic, A., Demirel, S., Uyanik, S., Cinar, O., 2011. Simultaneous heterotrophic and sulfur-oxidizing autotrophic denitrification process for drinking water treatment: Control of sulfate production. Water Res. 45, 6661–6667.

Soreanu, G., Béland, M., Falletta, P., Edmonson, K., Seto, P., 2008. Laboratory pilot scale study for H_2S removal from biogas in an anoxic biotrickling filter. Water Sci. Technol. 57, 201–207.

Soreanu, G., Béland, M., Falletta, P., Ventresca, B., Seto, P., 2009. Evaluation of different packing media for anoxic H_2S control in biogas. Environ. Technol. 30, 1249–1259.

Sun, M., Mu, Z.X., Chen, Y.P., Sheng, G.P., Liu, X.W., Chen, Y.Z., Zhao, Y., Wang, H.L., Yu, H.Q., Wei, L., Ma, F., 2009. Microbe-assisted sulfide oxidation in the anode of a microbial fuel cell. Environ. Sci. Technol. 43, 3372–3377.

Tabernacka, A., Zborowska, E., Łebkowska, M., Borawski, M., 2014. Air purification from TCE and PCE contamination in a hybrid bioreactors and biofilter integrated system. J. Hazard. Mater. 264, 363–369.

Tsubouchi, T., Koyama, S., Mori, K., Shimane, Y., Usui, K., Tokuda, M., Tame, A., Uematsu, K., Maruyama, T., Hatada, Y., 2014. *Brevundimonas denitrificans* sp. nov., a denitrifying bacterium isolated from deep subseafloor sediment. Int. J. Syst. Evol. Microbiol. 64, 3709–3716.

OSHA (U.S. Occupational, Safety and Health Administration), 2005. Fact sheet: Hydrogen sulfide. https://www.osha.gov/OshDoc/data_Hurricane_Facts/hydrogen_sulfide_fact.html, Accessed date: 21 September 2017.

Valle, A., Fernández, M., Ramírez, M., Rovira, R., Gabriel, D., Cantero, D., 2018. A comparative study of eubacterial communities by PCR-DGGE fingerprints in anoxic and aerobic biotrickling filters used for biogas desulfurization. Bioprocess Biosyst. Eng. 41, 1165–1175.

Villa-Gomez, D., Ababneh, H., Papirio, S., Rousseau, D.P.L., Lens, P.N.L., 2011. Effect of sulfide concentration on the location of the metal precipitates in inversed fluidized bed reactors. J. Hazard. Mater. 192, 200–207.

Yang, M., Zhong, Y., Zhang, B., Shi, J., Huang, X., Xing, Y., Su, L., Liu, H., Borthwick, A.G.L., 2018. Enhanced sulfide removal and bioelectricity generation in microbial

fuel cells with anodes modified by vertically oriented nanosheets. Environ. Technol. 1–10.

Yoshida, N., Yagi, K., Sato, D., Watanabe, N., Kuroishi, T., Nishimoto, K., Yanagida, A., Katsuragi, T., Kanagawa, T., Kurane, R., Tani, Y., 2005. Bacterial communities in petroleum oil in stockpiles. J. Biosci. Bioeng. 99, 143–149.

Zou, G., Papirio, S., Lakaniemi, A.-M., Ahoranta, S.H., Puhakka, J.A., 2016. High rate autotrophic denitrification in fluidized-bed biofilm reactors. Chem. Eng. J. 284, 1287–1294.

Chapter 6 Transient performance of an anoxic biotrickling filter (BTF) for treating H_2S and NO_3^--containing wastewater

This chapter will be submitted in modified form:

Khanongnuch, R., Di Capua, F., Lakaniemi, A.-M., Rene, E.R., Lens, P.N.L. 2019. Transient-state operation of an anoxic biotrickling filter for H_2S removal. *J. Hazard. Mater.*, In Press

The application of an anoxic biotrickling filter (BTF) for H_2S removal from contaminated gas streams is a promising technology for simultaneous H_2S and NO_3^- removal. Three transient-state conditions, i.e. different liquid flow rates, wet-dry bed operations and H_2S shock loads, were applied to a laboratory-scale anoxic BTF. In addition, bioaugmentation of the BTF with a H_2S removing-strain, *Paracoccus* MAL 1HM19, to enhance the biomass stability was investigated. Liquid flow rates (120, 60 and 30 L d^{-1}) affected the pH and NO_3^- removal efficiency (RE) in the liquid phase. Wet-dry bed operations at 2-2 h and 24-24 h reduced the H_2S elimination capacity (EC) by 60-80%, while the operations at 1-1 h and 12-12 h had a lower effect on the BTF performance. When the BTF was subjected to H_2S shock loads by instantly increasing the gas flow rate (from 60 to 200 L h^{-1}) and H_2S inlet concentration (from 112 ± 15 to 947 ± 151 ppm_v), the BTF still showed a good H_2S RE (>93%, EC of 37.8 g S m^{-3} h^{-1}). Bioaugmentation with *Paracoccus* MAL 1HM19 enhanced the oxidation of the accumulated S^0 to sulfate in the anoxic BTF.

6.1 Introduction

Hydrogen sulfide (H_2S) is one of the major gaseous pollutants emitted from wastewater treatment plants, landfill sites, anaerobic digesters and petroleum refinery processes and the H_2S concentration can be as high as 10,000 ppm_v (Khanal and Li, 2017; Muñoz et al., 2015; Yang et al., 2017). H_2S causes odor nuisance at concentrations as low as 0.025 ppm_v and represents an immediate hazard to human health at concentrations >600 ppm_v (Yalamanchili and Smith, 2008). Among the different biological techniques for H_2S removal from waste gas streams, biotrickling filters (BTFs) are widely used because they are easy to operate, economically viable and more efficient than conventional biofilters (Barbusinski et al., 2017). The major difference is that the trickling liquid in the BTF is continuously passed over the filter bed (packed with inert materials) to provide sufficient moisture and nutrients for the growth of microorganisms present in the BTF.

In recent years, H_2S removal in anoxic BTFs using nitrate (NO_3^-) as an electron acceptor has gained increasing interest (Almenglo et al., 2016b; Fernández et al., 2014; Jaber et al., 2017; López et al., 2017). NO_3^- can be cost-effectively fed to an anoxic BTF by using nitrified wastewater as the trickling liquid (Cano et al., 2018), resulting in a potential sustainable technology for combined H_2S and NO_3^- removal from waste streams. Anoxic H_2S removal is carried out by sulfur-oxidizing nitrate-reducing (SO-NR) bacteria, according to Eqs. (6.1) and (6.2) (Mora et al., 2014):

:

$$HS^- + 1.23\ NO_3^- + 0.093\ NH_4^+ + 0.438\ HCO_3^- + 0.573\ H^+ + 0.027\ CO_2 \rightarrow 0.093\ C_5H_7O_2N + 0.614\ N_2 + SO_4^{2-} + 0.866\ H_2O \quad (6.1)$$

$$HS^- + 0.350\ NO_3^- + 0.013\ NH_4^+ + 0.059\ HCO_3^- + 1.4\ H^+ + 0.004\ CO_2 \rightarrow 0.013\ C_5H_7O_2N + 0.175\ N_2 + S^0 + 1.21\ H_2O \quad (6.2)$$

During full-scale BTF operation, unexpected (transient) operating conditions, such as a process shut down during weekends, equipment malfunctions, sudden or unexpected changes in process conditions, are regularly encountered and can cause irregular inlet gas flow rates and variations in the inlet contaminant concentrations. This will affect the activity of microorganisms as well as the bioreactor stability (Rodriguez et al., 2014; San-Valero et al., 2017). Recent studies have investigated the impact of transient conditions, such as pollutant shock loads and starvation periods, on the performance of aerobic BTFs removing H_2S and other gaseous pollutants (Kim et al., 2008; López et al., 2017; Mohammad et al., 2017; Rene et al., 2010; Romero-Hernandez et al., 2013). Till to date, anoxic BTFs have only been studied under steady-state conditions to evaluate their performance using different packing materials, H_2S loading rates, gas flow rates or liquid flow rates (Almenglo et al., 2016a; Fernández et al., 2014, 2013; Montebello et al., 2012; Soreanu et al., 2009). The response of an anoxic BTF performing simultaneous waste gas desulfurization and wastewater denitrification to transient-state operation has, however, not yet been investigated.

The present study aimed, therefore, to evaluate the effect of several transient conditions on the performance of an anoxic BTF for H_2S removal using NO_3^--containing trickling liquid. Transient-state operation of the anoxic BTF included the application of: (i) different liquid flow rates, (ii) wet-dry bed operations, and (iii) H_2S shock loads by suddenly increasing both the gas flow rate and the inlet H_2S concentration in the gas stream. Furthermore, bioaugmentation of the BTF with a biomass dominated by *Paracoccus* MAL 1HM19 was performed to investigate if addition of a SO-NR bacterium enhances the biomass stability of an anoxic BTF for simultaneously treating H_2S and NO_3^- contaminated waste streams.

6.2 Materials and methods

6.2.1 BTF set-up and synthetic wastewater composition

The anoxic BTF used in this study was previously operated for 138 days under steady-state conditions (Khanongnuch et al., 2019). The BTF, having an inner diameter and height of 12 and 50 cm, respectively, was packed with polyurethane foam (PUF) cubes

(8 cm^3 each) to a volume of 2.11 L. The trickling liquid consisted of a NO_3^- rich medium containing (per 1 L): 0.07-0.46 g KNO_3, 1 g $NaHCO_3$, 0.2 g KH_2PO_4, 0.1 g NH_4Cl, 0.08 g $MgSO_4 \cdot 7H_2O$, 1 mL $FeSO_4 \cdot 7H_2O$ solution (2 mg L^{-1}) and 0.2 mL of trace element solution, as described by Khanongnuch et al. (2019). The inlet gas stream consisted of a mixture of N_2 and synthetic H_2S as described by Khanongnuch et al. (2019).

6.2.2 BTF operation

The BTF was operated for 78 days to evaluate three different transient-state conditions (phases I-III) and investigate the bioaugmentation of the BTF (phase IV) (Figure 6.1). Table 6.1 describes the operational conditions tested during each transient-state test and normal operation. The latter was applied for 1-4 days to stabilize the BTF performance at the end of each transient-state test. Under normal conditions, the BTF was fed with an inlet H_2S concentration of 116 (±2) ppm_v, gas flow rate of 60 L h^{-1}, a feed N/S molar ratio of 3 and a tricking liquid flow rate of 60 L d^{-1}. During phases I, II and III, the effect of, respectively, the liquid flow rates, wet-dry bed operation and H_2S shock load conditions was tested. In phase IV, the BTF was bioaugmented with a biomass dominated by *Paracoccus* MAL 1HM19 which is a SO-NR bacterium isolated from a hot spring in Thailand showing good capacity to grow at varied environmental conditions, e.g. NaCl concentrations of 0.03-7% *w/v* and temperatures of 20-50 °C (Watsuntorn et al., 2017).

During phase I (days 0-21), the liquid flow rates were increased stepwise from 30 L d^{-1} (days 0-6) to 60 L d^{-1} (days 7-12) and 120 L d^{-1} (days 13-19), while the gas flow rate was kept constant at 60 L h^{-1} (Table 6.1). On days 20-21, the BTF was operated under normal conditions before initiating the next transient condition.

During phase II (days 22-50), the BTF was tested under four different wet-dry bed operations by supplying the trickling liquid to the BTF at four different time intervals: (i) 12 h wet-12 h dry (days 22-30), (ii) 24 h wet-24 h dry (days 31-41), (iii) 1 h wet-1 h dry (days 42-45) and (iv) 2 h wet-2 h dry (days 46-50). The liquid flow rate was controlled using an automatic timer to switch the peristaltic pumps on or off.

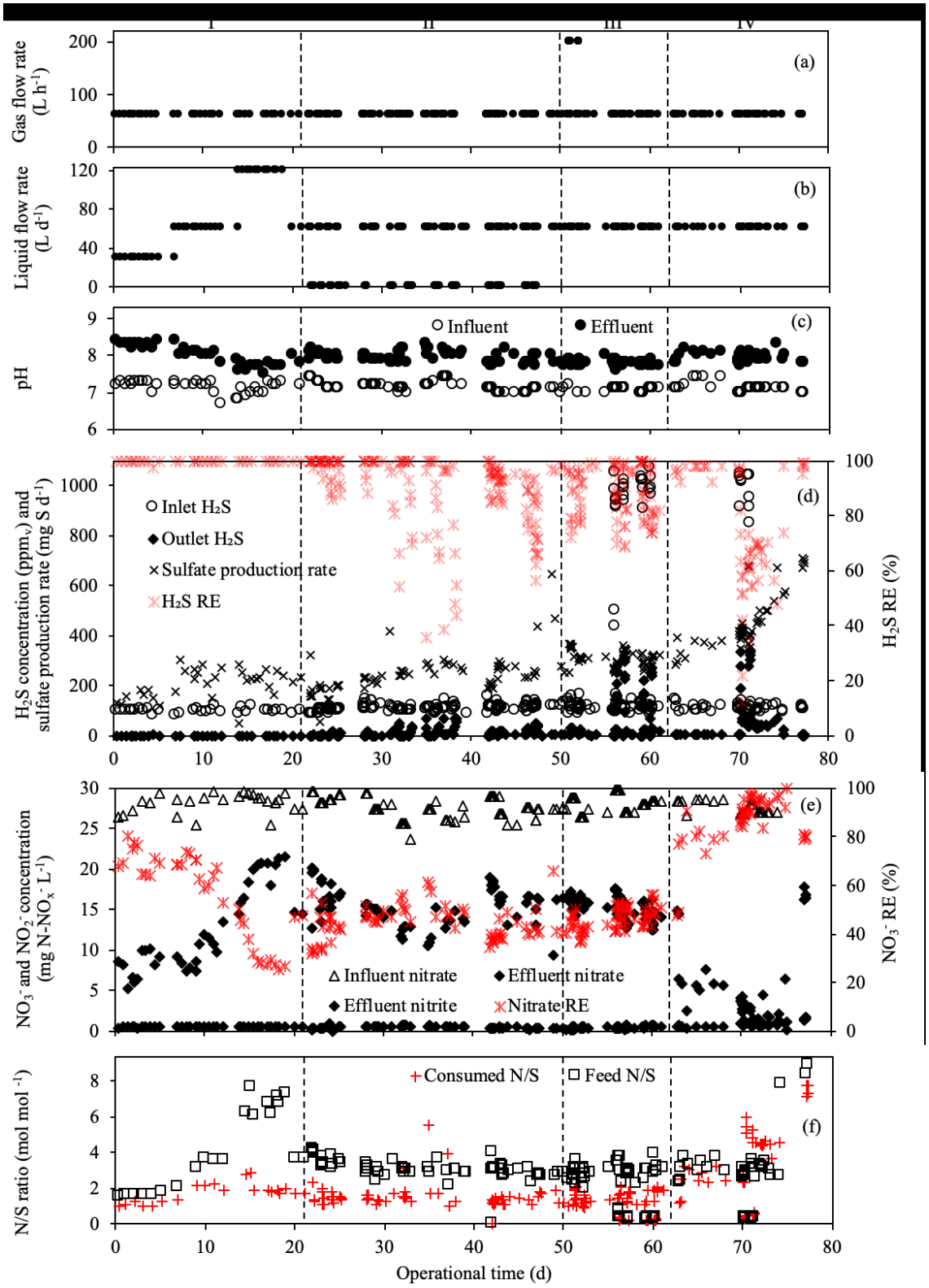

Figure 6.1. BTF performance during the entire operation (78 days): (a) different gas flow rates, (b) different liquid flow rates, (c) influent and effluent profiles of pH, (d) inlet and outlet concentrations of H_2S in the gas phase and sulfate production rate in liquid phase, (e) influent and effluent concentrations of nitrate and nitrite in the liquid phase and (f) consumed and feed N/S ratios.

Table 6.1. Transient-state operation of the anoxic biotrickling filter (BTF) for the simultaneous removal of H_2S and NO_3^-.

	Specific experiments	Inlet H_2S concentration (ppm_v)	H_2S loading rate (g S m^{-3} h^{-1})	Gas flow rate (L h^{-1})	EBRT[b] (min)	NO_3^- loading rate (g NO_3^--N m^{-3} h^{-1})	Liquid flow rate (L d^{-1})	Operational days	Days of normal conditions[a]
	Normal conditions[a]	116 (± 2)	4.3 (± 0.1)	60	3	3.8 (± 0.1)	60	-	-
I	Effect of liquid flow rate	98 (± 8)	3.7 (± 0.3)	60	3	3.9 (± 0.2)	30, 60 and 120	0-21	20-21
II	Effect of wet-dry bed operations	109 (± 12)	4.2 (± 0.4)	60	3	4.0 (± 0.1)	60		
	(i) 12 h wet-12 h dry							22-30	29-30
	(ii) 24 h wet-24 h dry							31-41	40-41
	(iii) 1 h wet-1 h dry							42-45	43-45
	(iv) 2 h wet-2 h dry							46-50	48-50
III	Effect of H_2S shock loads:								
	(i) increasing the gas flow rate	115 (± 18)	4.4 (± 0.8) and 14.0 (± 1.5)	60 and 200	3 and 0.9	3.8 (± 0.2)	60	51-55	54-55
	(ii) increasing the H_2S concentration	112 (± 15) and 947 (± 151)	4.2 (± 0.6) and 35.5 (± 5.6)	60	3	3.9 (± 0.2)	60	56-62	58, 61-62
IV	Bioaugmentation with *Paracoccus* MAL 1HM19 followed by the H_2S shock load test	110 (± 13) and 982 (± 70)	4.1 (± 0.4) and 36.8 (± 2.6)	60	3	3.8 (± 0.1) and 11.6 (± 0.1)	60	63-78	-

Note: [a]Normal operation was applied for stabilizing/recovering the H_2S RE of the BTF at the end of each transient-state tests.
[b]EBRT = empty bed residence time of the gas phase.

During phase III (days 51-62), H_2S shock loads were tested by suddenly increasing (i) the gas flow rate (days 51-55) and (ii) the inlet H_2S concentration (days 56-62). Each shock load was applied for 4 h and repeated for a duplicate test after 24 h of the first shock load (Table 6.1). First, the gas flow rate was instantly increased from 60 to 200 L h^{-1} while maintaining the inlet H_2S concentration constant at 115 (±18) ppm_v, resulting in an increase of the H_2S loading rate from 4.4 (±0.8) to 14.0 (±1.5) g S m^{-3} h^{-1} (days 51-55). Then, the inlet H_2S concentration was increased from 112 (±15) to 947 (±151) ppm_v at a constant gas flow rate of 60 L h^{-1}, resulting in an increase of the H_2S loading rate from 4.2 (±0.6) to 35.5 (±5.6) g S m^{-3} h^{-1} (days 56-62).

On day 63 (phase IV), the BTF was bioaugmented with PUF cubes obtained from another laboratory-scale anoxic BTF dominated by a facultative autotrophic denitrifying bacterium, *Paracoccus* MAL 1HM19 (Watsuntorn et al., 2017). One third of the PUF cubes (88 pieces) in the BTF of the present study were removed and replaced with PUF cubes of the other BTF containing *Paracoccus* MAL 1HM19. From day 70 onwards, the response of the BTF to H_2S shock loads of the bioaugmented BTF was tested. In this test, the inlet H_2S concentration was increased from 110 (±13) to 982 (±70) ppm_v for 4 h and repeated for a duplicate test at 24 h after the first shock load (Table 6.1).

6.2.3 Performance parameters of the anoxic BTF

The operation and performance parameters of the anoxic BTF were calculated as follows:

$$\text{Removal efficiency (RE, \%)} = \frac{\left(C_{H_2S\text{-in}} - C_{H_2S\text{-out}}\right)}{C_{H_2S\text{-in}}} \times 100 \quad (6.3)$$

$$\text{Elimination capacity (EC, g } m^{-3}\ h^{-1}) = \frac{\left(C_{H_2S\text{-in}} - C_{H_2S\text{-out}}\right)}{V} \times Q_G \quad (6.4)$$

$$\text{Feed N/S ratio (mol mol}^{-1}) = \frac{\left((C_{NO_3^-\text{-in}} \times Q_L\right)/MW_N}{\left(C_{H_2S\text{-in}} \times Q_G\right)/MW_S} \quad (6.5)$$

$$\text{Consumed N/S ratio (mol mol}^{-1}) = \frac{\left(\left(C_{NO_3^-\text{-in}} - C_{NO_3^-\text{-out}}\right) \times Q_L\right)/MW_N}{\left(\left(C_{H_2S\text{-in}} - C_{H_2S\text{-out}}\right) \times Q_G\right)/MW_S} \quad (6.6)$$

$$\text{Produced } SO_4^{2-} \text{ (mg S d}^{-1}) = \left(C_{SO_4^{2-}\text{-S-out}} - C_{SO_4^{2-}\text{-S-in}}\right) \times Q_L \times 24 \text{ h/d} \quad (6.7)$$

$$\%\ SO_4^{2-} \text{ production} = \frac{\left(C_{SO_4^{2-}\text{-S-out}} - C_{SO_4^{2-}\text{-S-in}}\right) \times Q_L}{\left(C_{H_2S\text{-in}} - C_{H_2S\text{-out}}\right) \times Q_G} \times 100 \quad (6.8)$$

where $C_{X\text{-}in}$ and $C_{X\text{-}out}$ are concentrations of H_2S-S, NO_3^--N or SO_4^{2-}-S in the influent and effluent (mg L^{-1}), respectively. V is the volume of the BTF packed bed (L), Q_G and Q_L are the flow rates of the gas and liquid phases (L h^{-1}), respectively. MW_S and MW_N are the molecular weights of sulfur and nitrogen (g mol^{-1}), respectively. The $\%SO_4^{2-}$ production was used for estimating the $\%S^0$ production in the system.

6.2.4 Analytical techniques

The influent and effluent pH was measured using a Präzision pH Meter (Metrohm, Switzerland) equipped with a SenTix 21 pH electrode (WTW, Germany). Liquid samples of the BTF influent and effluent were measured for total dissolved sulfide (HS^- and S^{2-}) and NO_2^- concentrations using colorimetric methods (APHA/AWWA/WEF, 1999) with a Lamda 365 UV/VIS spectrophotometer (Perkin-Elmer, USA). The liquid samples were filtered through 0.45 µm cellulose acetate syringe filters (Sigma-Aldrich, USA) prior to the measurements of NO_3^-, $S_2O_3^{2-}$ and SO_4^{2-} concentrations using ion chromatography Dionex ICS-1000 (Thermo Fisher, USA) (Villa-Gomez et al., 2011). The volatile suspended solids (VSS) of the BTF effluent were determined according to the procedure given in Standard Methods (APHA/AWWA/WEF, 1999). A Dräger X-am® 7000 gas detector (Dräger, Germany) was used to measure the H_2S concentration in the gas phase from 0-500 ppm_v, while H_2S concentration in the range of 500-5000 ppm_v were measured using a Geotech Biogas-5000 gas analyzer (Hatech Gasdetectietechniek BV, The Netherlands).

6.2.5 Microbial community analysis

Two pieces of randomly selected PUF cubes were collected from the BTF on days 0, 62 and 78. DNA was extracted, followed by polymerase chain reaction (PCR) of the 16S rDNA and denaturing gradient gel electrophoresis (DGGE) as well as the sequencing procedure was carried out according to the procedure described by Khanongnuch et al. (2018).

6.2.6 Data analysis

The experimental data sets from each phase of the BTF operation were compared and the statistical differences (significant difference at 95%) in the performance parameters during BTF operation, i.e. EC and RE, were determined using Tukey's multiple comparison tests (a one-way ANOVA, Minitab Inc., USA).

6.3 Results

6.3.1 Transient-state BTF operation

6.3.1.1 Effect of liquid flow rate

At different liquid flow rates from 30 to 60 and 120 L d^{-1} (phase I), the H_2S RE of the BTF was constant at 100% and corresponded to a H_2S EC of 3.7 (±0.3) g S m^{-3} h^{-1}. A partial oxidation of H_2S to S^0 likely occurred at a liquid flow rate of 30 L d^{-1}, as the produced SO_4^{2-} (136 ± 49 mg S d^{-1}) with respect to the removed H_2S was 84 (±12)% (Figure 6.2c, days 0-6).

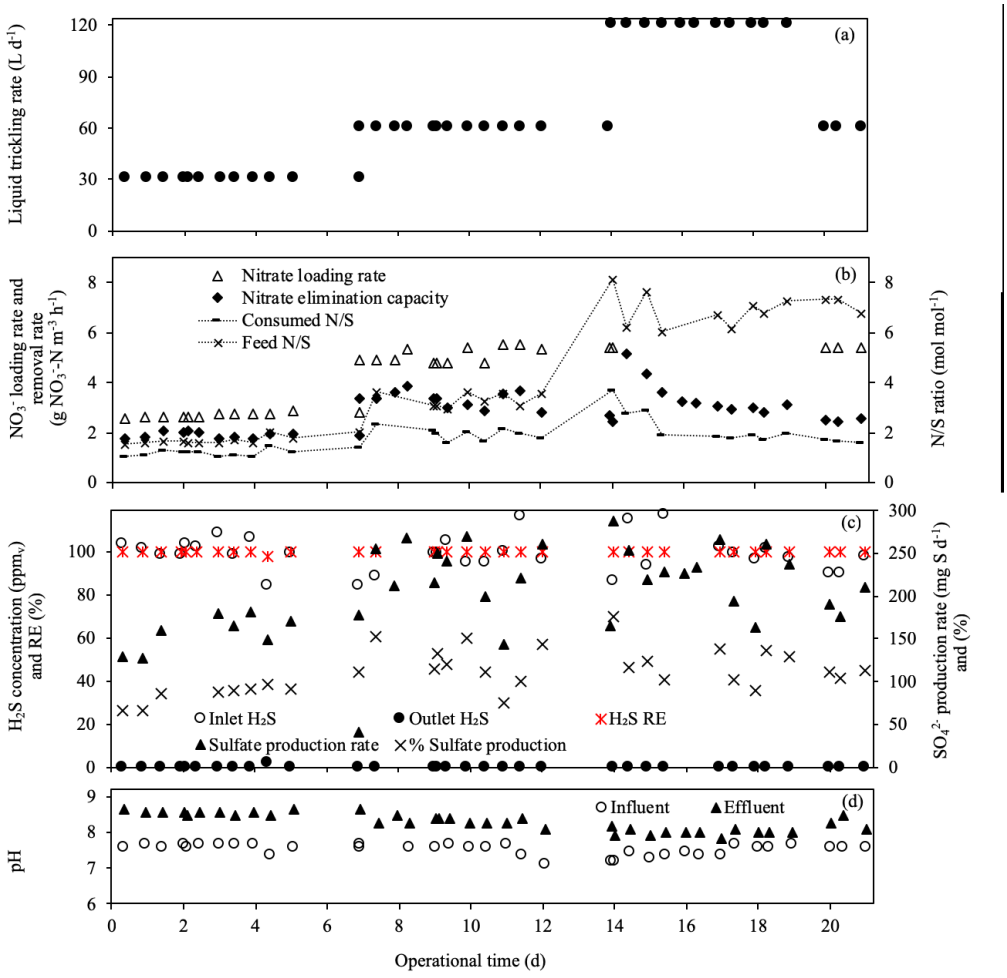

Figure 6.2. Effect of liquid flow rate on the BTF performance: (a) variation in liquid flow rates, (b) loading rate and elimination capacity of nitrate in the liquid phase and N/S ratio, (c) inlet and outlet concentrations of H_2S in the gas phase and sulfate production rate in the liquid phase, and (d) influent and effluent pH profiles.

The increase of the liquid flow rate from 30 to 60 L d^{-1} and 120 L d^{-1}, corresponding to an increase of the NO_3^- loading rate of 2.7 (±0.1) to 5.2 (±0.3) and 11.3 (±0.5) g NO_3^--N m^{-3} h^{-1}, resulted an increase of the NO_3^- removal rate from 1.4 (±0.1) to 2.3 (±0.3) and 2.6 (±0.6) g NO_3^--N m^{-3} h^{-1}, respectively (Figure 6.2b). However, the increase in the liquid flow rate from 30 to 60 L d^{-1} and 120 L d^{-1} resulted in a decrease of the effluent pH from 8.3 (±0.1) to 8.0 (±0.1) and 7.7 (±0.1), respectively (Figure 6.2d).

6.3.1.2 Effect of wet-dry bed operations

During 12 h wet-12 h dry operation, the NO_3^--containing liquid phase was fed to the BTF for 12 h, at an interval of 24 h from days 22-30 (Figure 6.3a). During days 24-30, the H_2S RE decreased from 100 to 87% after 6-h of dry operation (Figure 6.3b). During 12 h wet-12 h dry operation, the H_2S RE recovered to 100% within 5 h after resuming the trickling liquid supply. The NO_3^- RE fluctuated in the range of 32.0-56.8% during days 22-23, whereas a stable NO_3^- RE (45.9 ± 3.0%) were observed from day 25 onwards (Figure 6.3c).

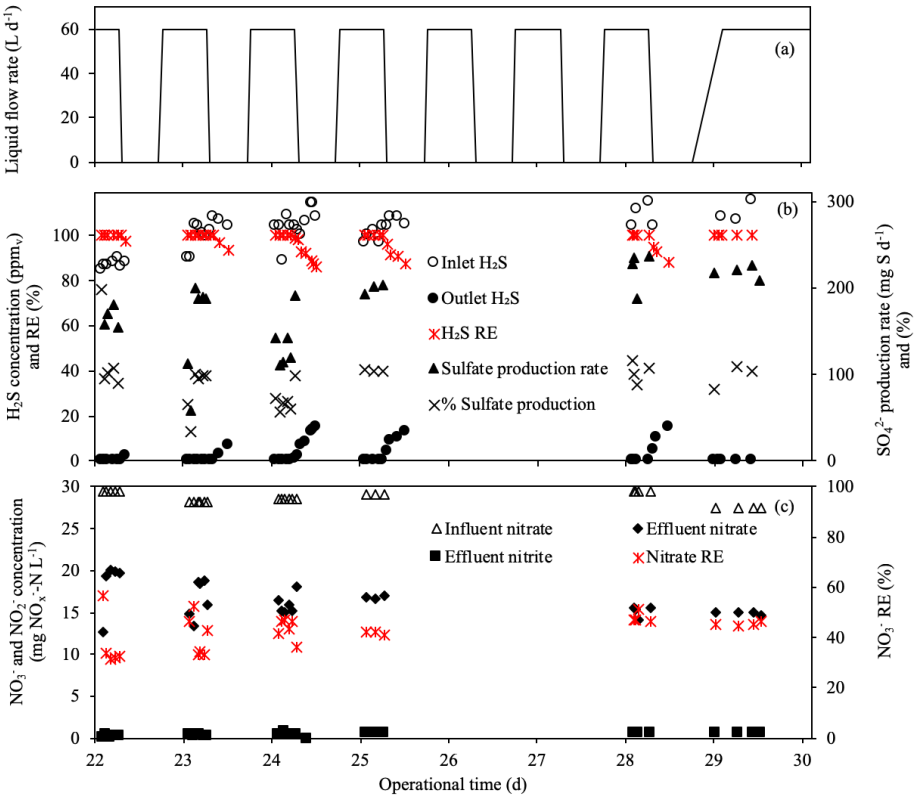

Figure 6.3. BTF performance during 12 h wet-12 h dry operation: (a) inlet and outlet concentrations of H_2S in gas phase, (b) sulfate production rate and (c) influent and effluent concentrations of nitrate and nitrite in the liquid phase.

During 24 h wet-24 h dry operation, the BTF was fed with the trickling liquid for 24 h at an interval of 48 h from days 31-41 (Figure 6.4a). During this test, the H_2S RE decreased from 100% to 35.6% (day 35) after 24 h of dry operation; however, the H_2S RE recovered to 100% within 3.5 h after resuming the trickling liquid supply (Figure 6.4b). At the end of the 24 h wet-24 h dry operation, the H_2S RE showed a longer recovery time, as complete H_2S removal was observed after 84 h of resuming the normal operating conditions (day 40). The $\%SO_4^{2-}$ production showed high variation with respect to the removed H_2S, in the range of 105-404% (Figure 6.4b). The average NO_3^- RE was 50.5 (±4.0)% during this test (days 31-41), except on day 36 on which an unexpected increase of the NO_3^- RE (61.6%) was observed (Figure 6.4c).

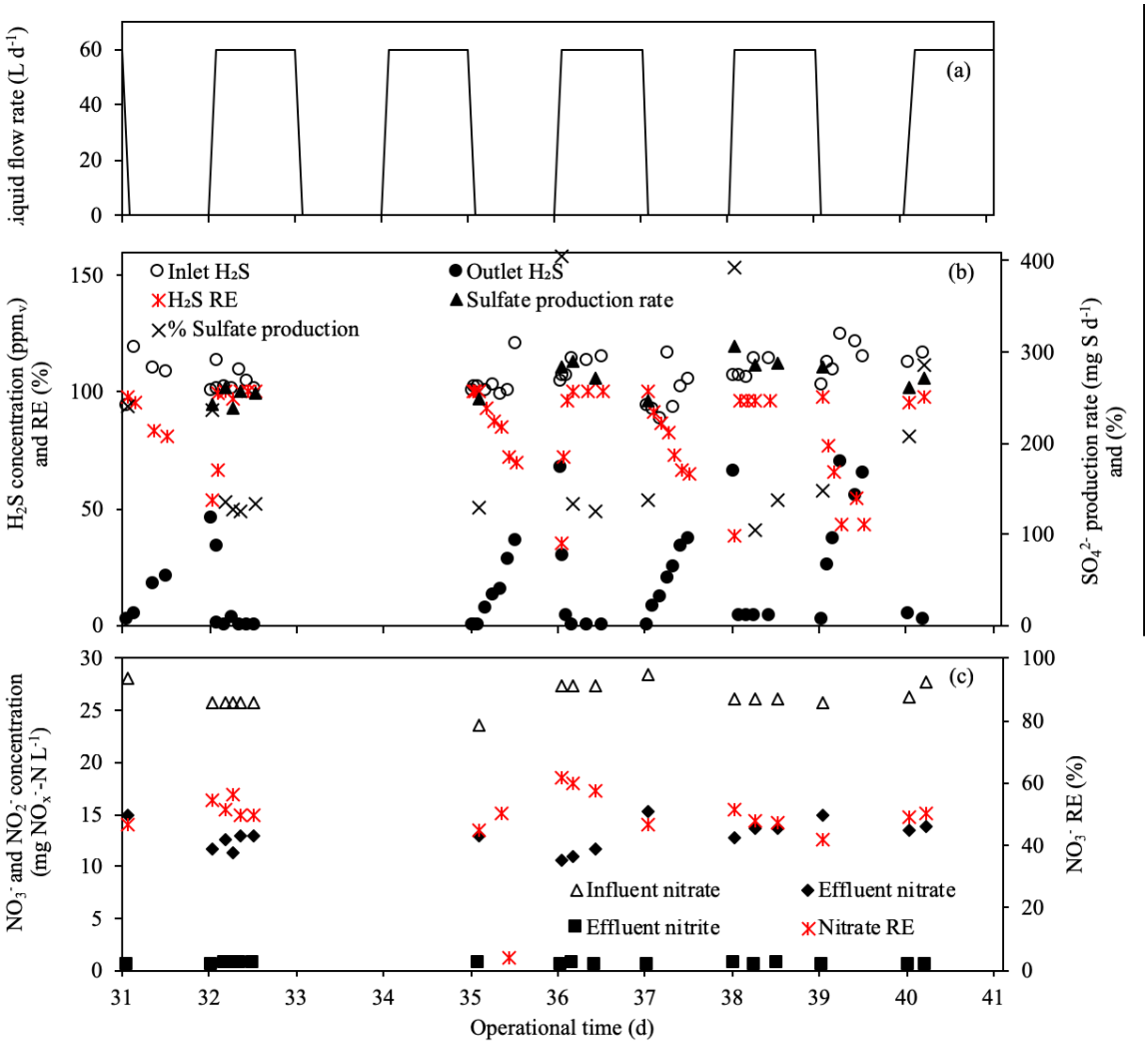

Figure 6.4. BTF performance during 24 h wet-24 h dry operation: (a) inlet and outlet concentrations of H_2S in the gas phase, (b) sulfate production rate and (c) influent and effluent concentrations of nitrate and nitrite in the liquid phase.

During 1 h wet-1 h dry operation (days 42-43), the H_2S RE was relatively stable in the range of 84.3-98.3% (Figure 6.5b) and the H_2S RE was still >98% when the BTF was operated under normal conditions (days 44-45). During 2 h wet-2 h dry operation, the H_2S RE decreased to 75.0% during days 46-47 and thereafter to 56.7% during days 47-48. The decrease of the H_2S RE did not significantly affect the NO_3^- removal from the liquid phase (Figure 6.5c). At the end of the wet-dry operations, the H_2S RE recovered to 98.3% after the trickling liquid had been continuously fed to the BTF for ~62 h (day 50).

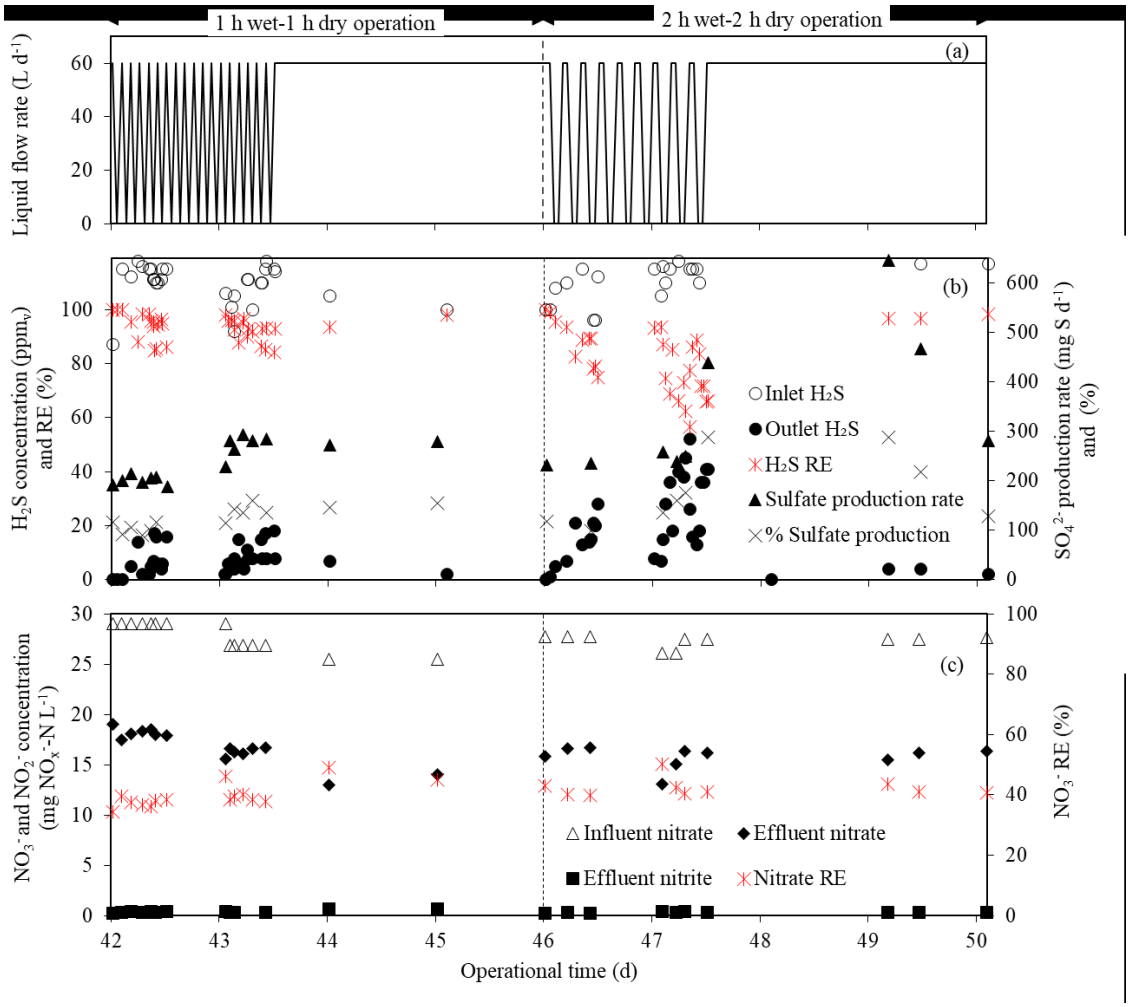

Figure 6.5. BTF performance during 1 h wet-1 h dry and 2 h wet-2 h dry operations: (a) inlet and outlet concentrations of H_2S in the gas phase, (b) sulfate production rate and (c) influent and effluent concentrations of nitrate and nitrite in the liquid phase.

6.3.1.3 Effect of H_2S shock loads

During the H_2S shock load tests by suddenly increasing the gas flow, a critical H_2S loading rate of 10.5 g S m^{-3} h^{-1} was achieved (Figure 6.6a). The sudden increasing the gas flow rate from 60 to 200 L h^{-1}, corresponding to increasing the H_2S loading rate from 4.4 to 14.0 g S m^{-3} h^{-1}, reduced the H_2S RE from 96.9 (±1.1)% to the lowest value of 72.0% (day 51). However, the H_2S RE recovered to 96.0 (±1.1)% within 16 h when the gas flow

rate was restored to 60 L h^{-1} (Figure 6.7a, days 53-55). Besides, SO_4^{2-} was mainly produced during this test (120 ± 40)% (Figure 6.7b, days 50-62).

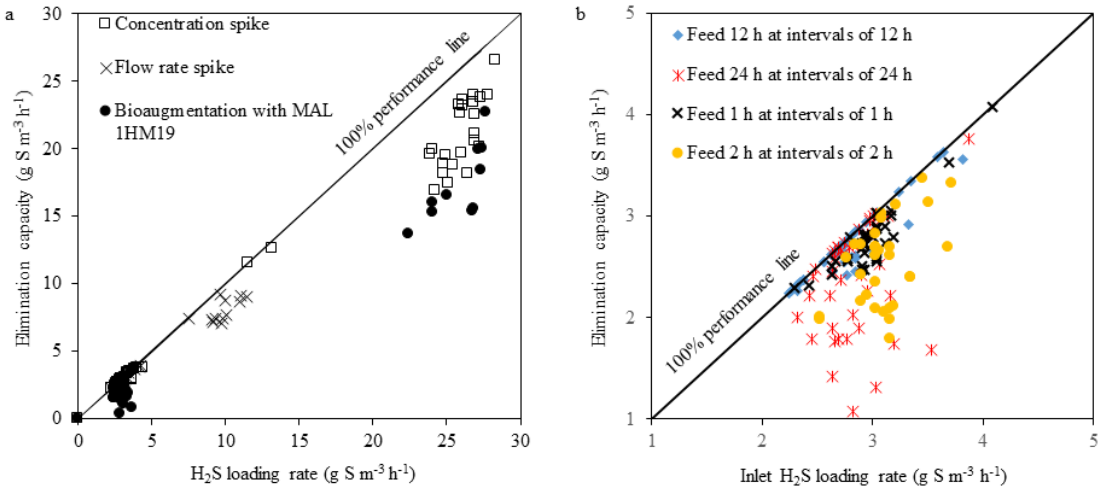

Figure 6.6. H_2S elimination capacity of the anoxic BTF under different transient-state operations tested in this study: (a) H_2S shock loads and bioaugmentation and (b) wet-dry bed operations.

During the subsequent H_2S shock load tests by increasing inlet H_2S from 110 (±13) to 982 (±70) ppm_v, the H_2S RE decreased to its lowest value of 68.9% (day 57). The critical H_2S loading rate was 17.9 g S m^{-3} h^{-1}, while the maximum H_2S EC was 37.8 g S m^{-3} h^{-1} (H_2S RE of 93.9%) (Figure 6.6a). During this test, the NO_3^- RE increased from 40.4% on day 51 to 56.0% on day 60 (Figure 6.7c). Moreover, the $\%SO_4^{2-}$ production based on the removed H_2S was below 20% during each H_2S shock load (Figure 6.7b). After this H_2S shock load test, when the inlet H_2S concentration was decreased to 116 (±2) ppm_v, the H_2S RE recovered to >98.0% within 40 h (Figure 6.7a).

6.3.2 Bioaugmentation with *Paracoccus* MAL 1HM19

After the BTF was bioaugmented with *Paracoccus* MAL 1HM19 (days 63-68), the H_2S RE was 96.8 (±2.1)% (Figure 6.8a), corresponding to a H_2S EC of 4.49 (±0.19) g S m^{-3} h^{-1} (Figure 6.6a). The bioaugmentation increased the NO_3^- RE from 46.3 (±1.2)% (phase III, days 50-61) to 80.4 (±5.0)% (phase IV, days 63-68), corresponding to an increase in the NO_3^- removal rate from 2.6 (±0.3) to 4.5 (±0.2) g NO_3^--N m^{-3} h^{-1} (Figure 6.8b). The consumed N/S ratio during normal operation prior to the bioaugmentation was 1.5 (±0.4) mol mol^{-1}, which increased to 9.9 (±3.6) mol mol^{-1} after subjecting the bioaugmented BTF to a H_2S shock load (Figure 6.1f, days 74-78).

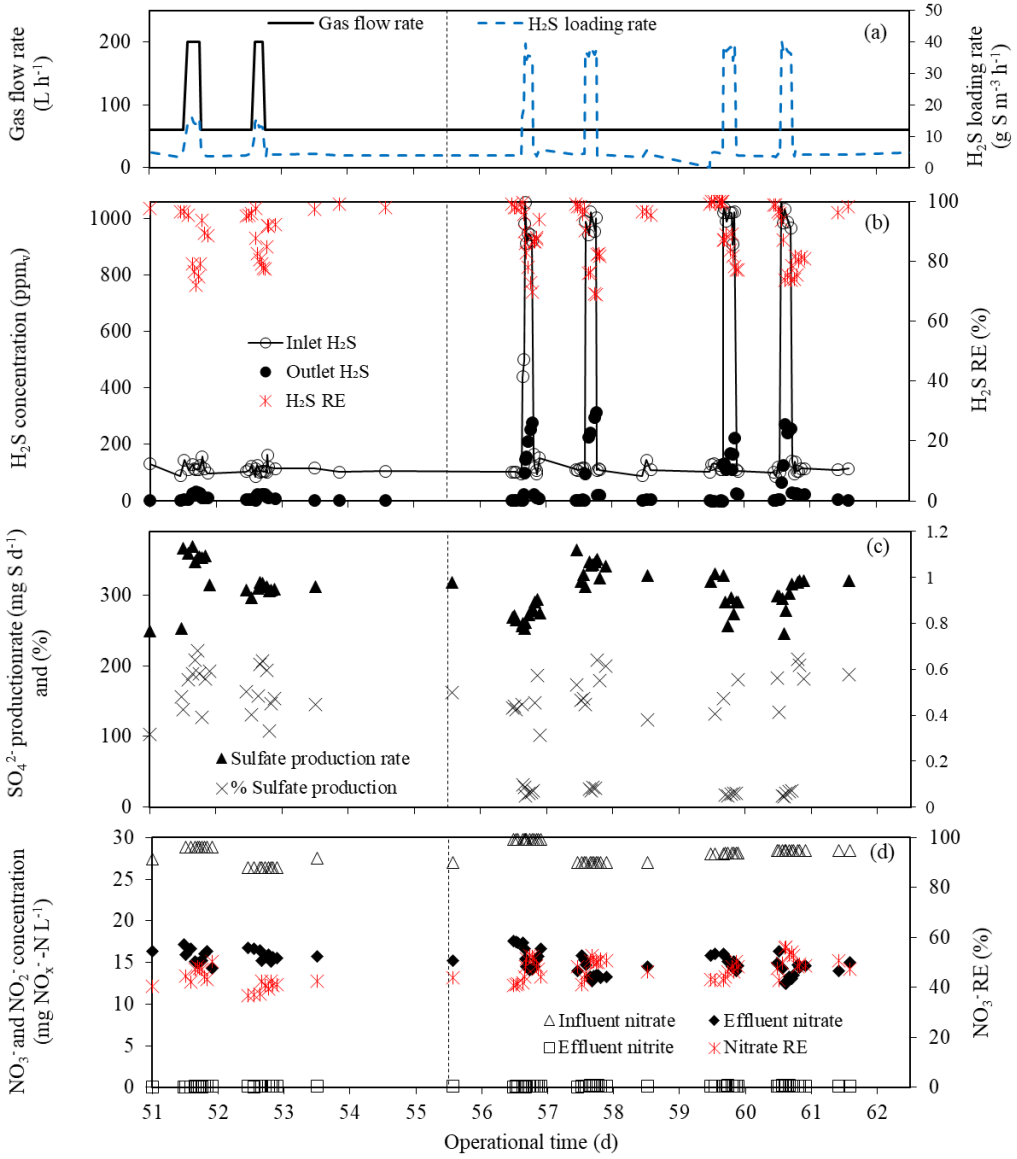

Figure 6.7. BTF performance under the influence of different H_2S shock loads: (a) inlet and outlet concentrations of H_2S in the gas phase, (b) sulfate production rate and (c) influent and effluent concentrations of nitrate and nitrite in the liquid phase.

When a H_2S shock load was applied to the bioaugmented BTF (days 70-71), the H_2S RE sharply decreased from 96.9 (±0.6)% to 12.0% (day 70) and 34.4% (day 71) after applying the first and second shock loads for 5.0 h and 4.3 h, respectively (Figure 6.8a). The SO_4^{2-} production rate gradually increased from 219 mg S d^{-1} (day 70) to 669 mg S d^{-1} (day 74). During days 71-73, the H_2S RE did not completely recover after the H_2S shock loads and fluctuated in the range of 34.4-70.6%. On day 74, when the influent NO_3^- concentration was increased from 27.8 (±1.2) to 84.0 (±0.6) mg L^{-1}, the H_2S RE increased to >98% (Figure 6.8a, days 75-78), corresponding to a H_2S EC of 4.0 (±0.2) g S m^{-3} h^{-1}. Besides, the NO_3^- RE was 87.1 (±9.1)% (Figure 6.8c, days 74-78), corresponding to a NO_3^- removal rate of 14.4 (±1.4) g NO_3^--N m^{-3} h^{-1}. The increase in SO_4^{2-} production rate

(713 mg S d^{-1}) on day 75 corresponded to a ~300% increased SO_4^{2-} production based on 190 mg H_2S-S d^{-1} removed (Figure 6.8b). During days 70-73, a higher turbidity and the presence of white/pale-yellowish particles, most likely S^0 particles, were visually observed in the effluent.

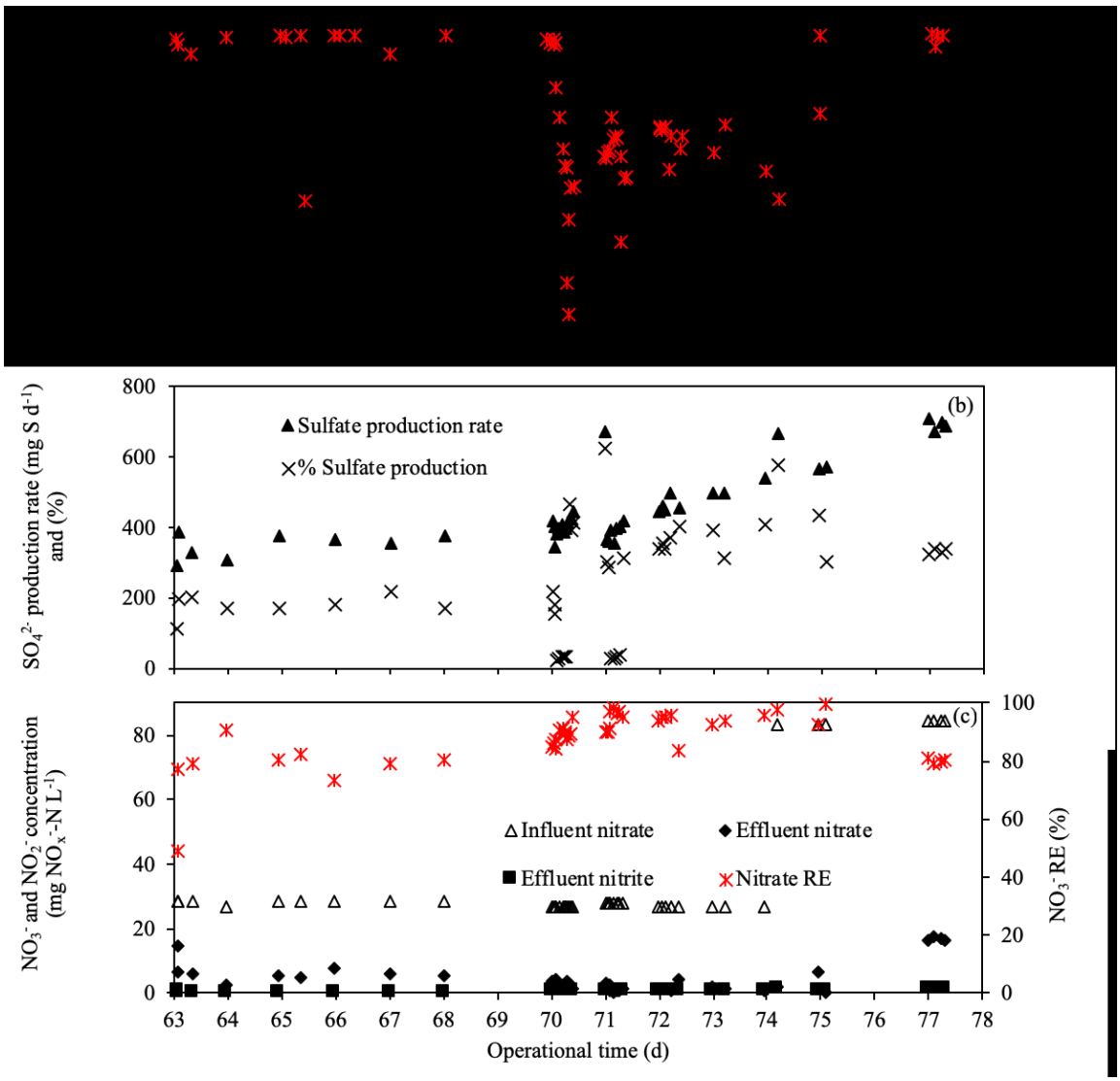

Figure 6.8. Effect of bioaugmentation with a facultative autotrophic biomass dominated by *Paracoccus* strain MAL 1HM19 on the BTF performance: (a) inlet and outlet concentrations of H_2S in the gas phase, (b) sulfate production rate and (c) influent and effluent concentrations of nitrate and nitrite in the liquid phase.

6.3.3 Microbial community composition in the BTF

The microbial community composition visualized by DGGE showed an increase in the number of individual bands after the transient-state tests (day 62) and the bioaugmentation (day 78) of the BTF (Figure 6.9). During all operational conditions, bacteria identified

as *Thiobacillus* sp. (bands 5, 7 and 8), *Rhodobacter* sp. (bands 2 and 15), *Stenotrophomonas* sp. (bands 1 and 11), *Rhodocyclales* bacterium (band 5) and bacteria belonging to *Bactroidetes* (bands 3 and 4) were detected (Figure 6.9). The bacteria with >99% similarity to the endosymbiont of *Acanthamoeba* sp. (band 14) and *Geobacter* sp. (band 16) were present after finishing the transient-state tests (day 62). After the bioaugmentation with *Paracoccus* MAL 1HM19 (day 78), DGGE bands of bacteria identified as *Paracoccus* sp. (bands 10 and 13) and *Simplicispira* sp. (band 9) were present in the BTF, while the band related to *Thiobacillus* sp. (band 5) and *Stenotrophomonas* sp. (band 11) had a lower intensity compared to days 0 and 62.

6.4 Discussion

6.4.1 Resistance of the BTF to intermittent H_2S loads

This study showed that H_2S shock loads only slightly affected the H_2S EC of an anoxic BTF, which maintained a stable performance in terms of H_2S RE and SO_4^{2-} production (Figure 6.7). H_2S shock loads occur frequently in industrial systems and can result in a rapid decrease of the empty bed residence time (EBRT) (Sharma et al., 2008). The sudden increase of the H_2S concentration likely resulted in partial oxidation of H_2S to S^0 due to NO_3^- limitation (feed N/S ratio was ~0.35) as the $\%SO_4^{2-}$ production was <20% of the consumed H_2S (Figure 6.7b) and visual observations suggested the presence of S^0 particles in the BTF effluent. However, the H_2S RE of the BTF recovered quite fast after the first H_2S shock load (Figure 7a). Moreover, the H_2S RE improved during the succeeding H_2S shock loads, resulting in a higher H_2S RE than when the first shock load was applied (Figure 6.7a). This suggests that the microorganisms adapted to the intermittent H_2S loading regime in the anoxic BTF.

The BTF showed a good resilience capacity to withstand a 10-fold increase in the H_2S loading rates (from 4.2 to 35.5 g S m^{-3} h^{-1}). In particular, the anoxic BTF showed a faster recovery time compared to those reported for an aerobic biofilter treating H_2S (loading rate of 1-6 g H_2S m^{-3} h^{-1}), which was subjected to a H_2S shock load of 10 g H_2S m^{-3} h^{-1} (Kim et al., 2008). Kim et al. (2008) showed that the recovery time to attain the H_2S RE of ~100% after restoring the initial H_2S load was 96 h. Jing et al. (2009) tested sulfide shock loads by applying (for 2 h) 1.5-3 times higher inlet concentrations (520 mg S^{2-}-S L^{-1}) in an anaerobic upflow bioreactor treating sulfide and NO_3^- in synthetic wastewater. The authors reported that the recovery time was 30 h at the highest tested concentration (1820 mg S^{2-}-S L^{-1}), which was similar to the recovery time observed in this study when the BTF was subjected to a 10-fold increase in the H_2S loading rate (Figure 7a).

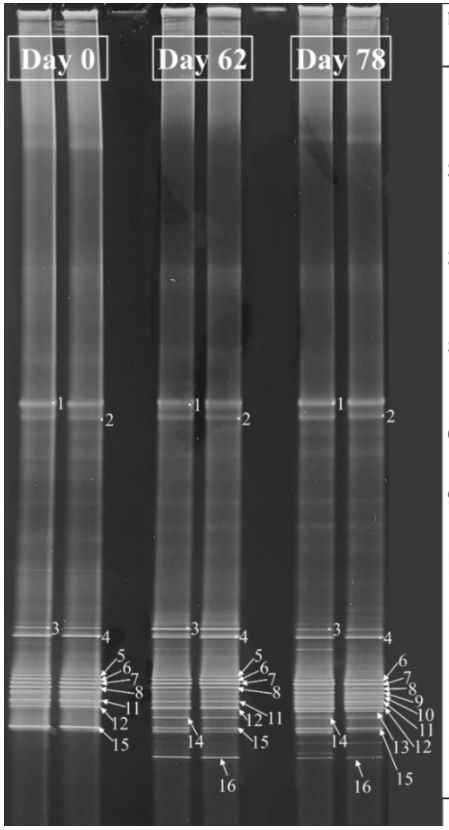

Band(s)[a]	Class/order/family	Affiliation[b]	Accession number	Similarity (%)	Sequence length
1, 11	γ -proteobacteria/Xanthomonadales/ Xanthomonadaceae	*Stenotrophomonas* sp.	KY490132.1, KM021209.1	91.8-94.5	456-510
2, 15	α-proteobacteria/Rhodobacterales/ Rhodobacteraceae	*Rhodobacter* sp.	LN879886.1, JN648234.1	92.6-99.1	415-429
3, 4	-	Bacteroidetes/Chlorobi group bacterium	KU685184.1, LN998004.1	96.2-96.3	416-418
5, 7, 8	β-proteobacteria/Nitrosomonadales/ Thiobacillaceae	*Thiobacillus* sp.	KM200026.1, JX530173.1, KM200014.1	98.0-100	433-508
6	β-proteobacteria/Rhodocyclales	*Rhodocyclales* bacterium	JQ723653.1, JQ723670.1	98.7	448
9	β-proteobacteria/Burkholderiales/ Comamonadaceae	*Simplicispira* sp.	KY476421.1	89.8	440
10, 13	α-proteobacteria/Rhodobacterales/ Rhodobacteraceae	*Paracoccus* sp.	KY427435.1	98.0	482
12	-	Uncultured β proteobacterium	EF667513.1	92.4	431
14	α-proteobacteria/Holosporales/ Holosporaceae	Endosymbiont of *Acanthamoeba* sp.	CP004403.1	99.1	430
16	δ-proteobacteria/Desulfuromonadales/ Geobacteraceae	*Geobacter* sp.	EF658628.1	99.3	433

Note: [a] Band label of DGGE-separated DNA fragments, and [b] Closet relative DGGE-separated DNA fragment in Genbank

Figure 6.9. Microbial community profiles (left) and identification of the sequenced denaturing gradient gel electrophoresis bands (right) of the biomass samples collected before (day 0), after transient-state conditions (day 62) and bioaugmentation (day 78). Each sample was run in duplicate.

6.4.2 Effect of intermittent flow of the trickling liquid

The anoxic BTF showed a high resilience capacity to tolerate gas-phase H_2S (88-147 ppm_v) in the absence of the trickling liquid and NO_3^- for 24 h, as the H_2S RE recovered to 100% immediately after resuming the liquid recirculation (Figure 6.4). During NO_3^- starvation in an attached biofilm system, microorganisms can survive by utilizing the easily biodegradable biofilm components (i.e. extracellular polymeric substance, EPS) in the system as carbon and energy sources (Wang et al., 2015). The NO_3^- RE also increased during prolonged bed drying periods, from 45.9 (± 3.0%) at 12 h wet-12 h dry operation to 50.5 (± 4.0)% at 24 h wet-24 h dry operation. During these disturbances of the bed wetting pattern, the NO_3^- RE increase could be a stress response of microorganisms to pulses of NO_3^- starvation and elevated H_2S concentrations.

The 12 h wet-12 h dry operation likely showed a high and stable BTF performance, resulting in H_2S EC close to the 100% performance line (Figure 6.6b), while the operations at 1 h wet-1 h dry and 2 h wet-2 h dry are not recommended to be applied during long-term BTF operation. Those short pulse feeding regimes were likely more detrimental to the H_2S RE which likely continued to reduce during the operation and only recovered to almost 100% when the BTF was operated under normal conditions (Figure 6.5b). Short pulse feeding may lead to non-uniform trickling liquid distribution through the packed bed and the formation of a stagnant zone within the pores of the foam cubes. These can cause severe mass transfer limitation. In further studies, residence time distribution (RTD) tests should be performed to obtain a better understanding of the effects of different modes of wet-dry operations on the hydrodynamic behavior of anoxic BTF and their effects on microbial activity.

6.4.3 BTF response to changes in liquid flow rate

The increase in liquid flow rate from 30 to 60 and 120 L d^{-1} did not significantly affect the H_2S RE of the BTF (Figure 6.2c). This related to previous observations in BTFs showing that the liquid flow rate usually has only a slight effect on the removal of low concentrations of gas-phase pollutants, especially when the pollutants are water soluble (Fernández et al., 2013; Kennes et al., 2009). Also Fernández et al. (2013) reported that different liquid flow rates of 20 to 180 L h^{-1} did not affect H_2S RE of the BTF at H_2S loading rate of 48.8 g S m^{-3} h^{-1}, while at higher H_2S loading rates (201 g S m^{-3} h^{-1}), the H_2S RE dropped to <80% at liquid flow rates <80 L h^{-1}. Subjecting the BTF to a high liquid flow rate could, nevertheless, reduce the biofilm stability and generate increased shear stress causing biofilm to wash out from the system (Kennes et al., 2009). In this study, the low biomass concentration in the effluent (VSS <30 mg L^{-1}) suggested no biofilm sloughing has occurred.

At the lowest liquid flow rate tested (30 L d^{-1}), partial oxidation of H_2S to S^0 using NO_3^- as electron acceptor likely occurred, as the H_2S consumed (84 ± 12%) was converted to SO_4^{2-} (Figure 6.2c), although sufficient NO_3^- was supplied to the BTF (feed N/S ratio of 1.7 ± 0.2). However, the consumed N/S ratio was 1.2 (±0.1), which causes the partial H_2S oxidation to S^0 in typical anoxic BTFs (Fernández et al., 2014, 2013; Soreanu et al., 2008). In contrast, the higher liquid flow rates tested in the BTF, i.e. 60 and 120 L d^{-1}, increased the %SO_4^{2-} production to 122 (±24)% (Figure 6.2c). This indicated sufficient NO_3^- was supplied to the sulfide-oxidizing biofilm in the BTF when the liquid flow rate was higher than 30 L d^{-1}. However, the liquid flow rates at 120 L d^{-1} likely caused an overload of the NO_3^- supply to the anoxic BTF (11.3 ± 0.5 g NO_3^--N m^{-3} h^{-1}), wherein the NO_3^- removal rate was only <3.3 (±0.6) g NO_3^--N m^{-3} h^{-1} resulting in a NO_3^- RE of 32 (±7)% (Figure 6.2b, days 7-20). Besides, an increase in the liquid flow rate in the BTF decreased the NO_3^- retention time in the anoxic BTF causing NO_3^- breakthrough in the effluent as evidenced by the lower consumed N/S ratio at the liquid flow rate of 120 L d^{-1} compared to the N/S ratio at 60 L d^{-1} (Figure 6.2b).

6.4.4 Microbial community composition

The microbial community composition in the BTF after the transient-state tests, i.e. different liquid flow rates, H_2S shock loads and wet-dry operations was only slightly different compared to the initial biomass (Figure 6.9). Surprisingly, the microbial community was enriched with the endosymbiont of *Acanthamoeba* sp. and *Geobacter* sp., which likely do not play roles in sulfide oxidation (Cardenas et al., 2010; Lu et al., 2015; Satoh et al., 2009). It should be noted, however, that those bacteria might not be viable as they have a lower intensity at the end of the BTF operation (day 78) (Figure 6.9). This study showed the stability of microbial community composition in the anoxic BTF to withstand different transients-state conditions, resulting in stable H_2S EC (4.0 ± 0.2 g S m^{-3} h^{-1}) at the end of experiment (days 75-78).

Bioaugmentation of the BTF with *Paracoccus* MAL 1HM19 did not affect the H_2S EC but increased ~2 times of NO_3^- removal compared to the value prior to bioaugmentation. The bioaugmentation, followed by the H_2S shock load, stimulated the utilization of NO_3^- as electron acceptor to oxidize S^0 previously accumulated in the BTF (Eq. 6.2), resulting in high SO_4^{2-} production (~300%) at the end of experiment (days 74-78).

The BTF can be further developed for simultaneously treating H_2S contaminated gas streams and wastewater containing NO_3^- and COD. For this, mixotrophic or heterotrophic denitrification could be stimulated in the BTF by e.g. inoculating with the *Paracoccus* MAL 1HM19. These are able to utilize various organic carbon sources (e.g. acetate, glucose and pyruvate) during H_2S oxidation under anoxic conditions (Watsuntorn et al.,

2017). The microbial interactions between autotrophic and heterotrophic bacteria can occur in the SO-NR systems (Di Capua et al., 2017a, 2017d, 2019; Khanongnuch et al., 2019). The inorganic carbon used for biomass production during H_2S oxidation via autotrophic denitrification (Eqs. 6.1 and 6.2) can be excreted by the SO-NR cells as organic compounds, which subsequently served for mixotrophic or heterotrophic denitrifying bacteria which also dominated in the BTF (Figure 6.9).

6.5 Conclusions

H_2S shock loads up to 35.5 (± 5.6) g S m^{-3} h^{-1} only slightly affected the BTF performance, resulting in the highest EC of 37.8 g S m^{-3} h^{-1} with >93% H_2S RE. Modification of the BTF liquid supply, i.e. the liquid flow rate and wet-dry bed operation, should be taken into account in designing and operating anoxic BTFs to avoid the depletion of the electron acceptor and mass transfer limitations. Bioaugmentation with biomass dominated with the SO-NR bacterium, *Paracoccus* MAL 1HM19, revealed the feasibility of H_2S removal at high NO_3^- loading rates. Considering its good resiliency and resistance to various transient-state conditions, anoxic BTFs are an attractive option in full-scale applications combining waste gas clean-up (H_2S removal) with wastewater treatment (NO_3^- removal).

6.6 References

Almenglo, F., Bezerra, T., Lafuente, J., Gabriel, D., Ramírez, M., Cantero, D., 2016a. Effect of gas-liquid flow pattern and microbial diversity analysis of a pilot-scale biotrickling filter for anoxic biogas desulfurization. Chemosphere 157, 215–223.

Almenglo, F., Ramírez, M., Gómez, J.M., Cantero, D., 2016b. Operational conditions for start-up and nitrate-feeding in an anoxic biotrickling filtration process at pilot scale. Chem. Eng. J. 285, 83–91.

APHA/AWWA/WEF, 1999. Standard methods for the examination of water and wastewater, 20th ed. American Public Health Association/American Water Works Association/Water Environment Federation, Washington D.C.

Barbusinski, K., Kalemba, K., Kasperczyk, D., Urbaniec, K., Kozik, V., 2017. Biological methods for odor treatment – A review. J. Clean. Prod. 152, 223–241.

Cano, P.I., Colón, J., Ramírez, M., Lafuente, J., Gabriel, D., Cantero, D., 2018. Life cycle assessment of different physical-chemical and biological technologies for biogas desulfurization in sewage treatment plants. J. Clean. Prod. 181, 663–674.

Cardenas, E., Wu, W.M., Leigh, B.M., Carley, J., Carroll, S., Gentry, T., Luo, J., Watson, D., Gu, B., Ginder-Vogel, M., Kitanidis, P.K., Jardine, P.M., Zhou, J., Criddle, C.S., Marsh, T.L., Tiedje, J.M., 2010. Significant association between sulfate-reducing bacteria and uranium-reducing microbial communities as revealed by a combined massively parallel sequencing-indicator species approach. Appl. Environ. Microbiol. 76, 6778–6786.

Di Capua, F., Lakaniemi, A.-M., Puhakka, J.A., Lens, P.N.L., Esposito, G., 2017a. High-rate thiosulfate-driven denitrification at pH lower than 5 in fluidized-bed reactor. Chem. Eng. J. 310, 282–291.

Di Capua, F., Milone, I., Lakaniemi, A.-M., Hullebusch, E.D., Lens, P.N.L., Esposito, G., 2017b. Effects of different nickel species on autotrophic denitrification driven by thiosulfate in batch tests and a fluidized-bed reactor. Bioresour. Technol. 238, 534–541.

Di Capua, F., Pirozzi, F., Lens, P.N.L., Esposito, G., 2019. Electron donors for autotrophic denitrification. Chem. Eng. J. 362, 922–937.

Fernández, M., Ramírez, M., Gómez, J.M., Cantero, D., 2014. Biogas biodesulfurization in an anoxic biotrickling filter packed with open-pore polyurethane foam. J. Hazard. Mater. 264, 529–535.

Fernández, M., Ramírez, M., Pérez, R.M., Gómez, J.M., Cantero, D., 2013. Hydrogen sulphide removal from biogas by an anoxic biotrickling filter packed with Pall rings. Chem. Eng. J. 225, 456–463.

Jaber, M.B., Couvert, A., Amrane, A., Le Cloirec, P., Dumont, E., 2017. Hydrogen sulfide removal from a biogas mimic by biofiltration under anoxic conditions. J. Environ. Chem. Eng. 5, 5617–5623.

Jing, C., Ping, Z., Mahmood, Q., 2009. Simultaneous sulfide and nitrate removal in anaerobic reactor under shock loading. Bioresour. Technol. 100, 3010–3014.

Kennes, C., Rene, E.R., Veiga, M.C., 2009. Bioprocesses for air pollution control. J. Chem. Technol. Biotechnol. 84, 1419–1436.

Khanal, S.K., Li, Y., 2017. Biogas Production and Applications, in: Li, Y., Khanal, S.K. (Eds.), Bioenergy: Principles and Applications. John Wiley & Sons Inc., New York, pp. 338–360.

Khanongnuch, R., Di Capua, F., Lakaniemi, A.-M., Rene, E.R., Lens, P.N.L., 2019. H_2S removal and microbial community composition in an anoxic biotrickling filter under autotrophic and mixotrophic conditions. J. Hazard. Mater. 367, 397–406.

Khanongnuch, R., Di Capua, F., Lakaniemi, A.-M., Rene, E.R., Lens, P.N.L., 2018. Effect of N/S ratio on anoxic thiosulfate oxidation in a fluidized bed reactor: experimental and artificial neural network model analysis. Process Biochem. 68, 171–181.

Kim, J.H., Rene, E.R., Park, H.S., 2008. Biological oxidation of hydrogen sulfide under steady and transient state conditions in an immobilized cell biofilter. Bioresour. Technol. 99, 583–588.

López, J.C., Porca, E., Collins, G., Pérez, R., Rodríguez-Alija, A., Muñoz, R., Quijano, G., 2017. Biogas-based denitrification in a biotrickling filter: Influence of nitrate concentration and hydrogen sulfide. Biotechnol. Bioeng. 114, 665–673.

López, M.E., Rene, E.R., Boger, Z., Veiga, M.C., Kennes, C., 2017. Modelling the removal of volatile pollutants under transient conditions in a two-stage bioreactor using artificial neural networks. J. Hazard. Mater. 324, 100–109.

Lu, L., Zeng, C., Wang, L., Yin, X., Jin, S., Lu, A., Jason Ren, Z., 2015. Graphene oxide and H_2 production from bioelectrochemical graphite oxidation. Sci. Rep. 5, 16242.

Mohammad, B.T., Rene, E.R., Veiga, M.C., Kennes, C., 2017. Performance of a thermophilic gas-phase biofilter treating high BTEX loads under steady- and transient-state operation. Int. Biodeterior. Biodegrad. 119, 289–298.

Montebello, A.M., Fernández, M., Almenglo, F., Ramírez, M., Cantero, D., Baeza, M., Gabriel, D., 2012. Simultaneous methylmercaptan and hydrogen sulfide removal in the desulfurization of biogas in aerobic and anoxic biotrickling filters. Chem. Eng. J. 200–202, 237–246.

Mora, M., Fernández, M., Gómez, J.M., Cantero, D., Lafuente, J., Gamisans, X., Gabriel, D., 2014. Kinetic and stoichiometric characterization of anoxic sulfide oxidation by SO-NR mixed cultures from anoxic biotrickling filters. Appl. Microbiol. Biotechnol. 99, 77–87.

Muñoz, R., Meier, L., Diaz, I., Jeison, D., 2015. A review on the state-of-the-art of physical/chemical and biological technologies for biogas upgrading. Rev. Environ. Sci. Biotechnol. 14, 727–759.

Rene, E.R., López, M.E., Veiga, M.C., Kennes, C., 2010. Steady- and transient-state operation of a two-stage bioreactor for the treatment of a gaseous mixture of hydrogen sulphide, methanol and α-pinene. J. Chem. Technol. Biotechnol. 85, 336–348.

Rodriguez, G., Dorado, A.D., Fortuny, M., Gabriel, D., Gamisans, X., 2014. Biotrickling filters for biogas sweetening: Oxygen transfer improvement for a reliable operation. Process Saf. Environ. Prot. 92, 261–268.

Romero-Hernandez, A.C., Rodríguez-Susa, M.S., Andrès, Y., Dumont, E., 2013. Steady- and transient-state H_2S biofiltration using expanded schist as packing material. N. Biotechnol. 30, 210–218.

San-Valero, P., Gabaldón, C., Penya-roja, J.M., Quijano, G., 2017. Enhanced styrene removal in a two-phase partitioning bioreactor operated as a biotrickling filter: Towards full-scale applications. Chem. Eng. J. 309, 588–595.

Satoh, H., Odagiri, M., Ito, T., Okabe, S., 2009. Microbial community structures and in situ sulfate-reducing and sulfur-oxidizing activities in biofilms developed on mortar specimens in a corroded sewer system. Water Res. 43, 4729–4739.

Sharma, K., Haas, D.W. De, Corrie, S., Halloran, K.O., Keller, J., Yuan, Z., 2008. Predicting hydrogen sulfide formation in sewers: a new model. J. Aust. Water Assoc. 60–65.

Soreanu, G., Béland, M., Falletta, P., Edmonson, K., Seto, P., 2008. Laboratory pilot scale study for H_2S removal from biogas in an anoxic biotrickling filter. Water Sci. Technol. 57, 201–207.

Soreanu, G., Béland, M., Falletta, P., Ventresca, B., Seto, P., 2009. Evaluation of different packing media for anoxic H_2S control in biogas. Environ. Technol. 30, 1249–1259.

Wang, Y., Zhou, S., Wang, H., Ye, L., Qin, J., Lin, X., 2015. Comparison of endogenous metabolism during long-term anaerobic starvation of nitrite/nitrate cultivated denitrifying phosphorus removal sludges. Water Res. 68, 374–386.

Watsuntorn, W., Ruangchainikom, C., Rene, E.R., Lens, P.N.L., Chulalaksananukul, W., 2017. Hydrogen sulfide oxidation under anoxic conditions by a nitrate-reducing, sulfide-oxidizing bacterium isolated from the Mae Um Long Luang hot spring, Thailand. Int. Biodeterior. Biodegradation 124, 196–205.

Yalamanchili, C., Smith, M.D., 2008. Acute hydrogen sulfide toxicity due to sewer gas exposure. Am. J. Emerg. Med. 26, 7–9.

Yang, Z., Liu, J., Cao, J., Sheng, D., Cai, T., Li, J., 2017. A comparative study of pilot-scale bio-trickling filters with counter- and cross-current flow patterns in the treatment of emissions from chemical fibre wastewater treatment plant. Bioresour. Technol. 243, 78–84.

Chapter 7 Hydrogen sulfide removal from biogas mimic in anoxic biotrickling filter (BTF) inoculated with *Paracoccus versutus* strain MAL 1HM19

This chapter will be submitted in modified form:

Watsuntorn, W., Khanongnuch, R., Chulalaksananukul, W., Rene, E.R., Lens, P.N.L. 2019. Hydrogen sulfide removal from biogas mimic in anoxic biotrickling filter inoculated with *Paracoccus versutus* strain MAL 1HM19. *Submitted for publication*.

Biological hydrogen sulfide (H_2S) removal under brackish conditions (pH = ~7.0) was tested for 189 days in a biotrickling filter (BTF) inoculated with a pure culture of *Paracoccus versutus* strain MAL 1HM19. The BTF was packed with polyurethane foam cubes and operated in both fed-batch and continuous modes. The H_2S inlet concentrations to the BTF varied between ~100 and ~500 ppm_v during steady-state tests, and later to ~1000, ~2000, ~3000 and ~4000 ppm_v during shock-load tests. The H_2S removal efficiency (RE) ranged between 17 and 100% depending on the operational mode of the BTF and the presence of acetate as a carbon source. The maximum elimination capacity (EC_{max}) of the BTF reached 113.5 (± 6.4) g S m^{-3} h^{-1} (97% RE) during H_2S shock-load experiments at ~4000 ppm_v. The results from polymerase chain reaction denaturing gradient gel electrophoresis (PCR–DGGE) revealed that *P. versutus* remained dominant throughout the 189 days of BTF operation. The analysis using artificial neural networks (ANNs) predicted the H_2S and NO_3^--N removal efficiencies and SO_4^{2-} production in the anoxic BTF. Consequently, *P. versutus* strain MAL 1HM19 can be used in an anoxic BTF system for the treatment of high H_2S contaminated gas streams.

7.1 Introduction

Biogas is a renewable energy source produced during the anaerobic digestion (AD) of solid waste and high strength wastewater. The presence of hydrogen sulfide (H_2S) in biogas as an impurity (0.1-2% *v/v* or 1000-20,000 ppm_v) limits its use for power generation (Fernández et al., 2014). H_2S is highly toxic, malodorous and corrosive to the equipment such as biogas engines. Moreover, sulfur dioxide (SO_2) is generated during the combustion of H_2S, which results in toxic effects to human health and the environment (Li et al., 2016). Hence, H_2S should be removed from biogas prior to use for domestic or commercial applications.

There are many techniques to clean H_2S from the gas-phase including physio-chemical and biological processes. Physico-chemical methods such as absorption, adsorption or chemical scrubbing are effective but have high energy requirement, disposal of generated wastes and chemical costs and generate secondary waste streams (Ramírez et al., 2009; Abdehagh et al., 2011). Biological methods are efficient for the treatment of waste gases at low concentrations and high gas-flow rates, Besides, they require low amounts of chemical addition, have low energy requirements and lower operational and maintenance costs compared to physical and chemical processes (Díaz et al., 2011).

The biotrickling filter (BTF) is one of the conventional biological waste gas treatment processes (Kennes et al., 2009), mostly used to remove hydrophilic volatile pollutants. In this reactor configuration, the waste gas is passed through a filter bed containing inert

packing material, on which the microorganisms grow as a biofilm. The pollutants present in the waste gas are absorbed by the biofilm and used as energy source by the microorganisms. The continuously trickling liquid-phase allows to adjust the operational parameters to the required conditions such as pH and nutrient concentrations (Abdehagh et al., 2011; Vikrant et al., 2017).

The selection of a proper inoculum is important for the successful operation of any waste gas treatment system (Lee et al., 2006). For the treatment of H_2S containing waste gases, both mixed and pure cultures can be used as inoculum for the BTF (Rattanapan et al., 2010). Activated sludge from domestic wastewater treatment systems are frequently used to inoculate BTF systems (Solcia et al., 2014). However, the long period of acclimation ranging from several weeks to months is one of the drawbacks when using the activated sludge as the inoculum (Rattanapan et al., 2010).

The use of pure cultures of bacteria as inoculum for BTF can offer the following advantages: short start-up times, high removal efficiency of the target pollutant, tolerate fluctuating concentrations and high inlet loads (Vikromvarasiri and Pisutpaisal, 2017). Several sulfur oxidizing bacteria have been used as inoculum to remove H_2S under long-term operation such as *Pseudomonas putida*, *Thiobacillus thioparus* (Chung et al., 2001), *Thiobacillus denitrificans* (Ramírez et al., 2009), *Acidiothiobacillus thiooxidans* (Abdehagh et al., 2011) and *Halothiobacillus neapolitanus* (Vikromvarasiri and Pisutpaisal, 2017). Recently, the genus of *Paracoccus* has also been considered as a biocatalyst for the simultaneous removal of H_2S and NO_3^- removal (Vikromvarasiri et al., 2015; Watsuntorn et al., 2017; Watsuntorn et al., 2018). In a recent study, H_2S removal (700-800 ppm_v) was achieved within 10 h in batch tests by *Paracoccus* sp. strain MAL 1HM19, isolated from the Mae Um Long Luang hot spring in Thailand (Watsuntorn et al., 2017).

The modelling of the BTF performance is crucial to optimize the appropriate operating conditions. However, classical approaches are arduous to predict the performance of a bioprocess because of various factors, i.e. microbial community in the BTF, composition of synthetic wastewater and the operational parameters of BTF. ANNs are a powerful tool which have been applied for prediction and solution of the complex relationship between input and output parameters in many different applications such as biotechnology, air contamination and environmental problems (Rene et al., 2008; Zamir et al., 2011; Atasoy et al., 2013). There are, however, only few studies on the application of ANNs for the simultaneous anaerobic sulfide and nitrate removal process (Cai et al., 2015).

To the best of our knowledge, this is the first continuous long-term study of anoxic H_2S and NO_3^- removal in an anoxic BTF inoculated with *Paracoccus versutus* strain MAL

1HM19 using brackish synthetic wastewater as the trickling nutrient solution. The objectives of this study were: (i) to investigate the performance of an anoxic BTF inoculated with pure cultures of *P. versutus* strain MAL 1HM19 for H_2S removal using NO_3^- as an electron acceptor under brackish conditions, (ii) to investigate the stability of *P. versutus* strain MAL 1HM19 and the bacterial community present in the BTF using PCR-DGGE, and (iii) to examine the effect of shock loads, i.e. sudden variations of H_2S concentration, on the performance of the anoxic BTF.

7.2 Materials and methods

7.2.1 Inoculum and nutrient solution

The *Paracoccus* sp. strain MAL 1HM19 used as the inoculum of the BTF was previously isolated from the Mae Um Long Luang hot spring (Mae Hong Son province, Thailand) (Watsuntorn et al. 2017). Based on whole genome sequencing analysis, the strain was identified as *Paracoccus versutus* (unpublished results). A modified Coleville synthetic brine (mCSB) was maintained at brackish conditions using 7 g NaCl L^{-1}, because the *P. versutus* strain MAL 1HM19 demonstrated the highest growth and H_2S removal rates under brackish conditions (Watsuntorn et al. 2017).

7.2.2 Immobilization

The immobilization step was conducted using “the three-step immobilization method”, described by Liu et al. (2013) to avoid wash out by the recirculation of mCSB medium when the immobilization step is performed directly in the BTF. *P. versutus* strain MAL 1HM19 was cultured in 1000 mL serum bottles according to the protocol described in Watsuntorn et al. (2017). The active *P. versutus* strain MAL 1HM10 was subsequently transferred to anaerobic bottles containing the polyurethane foam (PUF) cubes and mCSB medium and incubated for 7 d. The PUFs were then transferred to the anoxic BTF.

7.2.3 BTF set up and operation

The laboratory scale anoxic BTF was made from cylindrical glass having a total height of 50 cm and a diameter of 12.8 cm. The total bed height of the BTF was 30 cm, corresponding to a working bed volume of 3 L. The biogas mimic consisted of a mixture of N_2 and H_2S generated by mixing 1 M H_2SO_4 and 0.1 and 0.3 M $Na_2S{\cdot}9H_2O$ to obtain the desired gas phase H_2S concentrations (100-4000 ppm_v). The inlet gas-flow rate was 60 L h^{-1}, corresponding to an empty bed residence time (EBRT) of 3 min, while the temperature of the BTF was maintained at 22-25 °C. The mCSB medium was trickled from the

top of the BTF over the filter bed using a peristaltic pump (Masterflex, USA) at a liquid rate of 2.5 L h^{-1} and 1.67 L h^{-1} at fed-batch and continuous mode, respectively. The operational parameters and conditions tested in the anoxic BTF are shown in Table 7.1.

Table 7.1. Operational characteristics of the anoxic biotrickling filter.

Parameters	Values
Temperature	25 °C
pH	7.0-8.0
Electron donor	H_2S
Electron acceptor	NO_3^-
Nutrient	Modified CSB medium
Nutrient loading rate (mL min^{-1})	41.5
Inlet gas flow rate (L h^{-1})	60
EBRT (min)	3
Volume of packed bed (L)	3

Note: EBRT= empty bed gas residence time; CSB = Coleville synthetic brine

PUF cubes were used as the packing material. Before inoculation, the PUF cubes were manually cut into cube-shaped (2 × 2 × 2 cm) pieces. The PUF cubes had a density of 28 kg m^{-3} and porosity of 98% (Eregowda et al., 2018). Before adding the PUF cubes to the BTF, they were sterilized by autoclaving for 15 min at 121 °C. After that, the PUFs were submerged in 1 L sterile mCSB medium containing 10% (*v/v*) of *P. versutus* strain MAL 1HM19. The cell concentration of the *P. versutus* strain MAL 1HM19 in the PUF cubes was 8.7×10^8 CFU mL^{-1}.

The BTF was operated for 189 days under anoxic conditions during which H_2S was continuously fed in the gas-phase and NO_3^--N was added as the electron acceptor in the mCSB medium. The BTF operation was divided into three phases (phases P1-P3) to evaluate the BTF performance under different operational strategies as described in Table 7.2. In phase P1 (days 0-107), the BTF was operated in fed-batch mode and divided into five experimental phases (P1-I to P1-V) with different H_2S and acetate concentrations. During fed-batch mode, the mCSB medium was refreshed every week following the recommendations of a previous study by Prado et al. (2004). In phase P2, the effect of the presence (phase P2-I, days 133-161) and an absence (phase P2-II, days 162-174) of acetate on the performance of the BTF was evaluated. To evaluate the resilient capacity of the biofilm, the BTF was subjected to H_2S shock-loads (472.7-4129.4 ppm_v) in phase P3 (days 175-178 and days 184-187). After that, the BTF was operated again under steady-state conditions to check the stability and recoverability of the system.

Table 7.2. Operating conditions during anoxic BTF operation.

Mode of operation	Phase	Carbon source (CH_3CHOO^-)	Duration (days)	Inlet H_2S concentration (ppm_v)	H_2S loading rate (g S m^{-3} h^{-1})
Fed-batch	P1-I	+	0-27	97.0 (± 11.0)	2.7 (±0.4)
Fed-batch	P1-II	-	28-54	94.9 (± 11.6)	2.7 (± 0.3)
Fed-batch	P1-III	+	55-69	93.7 (± 15.3)	2.7 (± 0.4)
Fed-batch	P1-IV	+	70-90	318.5 (± 23.7)	9.0 (± 0.7)
Fed-batch	P1-V	+	91-107	426.6 (± 48.0)	12.1 (± 1.4)
Continuous	P2-I	+	133-161	475.9 (± 119.2)	13.3 (±3.4)
Continuous	P2-II	-	162-174	567.6 (± 58.8)	16.1 (± 1.7)
Continuous	P3-I	-	175-178	472.7 (± 67.8)-4129.4 (± 146.1)	13.4 (± 1.9)-116.8 (± 4.1)
Continuous	P3-II	-	184-187	432.1 (± 44.2)-4015.0 (± 234.8)	11.9(± 1.9)-113.6 (±10.1)

Note: "+" refers to addition of CH_3CHOO^- "-" refers to no addition of CH_3CHOO^-

7.2.4 Calculations

The performance of the BTF was evaluated in term of removal efficiency (RE), inlet loading rate (ILR) and elimination capacity (EC) as follows:

$$\text{RE (\%)} = \frac{C_{in}-C_{out}}{C_{in}} \times 100 \quad (7.1)$$

$$\text{ILR (g S m}^{-3}\text{ h}^{-1}\text{)} = C_{in} \times \frac{Q}{V} \quad (7.2)$$

$$\text{Elimination capacity (EC) (g S m}^{-3}\text{ h}^{-1}\text{)} = Q \times \frac{C_{in}-C_{out}}{V} \quad (7.3)$$

Where C_{in} and C_{out} are the inlet and outlet H_2S concentrations (g S m^{-3}), Q is the gas flow rate (m^3 h^{-1}), V is the filter bed volume of the packing medium (m^3). The H_2S concentrations, RE, ILR and EC values were presented as mean ± SD values.

7.2.5 Analytical techniques

H_2S concentration (0-500 ppm_v) was measured using two H_2S sensors depending on the concentration range: (i) Dräger X-am 7000 (Dräger, Lübeck, Germany) (H_2S measurement range: 0-500 ppm_v), and (ii) Biogas 5000 (Geotech, UK) (H_2S measurement range: 0-5,000 ppm_v), as described by Khanongnuch et al. (2019). Sulfide (S^{2-}) was measured using the modified methylene blue color method as described by van den Hoop et al. (1997) using a UV/Vis spectrophotometer (PerkinElmer, USA) at an absorbance of 670 nm. NO_3^--N and NO_2^--N concentrations were measured using the standard 4500-NO_3^--

B ultraviolet spectrophotometric screening (at 220 and 275 nm) and 4500-NO_2^--B colorimetric methods (at 543 nm), respectively (APHA, 2005). The cell density was monitored in term of the colony forming units (CFU mL^{-1}) using the drop plate technique (Gronewold and Wolpert, 2008). Acetate concentration was measured using a Varian 430 gas chromatograph (GC) (Varian Inc., USA) (Eregowda et al., 2018).

7.2.6 Microbial community analysis

The proliferation of the microbial community in the BTF was evaluated by PCR-DGGE as described by Khanongnuch et al. (2019). PUF samples were collected from the sampling ports at different operational phases of the BTF, i.e. on days 2, 11, 28, 98, 161, 184 and 189. The forward and reverse primers for PCR were 357F-GC and Un907R, respectively. The amplified PCR-DGGE products were purified and sequenced by Macrogen (The Netherlands). Bioedit software (version 7.2.5, Ibis Biosciences, USA) was used to compare the available sequences based on the National Center for Biotechnology Information (NCBI) database (Dessì et al., 2017).

7.2.7 ANN model development

The experimental data from days 0 to 189 (158 data points) of BTF operation was used to develop the ANN model using the Neural Network Toolbox 11.0 of MATLAB® R2017b (MathWorks Inc., USA). The inlet N/S ratio, H_2S concentration and the effluent pH were used as the ANN input parameters, while the output parameters consisted of H_2S-RE, NO_3^--RE and SO_4^{2-} production. Figure 7.1 shows the schematic of the three-layered feed-forward network topology developed to predict the BTF performance. The Levenberg-Marquardt back-propagation algorithm was used to brain the network (Khanongnuch et al., 2018).

To determine the optimal neural network, the input data were transformed by multiplying with the connection weights (W_{ih}) and bias term values to create data in the hidden layer. Thereafter, the signal to the output layer is transferred by multiplying with the respective connection weights (W_{ho}) to generate the desired output (Rene et al., 2009). A tan-sigmoid and a linear transfer function were used in the hidden layer and the output layer, respectively.

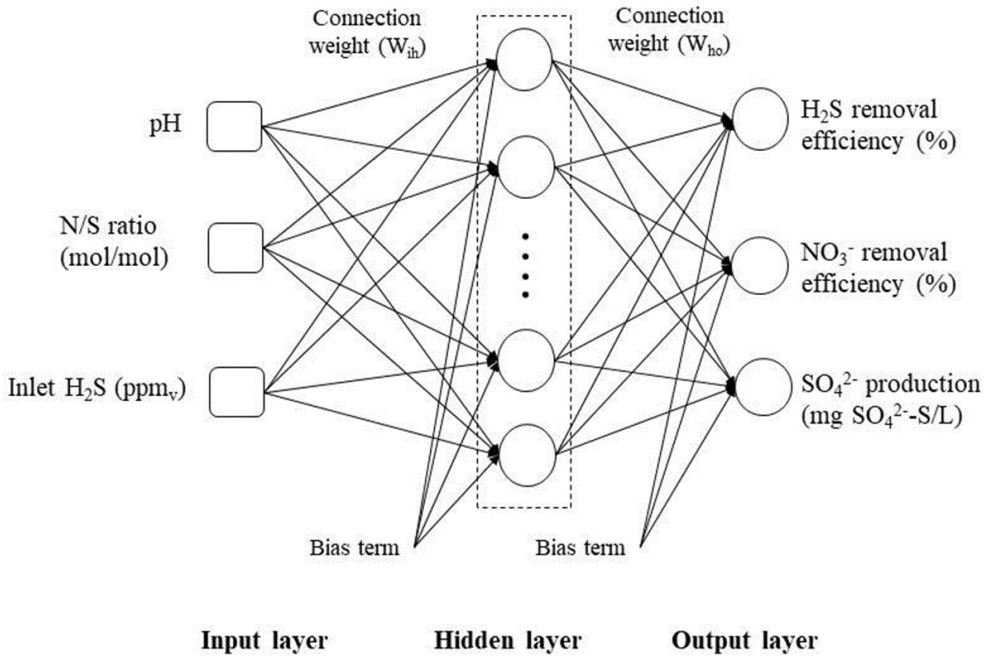

Figure 7.1. Three-layered network topology (3-9-3) for predicting the performance of the anoxic BTF.

The ANN model performance was evaluated using the mean squared error (MSE) and coefficient of determination (R^2) between the experimented and model fitted data. The basic statistics of the training, validation and test data sets are shown in Table 7.3. The experimental data from the BTF were normalized to values in the range of 0-1 according to Eq. (7.4):

$$\hat{X} = \frac{X - X_{min}}{X_{max} - X_{min}} \tag{7.4}$$

where $\hat{X}$ is the normalized value, X_{min} and X_{max} are the minimum and maximum values of X, respectively.

Table 7.3. Basic statistics of the training, validation and test data sets used to develop the artificial neural network (ANN) model.

	N	Mean	Minimum	Maximum
Input				
Inlet H_2S (ppm_v)	158	937	23.0	4456
Feed N/S ratio	158	0.14	0.002	0.70
Effluent pH	158	7.78	7.00	8.41
Output				
H_2S-RE (%)	158	91.2	20.9	100
NO_3^--RE (%)	158	80.3	21.0	100
SO_4^{2-} production (mg L^{-1})	158	670	193	1609

7.3 Results

7.3.1 H_2S removal and elimination capacity of the BTF

The H_2S RE was 99.6 (± 1.7)% within one day after BTF start-up (Figure 7.2A). During phase P1-II, i.e. the absence of acetate in the trickling liquid, the RE of H_2S decreased from 100% on day 28 to almost 17% on day 36. However, it reached a RE of 100% after replacing the nutrient medium on day 36 (Figure 7.2A). The H_2S RE decreased to values around 31-46% when the NO_3^--N concentration in the trickling medium was completely consumed, while the H_2S RE increased immediately to 100% when NO_3^--N was introduced to the BTF during medium replacement. During phase P1-III (days 55-69), acetate was added again to the nutrient medium. The H_2S RE was stable and >89% between days 60 and 69, even when NO_3^--N was completely consumed. During phase P1-IV (days 70-90), the inlet H_2S concentration was increased from 93.7 (± 15.3) (2.7± 0.4 g S m^{-3} h^{-1}) to 318.5 (± 23.7) ppm_v (9.0 ± 0.7g S m^{-3} h^{-1}). This resulted in a decrease of the H_2S RE from 97% (day 70) to 73% (day 75). Subsequently, in phase P1-V, when the inlet H_2S concentration was increased to 426.6 (± 48.0) ppm_v (12.1 (± 1.4) g S m^{-3} h^{-1}), the RE of H_2S was still >70% (Figure 7.2A). In phase P2 (days 133-174), the operational mode of the anoxic BTF was changed from fed-batch to continuous and the inlet H_2S concentration was 475.9 (± 119.2) ppm_v. The H_2S RE was >92% from the beginning of phase P2 (day 133) (Figure 7.2B) when NO_3^- was fed at a loading rate of 50.2 (± 15.0) g NO_3^--N m^{-3} h^{-1}.

During H_2S shock-load tests (phase P3, days 175-188), two sets of H_2S shock-loads were applied to ascertain the reproducibility of this phase of BTF operation. From days 175-178, the inlet H_2S concentration was maintained at 432.1 (± 44.2) ppm_v, while the H_2S shock-loads were applied once a day by increasing the H_2S concentration to 994.2 (±70.2) ppm_v on day 174, 1976.9 (± 96.1) ppm_v on day 175, 3008.3 (± 168.6) ppm_v on day 176, and 4129.4 (± 146.1) ppm_v on day 177, corresponding to an H_2S inlet load of 28.1 (± 2.0), 55.9 (± 2.7), 85.1 (± 4.8) and 116.8 (± 4.1) g S m^{-3} h^{-1}, respectively. Each step of H_2S shock-load was maintained for 4 h and repeated at 24 h intervals for 4 d. During the successive H_2S shock-load tests, the H_2S RE decreased from 96% to the lowest RE values RE 96%, 91%, >83% and 61%, respectively (Figure 7.2C). During the restoration of the normal inlet H_2S concentrations of 370 (± 0) ppm_v on day 178, the RE increased to values >95 %. During the second set of H_2S shock-load tests (days 184-187), the inlet H_2S concentration was increased from 432.1 (± 44.2) to 2174.3 (± 285.0), 3018.0 (± 211.0) and 4133.4 (± 234.8) ppm_v for each H_2S shock-load, corresponding to H_2S loading rates of 61.5 (± 8.1), 85.4 (± 6.0) and 116.9 (± 6.6) g S m^{-3} h^{-1}, respectively (Figure 7.2D). The H_2S RE was >96% during all the H_2S shock-load test. The H_2S RE

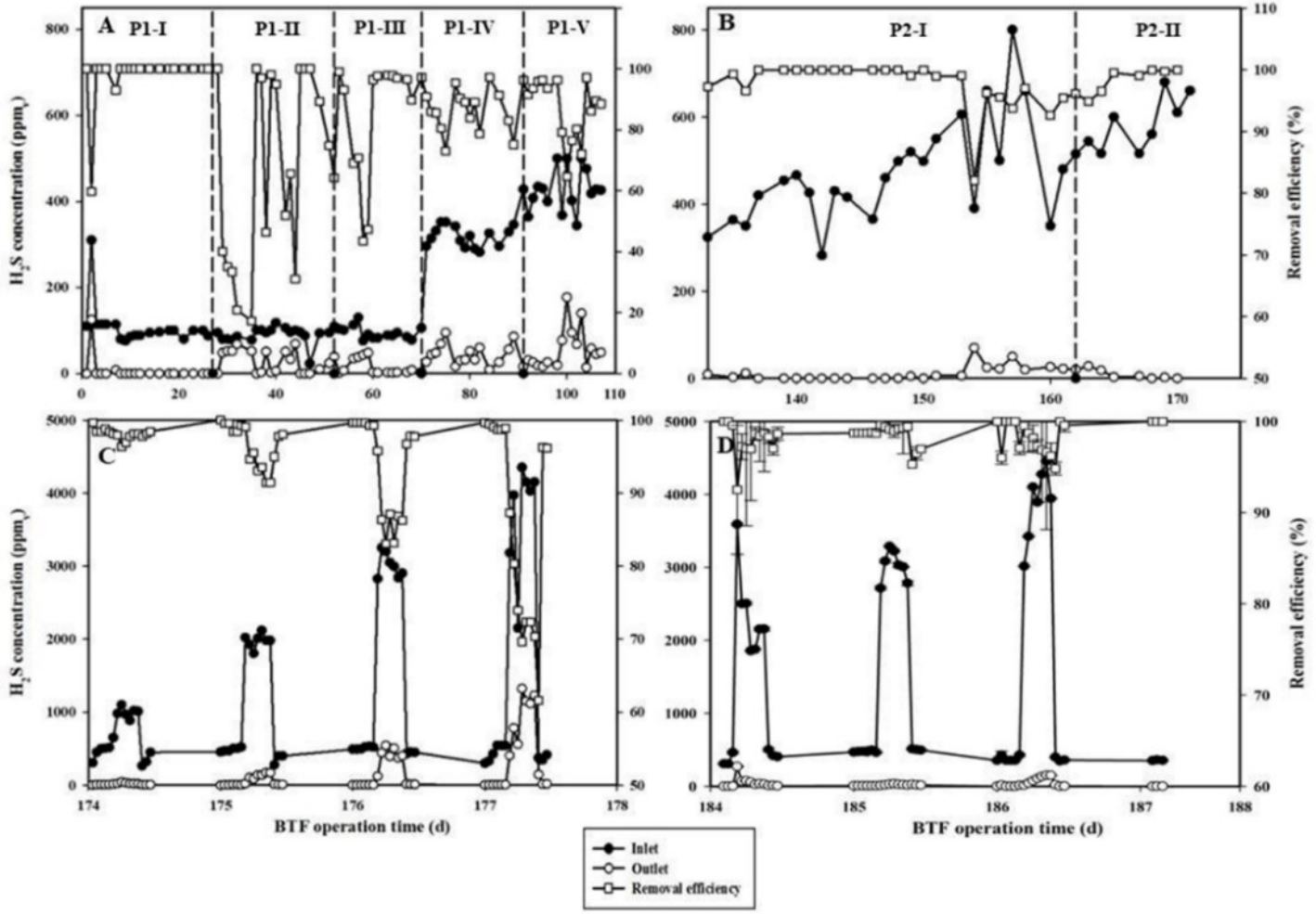

Figure 7.2. H_2S concentration and removal efficiency profiles during BTF operation: (A) fed-batch mode, (B) continuous mode, (C) 1st shock-load, and (D) 2nd shock-load.

increased to 98.1 (± 2.9)% within 1.5 h after decreasing the inlet load to 10.4 (±0.8) g S m^{-3} h^{-1} at an inlet H_2S concentration of 366.7 (± 27.1) ppm_v (Figure 7.2D).

Figure 7.3 shows the EC values and the inlet loading rates of the anoxic BTF. The EC of phase 1-I was 2.86 (± 0.66) g S m^{-3} h^{-1} at an inlet H_2S concentration of 97.0 (± 11.0) ppm_v. The EC_{max} values during fed-batch and continuous mode of BTF operation were, respectively, 10.67 and 21.22 g S m^{-3} h^{-1}. The EC_{max} value during the H_2S shock-load experiment was 113.5 (± 6.4) g S m^{-3} h^{-1} (RE = 96.5 %), which was achieved at an inlet loading of 116.9 (± 6.6) g S m^{-3} h^{-1}.

7.3.2 Sulfide and SO_4^{2-} profiles in the BTF

Trace amounts of sulfide in the liquid-phase (0-0.4 mg L^{-1}) were detected in the anoxic BTF during fed-batch mode of operation (Figure 7.4A). The sulfide concentration in the liquid-phase was below 0.7 mg L^{-1} during the H_2S shock-load tests (phase P3, days 174-188). The average SO_4^{2-} concentration was in the range of 900 to 1600 mg L^{-1} even when the H_2S concentration was increased from 99.6 (± 1.7) to 426.6 (± 48.0) ppm_v (Figure 7.4A). Consequently, an increase in the H_2S concentration did not affect the SO_4^{2-} profiles. The highest SO_4^{2-} concentration was 1600 mg L^{-1} during phase P1 of BTF operation (fed-batch mode) at an inlet H_2S concentration of 426.6 (± 48.0) ppmv (Figure 7.4A). During BTF operation in continuous mode, a cream-whitish layer of S^0 covered the PUFs in the BTF and results from EDX analysis confirmed these precipitates as S^0 particles (data not shown). The SO_4^{2-} concentrations during the continuous mode of BTF operation were lower than the SO_4^{2-} formed during fed-batch operation (247-593 mg L^{-1}) because S^0 was also produced as an end-product.

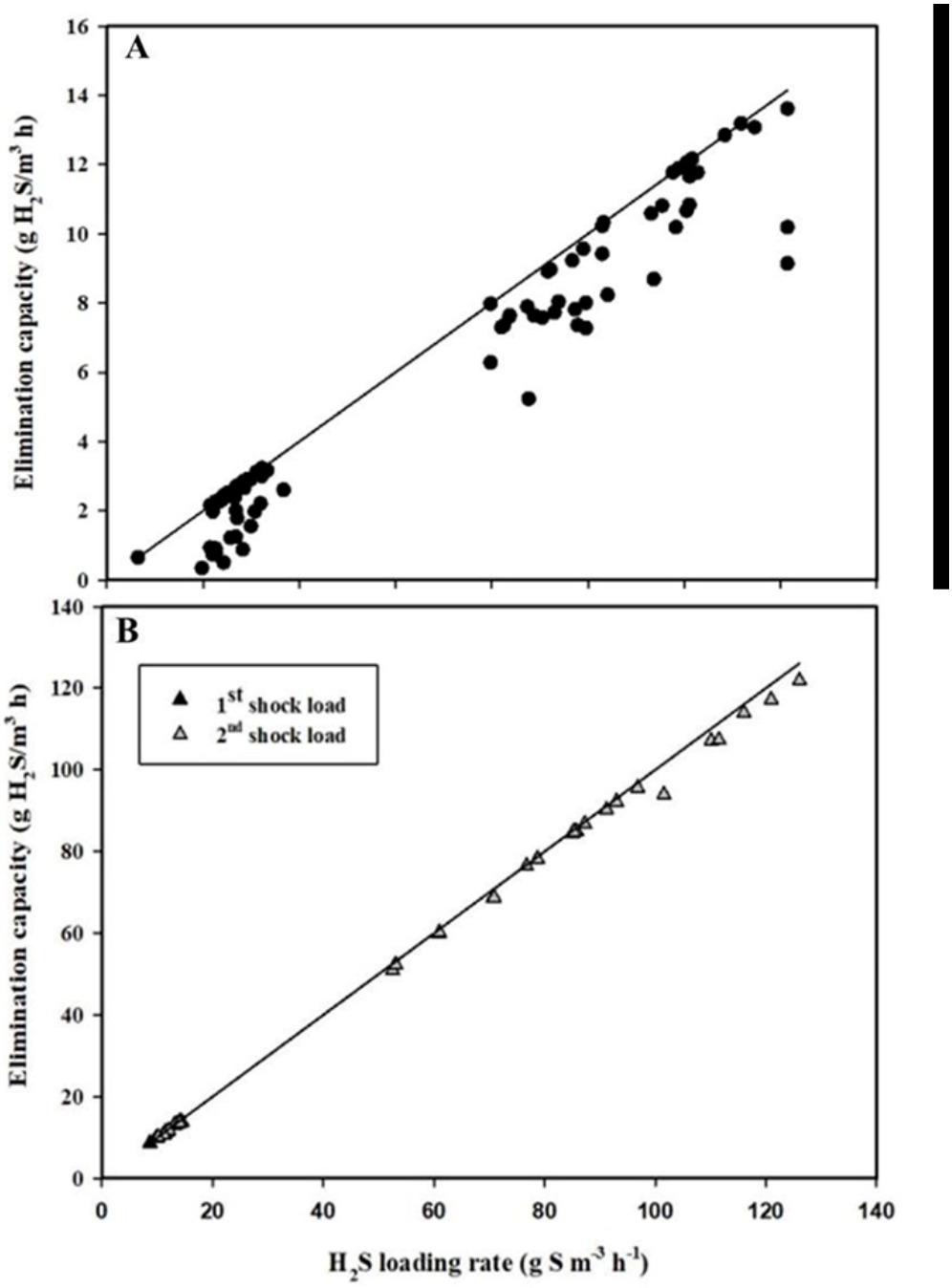

Figure 7.3. Influence of H_2S inlet load on the elimination capacity of the BTF during different modes of operation: (A) fed-batch and continuous, and (B) H_2S shock-load tests.

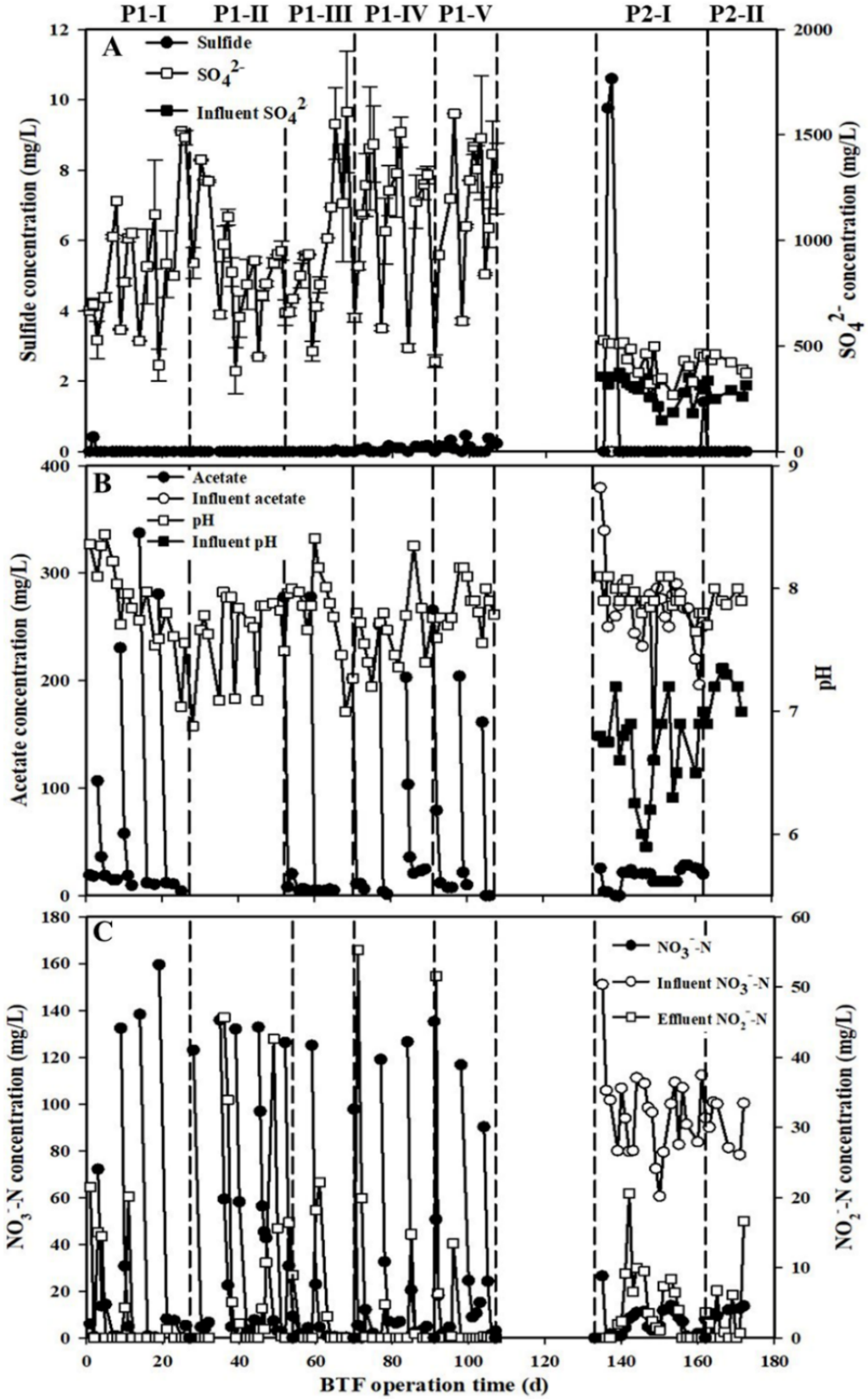

Figure 7.4. Profiles of different parameters in the BTF: (A) sulfide, and SO_4^{2-}, (B) acetate and pH, and (C) NO_3^--N and NO_2^--N.

During phase P1: I-III (IL = 2.7 ± 0.4 g S m^{-3} h^{-1}), SO_4^{2-} was detected as the major end-product (>83.4 ± 23.5)% formation) of sulfide oxidation, while S^0 was also detected as another end-product at high H_2S IL. During phases P1-IV and P1-V, 51.3 (± 3.7)% and 38.2 (± 13.3)% SO_4^{2-} was produced via the sulfide oxidation pathway at an H_2S IL of 9.0 (± 0.7) and 12.1 (± 1.4) g S m^{-3} h^{-1}, respectively. During continuous mode of BTF operation, 50.2 (± 19.9) and 42.4 (± 19.5%) of the sulfide was oxidized to SO_4^{2-} during phases P2-I and P2-II, respectively.

7.3.3 Acetate and pH profiles in the anoxic BTF

The acetate RE was 100% during the 189 days of anoxic BTF operation (Figure 7.4B). During phase P1-II, it was evident that the RE of H_2S decreased slightly from 70 to 52 ppm_v in the absence of acetate at day 31. However, after phase P2, the BTF was operated in continuous mode and acetate was not supplied to the reactor. The initial pH value was ~6.5-7.0 and the final pH value was ~7.7-8.1 without any adjustment of the pH throughout the entire BTF operation (Figure 7.4B).

7.3.4 NO_3^--N removal and NO_2^--N profile in the BTF

During fed-batch mode of operation (phase P1, days 0-107), the NO_3^- removal efficiency was almost 100% within 2 days for each cycle and NO_2^--N (0-55.0 mg NO_2^--N L^{-1}) was detected as an intermediate product of NO_3^- reduction (Figure 7.4C). During continuous mode of BTF operation (phase P2, days 133-175), the NO_3^- removal efficiency was only >82% and the effluent NO_2^--N was below 14 mg NO_2^--N L^{-1} (Figure 7.4C).

7.3.5 Stability of *P. versutus* strain MAL 1HM19 and microbial community analysis

At the end, three different phyla of bacteria were present in the anoxic BTF (Table 7.4): *Proteobacteria*, *Flavobacteria*, and *Actinobacteria*. The anoxic BTF was started using a pure culture of *P. versutus* strain MAL 1HM19. From the results of the PCR-DGGE analysis, the *Paracoccus* sp. strain MAL 1HM19 (*P. versutus*) (band 1), with a high similarity (98%), remained as the dominant microorganism during the BTF (Figure 7.5). Furthermore, CFU growth confirmed the presence of *P. versutus* strain MAL 1HM19 in the BTF biofilm (data not shown). Moreover, another dominant microorganism in the anoxic BTF was *Brevundimonas* sp. (band 2) with 95-99% similarity. Microbes having 97% similarity to *Microbacterium* sp. strain SFA13 (band 4) were observed only during phase P1-I. *Flavobacterium* sp. (band 3) and *Ochrobactrum* sp. AFO (band 8) were observed on day 161 and *Pseudomonas* sp. RAS29 (band 10) was detected on day 189, respectively (Figure 7.5).

Table 7.4 Identification of OTUs obtained from Genebank data (http://www.ncbi.nlm.nih.gov/genbank) based on DGGE band sequences.

Band ID	Closest relatives in the GenBank	Accession number	Identity (%)	Class	Matching length
1	*Paracoccusversutus* strain MAL 1HM1983	KY427435.1	98%	Alphaproteobacteria	482
2	*Brevundimonas* sp.	KU557513.1	96%	Alphaproteobacteria	446
		EF590244.1	99%		486
		HQ622538.1	95%		427
		MF285791.1	98%		513
		FN435943.1	97%		479
3	Uncultured *Flavobacterium* sp.	KM107820.1	95%	Flavobacteria	532
		KP875419.1	97%		503
4	*Microbacterium*sp. strain J13-49	MH470446.1	97%	Actinobacteria	502
5	*Sphingopyxis* sp. OTB55	KX022846.1	91%	Alphaproteobacteria	488
6	Uncultured *Rhizobiales* bacterium	HF678305.1	<90%	Alphaproteobacteria	377
7	Endosymbiont of*Acanthamoeba*sp. UWC8	CP004403.1	98%	-	438
8	*Ochrobactrum* sp. AFO	KJ127515.1	97%	Alphaproteobacteria	481
9	*Pseudomonas* sp. RAS29	FJ868601.1	98%	Gammaproteobacteria	521
10	Uncultured bacterium	AJ536818.1	98%	-	590

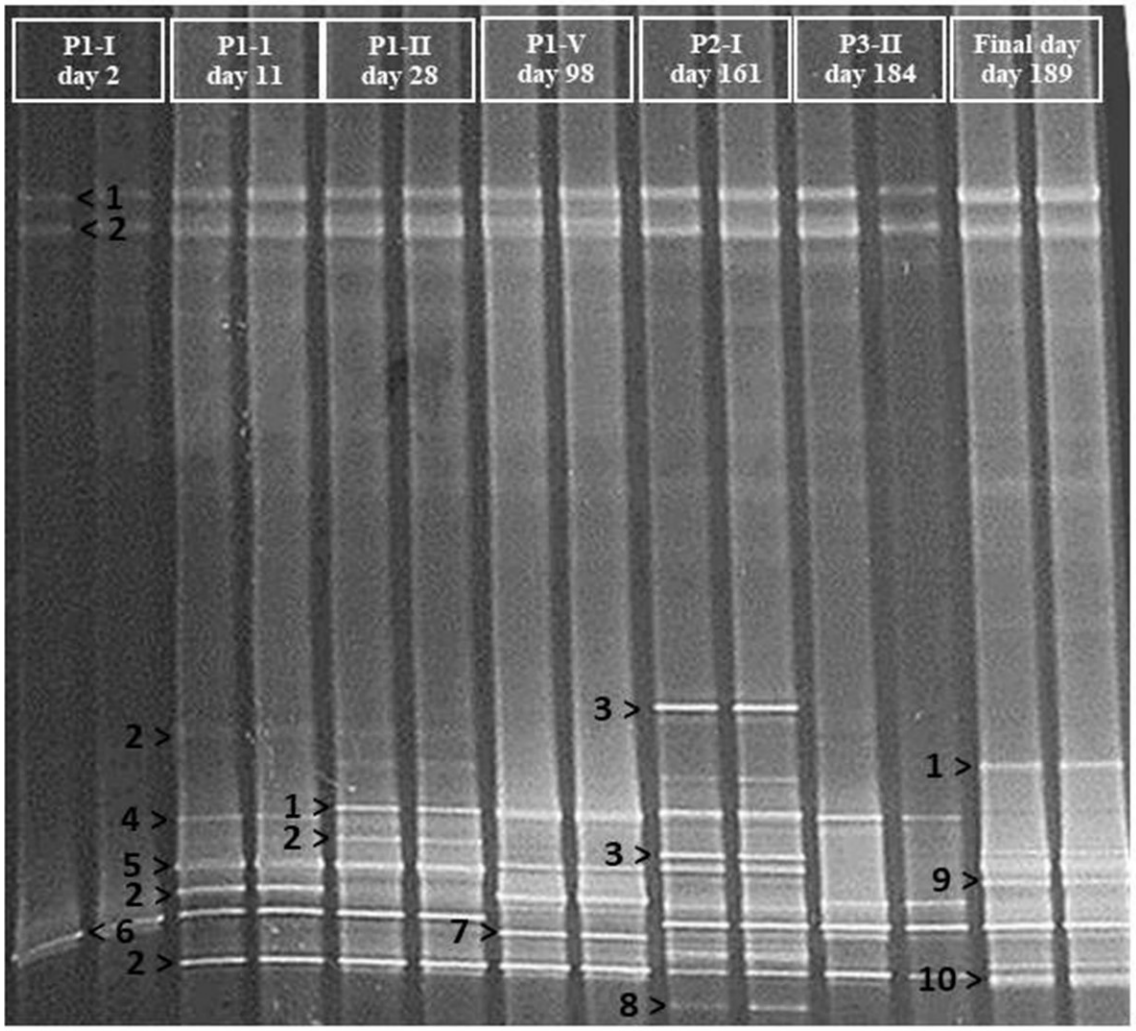

Figure 7.5. DGGE profiles based on 16S rDNA fragments amplified from DNA extracted from the biomass samples (7 pieces) collected on days 2, 11, 28, 98, 161, 184 and 189 from the BTF.

7.3.6 ANN modeling results

The ANN model developed could predict the H_2S-RE, NO_3^--RE and SO_4^{2-} production profiles in the BTF (Figure 7.6). The best network topology of the developed ANN model for the anoxic BTF consisted of 4 neurons in the input layer, 9 neurons in the hidden layer and 3 neurons in the output layer (3-9-3). The training of the network (Table 7.5) was achieved within 2 s and the best validation performance with an MSE of 0.01784 was achieved at an epoch size of 15. The R^2 of the training, validation and test data sets are 0.86, 0.91 and 0.81, respectively (Table 7.6).

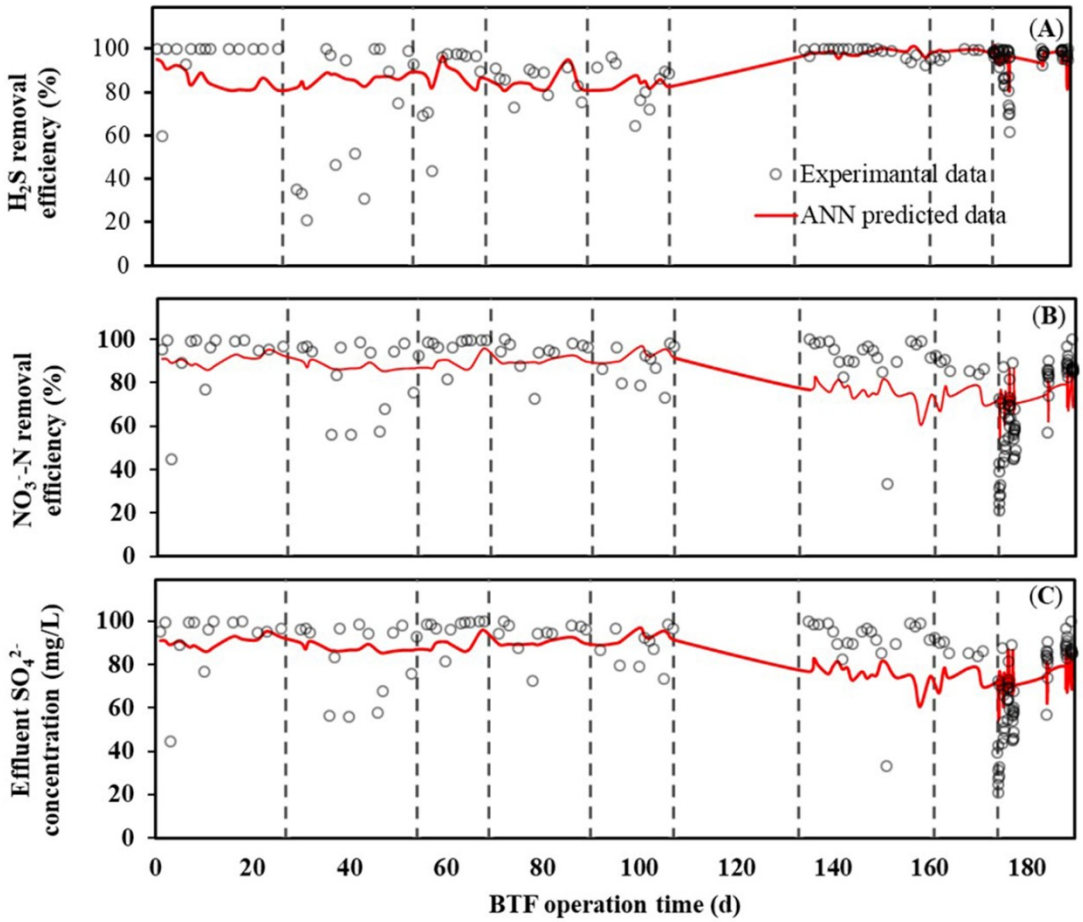

Figure 7.6. Experimental and ANN predicted profiles of: (A) H_2S removal efficiency, (B) NO_3^--N removal efficiency, and (C) SO_4^{2-} production in the BTF.

Table 7.5. Best values used to develop the ANN model for the anoxic biotrickling filter.

Training parameters	Range of value tested	Best value
Number of training data set	87-110	94 (60%)
Number of validation data set	40-24	32 (20%)
Number of test data set	16-32	32 (20%)
Number of neurons in input layer (N_I)	3	3
Number of neurons in hidden layer (N_H)	4-12	7
Number of neurons in output layer (N_O)	3	3
Epoch size	15	19
Momentum term (μ)	0-1	0.00001

Table 7.6. Connection weight between the input-hidden layer (W_{ih}) and hidden-output layer (W_{ho}) of the developed ANN models.

Input	Input-hidden layer (W_{ih})				Hidden-output layer (W_{ho})			
	H_2S_{in}	S/N ratio $_{in}$	pH	BT		H_2S RE	NO_3^- RE	Effluent SO_4^{2-}
HID-1	3.17911	1.49688	0.39428	-3.25933	HID-1	-0.9648	-1.20858	-0.02010
HID-2	-2.11596	-0.84500	-1.10522	2.82909	HID-2	-0.88392	-1.27784	-0.27479
HID-3	-2.78028	5.51576	1.10998	2.36456	HID-3	1.10869	-1.46237	-3.52432
HID-4	-1.41548	-0.94300	-1.78299	1.44844	HID-4	-0.51009	-0.57477	0.08760
HID-5	2.15991	1.60030	-1.67597	0.84400	HID-5	-0.14413	0.78937	-0.50398
HID-6	3.22409	0.39342	1.97824	2.53679	HID-6	-0.45921	0.90080	1.71352
HID-7	-2.56672	-0.42964	1.08732	-1.45408	HID-7	0.12283	0.80194	-0.82300
HID-8	1.38155	-1.18395	2.20227	1.28492	HID-8	-0.43005	0.09495	0.98716
HID-9	0.09249	-1.05230	2.53563	3.26122	HID-9	-0.09228	-0.12704	-0.14324
					BT	1.20774	1.66862	0.19080

Note: HID: hidden layer; W_{ih}: Input-hidden layer; W_{ho}: Hidden-output layer; BT: Bias term

7.4 Discussion

7.4.1 BTF performance

The good performance of the BTF in terms of reaching high EC_{max} values during shock-loading tests (Figure 7.3B) and consistently high H_2S removal efficiency (Figure 7.2) clearly indicates the versatility of the strain MAL 1HM19 to handle gas-phase H_2S. In a previous study, Aroca et al. (2007) tested the H_2S removal performance using *Acidithiobacillus thiooxidans* as the inoculum in an aerobic BTF, and an EC_{max} of 370 g S m^{-3} h^{-1} was reported at an EBRT of 45 sec. The anoxic BTF tested in this study had a moderately high EC_{max} value (116.9 ± 6.6 g S m^{-3} h^{-1}) compared to the EC_{max} observed in other bioreactors inoculated with mixotrophic sulfur oxidizing bacteria (SOB) as well as mixed cultures of autotrophic bacteria (Table 7.7).

The high H_2S RE noticed immediately after reactor start-up (Figure 7.2) indicated *P. versutus* strain MAL 1HM19 was active immediately. In a previous study, Wu et al. (2001) reported a start-up time of 80 days for the immobilization and acclimatization of microorganisms in a H_2S treating BTF inoculated with *Thiobacillus thiooxidans*. In another study, the acclimation step of a biofilter (BF) inoculated with a pure culture of *Acidithiobacillus thiooxidans* required 18 days (Aita et al., 2016). It should be noted that the initial H_2S concentration used in this study (~100 ppm_v) during start-up was higher than in previous studies where in the initial H_2S concentrations were usually in the range of 25-85 ppm_v (Nisola et al., 2010; Abdehagh et al., 2011).

Table 7.7. EC_{max} values reported in the literature for H_2S removal using different bioreactor configurations.

Microorganism	Electron acceptor	H_2S loading rate (g S m^{-3} h^{-1})	EBRT (S)	pH	EC_{max} (g S m^{-3} h^{-1})	Salinity (g L^{-1})	Reactor type	References
Acidithiobacillus thiooxidans	O_2	240	45	2-4	370	0	BTF	Aroca et al. (2007)
Bordetella sp. Sulf-8 BTF 94	O_2	104.5	5	7.0	94	0	BTF	Nisola et al. (2010)
Thiobacillus thioparus	O_2	30	26	6.8	14	0	BF	Aroca et al. (2007)
Thiobacillus denitrificans	NO_3^-	22	≥16	6.9-8.6	22.0	0	BTF	Solcia et al. (2014)
Mixed cultures of autotrophic bacteria	O_2	13	32	7.0	8	0	BF	Kim et al. (2008)
Consortium from activated sludge from a domestic wastewater treatment plant (Tougas, Nantes, France)	NO_3^-	18.5	300	N.D.	30.3	0	BTF	Jaber et al. (2017)
Consortium dominated by *Thiobacillus* sp.	NO_3^-	20.0	180	7.0	19.2	0	BTF	Khanongnuch et al. (2019)
Paracoccus versutus strain MAL 1HM19	NO_3^-	116.9 (± 6.6)	180	7.0-9.0	113.5 (± 6.4)	7	BTF	This study

Note: BF = biofilter; BTF = biotrickling filter; BS = bioscrubber; N/A = not available

The H_2S RE during the second set of shock-load experiments was higher than (>94%) the first successive shock-load experiments (>70%) and a satisfactory bioreactor performance was demonstrated (Figure 7.2D). Usually, in a BTF or BF, a sudden exposure to very high H_2S concentrations might cause toxicity to the microbial community, leading to an inhibition of the microbial activity and a decline of the RE by ~40 to 50% (Kim et al., 2008). This study clearly demonstrated the effective of anoxic BTF inoculated with *P. versutus* strain MAL 1HM19 for biological H_2S removal from contaminated gas stream at high concentration.

The removal of H_2S coupled to NO_3^--N reduction at pH 7.0 was mainly due to the biological activity of NR-SOB (Soreanu et al., 2008). Oh et al. (2001) reported that the optimum pH is in the range of 6.0-9.0 for autotrophic and heterotrophic denitrifying bacteria, which is also the same pH range used in this study.

Due to the absence of structured mathematical models to predict the BTF performance, artificial neural networks are an alternative way to identify the complicated patterns in datasets (López et al. 2014). The overall correlation coefficient (R^2) of the ANN model (0.93) confirms the reliable prediction of the biological processes in the BTF even though it was operated under transient-state conditions. The R^2 of training (0.86) indicated that the model was able to map the relation between the input and output parameters (i.e. H_2S RE, NO_3^- RE and SO_4^{2-} production), while the R^2 of validation (0.91) showed the good generalization capacity of the model (Antwi et al., 2017). The developed ANN in this study could be useful for predicting and optimizing the operational conditions of full-scale anoxic BTF for H_2S removal from gas streams using NO_3^- containing wastewater as the electron acceptor.

7.4.2 Complete or partial H_2S oxidation

The amount of sulfide produced in the liquid-phase (<0.7 mg L^{-1}, Figure 7.4A) had no inhibitory effect on the microorganisms present in the anoxic BTF. As reported in previous studies, the inhibitory concentration of undissociated and dissolved dissociated sulfide and H_2S are in the range of 50-400 and 100-800 mg L^{-1}, respectively (Pokorna et al., 2015). SO_4^{2-} is the main product in the sulfide bio-oxidation pathway under anoxic conditions and as reported previously by Vikromvarasiri and Pisutpaisal (2017), the SO_4^{2-} production rate is usually constant when the inlet H_2S concentration is <570 ppm_v. SO_4^{2-} formation or the presence of SO_4^{2-} in the trickling medium did not have an inhibitory effect on the microorganism nor an effect on the removal of gas-phase H_2S. This observation is consistent with the results reported in a previous BTF study for H_2S removal under aerobic conditions by Ramírez et al. (2009). In that study, the BTF was inoculated

with *T. thioparus* and repression was not reported at SO_4^{2-} concentrations as high as 5,000 mg L^{-1}.

The final product of the sulfide oxidation pathway not only depends on the NO_3^--N concentration following equations (Eqs. 7.5 and 7.6) (Moraes et al., 2012), but also on the amount of sulfide or other S compounds present in the bioprocess:

$5HS^- + 8NO_3^- + 3H^+ \rightarrow 5SO_4^{2-} + 4N_2 + 4H_2O$ (complete oxidation);

$\Delta G° = -3848$ kJ/reaction (7.5)

$5HS^- + 2NO_3^- + 7H^+ \rightarrow 5S^0 + N_2 + 6H_2O$ (partial oxidation);

$\Delta G° = -1264$ kJ/reaction (7.6)

With the NO_3^--N limiting conditions at phase P1-I (S/N = 0.25 ± 0.02), P1-II (S/N = 0.34 ± 0.03) and P1-III (S/N = 0.38 ± 0.1) under fed-batch operation, SO_4^{2-} was detected as the dominant end-product (>96%) according to equation (5) which is similar to the findings by Moraes et al. (2012), who reported the complete sulfide oxidation and SO_4^{2-} formation throughout the operation of a vertical fixed bed reactor treating H_2S and NO_3^--N at a S/N ratio = 0.37. In this study, the presence of excess H_2S, i.e. an increase of H_2S IL during phases P1-IV and P1-V might have caused insufficiency of NO_3^--N, which was supplied approximately once a week but was consumed within 1 d. This resulted in a severe fluctuation of the S/N ratio and the amount of S^0 generated increased relative to the amount of SO_4^{2-} formed. During NO_3^- limitation (phases P1-IV and P1-V), abiotic oxidation of H_2S to S^0 and polysulfides (S_x^{2-}) could be occurs in the BTF as a trace of oxygen can be contaminated with a trickling liquid (Beristain-Cardoso et al., 2006; Pokorna and Zabranska, 2015).

Another possible reason for the formation of S^0 as end-product of the H_2S oxidation might be the higher IL of H_2S during phases 1-IV and 1-V. Li et al. (2016) reported S^0 as the dominant end-product and the gradual decrease of SO_4^{2-} formation during BTF operation at an IL ranging between 16.3 and 54.5 g H_2S m^{-3} h^{-1}, i.e. S/N >0.625. The presence of S^0 might lower the chemolithotrophic denitrification rates because the solid Sº can cause unexpected clogging problems and also affect the mass transfer characteristics of the reactor (Beristain et al., 2005). Besides, changing of the operational mode of the BTF from fed-batch to continuous with high H_2S loading rates (>400 ppm_v or >12 g S m^{-3} h^{-1}) (S/N = 0.13 ± 0.02) in order to provide sufficient NO_3^--N to the BTF system, S^0 was also detected as the end-product (>45%), which is good agreement with Jaber et al. (2017) who reported the high amounts of S^0 (~53%) at high H_2S loading rates (>600 ppm_v). Interestingly, the S/N ratio tested under continuous mode of BTF operation was much

lower than the ratio used by Cai et al. (2008). In that study, 50% S^0 and 50% SO_4^{2-} were observed as the end-products at S/N ratio of 5/5.

7.4.3 Mixotrophic versus autotrophic growth

During mixotrophic conditions wherein both H_2S and acetate were supplied served as the electron donors, the removal of both H_2S and acetate occurred simultaneously which is concurrent with prior studies by Xu et al. (2015) who developed a heterotrophic and autotrophic denitrification (HAD) process for the simultaneous removal of sulfide, NO_3^- and acetate from synthetic wastewater in a Plexiglas reactor using sludge containing *Thiobacillus* sp., *Thauera* sp., *Xanthomonadaceae* sp. and *Chromatiales* sp. with the operating pH and temperature at 7.2-7.5 and 29.5-30.5 °C, respectively. However, this study contrasts An et al. (2010), where sulfide was used as an electron donor for NO_3^- reduction and acetate was used as an electron donor only when the reactor was depleted of sulfide. The different results of this study and An et al. (2010) might be due to the different inocula used.

The H_2S, NO_3^- and acetate removal pathways can be derived from the genetic data of strain MAL 1HM19, obtained by whole genome sequencing (unpublished results). *P. versutus* strain MAL 1HM19 contains the four enzymes including periplasmic nitrate reductase (Nap), nitrite reductase (Nir) and nitrous oxide reductase (Nos) encoded by the *nap*, *nir*, *nor* and *nos* genes for the four-step conversion NO_3^- to N_2 (Watsuntorn et al., 2017). As shown by the NO_2^--N concentrations produced (<14 mg NO_2^--N L^{-1}) during the continuous mode of BTF operation (Figure 7.4C) were not inhibitory to the microorganisms. The accumulation of NO_2^--N was usually followed by its complete conversion to N_2 gas within 3 days (Figure 7.4C). Also, the *sox* genes were present (unpublished results), which belong to the bacterial SOX system and are related to the sulfide oxidation pathway (Friedrich et al., 2005). Moreover, acetyl-CoA synthetase (ACS) or acetate-co A ligase involving the complete conversion of acetate to carbon dioxide (CO_2) as the end-product was present in the genetic profile of *P. versutus* strain MAL 1HM19. The ACS enzyme has the function to change the acetate and coenzyme A to acetyl Co A (Hattori et al., 2005).

7.4.4 Microbial community in the anoxic BTF

Most of the microbes which were observed during BTF operation belonged to denitrifying bacteria. The presence of these various types of denitrifying bacteria likely contributed to the NO_3^- removal in the anoxic BTF investigated. *Brevundimonas* sp., another dominant microorganism present in the anoxic BTF (band 2, Figure 7.5), is a denitrifying bacterium which belongs to the *Alphaproteobacteria* (Kavitha et al., 2009; Ji et al., 2016). Ji et al. (2016) isolated *B. diminuta* MTCC 8486 from groundwater and demonstrated its

ability to withstand NO_3^--N up to 10,000 mg L^{-1}, and 94% NO_3^--N removal was achieved within 36 h at an initial concentration of 148.8 NO_3^--N mg L^{-1} (Ji et al., 2016). Kavitha et al. (2009) reported NO_3^--N removal using *B. diminuta* isolated from marine soil of a coastal area near Trivandrum (Kerala, India). *B. diminuta* can tolerate NO_3^- concentrations up to 10,000 mg L^{-1}. *Microbacterium* sp. strain SFA13, isolated from Songhua River (China), showed good NO_3^- and ammonium (NH_4^+) removal, converting NO_3^- and NH_4^+ to N_2 at 5 °C under aerobic conditions and ~70% of the NO_3^- was reduced to N_2 within 30 h (Zhang et al., 2013). In addition, species from the genus *Pseudomonas* have also been reported to participate in the denitrification process (Zhang et al., 2011).

7.5 Conclusions

- An anoxic BTF inoculated with pure culture of *P. versutus* strain MAL 1HM19 required a short start-up time (1 d) and showed robustness for removal of H_2S from a biogas mimic. The *P. versutus* strain MAL 1HM19 was dominantly present in the BTF irrespective of the operational conditions and the strain showed good removal capacity during H_2S shock-load test.
- The EC_{max} values of the anoxic BTF in steady and transient state with continuous mode were 17.9 (± 2.1) and 113.5 (± 6.4) g S m^{-3} h^{-1}, respectively.
- The *P. versutus* strain MAL 1HM19 was dominantly present in the BTF irrespective of the operational conditions and the strain showed a good removal capacity during H_2S shock-load test.

7.6 References

Abdehagh, N., Namini, M.T., Heydarian, S.M., Bonakdarpour, B., Zare, D., 2011. Performance of a biotrickling filter employing *Thiobacillus thioparus* immobilized on polyurethane foam for hydrogen sulfide removal. Iran. J. Environ. Health. Sci. 8, 245-254.

Aita, B.C., Mayer, F.D., Muratt, D.T., Brondani, M., Pujol, S.B., Denardi, L.B., Hoffmann, R., Da Silveira, D.D., 2016. Biofiltration of H_2S-rich biogas using *Acidithiobacillus thiooxidans*. Clean Technol. Environ. Policy. 18, 689-703.

An, S., Tang, K., Nemati, M., 2010. Simultaneous biodesulphurization and denitrification using an oil reservoir microbial culture: effects of sulphide loading rate and sulphide to nitrate loading ratio. Water Res 44, 1531-1541.

Antwi, P., Li, J., Boadi, P.O., Meng, J., Shi, E., Deng, K., Bondinuba, F.K., 2017. Estimation of biogas and methane yields in an UASB treating potato starch processing wastewater with backpropagation artificial neural network. Bioresour. Technol. 228, 106-115.

APHA (2005) Standard methods for the examination of water and wastewater, 21st ed. American Public Health Association, Washington, DC.

Aroca, G., Urrutia, H., Núñez, D., Oyarzún, P., Arancibia, A., Guerrero, K., 2007. Comparison on the removal of hydrogen sulfide in biotrickling filters inoculated with *Thiobacillus thioparus* and *Acidithiobacillus thiooxidans*. Electron. J. Biotechnol. 10, 514-520.

Atasoy, A.D., Babar, B., Sahinkaya, E., 2013. Artificial neural network prediction of the performance of upflow and downflow fluidized bed reactors treating acidic mine drainage water. Mine Water Environ. 32, 222-228.

Beristain, R., Sierra-Alvarez, R., Salazar, M., Fernández, N., Gomez, J., Razo-Flores, E., Field, J.A., 2005. Autotrophic denitrification with elemental sulfur. In VIII International Water Association Latin American Symposium on Anaerobic Digestion, Oct. 2-5, Punda del Este, Uruguay, pp. 383-388.

Beristain-Cardoso, R., Sierra-Alvarez, R., Rowlette, P., Flores, E.R., Gómez, J., Field, J.A., 2006. Sulfide oxidation under chemolithoautotrophic denitrifying conditions. Biotechnol. Bioeng. 95, 1148–1157.

Cai, J., Zheng, P., Mahmood, Q., 2008. Effect of sulfide to nitrate ratios on the simultaneous anaerobic sulfide and nitrate removal. Bioresour. Technol. 99, 5520-5527.

Cai, J., Zheng, P., Mahmood, Q., Luo, T., 2015. Prediction and quantifying parameter importance in simultaneous anaerobic sulfide and nitrate removal process using artificial neural network. Environ. Sci. Pollut. Res. Int. 22, 8272–8279.

Chung, Y.C., Huang, C., Tseng, C.P., 2001. Biological elimination of H_2S and NH_3 from

waste gases by biofilter packed with immobilized heterotrophic bacteria. Chemosphere. 43, 1043-1050.

Díaz, I., Pérez, S.I., Ferrero, E.M., Fdz-Polanco, M., 2011. Effect of oxygen dosing point and mixing on the microaerobic removal of hydrogen sulphide in sludge digesters. Bioresour. Technol. 102, 3768-3775.

Eregowda, T., Matanhike, L., Rene, E.R., Lens, P.N.L., 2018. Performance of a biotrickling filter for the anaerobic utilization of gas-phase methanol coupled to thiosulphate reduction and resource recovery through volatile fatty acids production. Bioresour. Technol. 263, 591-600.

Fernández, M., Ramírez, M., Gómez, J.M., Cantero, D., 2014. Biogas biodesulfurization in an anoxic biotrickling filter packed with open-pore polyurethane foam. J. Hazard. Mater. 264, 529-535.

Friedrich, C.G., Bardischewsky, F., Rother, D., Quentmeier, A., Fischer, J., 2005. Prokaryotic sulfur oxidation. Curr. Opin. Microbiol. 8, 253-259.

Gronewold, A.D., Wolpert, R.L., 2008. Modeling the relationship between most probable number (MPN) and colony-forming unit (CFU) estimates of fecal coliform concentration. Water Res. 42, 3327-3334.

Hattori, S., Galushko, A. S., Kamagata, Y., Schink, B., 2005. Operation of the CO dehydrogenase/acetyl coenzyme A pathway in both acetate oxidation and acetate formation by the syntrophically acetate-oxidizing bacterium *Thermacetogenium phaeum*. J. Bacteriol. 187, 3471-3476.

Jaber, M.B., Couvert, A., Amrane, A., Le Cloirec, P., Dumont, E., 2017. Hydrogen sulfide removal from a biogas mimic by biofiltration under anoxic conditions. J. Environ. Chem. Eng. 5, 5617-5623.

Ji, B., Chen, W., Zhu, L., Yang, K., 2016. Isolation of aluminum-tolerant bacteria capable of nitrogen removal in activated sludge. Marine Poll. Bull. 106, 31-34.

Kavitha, S., Selvakumar, R., Sathishkumar, M., Swaminathan, K., Lakshmanaperumalsamy, P., Singh, A., Jain, S.K., 2009. Nitrate removal using *Brevundimonas diminuta* MTCC 8486 from ground water. Wat. Sci. Technol. 60, 517-524.

Khanongnuch, R., Di Capua, F., Lakaniemi, A.-M., Rene, E.R., Lens, P.N.L., 2018. Effect of N/S ratio on anoxic thiosulfate oxidation in a fluidized bed reactor: Experimental and artificial neural network model analysis. Process Biochem. 68, 171-181.

Khanongnuch, R., Di Capua, F., Lakaniemi, A-M., Rene, E.R., Lens, P.N.L., 2019. H_2S removal and microbial community composition in an anoxic biotrickling filter under autotrophic and mixotrophic conditions. J. Hazard. Mater. 367, 397-406.

Kennes, C., Rene, R.E., Veiga, C.M., 2009. Bioprocesses for air pollution control. J. Chem. Technol. Biotechnol. 84, 1419-1436.

Kim, J.H., Rene, E.R., Park, H.S., 2008. Biological oxidation of hydrogen sulfide under steady and transient state conditions in an immobilized cell biofilter. Bioresour.

Technol. 99, 583-588.

Lee, E.Y., Lee, N.Y., Cho, K.S., Ryu, H.W., 2006. Removal of hydrogen sulfide by sulfate-resistant *Acidithiobacillus thiooxidans* AZ11. J. Biosci. Bioeng. 101, 309-314.

Li, X., Jiang, X., Zhou, Q., Jiang, W., 2016. Effect of S/N ratio on the removal of hydrogen sulfide from biogas in anoxic bioreactors. Appl. Biochem. Biotechnol. 180, 930-944.

Liu, C., Liu, J., Li, J., He, H., Peng, S., Li, C., Chen, Y., 2013. Removal of H_2S by co-immobilized bacteria and fungi biocatalysts in a bio-trickling filter. Process Safe. Environ. 91, 145-152.

Moraes, B.D.S., Souza, T.S.O., Foresti, E., 2012. Effect of sulfide concentration on autotrophic denitrification from nitrate and nitrite in vertical fixed-bed reactors. Process Biochem. 47, 1395-1401.

Nisola, G.M., Tuuguu, E., Farnazo, D.M.D., Han, M., Kim, Y., Cho, E., Chung, W.G., 2010. Hydrogen sulfide degradation characteristics of *Bordetella* sp. Sulf-8 in a biotrickling filter. Bioproc Biosyst. Eng. 33, 1131-1138.

Oh, S.E., Yoo, Y.B., Young, J.C., Kim, I.S., 2001. Effect of organics on sulfur-utilizing autotrophic denitrification under mixotrophic conditions. J. Biotechnol. 92, 1-8.

Pokorna, D., Zabranska, J., 2015. Sulfur-oxidizing bacteria in environmental technology. Biotechnol. Adv. 33, 1246-1259.

Prado, Ó.J., Veiga, M.C., Kennes, C., 2004. Biofiltration of waste gases containing a mixture of formaldehyde and methanol. Appl. Microbiol. Biotechnol. 65, 235-242.

Ramírez, M., Gómez, J.M., Aroca, G., Cantero, D., 2009. Removal of hydrogen sulfide by immobilized *Thiobacillus thioparus* in a biotrickling filter packed with polyurethane foam. Bioresour. Technol. 100, 4989-4995.

Rattanapan, C., Kantachote, D., Yan, R., Boonsawang, P., 2010. Hydrogen sulfide removal using granular activated carbon biofiltration inoculated with *Alcaligenes faecalis* T307 isolated from concentrated latex wastewater. Int. Biodeter. Biodegradation, 64, 383-387.

Rene, E. R., Maliyekkal, S. M., Philip, L., Swaminathan, T., 2006. Back-propagation neural network for performance prediction in trickling bed air biofilter. Int. J. Environ. and Pollut. 28, 382.

Rene, E.R., Kim, J.H., Park, H.S., 2008. An intelligent neural network model for evaluating performance of immobilized cell biofilter treating hydrogen sulphide vapors. Int. J. Environ. Sci. Tech. 5, 287-296.

Rene, E.R., Veiga, M.C., Kennes, C., 2009. Experimental and neural model analysis of styrene removal from polluted air in a biofilter. J. Chem. Technol. Biotechnol. 84, 941–948.

Solcia, R.B., Ramírez, M., Fernández, M., Cantero, D., Bevilaqua, D., 2014. Hydrogen sulphide removal from air by biotrickling filter using open-pore polyurethane foam

as a carrier. Biochem. Eng. J. 84, 1-8.

Soreanu, G., Beland, M., Falletta, P., Edmonson, K., Seto, P., 2008. Investigation on the use of nitrified wastewater for the steady-state operation of a biotrickling filter for the removal of hydrogen sulphide in biogas. J. Environ. Eng. Sci. 7, 543-552.

van den Hoop, M.A., den Hollander, H.A., Kerdijk, H.N., 1997. Spatial and seasonal variations of acid volatile sulphide (AVS) and simultaneously extracted metals (SEM) in Dutch marine and freshwater sediments. Chemosphere. 35, 2307-2316.

Vikrant, K., Kim, K., Szulejko, J.E., Pandey, S.K., Singh, R.S., Giri, B.S., Brow, R.J.C., Lee, S.H., 2017. Bio-filters for the treatment of VOCs and odors - a review. Asian J. Atmos. Environ. 11, 139-152.

Vikromvarasiri, N., Boonyawanich, S., Pisutpaisal, N., 2015. Optimizing sulfur oxidizing performance of *Paracoccus pantotrophu*s isolated from leather industry wastewater. Energy Procedia. 79, 629-633.

Vikromvarasiri, N., Pisutpaisal, N., 2017. Hydrogen sulfide removal in biotrickling filter system by *Halothiobacillus neapolitanus*. Int. J. Hydrog. Energy. 41, 15682-15687.

Watsuntorn, W., Ruangchainikom, C., Rene, E.R., Lens, P.N.L., Chulalaksananukul, W., 2017. Hydrogen sulfide oxidation under anoxic conditions by a nitrate-reducing, sulfide-oxidizing bacterium isolated from the Mae Um Long Luang hot spring, Thailand. Int. Biodeterior. Biodegradation. 124, 196-205.

Watsuntorn, W., Ruangchainikom, C., Rene, E.R., Lens, P.N.L., Chulalaksananukul, W., 2018. Comparison of sulphide and nitrate removal from synthetic wastewater by pure and mixed cultures of nitrate-reducing, sulphide-oxidizing bacteria. Bioresour. Technol. 272, 40-47.

Wu, L., Loo, Y.Y., Koe, L.C.C., 2001. A pilot study of a biotrickling filter for the treatment of odorous sewage air. Water Sci. Technol. 44, 295-299.

Xu, G., Peng, J., Feng, C., Fang, F., Chen, S., Xu, Y., Wang, X., 2015. Evaluation of simultaneous autotrophic and heterotrophic denitrification processes and bacterial community structure analysis. Appl. Microbiol. Biotechnol. 99, 6527-6536.

Zamir, M., Halladj, R., Saber, M., Ferdowsi, M., Nasernejad, B., 2011. Biofiltration of hexane vapor: experimental and neural model analysis. Soil Air Water. 39, 813-819.

Zhang, J., Wu, P., Hao, B., Yu, Z., 2011. Heterotrophic nitrification and aerobic denitrification by the bacterium *Pseudomonas stutzeri* YZN-001. Bioresour. Technol. 102, 9866-9869.

Zhang, D., Li, W., Huang, X., Qin, W., Liu, M., 2013. Removal of ammonium in surface water at low temperature by a newly isolated *Microbacterium* sp. strain SFA13. Bioresour. Technol 137, 147-152.

Chapter 8 General discussion

8.1 Introduction

In this thesis, various anoxic bioreactor configurations were successfully used for treating waste streams contaminated with RSCs, i.e. $S_2O_3^{2-}$ and H_2S, using NO_3^- as an electron acceptor (Table 8.1). These processes relied on the activity of sulfur-oxidizing nitrate-reducing (SO-NR) bacteria, the ratio of nitrogen-to-sulfur (N/S ratio), the source of an inoculum and different bioreactor configurations. Two different anoxic bioreactor configurations, i.e. a fluidized bed reactor (FBR) and a moving bed biofilm reactor (MBBR) were successfully developed for the treatment of sulfur-containing liquid streams by using $S_2O_3^{2-}$ and NO_3^- as the sulfur source and electron acceptor, respectively (**Chapters 3 and 4**). To develop an integrated and sustainable approach, an anoxic biotrickling filter (BTF) was developed for the simultaneous treatment of H_2S contaminated gas streams and NO_3^--containing wastewater as well as the effect of organic matter present in the systems (**Chapter 5**). Besides, the inoculation and bioaugmentation with a facultative autotrophic bacterium, *Paracoccus* sp. strain 1MAL19, in the anoxic BTF was investigated to improve the bioreactor's resistance to high steady and transient loading rates of gas and liquid phase pollutants (**Chapters 6 and 7**). This research provides valuable insights to the anoxic treatment of RSCs contaminated waste streams and the reliability of different sulfur-oxidizing anoxic bioreactors. The integrated technologies based on the major findings obtained in this research are illustrated in Figure 8.1.

Table 8.1. Overview of the operational conditions and performance of the anoxic sulfur oxidizing bioreactors used in this PhD thesis.

	Fluidized bed reactor	Moving bed biofilm reactor	Biotrickling filter	Biotrickling filter
Inoculum	*Thiobacillus*-dominated biofilm	*Thiobacillus*-dominated biofilm	*Thiobacillus*-dominated biofilm	Pure culture of *Paracoccus* sp. strain MAL
Carriers	Granular activated carbon	Kaldnes-K1	Polyurethane foam	Polyurethane foam
Sulfur source	$S_2O_3^{2-}$	$S_2O_3^{2-}$	H_2S	H_2S
Feed N/S ratio (mol mol^{-1})	0.1-0.5	0.1-0.5	1.2-1.7	1.9-11.4
Inlet sulfur loading rate (g S m^{-3} h^{-1})	37.0	37.0	3.5-20.0 (40.0)[a]	2.0-18.0 (125)[a]
Maximum sulfur removal rate (g S m^{-3} h^{-1})	33.8	35.8	19.2 (37.8)[a]	17.0 (122)[a]
NO_3^- loading rate (g N m^{-3} h^{-1})	2.0-7.5	2.0-7.9	9.9-11.1	17.0

Note: [a]maximum value during shock load tests

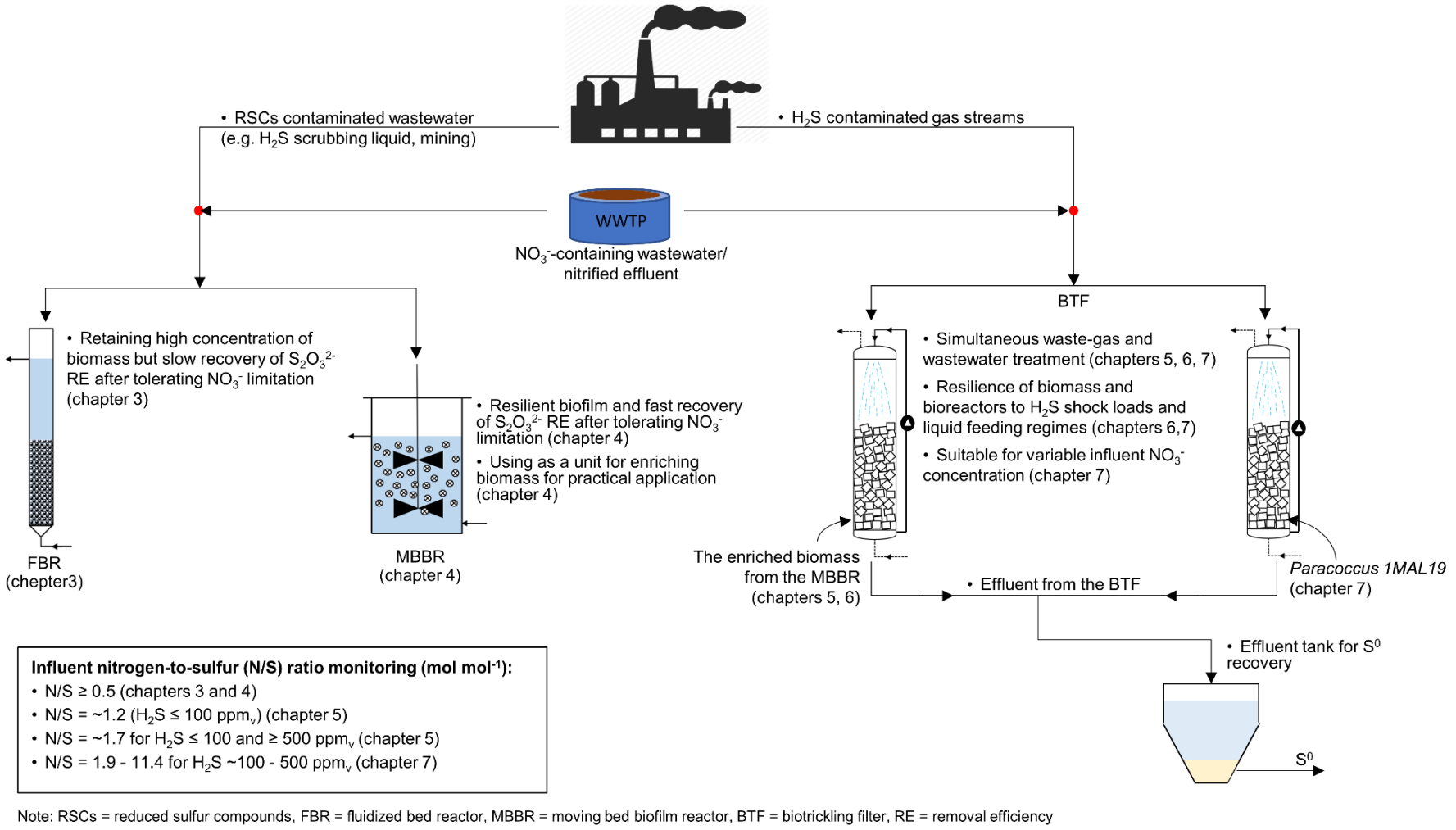

Note: RSCs = reduced sulfur compounds, FBR = fluidized bed reactor, MBBR = moving bed biofilm reactor, BTF = biotrickling filter, RE = removal efficiency

Figure 8.1. Schematic for the integrated treatment of reduced sulfur contaminated waste streams in anoxic bioreactors based on the major findings of this thesis.

8.2 H_2S removal from synthetic biogas

8.2.1 Application of anoxic bioreactors for the removal of reduced sulfur compounds (RSCs) from waste streams

The attached-biofilm reactors, including a FBR and MBBR, have been reported as effective bioreactors for NO_3^- removal from wastewater (Di Capua et al., 2015; Papirio, 2012; Yuan et al., 2015). However, the research and development of these bioreactors for treatment of RSCs contaminated wastewater is still limited. As these bioreactors have shown good ability to retain biofilms in the system and protect the microorganisms in the biofilms from high toxic and harmful environments, the performances of anoxic FBR and MBBR for $S_2O_3^{2-}$ oxidation were investigated in **Chapters 3 and 4**. The performance of the FBR and MBBR in terms of $S_2O_3^{2-}$ removal efficiency (RE) showed no difference when sufficient NO_3^- was supplied in the feed (N/S ratio of 0.5). In addition, the FBR and MBBR used in this study demonstrated higher resiliency to long-term operation under excess $S_2O_3^{2-}$ (N/S ratio of 0.5) compared to the optimal N/S ratios obtained in anoxic completely stirred tank reactors (CSTR), at 1.0 and 0.8-0.9 mol mol^{-1} for the removal of $S_2O_3^{2-}$ and S^{2-}, respectively (Dolejs et al., 2015; Manconi et al., 2007).

The MBBR showed a slightly higher $S_2O_3^{2-}$ RE than the FBR during the operation at NO_3^- limited conditions (N/S ratios of 0.3 and 0.1). The MBBR also showed a faster recovery of the $S_2O_3^{2-}$ RE, which increased from 37.7% to >99% within 2 days after increasing the N/S ratio from 0.1 to 0.5. The $S_2O_3^{2-}$ RE in the FBR recovered from 26.0% to 80.8 (± 4.1)% in 3 days and did not further improve although the experiment was continued for 64 d. Additionally, the metabolic activity of the MBBR biomass, i.e. the maximum specific rate of $S_2O_3^{2-}$ oxidation, was also enhanced after operation under severe NO_3^- limitation. The different bioreactor configurations and mixing conditions provided slightly higher dissolved oxygen concentrations to the MBBR (0.45 ± 0.08 mg L^{-1}) than to the FBR (0.25 ± 0.05 mg L^{-1}). Thus, one of the reasons for the slightly better performance of the MBBR compared to the FBR might be the higher level of free oxygen stimulating the sulfur-oxidizing activity of the MBBR biofilm during NO_3^- limitation (N/S ratio 0.3 and 0.1). Oxygen likely served as an alternative electron acceptor for facultative autotrophs, i.e. *Thiobacillus thioparus and Thiomonas sp.*, which were present in the systems (**Chapter 4**, Figure 4.8).

The different characteristics of the carrier materials used in the two systems also likely affected the bioreactor performance. Compared to the FBR biofilm developed onto granular activated carbon, the biofilm attached on the internal structure of the MBBR carriers

(Kaldnes-K1 carriers) could be more efficient in protecting the microorganisms against harsh environmental conditions (Barwal and Chaudhary, 2014). However, the FBR contained higher biomass concentrations than the MBBR (**Chapters 3 and 4**) that can further benefit when treating pollutants at high loading rates (Di Capua et al., 2015; Papirio et al., 2013).

In practical applications, RSCs contaminated waste streams, i.e. scrubbing liquid from the desulfurization unit or biogas production from anaerobic digestion of WWTP sewage could be simultaneously treated with NO_3^- containing wastewater from post-treatment using nitrification-denitrification to avoid the addition of external organic carbon (Baspinar et al., 2011; Guerrero et al., 2015). Due to the good performance of the MBBR in this study (**Chapter 3**), a long-term operated MBBR (306 days) can be used for enriching SO-NR biomass prior to the inoculation of other bioreactors, e.g. an anoxic BTF for H_2S removal or an anoxic MBBR. Furthermore, the FBR and MBBR can also be used for treating scrubbing liquid containing HS^-, S^{2-} and/or $S_2O_3^{2-}$ from scrubbers for H_2S removal coupled with nitrogen removal, which has been previously demonstrated as potential application for packed columns and activated sludge bioreactors (Baspinar et al., 2011; Deng et al., 2009).

8.2.2 Application of anoxic BTFs for H_2S removal from gas streams

Anoxic biotrickling filters for H_2S removal provide higher availability of electron acceptor for microbial metabolism than aerobic systems due to the high solubility of NO_3^- (Brito et al., 2017). In **Chapters 5 and 6**, the anoxic BTFs were used for H_2S removal from the gas stream (the mixture of N_2 and H_2S) and a H_2S RE >99% was obtained under steady-state operation with outlet H_2S concentrations of 0 and 0-10 ppm_v for inlet concentrations of 100 and 500 ppm_v, respectively. The highest H_2S elimination capacity (EC) of 19.2 g S m^{-3} h^{-1} was observed after 42 days of operation. The highest H_2S EC reported in anoxic BTFs was ~170 g S m^{-3} h^{-1} at high inlet H_2S concentrations in the range of ~1000-14600 ppm_v (Almenglo et al., 2016; Brito et al., 2017; Fernández et al., 2014, 2013; López et al., 2018). Those studies focused on the use of NO_3^- from chemical sources, i.e. $Ca(NO_3)_2$, KNO_3 and $NaNO_3$; and the determination of optimal operational conditions controlled by automatic systems, i.e. gas-liquid flow patterns and the use of proportional-integral-derivative (PID) control systems. Several applications of biogas, such as gas stoves and fuel cells, require biogas containing a very low H_2S concentration, e.g. <10 ppm_v. Furthermore, the outlets from full-scale desulfurization units often still contain H_2S concentrations of 20-1000 ppm_v (Baspinar et al., 2011). The results obtained from this thesis suggest that anoxic BTFs can also be used as a secondary treatment unit to remove H_2S from the effluent of full-scale desulfurization units treating high H_2S concentrations (10000-40000 ppm_v) to reach the regulatory limits.

When considering the use of NO_3^--containing wastewater as the electron acceptor source in anoxic sulfide oxidizing bioreactors, the composition of the wastewater should be analyzed carefully because many wastewaters also contain organic compounds which can affect the sulfur-oxidizing process and the microbial community in the bioreactor. Results of **Chapter 5** revealed that the addition of acetate under autotrophic conditions stimulated the growth and activity of heterotrophic denitrifying bacteria and the microbial community composition in the bioreactor changed significantly. The NO_3^- demand was high because NO_3^- was used for both autotrophic and heterotrophic denitrification. This led to a decrease of the H_2S RE in the BTF; however, the efficiency increased immediately after increasing the NO_3^- loading rate (**Chapter 6**). The mass balance analyses of sulfur, nitrogen and carbon carried out for the anoxic BTF showed high amounts of carbon release from the system during the addition of acetate in the form of high CO_2 production due to biodegradation of the feed acetate and wash out of biomass previously formed in the system. These results suggest that the BTF can be operated with wastewater containing organic carbon as it increases the NO_3^- RE via mixotrophic denitrification and provides CO_2 as the endogenous carbon source instead of adding external inorganic carbon (Bayrakdar et al., 2016). Furthermore, **Chapter 5** demonstrated that the N_2 and CO_2 concentrations produced during the autotrophic and/or mixotrophic H_2S oxidation did not affect the outlet gas composition of the system. Therefore, the anoxic BTF can be used for biogas desulfurization without dilution of the CH_4 content.

The variation in the feed N/S ratios from 1.2 to 1.7 mol mol^{-1} did not affect the main H_2S oxidation product, which was mainly SO_4^{2-}, when the anoxic BTF was operated at NO_3^- loading rates of 9.9-11.1g N m^{-3} h^{-1} for treating H_2S in the range of 100-500 ppm_v (**Chapter 5**). However, **Chapter 6** demonstrated that the trickling liquid flow rate at 30 L h^{-1} could lead to the partial S^0 production of ~20% at a feed N/S ratio of ~1.7 and NO_3^- loading rate of 2.7 g N m^{-3} h^{-1}. Nevertheless, the H_2S RE was stable at 100% compared to the trickling liquid flow rates at 60 and 120 L d^{-1}. Apart from the operation at high inlet H_2S concentrations (Fernández et al., 2014, 2013), the results of this study suggest that the operation at low trickling liquid flow rate or low NO_3^- loading rate also results in the production of S^0. S^0 can be used in commercial products, e.g. biological S^0 and fertilizer. However, the recovery techniques for S^0 from anoxic BTFs are still limited. Thus, the increase of the NO_3^- loading rate allows the removal of the accumulated S^0 and avoids clogging problems in the bioreactor (Brito et al., 2017).

Chapter 7 describes the performance of an anoxic BTF (189 operational days) inoculated with a pure culture of *Paracoccus* sp. 1MAL19 for H_2S removal. Watsuntorn et al. (2017) previously reported that *Paracoccus* sp. 1MAL19 could grow in varying operating conditions, i.e. temperatures of 20-50 °C and high salinity (7% *w/v* of NaCl). **Chapters 5 and 6** demonstrated that bioaugmentation with *Paracoccus* sp. 1MAL19 enhanced the

tolerance of bioreactors to varying influent acetate concentrations. Furthermore, the BTF bioaugmented with *Paracoccus* sp. 1MAL19 required organic carbon (10.2 g acetate m^{-3} h^{-1}) to achieve sulfide oxidation efficiencies >90% (**Chapter 6**). Additionally, it was shown that the BTF inoculated with *Paracoccus* sp. 1MAL19 could be operated at N/S ratios in the range of 1.9-11.4 mol mol^{-1}, while maintaining the H_2S removals efficiencies >90% (**Chapter 7**). This demonstrated that the *Paracoccus* sp. 1MAL19 could be used either as an inoculum or bioaugmented to an existing BTF for the simultaneous removal of H_2S, NO_3^- and organic carbon. Although anoxic BTFs have been developed for biological gas desulfurization, their practical application may encounter high variations in operating conditions, e.g. increase of heterotrophic bacteria growth and unexpected (transient) operating conditions. **Chapters 5, 6 and 7** also demonstrated the robustness of the anoxic BTF to H_2S shock loads, resiliency to recover the performance of two anoxic BTFs inocula with different inoculum as well as the microbial activity and community composition under transient conditions.

8.2.3 Microbial community composition of the anoxic bioreactors used for treatment of waste streams contaminated with RSCs

A similar microbial community composition was observed in the different bioreactors tested in this study (**Chapters 3, 4, 5 and 6**). During the entire operation of the FBR, MBBR and BTF, *Thiobacillus* sp. and *Chryseobacterium* sp., were the dominant microorganisms detected in the bioreactors under both autotrophic and heterotrophic denitrification conditions. Although the BTF was inoculated with biomass from the MBBR, the BTF showed the presence of only one species of known sulfur-oxidizing bacteria, i.e. *Thiobacillus* sp. (**Chapter 5**), while the FBR and MBBR retained various species that can oxidize RSCs, i.e. *Thiobacillus denitrificans*, *Thiobacillus* sp., *Sulfuritalea* sp. and *Thiomonas* sp. (**Chapters 3, 4**). This indicates that submerged attached growth bioreactors (FBR and MBBR) are able to better retain various microorganisms compared to BTFs. However, the BTF was preferable for the treatment of waste gas due to enhanced pollutant transfer characteristics from the gas-phase to the biofilm and its ability to handle transient-state conditions that are usually prevalent in industrial operations (Kennes et al., 2009).

During stress conditions in anoxic bioreactors for sulfur oxidation, i.e. NO_3^- limitation (**Chapters 3 and 4**), sulfate reducing bacteria (e.g. *Desulfovibrio* sp.) were detected from the biofilm samples and likely grew by reducing $S_2O_3^{2-}$ or SO_4^{2-} in the bioreactor. However, their representative DGGE bands faded away in the later stages of bioreactor operation likely because the conditions favored the dominance of sulfide-oxidizing bacteria in the system. This observation clearly confirms that the operating conditions of the reactor and the microbial community composition should be monitored carefully in order to

maintain the dominant microorganisms and bioreactor efficiency during long-term operation. Based on the results obtained from the BTF tested under various transient-state conditions (**Chapter 6**), it was evident that the growth of heterotrophic bacteria was stimulated during stress conditions when the sulfur-oxidation efficiency decreased. In such situation, heterotrophic and *Desulfovibrio*-like bacteria could utilize organic carbon sources excreted by and from the autotrophs or other bacteria present in the system.

8.2.4 Use of artificial neural networks for modeling the performance of different bioreactors

The artificial neural network (ANN) is one of the most efficient black-box modelling tools used widely to predict and describe the performance of biological processes (Jiang et al., 2016; Nair et al., 2016; Rene et al., 2011; Sahinkaya, 2009). ANN models were successfully used to predict the $S_2O_3^{2-}$ RE and NO_3^- RE and SO_4^{2-} production in the FBR and MBBR during long-term operation for 306 days (**Chapters 3 and 4**). The performance of the anoxic BTF that was operated under both steady-state and transient conditions for 189 days was also successfully predicted by the developed ANN model (**Chapter 7**). However, the application of ANN models can also have some drawbacks, e.g. the requirement of large data sets to represent the process behavior, possibility of over-training, problems with error convergence and need to use a trial and error approach to determine the optimal network topology. However, ANN models, such as fuzzy neural network, have been continuously developed and tested to solve the fluctuation of operational conditions in full-scale applications (Han et al., 2018; Mingzhi et al., 2009).

At industrial scale, wastewater and waste gas treatment systems are usually controlled with online monitoring instruments, and programmable sensors can be integrated with the ANN model in order to control and predict the reactor performance using online and/or off-line mode (Figure 8.2). In such cases, the software can be programmed to monitor the performance of the bioreactor treating wastewater/waste gas in real time and generate a set of signals that will raise an alarm to the plant operator about the faults that are occurring and enable suitable changes in the operational parameters to prevent failure of the bioreactor using an optimal set-point decided by neural networks (López et al., 2017; Sadeghassadi et al., 2018).

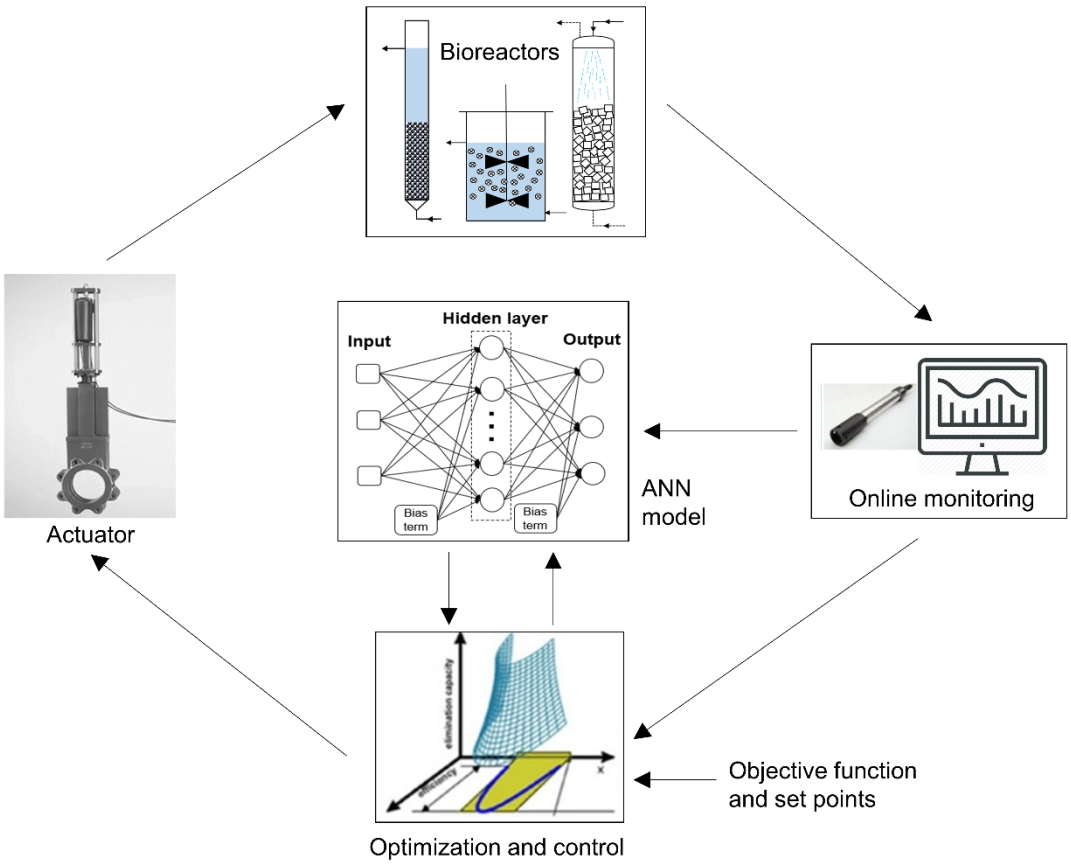

Figure 8.2. Example of an ANN application for the automated control and optimization of bioreactor performance (adapted from López et al., 2017).

8.3 Future research perspectives

8.3.1 Novel processes for H_2S and NO_3^- removal from waste streams

In this thesis, the anoxic MBBR showed a high performance for the removal of $S_2O_3^{2-}$ via autotrophic denitrification as well as good resilience under NO_3^- limitation (**Chapter 4**). However, the application of an anoxic MBBR for H_2S removal from biogas is non-practical due to a major limitation of gas-liquid mass transfer. MBBRs have commonly been used for the nitrogen removal process comprised of nitrification and denitrification steps in WWTP (Bassin and Dezotti, 2018; Yuan et al., 2015). It would be interesting to integrate the MBBR denitrification with biogas desulfurization which is able to provide sulfide as an electron donor during denitrification (NO_3^- removal) without the addition of external organic carbon. A bubble column is one of the most common reactors for simultaneous removal H_2S and CO_2 from biogas (Bahr et al., 2014; Kantarci et al. 2005; Kennedy et al., 2015). The alternative system could be an integration of a bubble column used for H_2S and CO_2 removal from biogas and a MBBR used for denitrification (Figure 8.3a).

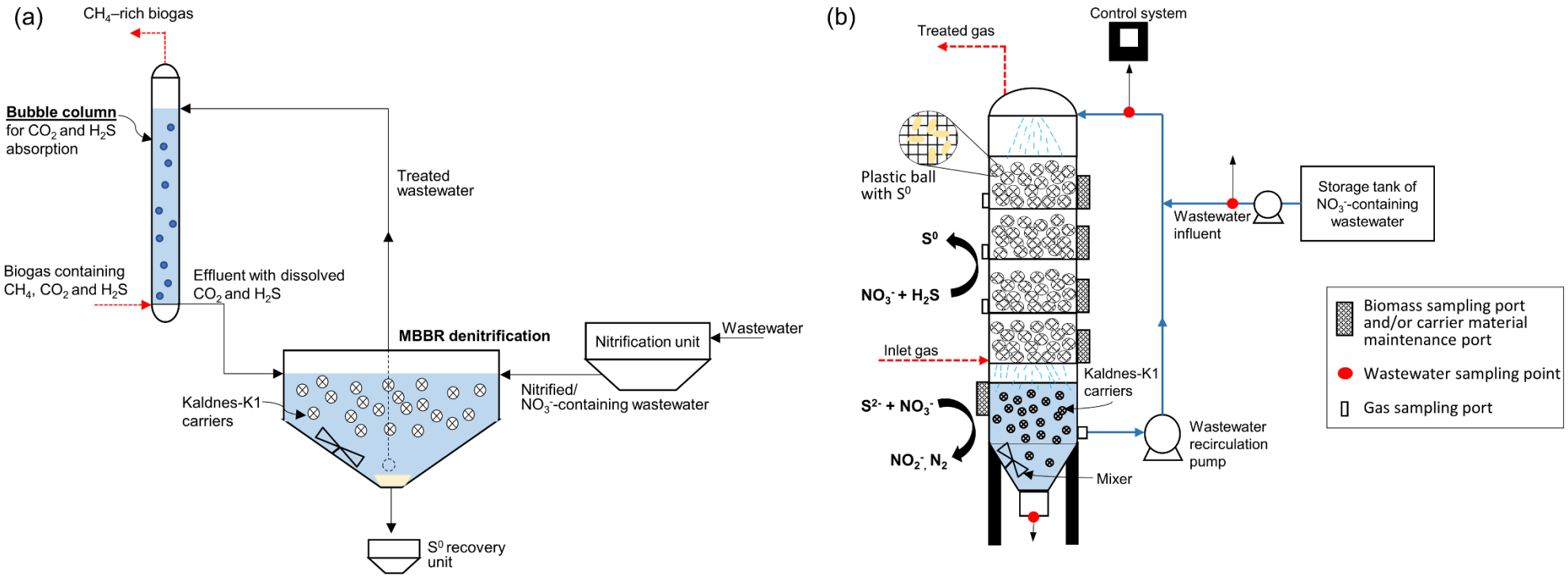

Figure 8.3. Novel processes for simultaneous removal of H_2S and NO_3^- from waste streams: (a) a moving bed biofilm reactor (MBBR) denitrification integrated with bubble column for biogas upgrading and (b) a hybrid biotrickling filter and MBBR for biogas desulfurization with S^0 recovery.

The effluent from the bubble column, also containing dissolved CO_2 (e.g. HCO_3^-), could serve as carbon source for the SO-NR process in the MBBR. However, this warrants further research since the integration of these processes has not yet been studied and the optimal operational conditions are unknown, e.g. the effect of dissolved CO_2 concentration on the SO-NR process and the optimization between concentrations of gaseous H_2S and NO_3^- in the MBBR.

Moreover, H_2S can be simultaneously removed with other contaminants such as CO_2 and NH_3 in biogas as well as the NO_3^-/nitrified wastewater from the post-treatment units of WWTPs (Baspinar et al., 2011; Garcia et al., 2015). The H_2S removal has also been done simultaneously with the removal of both NH_4^+ and NO_3^- from wastewater (anammox and autotrophic denitrification) as well as S^0 recovery (Franco-Morgado et al., 2018; Rios-Del Toro and Cervantes, 2016). In simultaneous desulfurization and denitrification process, the N_2O emission and other nitrate species (e.g. NH_3 and NH_4^+) should be also taken into account and evaluated during the process.

Anoxic bioreactors for gaseous H_2S removal have only been tested in laboratory and pilot scales. Cano et al. 2018 carried out a life cycle assessment (LCA) of different techniques for H_2S removal, i.e. an aerobic BTF, an anoxic BTF, chemical scrubber and impregnated activated carbon. The results showed that the anoxic BTF had lower operational costs than the chemical scrubber and impregnated activated carbon despite using chemicals (e.g. KNO_3 and $Ca(NO_3)_2$) as a NO_3^- source. Furthermore, the anoxic BTF had lower operational costs than the aerobic BTF when using NO_3^--containing wastewater from a nearby location. The use of the anoxic BTF for H_2S removal from synthetic biogas streams using NO_3^- as an electron acceptor required long hydraulic retention times (**Chapter 5**).

Further studies should be focused on the improvement of performance, elimination capacity and design of the packed bed structure of the BTF. The anoxic BTF packed with polyurethane foam likely caused rapid biomass accumulation, particularly when the wastewater contains organic carbon (**Chapters 5 and 6**). The maintenance of the BTF was also difficult due to the accumulation of S^0 in the BTF packed bed. During the anoxic BTF operation, Almenglo et al. (2017) suggested that switching off biogas and feeding only NO_3^- could remove accumulated S^0 which is oxidized to SO_4^{2-}. For a sustainable and cost-effective solution, a bioreactor configuration should be capable of directly recovering S^0. To combine the advantages of the MBBR and BTF, it would be interesting to develop a hybrid anoxic bioreactor (Figure 8.3b) for the simultaneous treatment of H_2S contaminated gas streams and NO_3^- containing wastewater. This alternative bioreactor configuration could potentially overcome high biomass accumulation in the BTF and facilitate S^0 recovery.

In practical applications, the use of real biogas in long-term operations should be further investigated because H_2S concentrations in real biogas can have significant fluctuations. Feeding biogas consisting mainly of CH_4 and CO_2 and low amounts of H_2S to a bioreactor over a long period of time might enrich new consortia under anoxic conditions as NO_3^- and NO_2^- can function as electron acceptors for methane oxidizing bacteria (López et al., 2017). Some sources of biogas containing insufficient CH_4 content (<30% *v/v*) cannot be used as an alternative energy source and CH_4 should not be released to the atmosphere as it is a greenhouse gas. In this context, the study of CH_4 oxidation in anoxic BTF is important for the removal of H_2S. As the end-product of H_2S is SO_4^{2-}, the effect of the SO_4^{2-} concentration should be further investigated as it can be an electron acceptor for CH_4 oxidation (Bhattarai et al., 2018; Cassarini et al., 2018). However, there are so far no studies of simultaneous CH_4 oxidation, SO_4^{2-} reduction and H_2S removal in anoxic BTF using NO_3^- as electron acceptor. The H_2S removal coupled with CH_4 oxidation could be done in the suggested hybrid bioreactor as illustrated in Figure 8.3b.

8.3.2 Advanced biofilm bioreactor analyses

8.3.2.1 Fluid dynamics

Fluid flow in biofilm reactors (e.g. MBBR and BTF) has the high impact on the biofilm development and mass transfer between microorganisms and pollutants (Bassin and Dezotti, 2018; Fortuny et al. 2011). The residence time distribution (RTD) tests carried out in this thesis to characterize the hydrodynamics in the bioreactors could be used to detect the axial dispersion occurring due to nonuniform liquid flow during the anoxic BTF operation (**Chapter 5**). However, the data obtained from the RTD tests is not suitable for the development of a dynamic model because it might critically affect the biofilm dynamics in the system (Prades et al., 2016). In further studies, mathematical modeling tools such as Computational Fluid Dynamics (CFD) for hydrodynamics in conjunction with biokinetic models as AquaSim could potentially be used to model integrated processes like the biogas desulfurization and wastewater denitrification process studied in this thesis.

8.3.2.2 Microbial ecology

Polymerase chain reaction-denaturing gradient gel electrophoresis (PCR-DGGE) followed by sequencing was used to identify the dominant species present in the biofilms in the different bioreactors under the influence of different operational conditions. It is a useful tool to enhance the understanding of the bioreactor performance and link the observed changes to the change in microbial community structure. However, PCR-DGGE is only able to provide information on what species are dominating the communities, but it does not reveal which microorganisms are active and what species are present in minor

amounts during the different operational conditions. For example, as the performance of bioreactors improved after transient-state operation such as NO_3^- limitation in the MBBR (**Chapter 4**) or the intermittent inlet concentrations of H_2S and NO_3^- in the BTF (**Chapter 6**), it would be interesting to investigate the microbial abundance and interactions in more detail. Illuminar Miseq sequencing is a powerful instrument to investigate the diverse microbial community (Giordano et al., 2018). Moreover, MiSeq can also be done on RNA level to identify the active species. This could allow to identify the microbial species and the abundance of the microbial community present in bioreactors during operations at different N/S ratios and after transient-state operations.

In addition to the comparative studies between the performance of different bioreactors, it would be interesting to study the biofilm characterization and/or the biofilm response to different operational conditions. For example, the use of fluorescent in situ hybridization with taxon specific probes can be an effective tool for identifying the dominant microorganisms and the changes in cell morphology and aggregates in biofilm samples. Zhang et al. (2013) demonstrated that FISH followed by confocal laser-scanning microscopy (CLSM) could be used to better understand the interaction between microorganisms and bioreactor performance. Thus, these methods could potentially be used to describe the interaction between sulfur-oxidizing bacteria and other autotrophic and heterotrophic bacteria as well as linking the biofilm characteristics to the performance of the bioreactors.

8.4 Conclusions

Reduced sulfur compound pollutants (i.e. H_2S and $S_2O_3^{2-}$), NO_3^- and organic carbon were simultaneously removed using different anoxic bioreactor configurations. This research demonstrated that the selection of bioreactor configurations is based on the types and composition of contaminants. In anoxic sulfur-oxidizing bioreactors, the NO_3^- loading rate and N/S ratio can be used as the key operational parameters to maintain the good bioreactor performance and the effective microorganisms in the bioreactor system. In this work, anoxic sulfur-oxidizing bioreactors were shown to be resilient and resistant to various transient-state conditions, e.g. NO_3^- limited conditions, H_2S shock loads and intermittent inlet flow rates of pollutants, that are important variables in practical applications. Besides, the activity of the sulfur-oxidizing biofilms was enhanced by applying harsh operating conditions, e.g. NO_3^- limited conditions, which could be used to enrich and strengthen microorganisms for being used as an inoculum for further applications. The collection of data of bioreactor performance (e.g. removal efficiencies and effluent con-

centration of pollutants) implemented with neural network-based models can help to optimize the operational conditions and deal with the low performance during transient-state conditions.

8.5 References

Almenglo, F., Bezerra, T., Lafuente, J., Gabriel, D., Ramírez, M., Cantero, D., 2016. Effect of gas-liquid flow pattern and microbial diversity analysis of a pilot-scale biotrickling filter for anoxic biogas desulfurization. Chemosphere 157, 215–223.

Bahr, M., Díaz, I., Dominguez, A., González-Sánchez, A., Muñoz, R., 2014. Microalgal-biotechnology as a platform for an integral biogas upgrading and nutrient removal from anaerobic effluents. Environ. Sci. Technol. 48, 573–581.

Barwal, A., Chaudhary, R., 2014. To study the performance of biocarriers in moving bed biofilm reactor (MBBR) technology and kinetics of biofilm for retrofitting the existing aerobic treatment systems: A review. Rev. Environ. Sci. Biotechnol. 13, 285–299.

Baspinar, A.B., Turker, M., Hocalar, A., Ozturk, I., 2011. Biogas desulphurization at technical scale by lithotrophic denitrification: Integration of sulphide and nitrogen removal. Process Biochem. 46, 916–922.

Bassin, J.P., Dezotti, M., 2018. Moving bed biofilm reactor (MBBR), in: Dezotti, M., Lippel, G., Bassin, J.P. (Eds.), Advanced Biological Processes for Wastewater Treatment. Springer, Rio de Janeiro.

Bayrakdar, A., Tilahun, E., Calli, B., 2016. Biogas desulfurization using autotrophic denitrification process. Appl. Microbiol. Biotechnol. 100, 939–948.

Bhattarai, S., Cassarini, C., Naangmenyele, Z., Rene, E.R., Gonzalez-Gil, G., Esposito, G., Lens, P.N.L., 2018. Microbial sulfate-reducing activities in anoxic sediment from Marine Lake Grevelingen: screening of electron donors and acceptors. Limnology 19, 31–41.

Brito, J., Almenglo, F., Ramírez, M., Gómez, J.M., Cantero, D., 2017. PID control system for biogas desulfurization under anoxic conditions. J. Chem. Technol. Biotechnol. 92, 2369–2375.

Cano, P.I., Colón, J., Ramírez, M., Lafuente, J., Gabriel, D., Cantero, D., 2018. Life cycle assessment of different physical-chemical and biological technologies for biogas desulfurization in sewage treatment plants. J. Clean. Prod. 181, 663–674.

Cassarini, C., Bhattarai, S., Rene, E.R., Vogt, C., Musat, N., Esposito, G., Lens, P.N.L., 2018. Enrichment of anaerobic methanotrophs in biotrickling filters using different sulfur compounds as electron acceptor. Environ. Eng. Sci. (in press).

Deng, L., Chen, H., Chen, Z., Liu, Y., Pu, X., Song, L., 2009. Process of simultaneous hydrogen sulfide removal from biogas and nitrogen removal from swine wastewater. Bioresour. Technol. 100, 5600–5608.

Di Capua, F., Papirio, S., Lens, P.N.L., Esposito, G., 2015. Chemolithotrophic denitrification in biofilm reactors. Chem. Eng. J. 280, 643–657.

Dolejs, P., Paclík, L., Maca, J., Pokorna, D., Zabranska, J., Bartacek, J., 2015. Effect of S/N ratio on sulfide removal by autotrophic denitrification. Appl. Microbiol. Biotechnol. 99, 2383–2392.

Fernández, M., Ramírez, M., Gómez, J.M., Cantero, D., 2014. Biogas biodesulfurization in an anoxic biotrickling filter packed with open-pore polyurethane foam. J. Hazard. Mater. 264, 529–535.

Fernández, M., Ramírez, M., Pérez, R.M., Gómez, J.M., Cantero, D., 2013. Hydrogen sulphide removal from biogas by an anoxic biotrickling filter packed with Pall rings. Chem. Eng. J. 225, 456–463.

Fortuny, M., Gamisans, X., Deshusses, M.A., Lafuente, J., Casas, C., Gabriel, D., 2011. Operational aspects of the desulfurization process of energy gases mimics in biotrickling filters. Water Res. 45, 5665–5674.

Franco-Morgado, M., Toledo-Cervantes, A., González-Sánchez, A., Lebrero, R., Muñoz, R., 2018. Integral (VOCs, CO_2, mercaptans and H_2S) photosynthetic biogas upgrading using innovative biogas and digestate supply strategies. Chem. Eng. J. 354, 363–369.

Garcia, G.P.P., Diniz, R.C.O., Bicalho, S.K., Franco, V.A.S., Gontijo, E.M.O., Toscano, R.A., Canhestro, K.O., Santos, M.R., Carmo, A.L.R.D., Lobato, L.C.S., Brandt, E.M.F., Chernicharo, C.A.L., Araujo, J.C, 2015. Biological sulphide removal from anaerobically treated domestic sewage: reactor performance and microbial community dynamics. Environ. Technol. 36, 2177–2189.

Giordano, C., Spennati, F., Mori, G., Munz, G., Vannini, C., 2018. The microbial community in a moving bed biotrickling filter operated to remove hydrogen sulfide from gas streams. Syst. Appl. Microbiol. 41, 399–407.

Guerrero, L., Montalvo, S., Huiliñir, C., Campos, J.L., Barahona, A., Borja, R., 2015. Advances in the biological removal of sulphides from aqueous phase in anaerobic processes: A review. Environ. Rev. 24, 84–100.

Han, H.G., Zhang, L., Liu, H.X., Qiao, J.F., 2018. Multiobjective design of fuzzy neural network controller for wastewater treatment process. Appl. Soft Comput. J. 67, 467–478.

Jiang, G., Keller, J., Bond, P.L., Yuan, Z., 2016. Predicting concrete corrosion of sewers using artificial neural network. Water Res. 92, 52–60.

Kantarci, N., Borak, F., Ulgen, K.O., 2005. Bubble column reactors. Process Biochem. 40, 2263–2283.

Kennedy, N., Zhao, Q.B., Ma, J., Chen, S., Frear, C., 2015. The selective removal of H_2S over CO_2 from biogas in a bubble column using pretreated digester effluent. Sep. Purif. Technol. 144, 240–247.

Kennes, C., Rene, E.R., Veiga, M.C., 2009. Bioprocesses for air pollution control. J. Chem. Technol. Biotechnol. 84, 1419–1436.

Khoshnevisan, B., Tsapekos, P., Alfaro, N., Díaz, I., Fdz-Polanco, M., Rafiee, S., Angelidaki, I., 2017. A review on prospects and challenges of biological H2S removal from biogas with focus on biotrickling filtration and microaerobic desulfurization. Biofuel Res. J. 4, 741–750.

López, J.C., Porca, E., Collins, G., Pérez, R., Rodríguez-Alija, A., Muñoz, R., Quijano, G., 2017. Biogas-based denitrification in a biotrickling filter: Influence of nitrate concentration and hydrogen sulfide. Biotechnol. Bioeng. 114, 665–673.

López, L.R., Brito, J., Mora, M., Almenglo, F., Baeza, J.A., Ramírez, M., Lafuente, J., Cantero, D., Gabriel, D., 2018. Feedforward control application in aerobic and anoxic biotrickling filters for H_2S removal from biogas. J. Chem. Technol. Biotechnol. 93, 2307–2315.

López, M.E., Rene, E.R., Boger, Z., Veiga, M.C., Kennes, C., 2017. Modelling the removal of volatile pollutants under transient conditions in a two-stage bioreactor using artificial neural networks. J. Hazard. Mater. 324, 100–109.

Manconi, I., Carucci, A., Lens, P., 2007. Combined removal of sulfur compounds and nitrate by autotrophic denitrification in bioaugmented activated sludge system. Biotechnol. Bioeng. 98, 551–560.

Mingzhi, H., Ma, Y., Jinquan, W., Yan, W., 2009. Simulation of a paper mill wastewater treatment using a fuzzy neural network. Expert Syst. Appl. 36, 5064–5070.

Muñoz, R., Meier, L., Diaz, I., Jeison, D., 2015. A review on the state-of-the-art of physical/chemical and biological technologies for biogas upgrading. Rev. Environ. Sci. Biotechnol. 14, 727–759.

Nair, V. V., Dhar, H., Kumar, S., Thalla, A.K., Mukherjee, S., Wong, J.W.C., 2016. Artificial neural network based modeling to evaluate methane yield from biogas in a laboratory-scale anaerobic bioreactor. Bioresour. Technol. 217, 90–99.

OSHA (U.S. Occupational, Safety and Health Administration), 2005. Fact sheet: Hydrogen sulfide. https://www.osha.gov/OshDoc/data_Hurricane_Facts/hydrogen_sulfide_fact.html, Accessed date: 21 September 2017.

Papirio, S., Villa-Gomez, D.K., Esposito, G., Pirozzi, F., Lens, P.N.L., 2013. Acid mine drainage treatment in fluidized-bed bioreactors by sulfate-reducing bacteria: a critical review. Crit. Rev. Environ. Sci. Technol. 43, 2545–2580.

Pokorna, D., Zabranska, J., 2015. Sulfur-oxidizing bacteria in environmental technology. Biotechnol. Adv. 33, 1246–1259.

Prades, L., Dorado, A.D., Climent, J., Guimerà, X., Gamisans, X., 2016. CFD modeling of a fixed-bed biofilm reactor coupling hydrodynamics and biokinetics. Chem. Eng. J. 680–692.

Rene, E.R., López, M.E., Veiga, M.C., Kennes, C., 2011. Neural network models for biological waste-gas treatment systems. N. Biotechnol. 29, 56–73.

Rios-Del Toro, E.E., Cervantes, F.J., 2016. Coupling between anammox and autotrophic denitrification for simultaneous removal of ammonium and sulfide by enriched marine sediments. Biodegradation 27, 107–118.

Rodriguez, G., Dorado, A.D., Fortuny, M., Gabriel, D., Gamisans, X., 2014. Biotrickling filters for biogas sweetening: Oxygen transfer improvement for a reliable operation. Process Saf. Environ. Prot. 92, 261–268.

Sadeghassadi, M., Macnab, C.J.B., Gopaluni, B., Westwick, D., 2018. Application of neural networks for optimal-setpoint design and MPC control in biological wastewater treatment. Comput. Chem. Eng. 115, 150–160.

Sahinkaya, E., 2009. Biotreatment of zinc-containing wastewater in a sulfidogenic CSTR: Performance and artificial neural network (ANN) modelling studies. J. Hazard. Mater. 164, 105–113.

Sulonen, M.L.K., Kokko, M.E., Lakaniemi, A.-M., Puhakka, J.A., 2014. Electricity generation from tetrathionate in microbial fuel cells by acidophiles. J. Hazard. Mater. 284, 182–189.

Watsuntorn, W., Ruangchainikom, C., Rene, E.R., Lens, P.N.L., Chulalaksananukul, W., 2017. Hydrogen sulfide oxidation under anoxic conditions by a nitrate-reducing, sulfide-oxidizing bacterium isolated from the Mae Um Long Luang hot spring, Thailand. Int. Biodeterior. Biodegradation 124, 196–205.

Yuan, Q., Wang, H., Hang, Q., Deng, Y., Liu, K., Li, C., Zheng, S., 2015. Comparison of the MBBR denitrification carriers for advanced nitrogen removal of wastewater treatment plant effluent. Environ. Sci. Pollut. Res. 22, 13970–13979.